Single droplet analysis for spray drying of foods

Jimmy Perdana

Thesis committee

Promotor

Prof. Dr *ir*. Remko M. Boom
Professor of Food Process Engineering
Wageningen University

Co-promotors

Dr *ir*. Maarten A.I. Schutyser
Assistant Professor, Laboratory of Food Process Engineering
Wageningen University

Dr Martijn B. Fox
Project Manager Processing
NIZO Food Research, Ede

Other members

Prof. Dr *ir*. Marcel H. Zwietering, Wageningen University
Prof. Dr *ir*. Gerrit Meerdink, Bangor University, Gwynedd, United Kingdom
Dr *ir*. Koen C. van Dijke, Danone Research, Utrecht, The Netherlands
Dr *ir*. A.J.B. (Ton) van Boxtel, Wageningen University

This research was conducted under the auspices of the Graduate School VLAG (Advanced Studies in Food Technology, Agrobiotechnology, Nutrition and Health Sciences).

Single droplet analysis for spray drying of foods

Jimmy Perdana

Thesis

submitted in fulfilment of the requirements for the degree of doctor
at Wageningen University
by the authority of the Rector Magnificus
Prof. Dr M.J. Kropff,
in the presence of the
Thesis Committee appointed by the Academic Board
to be defended in public
on Tuesday 3 September 2013
at 11 a.m. in the Aula.

Jimmy Perdana

Single droplet analysis for spray drying of foods,

254 pages.

PhD thesis, Wageningen University, Wageningen, The Netherlands (2013)

With references, with summary in English

ISBN 978-94-6173-587-4

Table of contents

Chapter 1

General Introduction

Introduction

Many food products and ingredients are dried in powdered form to provide shelf-life and retain the activity of bioactive components (1-7). One of the most popular techniques is spray drying, which processes liquid concentrates into powders that can be reconstituted. It is a mild technique due to its very short drying time and the low temperatures to which the product is exposed (8-11). However, in practice freeze drying is usually applied to dehydrate heat sensitive components such as enzymes, vitamins, volatile components, and probiotic bacteria since the activity of the heat sensitive components is better retained (12-14). Because spray drying is much more cost effective compared to freeze drying, many attempts have been made to optimise spray drying and product formulations towards minimal activity losses (1, 15-18). Although many successes have been reported, optimisation results, especially from pilot-scale experiments, have been difficult to translate into general optimisation rules (19), especially for its application on industrial scale.

Optimal spray drying of heat sensitive ingredients

Optimal drying should be targeted at minimising the loss of the functionality of the dried material and maximising the energy efficiency. For example, the survival of probiotics increases with decreasing the outlet temperature and the residence time (17, 20). However, a too low outlet temperature will reduce the drying capacity and result in a higher residual moisture contents, leading to subsequent loss of probiotic viability during storage (21). The sensitivity of micro-organisms towards the outlet temperature varies strongly with each bacterial strain (22). Additionally, the residence time is a critical parameter, which can vary considerably within different industrial dryer types and possible following steps, such as fluidised bed drying at low temperatures. Other drying parameters of influence are related to the exact spray dryer configuration, such as nozzle type, positioning of air flow and injection of feed, and chamber design (23).

Optimal spray drying of heat sensitive ingredients involves the use of tailored formulations to enhance the stability of the components. Carbohydrates are frequently added to obtain glassy, amorphous powders (24, 25). For each powder a glass transition temperature can be defined below which molecular mobility decreases dramatically (26-28). The glass transition temperature is a function of the temperature and the moisture content and thus

varies during the drying process (29-31). Formulations with a high glass transition temperature have been correlated to increased enzyme and bacterial stability (32, 33).

Rapid screening method for optimum spray drying procedures

Sensitivity to the drying process differs strongly between components (5). Therefore, optimum drying parameters are unique for a given component of interest. Moreover, feed formulation co-determines the impact of the drying on the activity of the component. The overall result of the drying process is a very complex function of both the formulation and the process parameters. Finding this relation between result and parameters with a limited set of experiments (or with straightforward modelling) is a great challenge. Therefore, in this thesis, a rapid yet robust method is proposed to screen for optimal conditions on the basis of a single droplet approach. This method should be able to handle a wide variety of parameters (e.g. drying temperature, droplet size, drying time, feed type and its physical properties) comparable to those in a spray dryer. Besides mimicking the drying process itself, it should facilitate subsequent rapid analysis of the functionality of the product.

The inactivation kinetics of heat sensitive components as a function of temperature has been extensively studied (34-38). However, the combined effect of temperature and moisture content on the inactivation kinetics is less well understood. Furthermore, for the application in drying of heat sensitive components, the complication emerges that during drying heat and mass transfer are distributed in both time and space. Mechanistic understanding of these distributions and the connected inactivation of components is expected to give insight in optimal drying conditions of heat sensitive components. The single droplet drying approach employed in this thesis is a well-defined and robust drying procedure, which can provide the necessary data to establish this insight with underlying inactivation mechanisms. Moreover, the well-defined experiments allow systematic variation of drying conditions to establish inactivation kinetics of heat sensitive components. These kinetics can be captured with predictive models to scale the obtained insight from the single droplet scale to the drying processes at the industrial scale.

Probiotic products

Probiotics are live microorganisms that may confer a health benefit on the host (9, 26, 28). Health benefits are related to the influence of probiotic bacteria on the microbial balance in

the hosts' intestine or via modulation of the gut-associated immune system (6, 10, 15, 17, 20). Probiotic cultures are applied mostly in yogurt or fermented milks, whereas applications in other dairy foods such as some cheese varieties, frozen yogurts, and ice cream have been explored (39). In 1997, the European market for probiotic yoghurt and milk (drinks) accounted for approximately USD 889 million; a number which is increasing rapidly every year (40, 41). Typical products such as Yakult or Danone Activia are composed of carbohydrates, milk, flavours and live probiotic bacteria and have a typical shelf-life of 40 days under refrigerated conditions (42). The living probiotic bacteria are supplied to manufactures either in frozen or (freeze-) dried formulations for prolonged shelf-life.

Drying of probiotics

The focus of this thesis is on the drying of probiotic bacteria. Probiotics formulations are dried to prolong their shelf life (43), and to facilitate their incorporation into products. Unfortunately, spray drying of living probiotic bacteria is challenging and poor survival rates are obtained, for example compared to freeze drying (1, 5). As mentioned before, spray drying is competitive due to its lower cost level and energy consumption and therefore could be an attractive alternative, provided that the survival percentages and shelf life are acceptable (12).

The single droplet drying approach is employed to derive a more accurate mechanistic description of the drying of probiotics. In addition to the temperature and the moisture content also for example the drying rate can be considered a critical parameter influencing survival (44). Predictive models are developed on the basis of systematic single droplet drying experimentation to more accurately describe microbial survival as function of relevant parameters. In addition the single droplet drying approach is used to investigate interaction behaviour between protective solid carriers and microbial cell membranes in a more systematic way (24, 33, 45, 46).

Optimisation of spray drying conditions and addition of protective agents are necessary to retain the maximum viability of the probiotics (2, 8, 38). The sensitivity of micro-organisms towards drying varies strongly with each bacterial strain (22). The cause of this is not yet understood well, since the underlying mechanisms are many and complex. In

practice, several expensive pilot-scale trials are needed to explore different formulations and determine optimum drying conditions. The need for a systematic screening methodology is clear when considering the laborious pilot scale experimentation and the number of parameters involved in the optimisation of spray drying, e.g. processing conditions, formulation, and component-specific sensitivity. Use of laboratory-scale spray dryers for optimisation is troublesome, because it is difficult to scale up drying time and particle size distribution to spray drying at the industrial scale (11, 39, 40). Moreover, the drying behaviour at the laboratory-scale induces specific physical and chemical changes which are not comparable to spray drying at the industrial scale (41-43). Thus, a rapid yet robust method is proposed to screen for optimal conditions on the basis of a single droplet approach, which will be used for obtaining further insight into the crucial mechanisms that limit the survival of probiotic bacteria during spray drying.

This thesis is the result of a project that was embedded in the NWO – Process on a Chip (PoaC) program and part of a larger project entitled “High throughput experimentation on spray drying”. The aim of this larger project was the development of a platform for screening of conditions and formulations for drying of probiotics, which included obtaining more insight in the influence of drying at the bacterial level. The research carried out on the bacterial level was done out at the Laboratory of Microbiology (by Dr. Bereschenko, Dr. Kutahya, and Prof. Kleerebezem) who were responsible for the development of the rapid viability enumeration assay interfacing with the single droplet drying. Additionally, this part of the project aimed at identification of the mechanisms that are responsible for a higher (drying) resistance bacterium using a molecular analysis approach.

Objective and outline of the thesis

The objective of the research reported in this thesis was the development of a single droplet based drying approach to screen for optimal spray drying. More specifically, this approach is to be used for identification and optimisation of formulations and drying conditions that result in maximum survival of probiotic bacteria or other heat sensitive ingredients. This then leads to better insight into the mechanisms that limit the survival of spray dried probiotics. In addition to the development of an experimental platform, predictive modelling tools were developed to translate the gained insight towards the design of spray drying processes, and to their scale up (Figure 1-1).

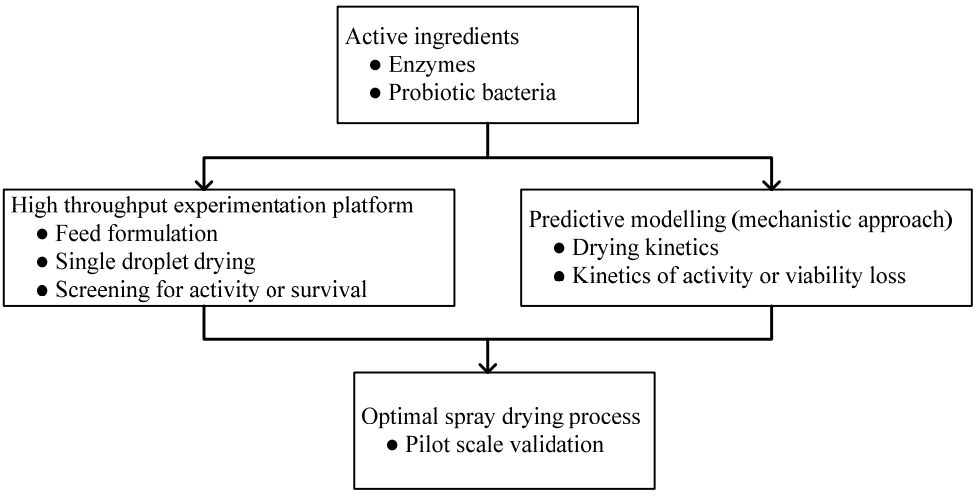

Figure 1-1. Schematic diagram of the approach to study the spray drying of heat sensitive products

In **chapter 2**, the design of a single droplet drying platform is described, including a method for accurately dispensing small droplets. The heat and mass transfer during evaporation of sessile water droplets is characterised, which is related to spray drying. The accurate estimation of moisture diffusivity is critical to calculate the temperature and moisture content history of droplets during drying. In **chapter 3**, a method is therefore presented to measure moisture diffusivities in solid materials. This method is based on gravimetric analysis of a drying thin film in a dynamic vapour sorption (DVS) analyser. The measured diffusivities are compared to predictions based on first principles, using only the physical properties and thermodynamics of the system.

The enzyme β-galactosidase was chosen as a model system to investigate the effect of temperature and moisture content on activity loss during heating and drying. In **chapter 4**, the isothermal inactivation kinetics of β-galactosidase at specific combinations of temperature and water content is reported. A mathematical model based on Eyring's transitional-state theory is employed to describe the inactivation kinetics of this enzyme as function of temperature and water content. In **chapter 5**, the single droplet drying system was validated by studying β-galactosidase inactivation. The histories of temperature and

moisture content in single droplets are predicted with an effective diffusion model. This model is then combined with the inactivation kinetics of the enzyme to predict the residual activity of the enzyme after drying of a single droplet. This predicted residual activity prediction is compared to the experimental results from the single droplet drying experiments.

Lactobacillus plantarum WCFS1 was selected as a model probiotic bacterium during subsequent single droplet drying experimentation. In **chapter 6**, a novel enumeration method of viable cells is presented on the basis of rehydration of single powder particles on an Anopore chip and subsequent fluorescence staining. The method is verified and compared towards conventional plate counting. Additionally, it is applied to analyse powder samples obtained from laboratory-scale spray drying experiments. In **chapter 7**, the inactivation kinetics of *L. plantarum* WCFS1 are reported on the basis of experiments with the single droplet drying platform. Both thermal and dehydration inactivation mechanisms are distinguished when operating at different drying conditions. Survival of *L. plantarum* WCFS1 is modelled taking into account both inactivation mechanisms adopting a Weibull distribution model. The modelling approach is used to predict retention of viability during laboratory scale spray drying and compared to experiments. Finally, various drying methods (operating at different time scales) are compared for their impact on (especially dehydration) inactivation.

The influence of the formulation and of the drying conditions on the residual viability of *L. plantarum* WCFS1 is presented in **chapter 8**. The influence of glass transition temperatures and other physical properties of the carrier formulations (e.g. molecular weight and degree of crystallinity) are related to survival after drying of *L. plantarum* WCFS1. In **chapter 9**, the cell-integrity based enumeration method on the basis of fluorescent staining is compared to another enumeration method relying on the microbial growth profile. Combining both enumeration methods provides more insight in the capacity to resume growth after reconstitution of the droplets.

A general discussion on the results and consequences of this thesis is presented in **chapter 10**. This includes the implementation of the rapid screening method for spray drying optimisation procedures. Finally, an outlook to further application of the acquired insight and future research lines are discussed.

Chapter 2

Single droplet experimentation on spray drying: evaporation of a sessile droplet

Published as:

J. Perdana, M.B. Fox, M.A.I. Schutyser, and R.M. Boom. 2011. Single-droplet experimentation on spray drying: evaporation of a sessile droplet. Chem. Eng. Technol. 34:1151-1158.

Abstract

This work forms the basis for the development of a platform for high throughput experimentation on spray drying. To mimic the drying of single droplets during spray drying individual droplets are dispensed and dried on a flat surface. A dispensing process is used that is able to dispense viscous liquids and generates small droplets (d_p > 150 µm). The dispensed droplet size for varying liquids could be accurately described with a predictive model based on Bernoulli's law. The drying of droplets is monitored with a camera and modelled with mass balance equations. Finally, a Sherwood correlation is derived to describe the mass transfer between the sessile droplet and the drying air.

Keywords: spray drying, sessile droplet, fluid dispensing, Sherwood correlation

Introduction

Spray drying has a long history in food processing and other areas of industrial production. For more than 30 years, spray drying is the most common method to dehydrate for example milk products (47). Nowadays, spray drying is widely used for manufacturing e.g. milk powder, whey powder, infant formula, lactose powder, and maltodextrin due to its advantages (11):

1. Instant properties of the powder can be effectively controlled,
2. Spray drying allows high production capacity in continuous operation,
3. Heat-sensitive foods, biological products and pharmaceuticals can be dehydrated under relatively mild drying conditions.

Although spray drying is well-established, it is difficult to find the optimal drying conditions for a given product. Numerous process parameters and feed properties during spray drying influence final product quality and process efficiency. To avoid up-scaling issues, it is necessary to carry out trials in representative pilot-scale spray dryers. These trials are costly and increase the time to market. Other disadvantages of existing spray dryers are the given design and operational parameters, e.g. operating temperatures, residence time, and liquid feed viscosity (have to be within certain limits), which makes it difficult to discover new windows of operation in combination with the development of new products.

Researchers have attempted to scale down the experimental conditions from pilot-scale to as small as a single droplet (48, 49). Major advantage of this approach is the reduction of the number of pilot-scale tests. Drying of single droplets was for example assessed by using acoustic levitation to suspend a free droplet in the air. From imaging the shrinking droplets, it was possible to determine the drying kinetics at different drying conditions (48, 50). In the current study we aim at the drying of single droplets dispensed on a flat surface. Advantages of the proposed approach is that multiple droplets can be dried simultaneous, residence time can be easily varied, and particles can be collected for further analysis (e.g. to monitor survival of bacteria after drying). Disadvantage of the drying of a droplet on a surface is that it is physically different from the drying of a free flowing droplet suspended in the air (which occurs during spray drying). However, despite the differences, there are also still many aspects of the drying process alike and parameters, e.g. initial droplet size

and air flow rate, can be set similar. The compromise of drying droplets on a surface facilitates that we can dry multiple droplets simultaneously and thus in principle perform high throughput experimentation on drying of droplets.

In this study a pneumatic dispensing method is investigated to produce a small initial droplet size of various liquids. The properties of the target surface are selected such that the droplets retain their spherical shape but do not move by the applied air flow. In this way the difference in drying behaviour between a sessile and a free falling droplet is minimized. Finally, the drying behaviour of the sessile droplets are investigated are compared to that of droplets in spray drying.

Materials and methods

The experimental set-up consists of the following units:

1. Micro-dispenser
2. Drying chamber
3. Camera system

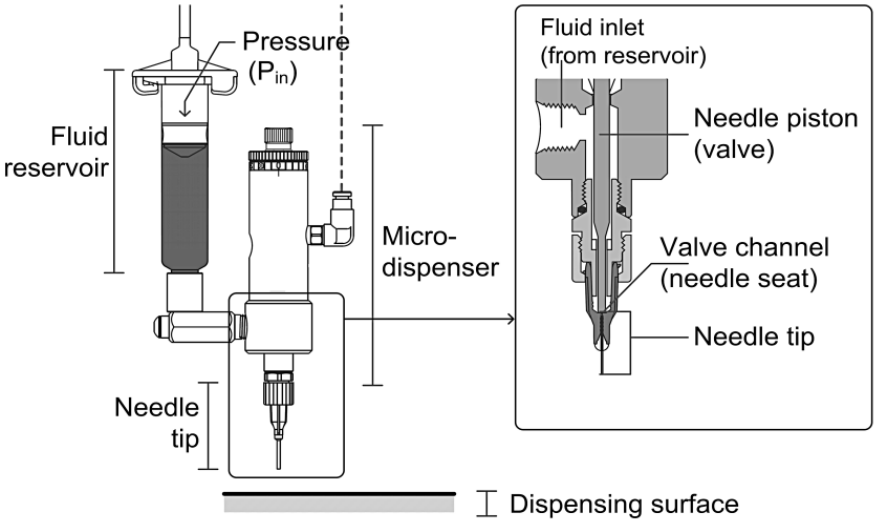

Figure 2-1. Pneumatically driven micro-dispenser.

The micro-dispenser was a Microdot 741MD-SS Dispense Valve (Nordson Engineering Fluid Dispensing, USA). Nitrogen (6 barG) was used to operate the micro-dispenser. As shown in Figure 2-1, a static pressure is applied to the fluid in the cylindrical fluid reservoir. The needle valve or piston opening time is controlled by the actuating pressure. When the valve is opened, liquid is dispensed through the needle tip. Inner diameter of the needle used in this study was 0.12 mm. An Ultra TT positioning system (Nordson Engineering Fluid Dispensing, USA) was used to automate the dispensing process and to position the dispensed droplets.

To evaluate the micro-dispensing process, three different fluids were dispensed; monoethylene glycol (MEG), diethylene glycol (DEG), and polyethylene glycol 400 (PEG-400). Analytical grade fluids (Merck Chemicals, Germany) were used. Milli-Q water (Millipore, USA) was dispensed for the drying experiments.

The pre-conditioning of the drying air was carried out with two heat exchangers and a packed bubble column. The dry air stream was then split into two streams of which the flow rates were measured and controlled independently. The first stream was saturated with water in a packed bubble column (A). The second stream was passed through a heat exchanger to increase the air temperature to a set value. Both streams were then mixed and led through the second heat exchanger (B). Thus, the first heat exchanger was used to control the humidity of the air and the second heat exchanger was used to control the outlet air temperature.

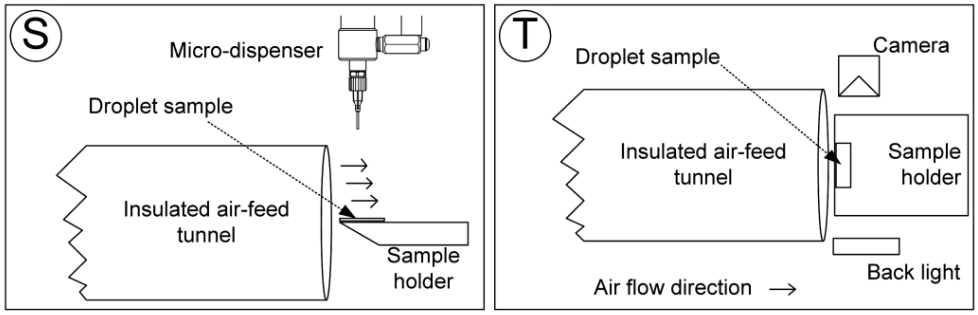

Figure 2-2. Spray drying screening tool setup, side view (S) and top view (T).

Drying air was fed to the drying chamber via an insulated channel. In this channel, the air flow was developed while the temperature was maintained constant. In the current study, the bulk drying air temperature in the tunnel was 80 °C. A similar air temperature was assumed near the droplet, although in practice this will be somewhat lower due to heat transfer between the solid surface and the air. The droplet was dispensed on the solid surface with the aid of the Ultra TT system. The position of the droplet sample was exactly in the centre of the outlet of the channel as shown in Figure 2-2.

The surface on which the droplets were deposited was a hydrophilic membrane, i.e. Accurel® type PP 2E-HF (Akzo Nobel Faser Ag., Netherlands). The water contact angle of this membrane was 130^{O}. The camera system used to monitor droplet geometry change consisted of a μEye 1480ME CCD camera (Imaging Development System GMBH, Germany) with a magnification lens. The droplet was illuminated from the back using a diffused light Lumimax SQ50-W (Lumimax, USA).

Theory

Micro-dispensing

The micro-dispensing process can be considered as a fluid flowing through a series of channels. To describe the micro-dispensing process, a model based on Bernoulli's law is proposed. Several assumptions and considerations were checked and found to hold:

- Newtonian flow behaviour of the dispensed fluids,
- The dispensing resistance is (> 99 %) dominated by the needle tip, which is the narrowest channel in the dispensing system (51),
- The small increase in temperature (< 3^{o}C) has no significant effect on fluid viscosity,
- The Laplace pressure is less than 5 % of the applied pressure for dispensing the smallest droplets and thus assumed negligible.

For non-compressible fluids, Bernoulli's equation (52, 53) can be written as

$$\left(\frac{P_o - P_i}{\rho}\right) + g(z_o - z_i) + \frac{1}{2}\alpha\left(v_o^{\,2} - v_i^{\,2}\right) + w + e_f = 0 \qquad (2\text{-}1)$$

which gives the energy per unit mass due to the applied pressure difference (first term in Eq. 2-1), the potential energy difference (second term), the kinetic energy difference (third

term), the shaft work (fourth term), and the friction in pipes and appendages (fifth term). The value of the kinetic energy correction factor (α) is taken as 2, which is valid for laminar flow (51). The piston movement in the dispenser (to open and close the valve) can be regarded as shaft work and determines the minimum dispensed fluid that can be achieved.

The total friction loss of the system is the summation of all frictions due to the length of the pipes, valves, fittings, contractions or expansions

$$e_f = \sum_i \frac{K_{f_i} v_i^2}{2} \tag{2-2}$$

It was calculated that 99 % of the resistance to liquid flow is contributed by the needle tip due to contraction and flow in the small channel. The flow in the small channel is laminar. The friction coefficient (K_f) can be estimated using the Fanning friction factor (f), which is dependent on the Reynolds number for laminar flow:

$$K_f = 4f\frac{L}{d_h};\ f = \frac{16}{Re} \tag{2-3}$$

To predict the resistance to flow due to contraction between the needle and the needle chamber, the following friction coefficient was used (54)

$$K_f = K + \frac{K'}{Re} \tag{2-4}$$

with K = 2.4 and K'= 295. This correlation is derived for a contraction factor ($d_{c,o}/d_{c,i}$) of 0.016 and 6<Re<2000, which is relevant to the dispensing process used; the contraction factor in the micro dispenser used is between 0.026 and 0.048 and the Reynolds number is larger than 8.

Eq. 2-1 is numerically solved and yields the outlet fluid velocity (v_o) of the dispensed fluid. The droplet volume can then be calculated as follows

$$V_d = \frac{1}{4}\pi d_{c,o} v_o t_{dis} \tag{2-5}$$

Drying of a single sessile droplet

The evaporation of a single sessile droplet cannot be considered similar to that of an ideal spherical body because of the evolution in geometry during the drying. In Figure 2-3 the evolution of a drying sessile droplet is sketched. It is found that during our drying experiments the wetted droplet surface ($2 \cdot l_d$) remained constant. Thermodynamically, one would expect a constant contact angle. However, due to surface roughness a constant base diameter is often observed as well. This phenomenon is also known as contact angle hysteresis (55). It is noted that during the drying of actual food suspensions (e.g. concentrated milk) the droplet height will only be reduced with approximately 30 % and thus the final particle shape will not be completely flat.

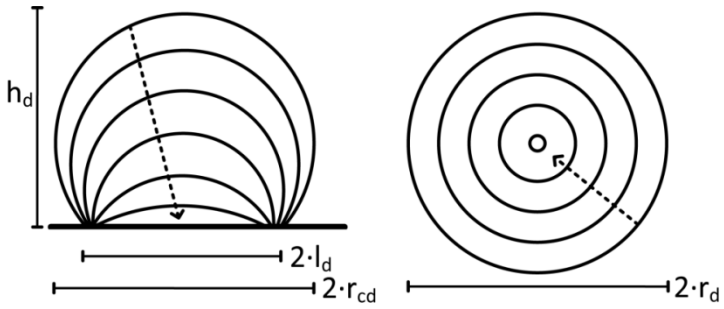

Figure 2-3. Droplet evolution due to evaporation of a pure liquid; sessile droplet (left) and spherical body (right).

Drying of single droplets has been investigated in numerous studies, e.g. the work of Ranz-Marshall (56). The mass transfer coefficient can be obtained from Sherwood correlation that describe the mass transfer coefficient as a function of hydrodynamic conditions and the geometry of the drying object. The general Sherwood correlation is the following (57)

$$Sh = \frac{k_{ev} l_c}{D} = P_1 + P_2 \, Re^{P3} \, Sc^{P4} \qquad (2\text{-}6)$$

In which, the Reynolds and Schmidt numbers are defined as

$$Re = \frac{\rho_a d_p v_a}{\mu_a} \qquad (2\text{-}7)$$

$$Sc = \frac{\mu_a}{\rho_a D} \tag{2-8}$$

In the field of spray drying the Sherwood correlation for a free falling spherical body is mostly applied. The Sherwood and Nusselt relations for heat and mass transfer for this case are

$$Sh = \frac{k_{ev} l_c}{D} = 2.0 + 0.6\, Re^{1/2}\, Sc^{1/3} \tag{2-9}$$

$$Nu = \frac{h_c d_p}{k_a} = 2.0 + 0.6\, Re^{1/2}\, Pr^{1/3} \tag{2-10}$$

in which the Prandtl number is equal to

$$Pr = \frac{cp_a \mu_a}{k_a} \tag{2-11}$$

In this study we focus on the drying of a droplet deposited on a flat surface. Baines and James (58) indicate that the Sherwood correlation for a deposited droplet is comparable to that for flow across a flat plate

$$Sh = 0.664\, Re^{1/2}\, Sc^{1/3};\ Sc > 0.6 \tag{2-12}$$

Evaporation of water from a sessile droplet is a coupled heat and mass transfer process (50, 59). For a sessile droplet heat is partially transferred via the drying air and via the solid surface that is heated by the drying air. Therefore, the total heat balance is

$$m_d cp_l \frac{dT}{dt} = U_{conv} A_{la} \Delta T_{la} + U_{cond} A_{ls} \Delta T_{ls} - \frac{dm_d}{dt} \Delta H_{vap} \tag{2-13}$$

in which ΔT_{la} is the temperature difference between the droplet and the air; and ΔT_{ls} is the temperature difference between the droplet and the solid surface. The exact temperature of the droplet was not determined during this study. For the calculations on mass transfer it was assumed that the drying occurred at wet bulb temperature (60).

The change in droplet mass during evaporation can be described as

$$-\frac{dm_d}{dt} = -\rho_l \frac{dV_d}{dt} = k_{ev} A_{la} \frac{M_l}{R}\left(\frac{P_{sat}}{T_{sat}} - \frac{P_{ba}}{T_{ba}}\right) \tag{2-14}$$

in which P_{sat} is the saturated vapour pressure at 26 °C (the correlated wet bulb temperature of the drying air with temperature 80 °C and relative humidity 0 %) and P_{ba} is the vapour pressure of the drying air, which is taken zero.

The change in droplet volume can be related to the change in height

$$dV_d = 2\pi r_{cd} \frac{h_d}{2} dh_d \tag{2-15}$$

in which r_{cd} is the radius curvature of the droplet

$$r_{cd} = \frac{{h_d}^2 + {l_d}^2}{2h_d} \tag{2-16}$$

The contact area between the sessile droplet and the drying air (A_{la}) is given by

$$A_{la} = \pi\left({h_d}^2 + {l_d}^2\right) \tag{2-17}$$

Finally, the change in droplet height can then be described

$$-\frac{1}{2}\rho_l \pi\left({h_d}^2 + {l_d}^2\right)\frac{dh_d}{dt} = k_{ev}\pi\left({h_d}^2 + {l_d}^2\right)\frac{M_l}{R}\left(\frac{P_s}{T_s} - \frac{P_{ba}}{T_{ba}}\right) \tag{2-18}$$

The equation above can be simplified to

$$-\frac{dh}{dt} = 2\frac{k_{ev}}{\rho_l}\frac{M_l}{R}\left(\frac{P_s}{T_s} - \frac{P_{ba}}{T_{ba}}\right) \tag{2-19}$$

The mass transfer coefficient (k_{ev}) can be obtained by fitting Eq. 2-19 to the experimental data.

Results and discussion

Dispensing process

A pneumatic micro-dispenser was used to produce droplets of a size similar to the droplet size during spray drying. This micro-dispenser was selected as it is able to produce small droplets and at the same time dispense viscous liquids, which is a prerequisite for the dispensing of concentrated liquid foods. The top view of the deposited droplets was visualized with a microscope and subsequently the droplet volume could be calculated assuming a constant contact angle during drying. In Figure 2-4A, the droplet volume is shown as a function of applied dispensing pressure and valve opening time.

Figure 2-4A shows that droplet volume increases with pressure and valve opening time. In practice, the smallest droplet that can be generated has a diameter of 150 μm (~2 nl). This minimum droplet size is influenced by the moving needle valve (in the micro-dispenser) during opening and closing. The predicted droplet volume by a model based on Bernoulli's law (Eq. 2-1) was compared to the experimental results. As shown in Figure 2-4A, the predicted droplet size is in close agreement with the experimental data.

The viscosities of MEG, DEG, and PEG-400 at 30 °C are 13, 21, and 71 mPa.s, respectively. Rheological measurements showed that the fluids exhibit Newtonian behaviour in the range of shear rates applied. Figure 2-4B shows that droplet size decreases with increasing fluid viscosity. Bernoulli's law also includes the effect of viscosity on dispensed droplet size. As shown in Figure 2-4B, the predictions are in good agreement with the experimental data.

Three different sizes of needle tips were used; 27 gauge (0.22 mm), 30 gauge (0.16 mm), and 32 gauge (0.12 mm). As shown in Figure 2-4C, the model is in agreement with the experimental data. From these results, it is concluded that Bernoulli's law can account for the effects of applied pressure, valve opening time, needle tip size, and fluid viscosity on droplet size. Thus, if the liquid viscosity is known and an appropriate needle tip size is chosen, the pressure and valve opening time can be controlled to deposit the required droplet size.

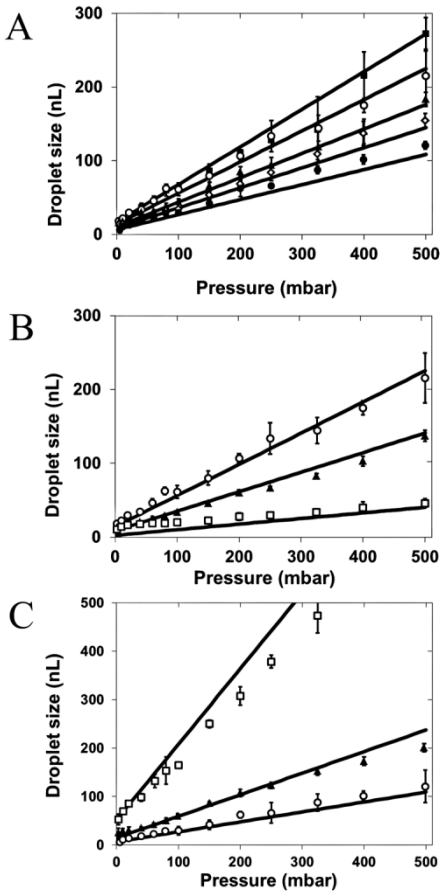

Figure 2-4. A: Effect of dispensing pressure and valve opening time on droplet volume for MEG. The symbols represent the experimental values at valve opening time 200 ms (■), 170 ms (○) 130 ms (▲) 110 ms (◊), and 80 ms (●). The lines represent the values predicted by the model based on Bernoulli's law.

B: Dispensed droplet size of MEG (○), DEG (▲), and PEG-400 (□) at valve opening time = 170 ms. C: Effect of needle tip size; 0.12 mm (○), 0.16 mm (▲), and 0.22 mm (□); on MEG dispensed volume at valve opening time = 80 ms.

Drying process

The evaporation of a single dispensed droplet was investigated as a function of the drying air conditions. The effect of the slip velocity between the droplet and drying air on the drying of a sessile water droplet was investigated here. In Figure 2-5, snapshots of a droplet are shown during the drying process.

Figure 2-5 show that the droplet geometry evolves mainly in height, while the contact area between droplet and the flat surface (base diameter) remains constant. This finding is in agreement with the observations of Hu and Larson (61) who observed that the contact angle of water droplets deposited on a glass surface changed from 40° to a minimum contact angle of 2–4°, while the base diameter remained constant. In the current study similar observations were obtained; the droplet base diameter tends to be constant during drying (Figure 2-5C). It was observed that during the drying experiment with the air slip velocity of 0.17 m/s, the droplet base diameter suddenly changed. Possibly, this was due to an irregularity in the microscopic surface of the membrane. After the sudden change, the droplet base diameter remained constant again with changing contact angle.

The experimental data on the change in height may be compared to Eq. 2-19. A characteristic length is used for the calculations of the Sherwood and Reynolds number. The characteristic length (l_c) is defined as:

$$l_c = \frac{object\ surface\ \ area}{perpendicular\ object\ \ perimeter}$$

For sessile droplets, the characteristic length is

$$l_c = \frac{\pi h_d}{\theta_d} \qquad (2\text{-}20)$$

The mass transfer coefficient (k_{ev}) for a free spherical droplet is calculated using the Sherwood number from the Ranz-Marshall correlation (Eq. 2-9 and 2-10). The mass transfer coefficient is then used to describe the height as a function of the drying time using Eq. 2-19 (Figure 2-6).

Figure 2-6 shows that the height of a free droplet decreases faster than that of a sessile droplet. It is concluded that the drying of the sessile droplet, even when with a high contact

angle (130°), cannot be approximated by directly using the mass transfer coefficient for a free spherical droplet. Therefore, different parameters for the Sherwood correlation were determined for the drying of a sessile droplet by fitting 2-6 to the experimental data.

Vapour-air diffusivity and air viscosity were taken at the wet bulb temperature of 26 °C and assumed constant in the experiments. The Schmidt number is thus constant in this study, i.e. 0.62. Therefore, it was not possible to estimate the power of the Schmidt number.

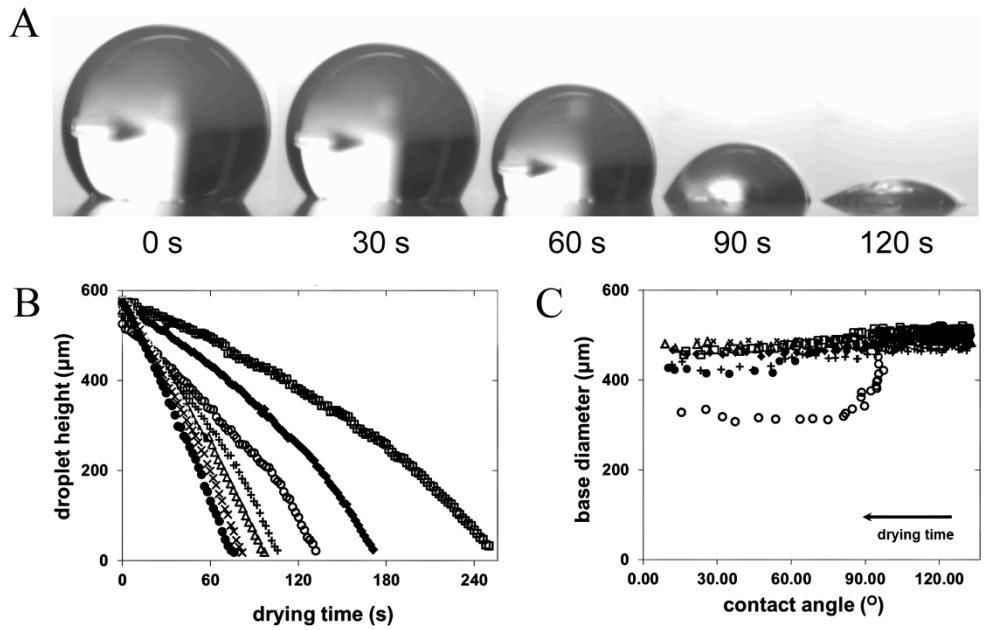

Figure 2-5. A: Snapshots of a shrinking droplet, drying at a constant bulk velocity of drying air 0.30 m/s, T_{air} = 80^{O}C, and RH ~ 0 %. B: Droplet height as a function of drying time at different bulk slip air velocities: 0.04 m/s (□), 0.11 m/s (♦), 0.17 m/s (○), 0.30 m/s (+), 0.38 m/s (Δ), 0.64 m/s (*), 0.98 m/s (●). C: Droplet base diameter as function of the contact angle during the drying process; bulk slip air velocities: 0.04 m/s (□), 0.11 m/s (♦), 0.17 m/s (○), 0.30 m/s (+), 0.38 m/s (Δ), 0.64 m/s (x), 0.98 m/s (●).

The estimated Sherwood correlation are shown in Table 2-1 and compared to the values from literature for several cases. The parameter values for the Sherwood correlation (Eq. 2-6) in this study were obtained by fitting the predictive model (Eq. 2-19) to the experimental height data as shown in Figure 2-6B.

Table 2-1 shows that the estimated parameter values in this study are different compared to those of the flat plate and the falling sphere. Specifically, the parameter value P_1 is found to be in between the two cases. The value of P_1 reflects the limiting Sherwood value where diffusional mass transfer occurs predominantly. The value of P_1 is 2.0 for a spherical object and 0 for a flat object. The sessile droplet changes from a nearly spherical to a flat object, which is reflected in a decreasing contact angle. The value of P_1 (0.24) in this study is only valid for a sessile droplet with an initial contact angle of 130^o that decreases to nearly 0^o. More information about the effect of contact angle on the Sherwood number for the diffusional regime can be found in literature (Baines and James, (58).

It is expected that the P_1 value for drying of a droplet from a suspension will be higher if the droplet will only partially evaporate. Furthermore, to better mimic the drying behaviour of a free falling droplet it is suggested to for example micro-fabricate a ‘hairy’ surface structure that is better able to retain the spherical shape of the drying droplet (i.e. making use of the Lotus effect).

The estimated value of P_2 for this work is 0.62, if it is assumed that P_4 is 1/3 (a common value for the power of the Schmidt number). For a free falling sphere P_2 is found equal to 0.60 and for a flat surface equal to 0.67. The value of the estimated parameter P_3 in this study (0.51) is comparable to the P_3 values in the Sherwood correlations for flow across a flat surface and a falling sphere.

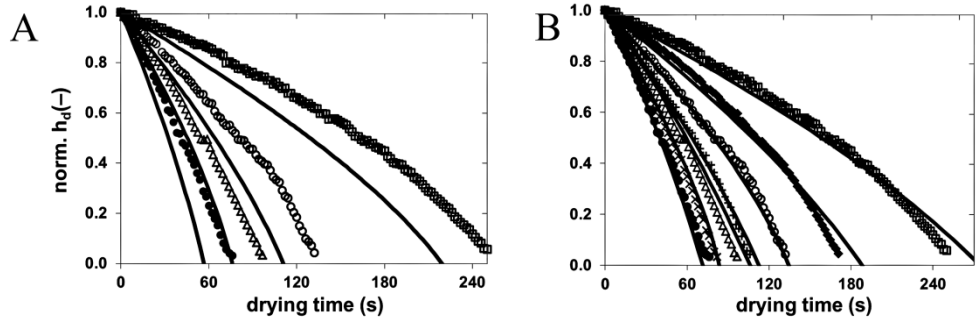

Figure 2-6. Normalized droplet height as a function of the drying time using the estimated Sherwood correlation (solid line) and the drying results at slip air velocity 0.04 m/s (□), 0.11 m/s (♦), 0.17 m/s (○), 0.38 m/s (Δ), and 0.98 m/s (●); the solid line represents the model with (A) Sherwood correlation for free falling sphere (Ranz-Marshall correlation) and (B) proposed Sherwood correlation for sessile droplet (this research).

Table 2-1. Estimated parameter values for the general Sherwood correlation for different cases.

$Sh = P_1 + P_2 Sc^{P4} Re^{P3}$			
P_1	$P_2 Sc^{P4}$	P_3	Case
0.24 ($2.7 \cdot 10^{-2}$)[a]	0.53 ($3.1 \cdot 10^{-2}$)	0.51 ($9.8 \cdot 10^{-3}$)	Sessile droplet, initial contact angle 130° This work, $0.6 \leq Re_d \leq 60$
2.0	0.51	0.50	Free sphere Ranz-Marshall (62)
0	0.56	0.50	Laminar flow across flat plate; Sc > 0.6 (58)

[a] The uncertainty of the parameters at 95 % confidence interval is provided between brackets

Conclusion

The dispensing of liquid droplets was carried out with a pneumatic dispenser and could be controlled accurately by varying applied pressure and valve opening time. A predictive model based on Bernoulli's law was developed and this model was found to predict the dispensed droplet volume as a function of liquid properties and dispensing parameters.

Drying of single sessile water droplets was experimentally monitored with a camera set-up. Drying was assumed to occur at the wet bulb temperature. Experimental data of the shrinking droplets were compared with a predictive model based on mass transfer for a single free falling sphere. It was found that the Sherwood correlation of a free falling sphere did not predict the appropriate mass transfer coefficient for the drying sessile droplet. Therefore, a Sherwood correlation was derived for the drying of sessile water droplets as $Sh = 0.24 + 0.62Re^{0.51}Sc^{1/3}$ for $Sc = 0.62$. This correlation was found almost similar to the Sherwood correlation for flow across a flat surface and a free falling sphere except for the value of P_1. It is expected that this value will increase when drying food suspensions or when a micro-fabricated 'hairy' surface structure is used.

It is planned to further investigate the drying of complex solutions, i.e. food products, which are highly viscous or contain specific heat sensitive ingredients. During drying of these products, the temperature of the product will start deviating from the wet bulb temperature. Furthermore, a challenge will be the subsequent analysis of very small particles. Therefore, it is intended to develop the platform into a high throughput experimentation system to dry multiple droplets at the same time.

Nomenclature

A	Surface area	m^2
c_p	Specific heat capacity at constant pressure	$J.kg^{-1}.K^{-1}$
d	Diameter	m
d_h	Channel diameter	m
D	Diffusion coefficient of water vapour in air	m^2s^{-1}

e_f	Friction loss per unit mass	$N.m.kg^{-1}$
f	Fanning friction factor	–
g	Acceleration gravity constant (9.8)	$m.s^{-2}$
h_c	Convective heat transfer coefficient	$W.m^{-2}K^{-1}$
h_d	Droplet height	m
ΔH_{vap}	Enthalpy of vaporization	$J.kg^{-1}$
K	Thermal conductivity	$W.m^{-1}K^{-1}$
k_{ev}	Convective mass transfer coefficient	$m.s^{-1}$
K	Hagenbach-Couette correction factor for narrow gap contraction	–
K'	Hagenbach-Couette correction factor for narrow gap contraction	–
K_f	Friction loss coefficient	–
l_c	Characteristic length in Sherwood number	m
l_d	Droplet base radius	m
L	Channel length	m
m	Mass	kg
M	Molecular weight	$kg.mol^{-1}$
Nu	Nusselt number	
P	Pressure	Pa
P_1	First parameter in generalized Sherwood correlation	
P_2	Second parameter in generalized Sherwood correlation	

P_3	Third parameter in generalized Sherwood correlation	
P_4	Fourth parameter in generalized Sherwood correlation	
Pr	Prandlt number	–
r_c	Radius curvature	m
R	Gas constant, 8.314	$J.mol^{-1}K^{-1}$
Re	Reynolds number	–
Sc	Schmidt number	–
Sh	Sherwood number	–
t	Time	s
T	Temperature	°C or K
U	Overall heat transfer coefficient	$W.m^{-2}K^{-1}$
v	Velocity	$m.s^{-1}$
V	Volume	m^3
w	Shaft work in micro-dispenser per unit mass	$N.m.kg^{-1}$
x	Length coordinate	m
z	Height coordinate	m

Greek letters:

α	Kinetic energy correction factor	–
Δ	Difference	–
μ	Dynamic viscosity	$kg.m^{-1}.s^{-1}$

π	Pi value; 3.14	
θ	Contact angle	rad
ρ	Density	$kg.m^{-3}$

Subscripts:

A	Air
ba	Bulk air
C	Dispensing needle channel
conv	Convection
cond	Conduction
D	Droplet
dis	Dispensing
i	In
l	Liquid, i.e. Water
o	Out
p	Particle
s	Solid
sat	Saturated

Chapter 3

Measuring and modelling of diffusivities in carbohydrate-rich matrices during thin film drying

Submitted for publication:

J. Perdana, R.G.M. van der Sman, M.B. Fox, R.M. Boom, and M.A.I. Schutyser. Measuring and modelling of diffusivities in carbohydrate-rich matrices during thin film drying.

Abstract

Knowledge about moisture diffusivity in solid matrices is a key for understanding drying behaviour of for example probiotic or enzymatic formulations. This paper presents an experimental procedure to determine moisture diffusivity on the basis of thin film drying and gravimetric analysis in a Dynamic Vapour Sorption (DVS) system. The extraction of moisture diffusivity is based on the "regular regime approach". The method was explored and verified for its assumptions. It provided insight in the effect of moisture content and temperature on moisture diffusivity. Moreover, it was found that moisture diffusivity in different carbohydrate systems was similar and decreased with moisture content. The latter was explained by similar molecular interactions in carbohydrate systems and formation of a percolating network at low moisture content that affects water mobility. Subsequently, measured moisture diffusivities were compared to model predictions based on first principles. It was found that predicted moisture diffusivities were in fair agreement with these, including the effect of moisture content and temperature on moisture diffusivity. At low moisture content the model overestimated the sensitivity of moisture diffusivity towards temperature. This was explained by the fact that the different water-solid interactions at lower moisture content (including relaxation behaviour in the glassy state) are not considered in the modelling. Finally, the methodology was successfully evaluated to other solid matrices such as glycerol, skimmed milk and casein, providing different moisture diffusivities as function of moisture content.

Keywords: moisture diffusion, thin film drying, modelling, regular regime, carbohydrate, ternary matrix

Introduction

Spray drying is frequently applied to encapsulate active ingredients for example in chemical, food, and pharmaceutical products (63-67). During spray drying, internal moisture gradients develop within drying particles due to diffusion limitation. In combination with temperature this is found critical to retention of biological activity of ingredients (68-70). Understanding and predictive modelling of diffusion-limited drying requires full description of diffusivity as a function of moisture contents and temperature. Unfortunately, these diffusivities and their relation on moisture and temperature are only available for homogeneous matrices, while for more complex mixtures, e.g. food matrices, these are rarely available. Current experimental methods for measuring diffusivities often require highly specialized equipment, such as the use of nuclear magnetic resonance spectroscopy (71, 72) or fluorescence photo-bleaching methods (73, 74) or are complicated and time consuming, especially when the diffusivity is dependent on both temperature and moisture content, which is usually case.

In this paper we present an efficient procedure to more rapidly determine diffusivities on the basis of thin film drying and gravimetric analysis in a Dynamic Vapour Sorption (DVS) system. The new procedure is demonstrated by measurements on drying of aqueous suspensions of different carbohydrates and their mixtures, which are frequently applied to formulate active ingredients (5, 75, 76). The method was evaluated for its potential to provide diffusivities for amorphous systems. The moisture diffusivities as a function of moisture content and temperature were extracted from the experimental data by adopting the more commonly applied regular regime approach (77-79).

To predict moisture diffusivity in complex solid matrices for a wide range of temperature and moisture content a semi-mechanistic modelling approach was developed as well (80). The approach was based on 1) the Darken relation for the mutual diffusivity, which has the advantage that it can be expanded to multicomponent systems, 2) the generalized Stokes-Einstein relation to describe the solute self-diffusivity, and 3) the free volume theory, which describes the solvent self-diffusivity. Following this approach, moisture diffusivity can be described according to the physical properties and thermodynamics of the system.

Predicted diffusivities were compared to the experimental results from thin film drying and the gravimetric analysis in the DVS system. The latter provided insight on the accuracy of

the prediction of the diffusivity by the semi-mechanistic model and indicated possibilities to generalize diffusivities in complex matrices.

Materials and methods

Materials

Alginic acid sodium salt (sodium alginate) powder (Sigma-Aldrich, USA), sucrose (Sigma-Aldrich, USA), Lactose (Sigma-Aldrich, USA), trehalose (Sigma-Aldrich, USA), and casein (Sigma-Aldrich, USA) were analytical grade and used as received. Maltodextrin DE 4-8 (Glucidex 6, Roquette, France), and technical agar (Sigma-Aldrich, USA) were used as received.

Thin film drying experiments in a Dynamic Vapour Sorption Analyser (DVS)

Thin films were prepared by dissolving 20 % $^{w}/_{w}$ of the selected solid substrates in Milli-Q water. For preparation of a consistent film, 1.5 % $^{w}/_{w}$ agar was added. It is noted that the addition of this agar has negligible effect on the diffusivity of water in the film (78, 81). To ensure that all ingredients were dissolved, the mixture was boiled in a microwave oven for 60 s. Subsequently, the mixture was casted in a mould (to prepare a film of 8 x 8 mm with a thickness of 1 mm) and slowly cooled down to solidify at room temperature.

The thin film drying experiments were performed in a Dynamic Vapour Sorption (DVS) Elevated Temperature (Surface Measurement System, England). The relative humidity of the drying air was set to 0.0 % and the air flow applied was 50 ml/s. Each drying experiment was carried out in three subsequent steps:

1. The thin film was first (nearly completed) dried at a desired temperature for 24 h.
2. The drying air temperature was raised to remove all the remaining water during a next period of 24 h.
3. Finally, the drying air was readjusted to the originally selected temperature in the first step.

During the first drying step the mass of the thin film was recorded each 2 s during the first 6 h, and after that the mass was recorded only every 10 s. The temperature in the second step was selected to be slightly higher than the glass transition of the solid substrate as

summarized in Table 3-1. The second step is important to "completely" remove the remaining water from the sample without significantly degrading the materials, which ensures measurement of the dry matter in the sample. Accurate measurement of the dry matter is required for proper estimation of the mutual diffusion coefficient of water at small water contents. After the second step, the air temperature was set to the value used at the first step to obtain the final dry matter mass of the sample, because the mass balance of the DVS was originally calibrated at this temperature.

Table 3-1. The selected temperatures for the second step involving high temperature drying to remove all water and measure the dry matter mass of the thin film.

Component	T_g (°C)	Reference	T for high temperature drying (°C)
Casein	206	(82)	200
Lactose	110	(83)	130
Sucrose	60	(84)	105
Trehalose	107	(84)	120
Maltodextrin DE 6	190	(30)	200
Sodium Alginate	95	(85)	120
Glycerol	-93	(86)	70
Skim milk	NA		200

X-ray diffraction for assessing the degree of crystallinity of the solid matrix

X-ray diffraction spectroscopy (XRD) was conducted with a PANalytical Expert Pro System (The Netherlands) by using nickel-filtered CuKα radiation (tube operating at 40 kV and 40 mA). The data were collected using an automated divergence slit (5 mm irradiated length) and a 0.5 mm receiving slit. Data were collected by step counting at 0.02° intervals for 2 seconds per data point.

The amorphous samples used as reference were obtained by spray drying 0.2 % $^{w}/_{w}$ samples diluted in Milli-Q water (Millipore, USA) in Buchi 190 mini spray dryer (Buchi Labotechnik, Switzerland) at an inlet air temperature of 120 °C and an outlet air temperature of 85 °C.

The degree of crystallinity was determined using external standard method (87). The volume fraction of the crystalline phase in the mixture was calculated from the measured integrated intensities of diffraction peaks produced by the samples compared to the amorphous samples

$$W_i = 1 - \frac{I_i}{I_a} \tag{3-1}$$

where W_i is the weight fraction of the crystalline phase, I_i is the integrated intensity of the samples and I_a is the integrated intensity of the reference phase (amorphous sample).

Extraction of mutual diffusivities of water from thin film drying experiments

The mutual diffusion coefficient of water in various water-solid mixtures predicted using Darken relation was validated using the results from experiments. The mutual diffusion coefficients from experimental data were determined on the basis of thin film drying and gravimetric analysis. The regular regime approach (77) was adopted to extract moisture diffusivity values as a function of moisture content and temperature.

Theory behind the regular regime approach for a drying slab

The generalized concentration-dependent diffusion equation for a shrinking slab is (88, 89):

$$\frac{\partial u}{\partial t} = \frac{\partial}{\partial z}\left[D {c_s}^2 \frac{\partial u}{\partial z}\right] \tag{3-2}$$

with t is time, D the mutual diffusion coefficient, c_s the mass concentration of the non-diffusing reference component (solids) and u the mass concentration of water on the mass basis of dry matter (c_w/c_s), and z the reference component mass-centered coordinate:

$$z = c_s \cdot r \tag{3-3}$$

with r is the absolute distance coordinate.

To solve the diffusion equation, the following dimensionless variables were introduced (77, 88):

$$\zeta = \frac{z}{Z} \tag{3-4}$$

$$\tau = \frac{D_0 c_{s,0}^2 t}{\rho_s^2 Z_s^2} \tag{3-5}$$

$$D_r = \frac{D c_s^2}{D_0 c_{s,0}^2} \tag{3-6}$$

with ζ is the reduced distance coordinate which corresponds to fractional increments in the reference component mass, τ the dimensionless time, ρ_s the density of the solid components, Z_s the slab thickness at u = 0, $c_{s,0}$ the reference mass concentration of the solids and D_0 the value of the diffusion coefficient at $c_{s,0}$, which is introduced to calculate a dimensionless reduced diffusion coefficient (D_r). The reduced diffusion coefficient is used to describe diffusion in a component-mass centered coordinate system. Substitution of the dimensionless variables in the diffusion equation returns a dimensionless "Fickian" diffusion model (77):

$$\frac{\partial u}{\partial \tau} = \frac{\partial}{\partial \zeta}\left(D_r \frac{\partial u}{\partial \zeta}\right) \tag{3-7}$$

With initial and boundary conditions:

$$u = u_0 \quad \text{for } \tau = 0 \text{ and } 0 \leq \zeta \leq 1 \tag{3-8}$$

$$u = u_{ss} \quad \text{for } \tau = \tau \text{ and } \zeta = 1 \tag{3-9}$$

$$\frac{\partial u}{\partial \zeta} = 0 \quad \text{for } \tau = \tau \text{ and } \zeta = 0 \tag{3-10}$$

In most cases, the diffusion equation above (Eq. 3-2) can only be resolved numerically by implementing the initial and boundary conditions (Eq. 3-8 to 3-10). Its solution can be divided into two regions, i) a penetration period and ii) a regular regime period. Schoeber (77) developed an approach to determine moisture diffusivity by exploiting a unique feature of the regular regime period. In the regular regime the desorption rate (dimensionless flux parameter F) can be assumed independent of the initial concentration of water in the slab (u). For desorption in a slab, the value of the dimensionless flux parameter (F) is calculated as

$$F = -(\rho_s Z_s)^2 \frac{d\bar{u}}{dt} \tag{3-11}$$

with

$$\bar{\boldsymbol{u}} = \frac{(\boldsymbol{m}-\boldsymbol{m_s})}{\boldsymbol{m_s}} \qquad \text{and} \qquad \frac{\boldsymbol{d\bar{u}}}{\boldsymbol{dt}} = \frac{\boldsymbol{d}[(\boldsymbol{m}-\boldsymbol{m_s})/\boldsymbol{m_s}]}{\boldsymbol{dt}} = \frac{\boldsymbol{1}}{\boldsymbol{m_s}}\frac{\boldsymbol{dm}}{\boldsymbol{dt}} \tag{3-12}$$

where m is the total mass of the sample at time t and m_s the solute mass.

Subsequently, the approach introduces a Sherwood number representing the mass transfer at the interface for the dispersed phase ($Sh = 2kL/D$) on the basis that the moisture concentration profile remains geometrically the same during the regular regime:

$$\overline{Sh_d} = \frac{2F/(\bar{u}-u_{ss})}{\overline{D_r}} \tag{3-13}$$

with $\overline{Sh_d}$ the Sherwood number for dispersed phase in relation to the average mass concentration of water $\bar{u}$, u_{ss} the mass concentration near the surface and $\overline{D_r}$ is the average value of the reduced diffusion coefficient. During the regular regime, when boundary values are fixed, the $\overline{Sh_d}$ can be assumed constant (for a slab $\overline{Sh_d}$ is $\pi^2/2$) (88). Thus,

$$F = \overline{D_r}(\bar{u} - u_{ss})\,\pi^2/4 \tag{3-14}$$

Next, a power law relationship is assumed between the diffusion coefficient and the moisture content:

$$D_r = u^a \tag{3-15}$$

with *a* is the power parameter to describe the reduced diffusion coefficient dependency on moisture content. This power law relationship allows for analytical solution of the inverse problem, i.e. enable the extraction of the diffusivity values. A more complex relation based on free-volume theory may be used but the extraction of the diffusivity values becomes very challenging. The reduced diffusion coefficient across the slab can be approximated as:

$$\int_{u_{ss}}^{\bar{u}} D_r du = \int_{u_{ss}}^{\bar{u}} u^a du \tag{3-16}$$

and thus the average value can be approximated as

$$\overline{D_r} = \frac{1}{\bar{u}-u_{ss}} \int_{u_{ss}}^{\bar{u}} u^a du \tag{3-17}$$

which leads to

$$\overline{D_r} = \frac{1}{\bar{u}-u_{ss}} \frac{1}{a+1} \bar{u}^{(a+1)} \tag{3-18}$$

Substituting Eq. 3-18 into Eq. 3-13 results in

$$\bar{u}^a = \frac{2F(a+1)/\overline{Sh_d}}{\bar{u}} \tag{3-19}$$

On the basis of Eq. 3-16, for u = $\bar{u}$, D_r can be estimated by differentiating Eq. 3-19

$$D_r = \frac{d(2F(a+1)/\overline{Sh_d})}{d\bar{u}} \tag{3-20}$$

Liou and Bruin (88) suggested to use $\overline{Sh_d}$ as a function of a (and thus indirectly to moisture content in contrast to the previous assumption). $\overline{Sh_d}$ was found linearly correlated to $a/(a+2)$:

$$\overline{Sh_{d,a}} = \frac{\pi^2}{2} + \frac{4}{\pi^2}\left(\frac{a}{a+2}\right) \tag{3-21}$$

with $\overline{Sh_{d,a}}$ is the Sherwood number for the dispersed phase as a function of the power law parameter a.

Following the relation in Eq. 3-6, the value of $D_0 c_{s,0}^2$ can be chosen arbitrarily. A value of 1 kg^2/m^{4}s is suggested so that D_r is numerically equal to Dc_s^2 (77). Thus,

$$D = D_r / c_s^2 \tag{3-22}$$

Taking into account the moisture content profile (u) across the slab, the moisture dependent diffusivity (D) can be reversely extracted from the measured sample mass data obtained during drying (77, 90):

$$D = c_s^{-2}\left(\frac{d\left(2F(a+1)/\overline{Sh_{d,a}}\right)}{d\bar{u}}\right) \tag{3-23}$$

When substituting F from Eq. 3-14 and $\overline{Sh_{d,a}}$ from Eq. 3-21 into Eq. 3-23 one obtains:

$$D = c_s^{-2}\left[\frac{d\left(2D_{r,\bar{u}}(\bar{u}-u_{ss})\frac{\pi^2}{4}(a+1)/\overline{Sh_{d,a}}\right)}{d\bar{u}}\right] \tag{3-24}$$

Subsequently this can be rearranged into the following equation:

$$D|_{u=\bar{u}} = c_s^{-2}\left[\frac{(a+1)\pi^2 D_{r,\bar{u}}}{2\overline{Sh_{d,a}}}\right] \tag{3-25}$$

Yamamoto (91) proposed to explicitly make power parameter a dependent on $\bar{u}$ to more accurately describe D(u) over a wide range of moisture contents. The value of D at a specific moisture content is approximated by estimating the value of a over a small interval of $\bar{u}$

$$a = \frac{\ln(D_{r,i}/D_{r,i+1})}{\ln(\bar{u}_i/\bar{u}_{i+1})} \tag{3-26}$$

with $\bar{u}_i > \bar{u}_{i+1}$.

Procedure to extract moisture diffusivities from the drying curve

The overall procedure for extraction of moisture diffusivity is schematically depicted in Figure 3-1. The procedure is started by determining the reduced moisture diffusion coefficient (D_r) for the component mass-centered coordinate system (Eq. 3-20). The value of F is calculated according to Eq. 3-11. For accuracy reasons, $d\bar{u}/dt$ is calculated for different time intervals; for small $d\bar{u}/dt$ values, longer time interval to calculate $d\bar{u}/dt$ are required.

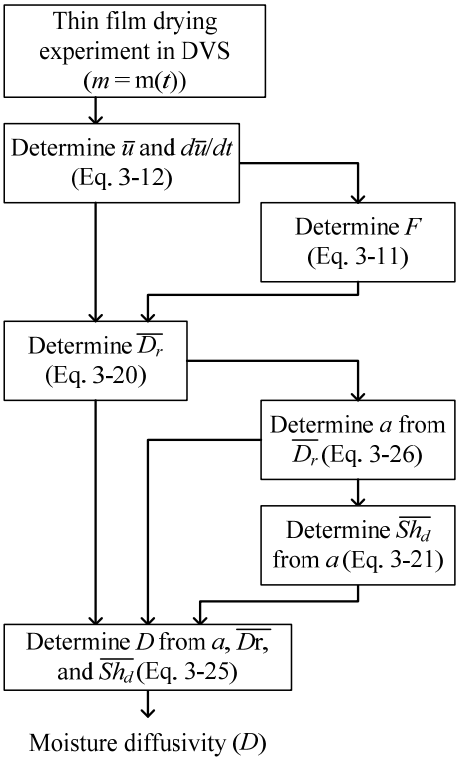

Figure 3-1. Procedure to extract the moisture diffusivity (D) from gravimetric data based on the regular regime method

From the reduced diffusion coefficient (D_r), the mutual diffusion coefficient D is determined using Eq. 3-25 with the Sherwood number of the dispersed phase $Sh_{d,a}$ and the moisture-dependent diffusion power parameter a (using Eq. 3-21 and Eq. 3-26, respectively).

For multicomponent systems, the composition of for example the two solids does not change during the experiment. Therefore, the mixture of the solid components was merged into a single density (d_s) and an overall solids concentration (c_s). For carbohydrate polymers, it can be further assumed that the density is constant and not dependent on molecular weight (30). We fixed the density for our systems to 1550 kg/m^3.

Modelling the mutual diffusion coefficient of water in binary systems

A semi-mechanistic model was used to predict the mutual diffusion coefficient, in which we used the approach by van der Sman and Meinders (80). The generalized Darken relation was used to describe the mutual diffusion coefficient of a binary *i*-*j* component system in a multicomponent mixture (92, 93)

$$D_{i,j} = \left(x_j D_{i,self} + x_i D_{j,self}\right) Q \tag{3-27}$$

where $D_{i,j}$ are the mutual diffusivity of component *i* in *i*-*j* system, *x* is the mole fraction, $D_{i,self}$ and $D_{j,self}$ are the self-diffusivities of components *i* and *j*, respectively, and Q is the thermodynamic factor.

Following a more commonly approach applied to polymer melts, it is proposed to use a volume fraction of polymer (ϕ) instead of a molar fraction (x) for food polymer systems. Therefore, Eq. 3-27 can be written as

$$D_{i,j} = \left(\phi_j D_{i,self} + \phi_i D_{j,self}\right) Q \tag{3-28}$$

The thermodynamic factor Q for polymer *j* in solvent *i* can be written following the Flory-Huggins free energy function as

$$Q = 1 - 2\chi\phi_j\left(1 - \phi_j\right) \tag{3-29}$$

where χ is Flory-Huggins interaction parameter.

For a water-carbohydrate mixture, the self-diffusion coefficient for water molecules is predicted using the free volume theory based on the work of Vrentas and Duda (94)

$$D_{w,self} = D_0 exp\left(-\frac{E}{RT}\right) exp\left[\frac{-(m_w\tilde{V}_w^* + m_s\xi\tilde{V}_s^*)}{m_w\left(\frac{K_{1w}}{\gamma}\right)(K_{2w} - T_{g,w} + T) + m_s\left(\frac{K_{1s}}{\gamma}\right)(K_{2s} - T_{g,s} + T)}\right] \quad (3\text{-}30)$$

with D_0 is the pre-exponential factor, E the energy to overcome the attractive forces from neighbouring molecules, R the gas constant, T the temperature, $\tilde{V}^*$ the specific critical free volume, ξ the ratio of solvent and polymer jumping units, K_{1w}, K_{2w}, K_{1s}, K_{2s} the free volume parameters, T_g the glass transition temperature, and γ the overlap factor for shared free volume (between 0.5 and 1). By equating the diffusion coefficient for pure water (95, 96) and using the Vrentas-Duda theory for self-diffusivity of water for pure water ($m_w = 1$), the value of D_0 and E can be determined (Table 3-2).

Table 3-2. Vrentas-Duda diffusion parameter values for pure water

Parameter	Value	The uncertainty of the parameter	
		Value	%
D_0 (m^2/s)	$1.48 \cdot 10^{-7}$	$2.38 \cdot 10^{-8}$	16.1
E (kJ/mol)	2.34	0.42	17.9

Based on molecular dynamics simulations, Limbach and Ubbink (97) showed that the self-diffusion coefficient of water in carbohydrate polymer systems is independent to the degree of polymerisation and therefore the free volume parameters for water in sucrose (Table 3-3) are applied to predict the self-diffusion coefficient of water in various carbohydrate polymers.

The self-diffusivity of a carbohydrate molecule s in a water-carbohydrate mixture is described using the Stokes-Einstein relation (98)

$$D_{s,self} = \frac{k_B T}{6\pi r_H \mu_{eff}} \quad (3\text{-}31)$$

with k_B is Boltzmann constant, T is temperature, r_H is the hydrodynamic radius of the molecules, and μ_{eff} is the effective viscosity. The hydrodynamic radius (r_H) is calculated from the degree of polymerization of a carbohydrate polymer applying the Mark-Houwink correlation (99)

$$r_H = \frac{a_u}{DP^{-0.49}} \quad (3\text{-}32)$$

with *DP* is the degree of polymerization of carbohydrate and a_u is the hard sphere radius of a monomeric subunit:

$$a_u = \left(\frac{M_U}{4/3\pi N_S \rho_S}\right)^{1/3} \quad (3\text{-}33)$$

with M_U is the molecular weight of the monomer, N_s is the degree of polymerisation of the carbohydrate polymer.

Table 3-3. Free volume parameters for water and sucrose[a]

Free volume parameters	Water	Sucrose
V^* (L/kg)	0.91	0.59
T_g (K)	136	347
ξ (-)	-	0.79
K_1/γ (L/kg·K)	1.945	0.336
K_2 (K)	-19.73	69.21

[a] The data is taken from van der Sman and Meinders (80)

The effective viscosities of the mixtures are calculated by a correlation proposed by Soesanto and William (26):

$$\mu_{eff} = 2.2414 \cdot 10^{-5} \cdot 10^{247.8/(T-140)} \cdot exp(-k(1-x_w)v_s) \quad (3\text{-}34)$$

with k is a constant given for carbohydrate solution is 282 mol/L (26), x_w is the mole fraction of water and v_s is the molar volume of the solid.

Results and discussion

Drying curves from the thin film drying

The mass decrease of thin films could be accurately monitored during drying experiments using the Dynamic Vapour Sorption (DVS) analyser. The decrease in the mass of the films was rapid in the beginning of the drying and became less with time. After 24 h of drying, the film was subjected to a high temperature drying period to remove the remaining water.

In this step, the mass of the sample decreased significantly in the beginning of the step, because: 1) remaining water was rapidly removed at this high temperature and 2) the DVS balance was not-calibrated for this high temperature. Therefore, readjusting the temperature to the original setting (third step drying) is necessary to obtain the right mass reading; as shown in Figure 3-2 the mass of the sample increased again before it equilibrated to a constant value and provided the appropriate reading for the final mass of the "complete" dry sample.

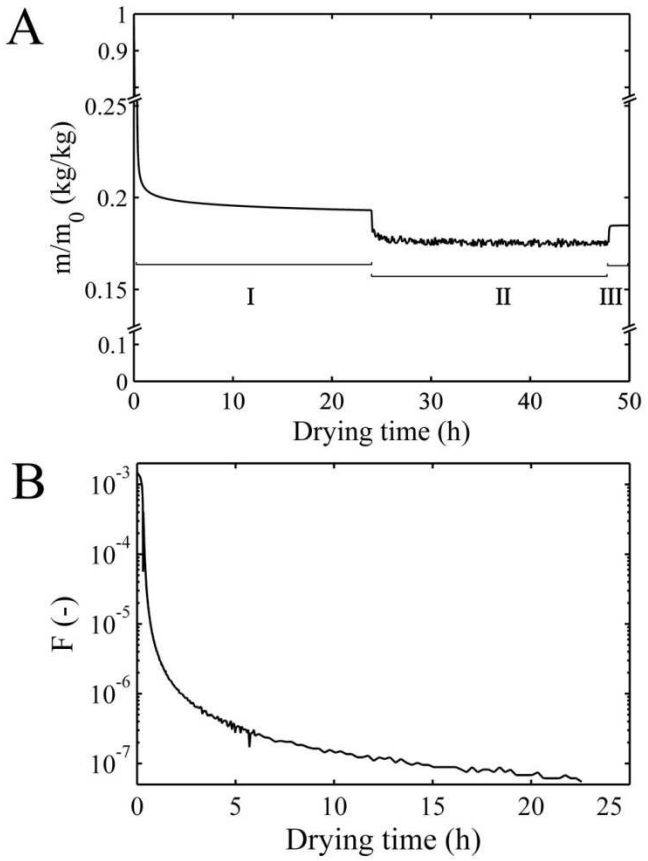

Figure 3-2. A: The normalised mass of a thin film consisting of a trehalose-water mixture as a function of time dried at an air temperature of 70 °C, showing the three drying steps applied. B: The rate of mass decrease as a function of time.

The main advantage of using the DVS analyser to monitor the drying curve is the high accuracy and stability of its mass balance. Additionally, mass readings can be recorded with a small time interval (order of magnitude: seconds), which is especially relevant at the beginning of the drying. This acquisition procedure allowed direct estimation of *dm*/*dt* without the need for regression.

Verification of the regular regime method on assumptions

Advantages of carrying out the measurements and determining the diffusion coefficient in the regular regime is that it can be assumed that: 1) the effect of the external mass transfer (in this case, between the sample and the drying air) is negligible and 2) the drying rate is not dependent on the initial water content (77, 78). We evaluated these assumptions by determining the moisture diffusivity using three different air flow rates. It was found that although different air flow rates were applied, identical values of moisture diffusivity were obtained (Figure 3-3A). It was also observed that equal moisture diffusivities were obtained for thin films with different initial water contents, although above 60-65 % $^{w}/_{w}$ a small deviation can be observed, which indicates that the initial drying is not in the regular regime (Figure 3-3B).

Crystallization of components in the thin film during the drying procedure can lead to an erroneous estimation of the mutual diffusion coefficient of water. During crystallization, water is excluded from growing crystals, which leads locally to a higher water concentration. It is advisable to check the degree of crystallinity of the thin films after drying; an amorphous structure is a prerequisite for accurate diffusivity estimation. For example, for experiments with lactose a high degree of crystallinity in the thin film was observed (Figure 3-4A, Table 3-4) and, additionally, the mutual diffusivity of water in the lactose-water system showed completely different behaviour compared to those of other carbohydrates (Figure 3-3C).

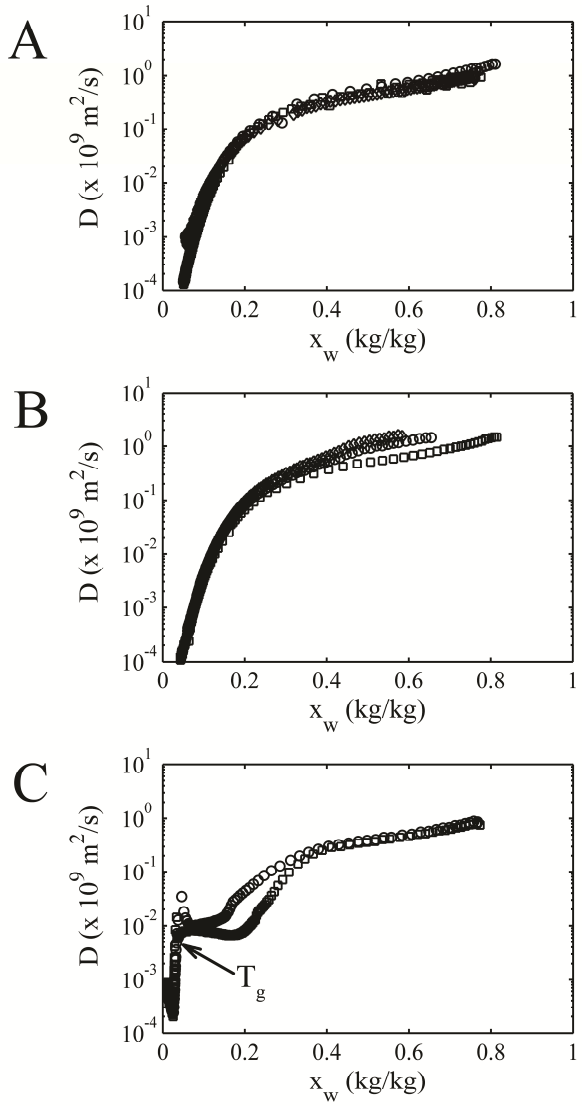

Figure 3-3. A: Moisture diffusion coefficient in sucrose at 70 °C determined at air flow rates of 10 (○), 50 (□), and 200 ml/min (◊). B: Moisture diffusion coefficient of sucrose at 70 °C determined at an air flow rate of 50 ml/min with varying initial water contents of 80 (□), 70 (○), and 60 % $^{w}/_{w}$ (◊). C: Moisture diffusion coefficient in water-lactose mixture (in duplicate). The T_g value shown was corrected with the crystal concentration.

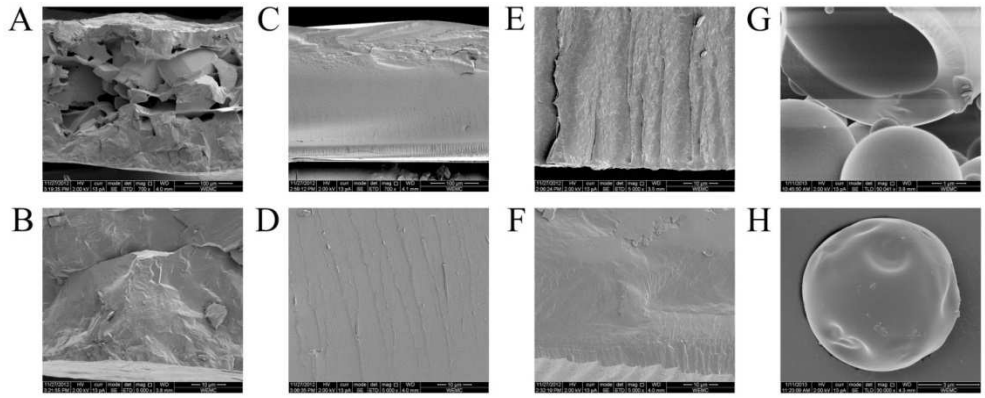

Figure 3-4. Cross sectional scanning electron microscope (SEM) images of a dried thin film sample of lactose at 700x magnification (A), lactose at 5000x magnification (B), trehalose at 700x magnification (C), trehalose at 5000x magnification (D), maltodextrin DE 6 at 5000x magnification (D), sucrose at 5000x magnification (F). SEM images of spray dried lactose particles at 50000x magnification (G), and maltodextrin DE 6 particles at 50000x magnification (H).

Table 3-4. Degree of crystallinity of thin films after drying at specific air temperature as determined using X-ray diffraction measurement

Thin film sample	Drying temperature (°C)	Crystallinity (%)
Trehalose	25	0
Trehalose	70	0
Lactose	25	70
Lactose	70	73
Sucrose	25	2
Sucrose	70	1
Maltodextrin DE 6	25	0

Mutual diffusion coefficients in binary carbohydrate systems

The mutual diffusivities of water in various binary systems were determined experimentally following the regular regime method. Generally, the moisture diffusivity decreases with decreasing moisture content, which becomes more pronounced at lower moisture content (Figure 3-5). These results were compared to the predicted moisture diffusivity of sucrose based on the Darken diffusion equation (Figure 3-5). The moisture diffusivity in various carbohydrate polymers is found in agreement with the predicted moisture diffusivity in sucrose. This indicates that the moisture diffusivity in the studied carbohydrate systems is mainly determined by local interactions between water molecules and individual hydroxyl groups of the polymer rather than the polymer as a whole (80). Slight difference between the prediction and the data of the moisture diffusivity was observed for the sodium alginate sample, especially because the model needs to be adjusted for gels (80). At moisture contents above 65 % $^{w}/_{w}$, the predicted diffusivities are not in full agreement with the moisture diffusivity determined from the drying experiments. This may be due to the fact that the drying did not yet reach the regular regime as discussed in the previous section.

As shown in Figure 3-6, the moisture diffusivity increases with increasing moisture content and temperature. At low moisture contents, especially in the glassy region, it can be observed that the moisture diffusivity is very sensitive towards small changes in moisture content. Reasonable agreement is obtained between the predicted and experimentally determined moisture diffusivities of water in the water-trehalose system at different temperatures, while the agreement for the water-maltodextrin system is less.

At moisture content lower than 0.2, the moisture diffusivity becomes less sensitive towards temperature, which is not well predicted by the model (Figure 3-6). Thus, the diffusion coefficient for maltodextrin is less temperature dependent than for trehalose at low moisture content. The observations are in-line with previous studies and were explained by decoupling of moisture diffusion and viscosity (100). This decoupling behaviour can be further explained by the change in relaxation times of the carrier network when going from rubbery to glassy state. In a rubbery system, relaxation is faster than the rate of diffusion of the penetrant (solvent). In the glassy region, relaxation rates are small due to time-dependent structural rearrangements (e.g. swelling to allow penetration) (101, 102).

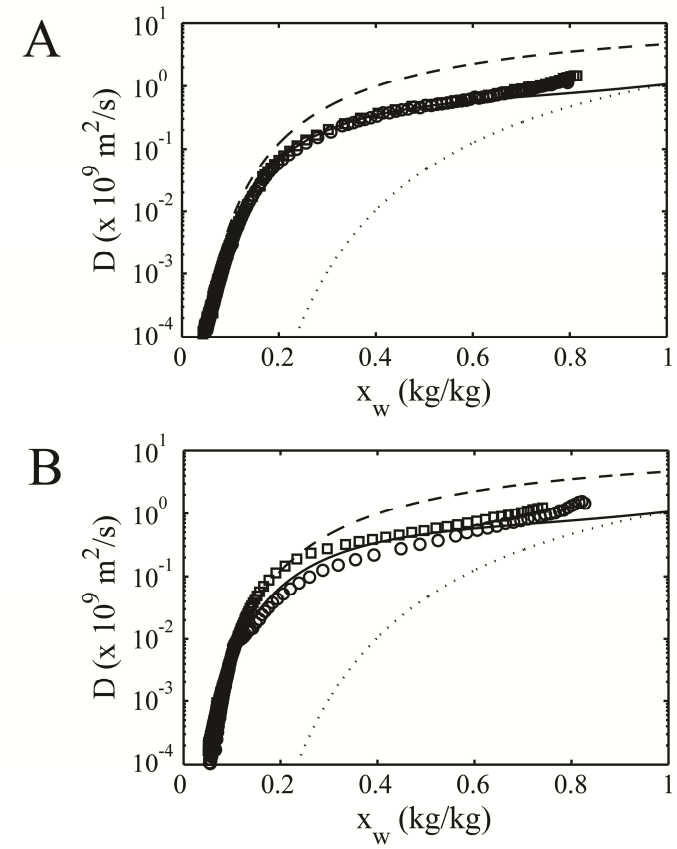

Figure 3-5. A: Mutual diffusion coefficients of water in a water-trehalose mixture (□) and in a water-sucrose mixture (○). B: Mutual diffusion coefficients of water in a water-sodium alginate mixture (□) and in a water-maltodextrin mixture (○).The symbols represent the mutual diffusivity of water determined using the regular regime method from drying experiments. The lines represent the predicted value based on the thermodynamic data of the water-sucrose mixture for the mutual diffusion coefficient of water (solid lines), the self-diffusion coefficient of water in sucrose (dashed lines), and the self-diffusion coefficient of the sucrose in water (dotted lines). The initial moisture content of the thin film was 80 % $^{w}/_{w}$.

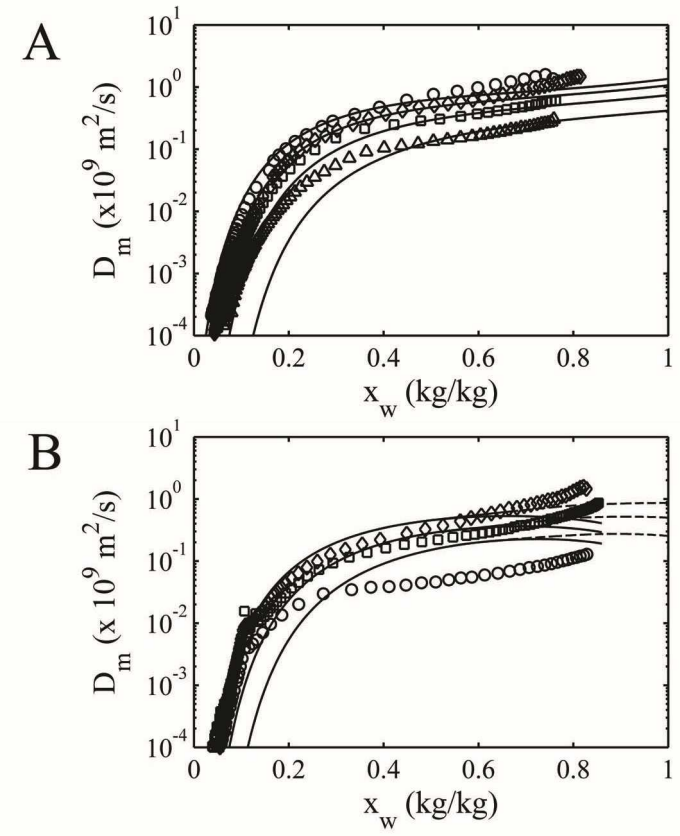

Figure 3-6. A: Mutual diffusion coefficients of water in a water-trehalose mixture at 25 (Δ), 50 (□), 70 (◊), and 85 °C (○). B: Mutual diffusion coefficients of water in water-maltodextrin mixture at 25 (○), 50 (□), and 70 °C (◊). The symbols represent the diffusivity data extracted from drying experiments and the solid lines represent the predicted diffusivities.

Relaxation can be categorized into α-relaxation (slow hierarchically constrained motions of the surrounding molecules) being virtually absent in glassy state (28, 80), while β-relaxation (associated to small angle rotational dynamics of the molecules) allows diffusion in the glassy state (27, 103). The temperature dependency of β-relaxation is lower in the

glassy region than in the rubbery region (104), which explains the limited sensitivity of the diffusion coefficient on temperature at low moisture contents (Figure 3-6).

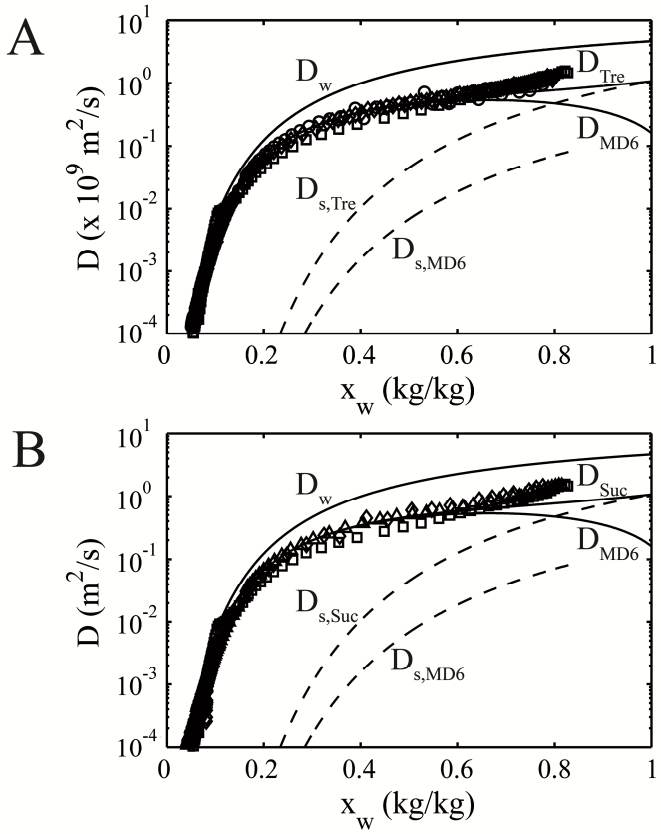

Figure 3-7. A: The mutual diffusivity of water in a ternary system of trehalose-maltodextrin-water (○) compared to in binary systems of trehalose-water (◊) and maltodextrin-water (□). B: The mutual diffusivity of water in a ternary system of sucrose-maltodextrin-water (Δ) compared to that in binary systems of sucrose-water (◊) and maltodextrin-water (□). Solid lines represent the predicted mutual diffusion coefficient of water in trehalose (Tre) or sucrose (Suc) or in maltodextrin (MD6). Solid lines represent self-diffusion coefficient of water (water). Dashed lines with text captions represent the self-diffusion of trehalose (Tre), or sucrose (Suc), or maltodextrin (MD6).

Mutual diffusion coefficients in ternary carbohydrate systems

For specific applications a mixture of solids can be preferred as the matrix. This is for example common practice in drying of probiotics (15, 105). Therefore, it is very useful to estimate mutual diffusion coefficients in ternary matrices. The mutual diffusion coefficients of water in ternary component systems were determined using the same approach. Despite the differences between the carbohydrate systems, it was found that the mutual diffusion coefficients of water were similar for both sucrose-maltodextrin-water and trehalose-maltodextrin-water systems (Figure 3-7).

The self-diffusivities of maltodextrin in water and disaccharides in water are very low compared to the self-diffusivities of water in either maltodextrin or disaccharides, counting for only $5 \cdot 10^{-3}$ and 0.2 times at moisture content of 0.6. Thus, the mutual diffusivity is determined mostly by the mobility of water molecules in the system, while the mobility of the solids (carbohydrates) can be considered negligible (106, 107). In concentrated regimes (x_w<0.5) both maltodextrin and disaccharides form a percolating network with viscoelastic properties via hydrogen bonding (108). This explains the mobility decrease of the carbohydrate molecules with decreasing moisture content (Figure 3-7). Furthermore, carbohydrates are generally build up from similar repeating monomers (e.g. glucose) which provides an analogous architecture of the percolating network (80). Therefore, it may be expected that the mobility of water and thus moisture diffusivity will not be very much affected by the type or composition of carbohydrates in the system (80).

Outlook on different applications of the methodology

Thin film drying in the DVS system combined with the regular regime method was successfully used to determine moisture diffusivity in carbohydrate matrices. It was found that moisture diffusivities of different carbohydrate systems were analogous, which could be explained on the basis of similar molecular interactions of water with all carbohydrates. It is expected that moisture diffusivities will be different for systems, containing for example proteins or fat. To check this, experiments were carried out for several other matrices (Figure 3-8). For verification, the new results were compared and fortunately found in agreement with previously reported diffusivity data, e.g. for glycerol-water mixtures (109). It was indeed observed that moisture diffusivities varied with the different tested materials. These variations are explained by different (or additional) interactions

between solutes and the water molecules, for example when ionic forces or charges are present.

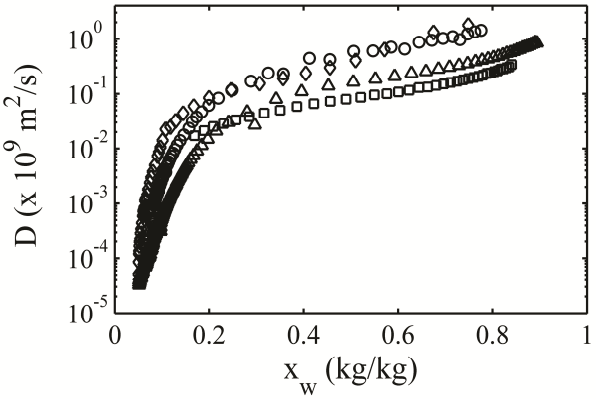

Figure 3-8. Mutual diffusivities of water of water-glycerol (□), water-skimmed milk (Δ), water-casein mixtures (◊), and compared to those of the water-trehalose system (○).

Conclusion

We presented an effective procedure to determine diffusivity on the basis of thin film drying and gravimetric analysis in a Dynamic Vapour Sorption (DVS) system. The approach was verified by checking the effect of the initial drying conditions i.e. mass transport in the drying air is not limiting and the initial water content has only limited influence on the measured diffusivities.

We observed that the mutual diffusion coefficients of water in various carbohydrate matrices were analogous, which indicates that moisture diffusivity in carbohydrate systems is mainly determined by local interactions between water molecules and individual hydroxyl groups. The experimental diffusivities were found comparable to model predictions of moisture diffusivities of the sucrose-water system, though the model underestimated the moisture diffusivity at very high moisture contents. Experimental data showed the influence of temperature on moisture diffusivity at different moisture contents. Model predictions of moisture diffusivity at different temperatures were found in reasonable agreement for the water-trehalose system. At low moisture contents the effect of

temperature was not predicted well. The latter was explained by the difference in relaxation behaviour interacting with the penetrating solute in the glassy state compared to the rubbery state. Finally, the methodology was applied to various other solid matrices and resulted in different moisture diffusivities as a function of moisture contents, which was explained by different molecular interactions between solutes and water.

Nomenclatures

a_u	Hard sphere radius of monomeric unit	m
c_s	the mass concentration of the non-diffusing reference component (solids)	$kg \cdot kg^{-1}$
D	mutual diffusion coefficient of water in solute	$m^2 \cdot s^{-1}$
D_0	pre-exponential diffusion factor in Vrentas-Duda equation	$m^2 \cdot s^{-1}$
D_a	apparent moisture diffusion coefficient in solute-fixed coordinate	$m^2 \cdot s^{-1}$
DP	Degree of polymerization of the carbohydrate molecule	–
E	energy to overcome the attractive force from neighbouring molecule to enable molecule diffusion	$J \cdot mol^{-1}$
F	dimensionless flux parameter	–
I	integrated intensity of the peaks from X-ray diffraction experiments	–
k_B	Boltzmann constant ($1.381 \cdot 10^{-23}$)	$J \cdot K^{-1}$
k	viscosity constant	$mol \cdot l^{-1}$
K_1	free volume parameter	$m^3 \cdot g^{-1} \cdot K^{-1}$
K_2	free volume parameter	K
m	mass	kg
M_U	molecular weight of monomeric carbohydrate molecule	$g \cdot mole^{-1}$
N	degree of polymerisation	–
Q	thermodynamic factor for diffusion coefficient	–
r_H	hydrodynamic radius of the molecules	m
r	absolute distance coordinate	m
R	ideal gas constant (8.314)	$J \cdot mol^{-1} \cdot K^{-1}$

Sh_d	Sherwood number of the dispersed phase	–
t	time	s
T	temperature	K
T_g	glass transition temperature	K
u	mass concentration on dry matter mass basis	$kg \cdot kg$ dry $solid^{-1}$
v	molar volume	$m^3 \cdot mole^{-1}$
$\tilde{V}^*$	specific critical hole free volume	$m^3 \cdot kg^{-1}$
w	weight fraction	$kg \cdot kg^{-1}$
x	molar fraction	$m \cdot mole^{-1}$
z	reference component mass centered coordinate	–
Z	thickness of the thin film in complete dry condition	m

Greek symbols

γ	overlap factor for shared free volume	–
ξ	ratio of solvent and polymer jumping units	–
ρ	density of pure components	$kg \cdot m^{-3}$
τ	dimensionless time in solute-fixed coordinate	–
φ	volume fraction	$m^3 \cdot m^{-3}$
χ	Flory-Huggins interaction parameter	–
ζ	reduced distance coordinate	–

Subscripts

i, j	components i and j
s	solute
ss	surface
ref	reference
w	water
self	self-diffusion coefficient for specific component

Chapter 4

Enzyme inactivation kinetics: coupled effects of temperature and moisture content

Published as:
J. Perdana, M.B. Fox, M.A.I. Schutyser, and R.M. Boom. 2012. Enzyme inactivation kinetics: coupled effects of temperature and moisture content. Food Chem. 133:116-123.

Abstract

Enzymes are often dried for stability reasons and to facilitate handling. However, they are often susceptible to inactivation during drying. It is generally known that temperature and moisture content influence the enzyme inactivation kinetics. However, the coupled effect of both variables on enzyme inactivation within a broad temperature-moisture content range is still not well understood. Therefore, the inactivation of β-galactosidase in maltodextrin matrix is investigated using a newly developed method. An improved kinetic modelling approach is introduced to predict the inactivation over large range of temperature-moisture values. The model assumes a two-step inactivation mechanism involving reversible unfolding and irreversible inactivation. The model is able to describe the inactivation kinetics of β-galactosidase accurately showing the temperature-dependent kinetic transition from reversible unfolding to irreversible inactivation limited. Application of this approach can provide immediate understanding of the effect of processing on enzyme inactivation and indicates the processes' critical points, which offer the possibility for optimisation.

Keywords: enzyme, inactivation kinetics, temperature, moisture content, drying

Introduction

Many applications have been developed in the chemical, food and biotechnological industry that utilize enzymes to produce or improve products. To facilitate handling and for stability reasons industrial enzymes are often dried. Unfortunately, enzymes are heat sensitive and thus may be inactivated during drying, either partly or completely, depending on the specific drying procedure applied (110-112). Enzymes that are susceptible for heat inactivation are for example glucose oxidase, β-galactosidase, alkaline phosphatase, and lactate hydrogenase (7). Generally, it is found that the rate of enzyme inactivation increases with temperature and moisture content (6, 10, 113, 114). Kinetic modelling of the enzyme inactivation helps to understand how to optimise drying processes with respect to maximum retention of enzyme activity (67).

One of the major challenges for kinetic modelling of enzyme inactivation during drying is to accurately describe the combined effect of temperature and moisture content on inactivation in a broad range. This is essential, since particles are subjected to this broad range of temperature-moisture content combinations during a single drying process. Luyben *et al.* (114) describe an approach to model the kinetics of enzyme inactivation during drying, which was later modified by Yamamoto and Sano (6). Both references include the combined effect of temperature and moisture content on inactivation. To calibrate kinetic models for a specific enzyme, usually heating experiments are carried out at a constant temperature and constant moisture content. Heat inactivation studies in dilute solutions are very much straightforward. However, collection of accurate inactivation data at lower moisture contents is less straightforward. Several procedures have been developed to investigate the inactivation at low moisture content, for example, in a dedicated inactivation cell (115).

In this paper an improved kinetic modelling approach is introduced to predict enzyme inactivation over a broad range of temperature and moisture values. The approach assumes a two-step enzyme inactivation mechanism that includes a reversible unfolding and an irreversible inactivation step. The major difference of this approach with previous work is that it also takes into account the reversible unfolding reaction instead of irreversible inactivation alone. Taking this approach, it is expected that we can describe enzyme inactivation over a large range of temperatures and (low) moisture levels, making it feasible

to more accurately describe enzyme inactivation during drying. A disadvantage of such a more complex inactivation model is that the number of parameters increases (from 5 to 9). To alleviate this complication, we adopted the conformational stability theory to better describe the reversible unfolding of proteins from a thermodynamic point of view (116). Besides the more mechanistic approach in describing the unfolding process the latter also leads to a reduction of the number of parameters in the model (to 8). Finally, the transitional-state theory (117) is adopted to replace the Arrhenius equation for describing the dependence of inactivation on temperature. The transitional-state theory provides a more mechanistic approach in describing enzyme inactivation as a thermodynamic transition (118).

The kinetic modelling approach introduced here was compared to the previously published model by Luyben *et al.* (1982) and was evaluated for its accuracy in describing enzyme inactivation as a function of temperature and moisture content. The model by Luyben is to our knowledge the only published semi-mechanistic model applied to describe enzyme inactivation for a wide range of moisture contents. We used β-galactosidase in a maltodextrin solution as a model system. The enzyme inactivation kinetic constants were collected from heating experiments with temperatures between 55 and 130 °C and with moisture contents between 0.01 and 0.98. Dedicated experimental procedures were used to obtain accurate data at these varying temperatures and moisture contents.

Theory

Enzyme inactivation kinetics

Enzyme inactivation can be described by a reversible unfolding reaction followed by an irreversible reaction. The latter reaction leads to complete inactivation of the enzyme (119-123). This can be captured in the following reaction scheme:

$$N \underset{k-1}{\overset{k1}{\leftrightarrow}} U \overset{k2}{\rightarrow} I$$

where N is the native enzyme, U is the unfolded enzyme, and I is the inactivated enzyme.

In the case of β-galactosidase and also for many other enzymes, the reactions involved are usually described by first order kinetics (6, 36). The formation rate of the inactivated enzyme, r_I, is thus

$$r_I = \frac{dI}{dt} = k_2 U \tag{4-1}$$

The unfolded enzyme U is assumed to refold completely upon cooling and convert back to N. By assuming that N and U are in instant equilibrium, the inactivation rate can be described by a first order reaction as a function of $N+U$, which is measured as N after cooling:

$$-\frac{d(N+U)}{dt} = k_{obs}(N+U) \quad ; \quad N+U+I = N_0 \tag{4-2}$$

with N_0 is the initial enzyme activity and k_{obs} (observed inactivation rate constant) described as (36)

$$k_{obs} = \left(\frac{K_1}{1+K_1}\right)k_2 ; \quad K_1 = \frac{k_1}{k_{-1}} \tag{4-3}$$

in which K_1 is the unfolding equilibrium constant, k_1, and k_{-1} are the unfolding and refolding kinetic constants, and k_2 is the irreversible inactivation kinetic constant.

Model 1

The temperature dependence of enzyme inactivation k_{obs} can be described with the following modified Arrhenius equation (6, 114):

$$k_{obs} = k_{ref}\ exp\left[-\frac{E_a}{\mathrm{R}}\left(\frac{1}{T}-\frac{1}{T_{ref}}\right)\right] \tag{4-4}$$

where T is temperature, T_{ref} is reference temperature, k_{ref} is the inactivation rate constant at T_{ref}, E_a is the activation energy, and R is the ideal gas constant.

A lower moisture content has a decreasing effect on the rate of inactivation of enzymes (6, 36, 114, 124). Luyben *et al*. (1982) modelled the influence of moisture content on enzyme inactivation by making the reaction rate coefficients (k_{ref} and E_a) of the Arrhenius equation

(Eq. 4-4) dependent on moisture content. The model, now referred to as Model 1, can then be rewritten into (see Appendix for the derivation of this equation from the original model by Luyben *et al*. (114)):

$$k_{obs}(T,x_w) = k_w(T) \cdot \exp\left[ln\left(\frac{k_s(T)}{k_w(T)} \right) exp\left(-p \cdot \frac{x_w}{1-x_w} \right) \right] \quad (4\text{-}5)$$

where x_w is the mass fraction of water, $k_{obs}(T,x_w)$ is the enzyme inactivation kinetic constant at specific T–x_w, $k_w(T)$ and $k_s(T)$ are the inactivation kinetic constants at infinite dilution (x_w = 1) and in pure solid form (x_w = 0) respectively as a function of temperature (as is described by Eq. 4-4), and p is an empirical parameter that describes the effect of the moisture content on the enzyme inactivation kinetic constant. Overall, this model contains five parameters; viz. k_{ref} and E_a for the inactivation at x_w = 1 and x_w = 0, and the parameter p.

Model 2

To describe enzyme unfolding, the conformational stability theory is adopted (125). The enzyme stability can be derived from measuring the free energy difference for enzyme unfolding in a solution and in pure water ($\Delta\Delta G$) (116). It is generally found that the free energy difference, and thus the conformational stability, is linearly related to the concentration of solids present in the solution (124, 126, 127):

$$\Delta\Delta G = -\mathrm{R}T\, ln\left(\frac{K_1}{K_{1,w}} \right) = mS \quad (4\text{-}6)$$

where the value of parameter m may be positive (promote enzyme unfolding) or negative (prevent the enzyme from unfolding), S is the solute concentration, and $K_{1,w}$ is the enzyme unfolding equilibrium constant in very dilute solution.

In this study, the concentration of solids is approximated by the solid mass fraction. This is valid if the volume change upon mixing is negligible (79). Rewriting Eq. 4-6 and approximating the solute concentration with the solids mass fraction, the native-denatured enzyme equilibrium constant at a specific moisture content can be described as

$$K_1 = K_{1,w}\, exp\left(-\frac{m\cdot(1-x_w)}{\mathrm{R}T}\right); \qquad x_w + x_s = 1 \tag{4-7}$$

with parameter *m* to quantify the effect of moisture content on protein unfolding.

The subsequent irreversible inactivation step is described similar to Model 1; the irreversible inactivation kinetic constant is as defined in Eq. 4-5. The temperature dependencies of $K_{1,w}$, $k_{2,w}$, and $k_{2,s}$ are described with the transitional-state theory (117). To reduce the correlation between parameters, the temperature is reparameterized (119)

$$k = \frac{\mathrm{k_B}T}{\mathrm{h}}\exp\left(\frac{\Delta S^{\ddagger}}{\mathrm{R}} - \frac{\Delta H^{\ddagger}}{\mathrm{R}T_{ref}}\right) exp\left(-\frac{\Delta H^{\ddagger}}{\mathrm{R}}\left(\frac{1}{T}-\frac{1}{T_{ref}}\right)\right) \tag{4-8}$$

where $\mathrm{k_B}$ is Boltzmann's constant ($1.381\cdot10^{-23}$ J.K^{-1}), h is Planck's constant ($6.626\cdot10^{-34}$ J.s^{-1}), $\Delta S^{\ddagger}$ is the activation entropy and $\Delta H^{\ddagger}$ is the activation enthalpy.

Eyring's transitional-state theory applied to the reversible unfolding kinetics (first step inactivation) gives

$$K_{1,w} = \frac{k_{1,w}}{k_{-1,w}} = \frac{\frac{\mathrm{k_B}T}{\mathrm{h}} exp\left(\frac{\Delta S^{\ddagger}_{1,w}}{\mathrm{R}} - \frac{\Delta H^{\ddagger}_{1,w}}{\mathrm{R}T_{ref}}\right) exp\left(-\frac{\Delta H^{\ddagger}_{1,w}}{\mathrm{R}}\left(\frac{1}{T}-\frac{1}{T_{ref}}\right)\right)}{\frac{\mathrm{k_B}T}{\mathrm{h}} exp\left(\frac{\Delta S^{\ddagger}_{-1,w}}{\mathrm{R}} - \frac{\Delta H^{\ddagger}_{-1,w}}{\mathrm{R}T_{ref}}\right) exp\left(-\frac{\Delta H^{\ddagger}_{-1,w}}{\mathrm{R}}\left(\frac{1}{T}-\frac{1}{T_{ref}}\right)\right)} \tag{4-9}$$

which can be simplified to

$$K_{1,w} = exp\left(\frac{\Delta\Delta S^{\ddagger}_{1,w}}{\mathrm{R}} - \frac{\Delta\Delta H^{\ddagger}_{1,w}}{\mathrm{R}T_{ref}}\right) exp\left(-\frac{\Delta\Delta H^{\ddagger}_{1,w}}{\mathrm{R}}\left(\frac{1}{T}-\frac{1}{T_{ref}}\right)\right) \tag{4-10}$$

with $\Delta\Delta S^{\ddagger}_{1,w}\left(=\Delta S^{\ddagger}_{1,w} - \Delta S^{\ddagger}_{-1,w}\right)$ and $\Delta\Delta H^{\ddagger}_{1,w}\left(=\Delta H^{\ddagger}_{1,w} - \Delta H^{\ddagger}_{-1,w}\right)$ being the activation entropy and activation enthalpy differences between unfolding and refolding reactions, respectively. Therefore, Eq. 4-7 can be rewritten into

$$K_1 = exp\left(\frac{\Delta\Delta S^{\ddagger}_{1,w}}{\mathrm{R}} - \frac{\Delta\Delta H^{\ddagger}_{1,w}}{\mathrm{R}T_{ref}}\right) exp\left(-\frac{\Delta\Delta H^{\ddagger}_{1,w}}{\mathrm{R}}\left(\frac{1}{T}-\frac{1}{T_{ref}}\right)\right) exp\left(-\frac{m\cdot(1-x_w)}{\mathrm{R}T}\right) \tag{4-11}$$

For the second, irreversible inactivation step, the moisture content is believed to influence $\Delta S^{\ddagger}$ and $\Delta H^{\ddagger}$ (6, 114). To reduce the number of parameters a new parameter T_{int} is introduced, instead of describing $\Delta S^{\ddagger}$ and $\Delta H^{\ddagger}$ as a function of moisture content. T_{int} is the temperature at which k_2 is not temperature dependent. Via the introduction of this parameter, the model equations can be simplified, which has also its advantage for the parameter optimization procedure. Equalizing the value of k_2 using transitional state theory (Eq. 4-8) for $x_w = 1$ and $x_w = 0$ gives

$$\frac{\Delta S^{\ddagger}_{2,w}}{\mathrm{R}} - \frac{\Delta H^{\ddagger}_{2,w}}{\mathrm{R}T_{int}} = \frac{\Delta S^{\ddagger}_{2,s}}{\mathrm{R}} - \frac{\Delta H^{\ddagger}_{2,s}}{\mathrm{R}T_{int}} \tag{4-12}$$

Therefore, the ratio between $k_{2,s}$ and $k_{2,w}$ at a given temperature is

$$\frac{k_{2,s}}{k_{2,w}} = \frac{exp\left(-\frac{\Delta H^{\ddagger}_{2,s}}{\mathrm{R}}\left(\frac{1}{T}-\frac{1}{T_{int}}\right)\right)}{exp\left(-\frac{\Delta H^{\ddagger}_{2,w}}{\mathrm{R}}\left(\frac{1}{T}-\frac{1}{T_{int}}\right)\right)} \tag{4-13}$$

Substitution of Eq. 4-13 into Eq. 4-5 gives

$$k_2 = \frac{\mathrm{k_B}T}{\mathrm{h}} exp\left(\frac{\Delta S^{\ddagger}_{2,w}}{\mathrm{R}} - \frac{\Delta H^{\ddagger}_{2,w}}{\mathrm{R}T_{ref}}\right) exp\left(-\frac{\Delta H^{\ddagger}_{2,w}}{\mathrm{R}}\left(\frac{1}{T}-\frac{1}{T_{ref}}\right)\right) exp\left[-\frac{\Delta H^{\ddagger}_{2,s}-\Delta H^{\ddagger}_{2,w}}{\mathrm{R}}\left(\frac{1}{T}-\frac{1}{T_{int}}\right) exp\left(-p\cdot\frac{x_w}{1-x_w}\right)\right] \tag{4-14}$$

The kinetic constants of the two-step enzyme inactivation are described by Eq. 4-11 and Eq. 4-14. In Eq. 4-11, three parameters need to be optimized, viz. $\Delta\Delta S^{\ddagger}$, $\Delta\Delta H^{\ddagger}$, and m. In Eq. 4-14, five parameters need to be optimized, viz. $\Delta S^{\ddagger}_{2,w}$, $\Delta H^{\ddagger}_{2,w}$, $\Delta H^{\ddagger}_{2,s}$, T_{int}, and p. Therefore, in total, eight parameters have to be fitted to the k_{obs} calculated from the experimental data.

Materials and methods

Sample preparation

The enzyme solution was prepared by dissolving 250 mg β-galactosidase from *A. oryzae* (Sigma-Aldrich, Germany) into 4750 µl buffer solution and filtered with 0.2 µm sieve (Sartorius Stedim Biotech GMBH, Germany). The maltodextrin solutions were prepared by dispersing maltodextrin DE 4-7 (Sigma-Aldrich, Germany) in buffer solution. The buffer solution was prepared by mixing 0.2 M Na_2HPO_4 (Sigma-Aldrich, Germany) and 0.1 M Citric Acid ($C_6H_8O_7$) solutions (Sigma-Aldrich, Germany); pH of the buffer was adjusted to 6.00 ± 0.01.

Heating tests

Heating tests were carried out following two different methods. The first method is for high moisture content (<40 % $^{w}/_{w}$ maltodextrin), whereas the second method is required for the more concentrated mixtures (> 40 % $^{w}/_{w}$ maltodextrin).

1. At high moisture content: A sample of 480 µl maltodextrin solution (0 %, 10 %, 20 % and 40 % $^{w}/_{w}$) was heated to the desired temperature in a 2 ml vial (Eppendorf AG, Germany) using a Thermomixer (Eppendorf AG, Germany). Subsequently, 20 µl of a 5 % $^{w}/_{w}$ enzyme solution was added to the heated matrix solution. After heating for the required time, 1500 µl cold buffer solution was added and the tube was immediately submerged into an ice bath to quickly decrease the temperature and avoid further inactivation. Subsequently, the sample was stored at 7 °C for 12 h prior to the activity measurement to allow refolding of the unfolded enzyme.

2. At low moisture content: 10 µl of 5 % $^{w}/_{w}$ enzyme solution was mixed with 90 µl of 20 % $^{w}/_{w}$ maltodextrin solution and dispensed on an Accurel® type PP 2E HF membrane (Akzo Nobel, The Netherlands). Subsequently, the solution was dried with an air flow at ambient temperature. The relative humidity of the contacting air was adjusted to obtain specific final moisture content. The drying time was dependent on the amount of water to be removed, e.g. for a final moisture content of < 1 %, the drying time was 72 h, while for a final moisture content larger than 10 %, 24 h of drying was sufficient. Subsequently, the preconditioned sample was sealed airtight in a pipette tube (Thermo Fischer Scientific, USA) prior to the heating tests. The sample was heated to the

desired temperature by contacting it with dry air of the desired temperature for a certain time. Heating up of the sample was on average complete within 1 minute, which is negligible compared to the time for which a sample was generally kept at the desired temperature. After heating, the sample was dispersed into cold buffer solution and the final water content was adjusted to 95 % $^{w}/_{w}$. After being re-dissolved, the sample was stored at 7 °C for 12 h prior to the activity measurement to allow refolding of the unfolded enzyme.

Measurement of β-galactosidase activity

The activity of β-galactosidase was measured using an o-nitrophenyl-ß-D-galactopyranoside (ONPG) assay (Sigma-Aldrich, Germany). A sample of 20 µl was added to 980 µl 0.2 % ONPG solution at 40 °C and incubated for 10 minutes. The ONPG solution was pre-heated to 40 °C prior to the sample incubation. The active enzyme cleaved ONPG into galactose and o-nitrophenol; o-nitrophenol gave a yellow colour to the solution. The enzyme was inactivated by adding 1000 µl 10 % Na_2CO_3 (Sigma-Aldrich, Germany). The absorbance of the sample was immediately measured at 420 nm wavelength using spectrophotometer (Beckman Coulter, Inc., USA).

Data acquisition and modelling procedures

The observed inactivation kinetic constant (k_{obs}) at specific T-x_w combination is calculated from the residual enzyme activity applying the first order inactivation kinetics (Eq. 4-2). The first order kinetic model was first tested to describe the effect of treatment time at 60 °C and x_w = 0.98, 0.88, and 0.78. It was found that the first order kinetics was sufficient to describe the β-galactosidase inactivation and therefore for further analysis, only one specific treatment time was used for each T-x_w combination. This treatment time was chosen at the most sensitive inactivation region (N/N_0 around 0.5), for example, at T = 121.5 °C and x_w = 0.01, the treatment time applied was 750 s while at T = 60 °C and x_w = 0.98, the treatment time applied was 600 s. The experiments at specific T-x_w combination were carried out in triplicate. The observed inactivation kinetic constant at a specific T-x_w combination was then calculated from the average residual enzyme activity using first order inactivation kinetics (Eq. 4-2).

The parameter optimisation was carried out using a non-linear least square method solved using the Levenberg-Marquardt algorithm (128). The optimization was split in two parts. A first optimisation was performed for the experimental data assuming infinite dilution (x_w = 0.98). From this the following parameters were obtained, viz. $\Delta\Delta S^{\ddagger}_{1,w}$, $\Delta\Delta H^{\ddagger}_{1,w}$, $\Delta S^{\ddagger}_{2,w}$, and $\Delta H^{\ddagger}_{2,w}$. The second optimization was carried out for the entire dataset to obtain the values of parameters $\Delta H^{\ddagger}_{2,s}$, m, p, and T_{int}. Following this procedure, the parameter optimization was less troubled by local optimum values and thus provided the most accurate results. The confidence intervals of the parameters (P = 0.95) were estimated using the Hessian matrix, which was derived from the Jacobian matrix of the solution (129). All the calculations were performed with MATLAB version 7.10.

Results and discussion

Experimental and modelling results

Figure 4-1 shows the observed inactivation rate constant of β-galactosidase as function of the temperature and moisture content. The observed inactivation rate constants from experimental data were calculated using Eq. 4-2. For this calculation it was taken into account that $N_0 = N + U + I$ and that the unfolded enzyme U refolds back to the native enzyme N upon cooling.

The observed inactivation kinetic constant increases with increasing temperature and moisture content (Figure 4-1). If we observe the inactivation kinetic constant as a function of temperature at low temperatures in, i.e. below 60 °C for x_w = 0.98 and below 80 °C for x_w = 0.01, then it can be concluded that the slope of the curve is similar for the different moisture contents and thus has similar dependency on temperature. Meanwhile, at higher temperatures, the effect of temperature on the inactivation kinetic constant is larger for higher moisture contents. The experimental data as represented in Figure 4-1B also show that the inactivation kinetic constant of β-galactosidase increases at low moisture content, while it remains constant at moisture contents above x_w = 0.6, especially between 65 and 73 °C.

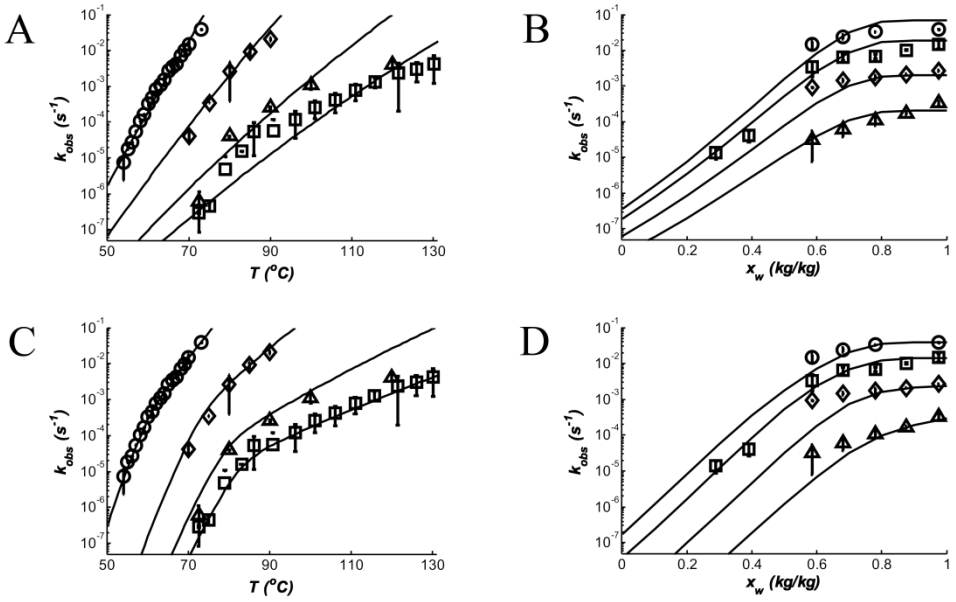

Figure 4-1. Inactivation kinetic constant of β-galactosidase; A and C: at x_w = 0.98 (○), 0.39 (◊), 0.14 (Δ), and 0.01 (□), B and D: at T = 60 (Δ), 65 (◊), 70 (□), and 73 °C (○). Solid lines represent the fitted model 1 (A and B) and model 2 (C and D). The error bar shows the confidence interval (P = 0.95) of the experimental data.

Figure 4-1A and B also show the observed inactivation kinetic constant calculated with Model 1. It can be visually observed that the model does not fit well to the experimental data. Moreover, the large standard errors for the model parameters as shown in Table 4-1 indicate that the model fails to adequately describe the experimental results. Specifically, the model underestimates the observed inactivation kinetic constant between 80 and 100 °C and at lower moisture contents (x_w = 0.14 and x_w = 0.01). In addition, the Model 1 does not include a description of the change in kinetics observed (bend in the curve) at 60 °C for a moisture content of 0.98 and at 80 °C for a moisture content of 0.01. This kinetic shift has been observed before and is explained by the transition from a rate limiting unfolding reaction at lower temperatures, to a rate limiting denaturation reaction at higher temperatures (120, 122). The new model proposed here (Model 2) does include this two-

step reaction mechanism of unfolding and denaturation. Figure 4-1C and D show that the model presented in this paper is in better agreement with the experimental data.

At temperatures below 60 °C with x_w = 0.98 and below 80 °C for x_w = 0.01, the inactivation kinetics is limited by protein unfolding (K_1). At higher temperatures, where K_1 is much larger than 1, the term in [K_1/(K_1+1)] in Eq. 4-3 approaches 1. Thus the observed reaction rate depends primarily on k_2; the rate constant for the irreversible reaction from unfolded to inactivated enzyme. The difference in temperature at which this transition takes place shows that the unfolding behaviour of β-galactosidase is influenced by the water content. This kinetic shift temperature is also sometimes referred to as melting temperature or denaturation temperature (36).

The effect of temperature on the unfolding equilibrium constant (K_1) is described using Eq. 4-10. The parameter values of $\Delta\Delta H^{\ddagger}$ in Eq. 4-10 at T < 60 °C for moisture content 0.98 and at T < 80 °C for moisture content 0.01 are similar, viz. $\Delta\Delta H^{\ddagger} = 3.57 \cdot 10^5 \pm 0.81 \cdot 10^5$ for x_w 0.98 and $\Delta\Delta H^{\ddagger} = 3.07 \cdot 10^5 \pm 1.21 \cdot 10^5$ for x_w = 0.01 (the confidence interval P = 0.95 is presented after the estimated parameter value). These values are in accordance with the similar slopes of the curves at the low temperatures for different moisture contents (Figure 4-1). This indicates that at temperatures below the melting temperature of the protein, the increase of k_{obs} with temperature is similar for different moisture contents. At the same time, the increase of k_{obs} with moisture content at low temperature is similar (Figure 4-1D). We know that k_{obs} at these temperatures is primarily determined by the unfolding equilibrium (K_1). The exponential term in the conformational stability theory (Eq. 4-7) describes the dependency of K_1 on moisture content, in which parameter m is independent of temperature.

At higher temperatures (> 60 °C for x_w = 0.98 and > 80 °C for x_w = 0.01), the irreversible inactivation is rate limiting. In this regime, the dependence of k_{obs} on the temperature becomes stronger as the moisture content increases. This effect is described by the model via the dependency of the activation enthalpy on moisture content. The latter effect is difficult to comprehend from mechanistic point of view. It can be said that the irreversible inactivation (second step reaction) of β-galactosidase is a complex reaction and may for

example involve agglomeration of two or more molecules (36). Decrease of moisture content reduces the mobility of the unfolded enzyme and thus decreases the reaction rate.

Table 4-1. Estimated parameter values for Model A and Model B

Estimated parameter[a]		
Model A		
$k_{ref,w}$ (s^{-1})	0.340	(0.088)
$E_{a,w}$ (kJ/mol)	431.50	(16.15)
$k_{ref,s}$ (s^{-1})	$7.87 \cdot 10^{-7}$	$(2.64 \cdot 10^{-7})$
$E_{a,s}$ (kJ/mol)	214.0 4	(12.66)
p	1.16	(0.0018)
T_{ref} (°C)[b]	76.7	
Standard error[c]	$7.52 \cdot 10^{-2}$	
Akaike Criterion	139	
Model B		
$\Delta\Delta S^{\ddagger}_{1,w}$ ($J \cdot mol^{-1}K^{-1}$)	$1.08 \cdot 10^{3}$	$(0.250 \cdot 10^{3})$
$\Delta\Delta H^{\ddagger}_{1,w}$ ($J \cdot mol^{-1}$)	$3.57 \cdot 10^{5}$	$(0.806 \cdot 10^{5})$
$\Delta S^{\ddagger}_{2,w}$ ($J \cdot mol^{-1}K^{-1}$)	$6.75 \cdot 10^{2}$	$(1.173 \cdot 10^{2})$
$\Delta H^{\ddagger}_{2,w}$ ($J \cdot mol^{-1}$)	$3.28 \cdot 10^{5}$	$(0.401 \cdot 10^{5})$
$\Delta H^{\ddagger}_{2,s}$ ($J \cdot mol^{-1}$)	$1.28 \cdot 10^{5}$	$(0.196 \cdot 10^{5})$
m	$2.60 \cdot 10^{4}$	$(0.00936 \cdot 10^{4})$
p	1.16	(0.00562)
T_{int} (°C)	33.85	(0.00648)
T_{ref} (°C)[b]	60.5	
Standard error[c]	$5.77 \cdot 10^{-2}$	
Akaike Criterion	122	

[a] The uncertainty of the parameters at 95 % confidence interval is provided between brackets

[b] Not optimized

[c] Standard error of $\ln(k_{obs})$

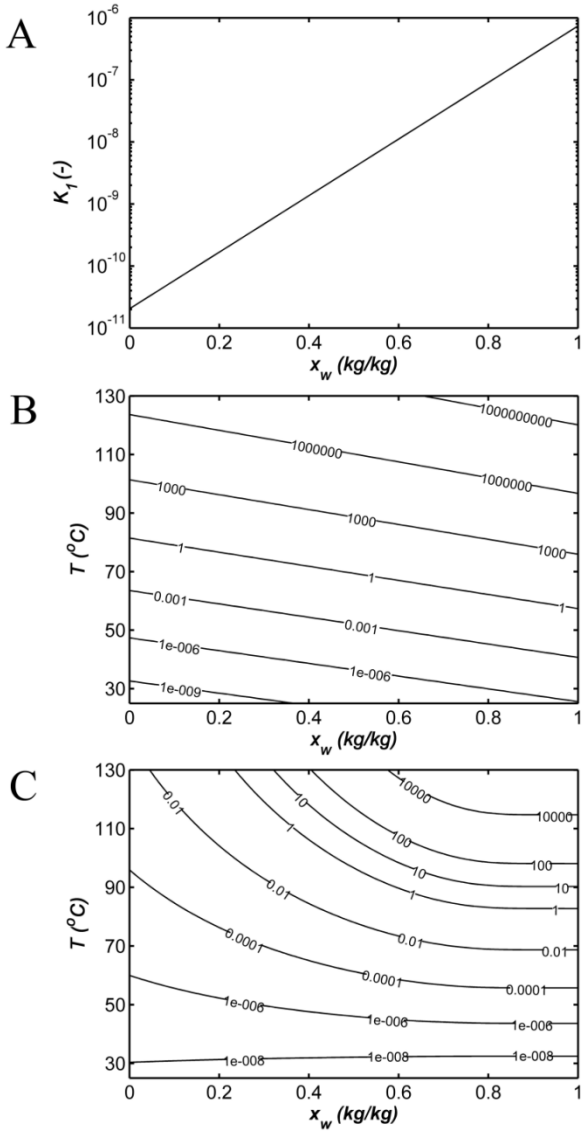

Figure 4-2 A: The unfolding equilibrium constant (K_1) as a function of moisture value at cooled temperature (25 °C). B: Contour plot of the unfolding equilibrium constant (K_1) as a function of temperature and moisture value. C: Contour plot of the second step inactivation kinetic constant (k_2) as a function of temperature and moisture value.

In Figure 4-2 we show K_1 as a function of moisture content at ambient temperature. It can be observed that the value of K_1 at 25 °C is smaller than 10^{-6}, which indicates that the equilibrium instantly shifts towards the native enzyme after cooling to ambient temperature. This supports our assumption that the unfolded enzyme will refold completely upon cooling.

The obtained model parameter values and their statistical analysis are shown in Table 4-1. Despite the large number of parameters for both models, all parameters have reasonable narrow confidence intervals. Statistical analyses were carried out for both model fitting results. Besides the standard error also the Akaike criterion, which is based on the principle of parsimony, was used (130).

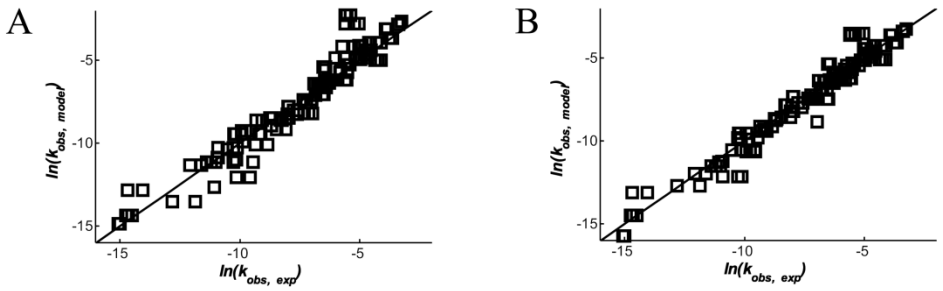

Figure 4-3. Parity plots of the observed inactivation kinetic constants for model 1 (left) and model 2 (right). The symbol (□) represents the parity between the experimental data and their model prediction and solid line represents experimental data = model prediction.

The standard error of Model 2 is lower than that of the Model 1. This indicates that Model 2 fits better to the inactivation kinetics constant from the experimental results than Model 1. The Akaike criterion of Model 2 is found lower than that for Model 1. This indicates that Model 2, despite having three fitted parameters more, is preferred above Model 1. This preference can be explained by the more adequate description of the kinetic shift, which is absent in Model 1.

Figure 4-3 shows the parity plots of the natural logarithmic values of the inactivation kinetics constants obtained from the experimental data and calculated by the models. From the plots it can be observed that there are less outliers for Model 2 compared to Model 1. Therefore, we conclude that Model 2 is more suitable to describe the inactivation kinetics constant of β-galactosidase.

Practical application

A contour plot of the observed inactivation kinetic constant of β-galactosidase estimated with the proposed model is presented in Figure 4-4. This contour plot can be helpful to optimize the drying of β-galactosidase. Plotting the temperature and moisture content history of a certain treatment involving elevated temperatures in the contour plot, can give a first insight on the impact of the treatment on the enzyme activity. For example, in case of spray drying, inactivation can be reduced by adjusting the temperature and moisture content history in such a way to avoid a region with a high inactivation kinetic constant.

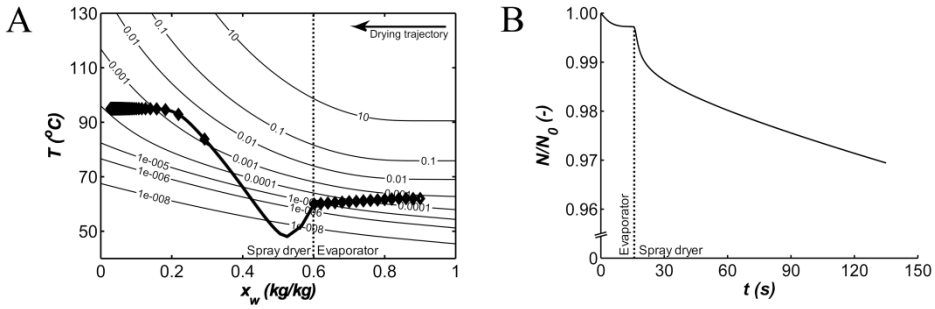

Figure 4-4. Contour plot of the inactivation kinetic constant of β-galactosidase. The isolines represent the inactivation kinetic constant of β-galactosidase. The solid line is the average temperature-moisture content history of a virtual spray dried product; symbols (◊) in the line represent a time step of 1 s (note that the times steps taken in the calculations are as small as 25 ms).

In Figure 4-4A, the temperature and moisture content history of a virtual product processed in an evaporator (15 s) and subsequently in a spray dryer (120 s) is plotted. In the evaporator, most of the inactivation takes place in the beginning of the process where the

temperature and moisture content are at the highest. To reduce the inactivation rate, one may propose a lower initial temperature, which could be compensated by a slowly increasing temperature when the moisture level has decreased.

During drying, the temperature of the product first cools to the wet bulb temperature, and then gradually increases again as internal diffusion becomes limiting. The temperature and moisture content of the product is assumed uniform, although we are aware that this is not the case in reality, especially in spray drying. Figure 4-4A shows that the highest inactivation rate constant occurs at moisture contents between 0.2 and 0.25 in the example drying process. At this relatively high moisture content, the drying is diffusion limited and the temperature approaches the air temperature, with consequently a high inactivation kinetic constant. Later in the drying process, the inactivation kinetic constant decreases with decreasing moisture content. A criterion can be defined for inactivation, e.g. k_{obs} should not exceed $3 \cdot 10^{-3}$ s^{-1}. Therefore, on the basis of Figure 4-4A, one may suggest to decrease the temperature of the drying air to decrease the temperature of the product during the later stages of the drying process.

Figure 4-4B shows that the enzyme activity decreases less than 0.5 % after dehydration in the evaporator and decreases 3 % after spray drying. The decrease of the activity is faster in the beginning of dehydration in evaporator and in spray dryer (Figure 4-4B). This is related to the high inactivation rate constant because of the combination of high moisture content and high temperature. In a prolonged drying, the residual enzyme activity levels off because of the decrease of the moisture content which implies to the decrease of the enzyme inactivation kinetic constant.

The inactivation kinetic constant is exponentially dependent on temperature and moisture content, which means that small deviations in kinetic constant have large consequences for the final enzyme activity. Therefore, good quantification of the inactivation kinetics is a prerequisite for accurate prediction of the influence of thermal processing on residual activity of a component. The developed kinetic modelling approach can be supportive in this respect.

Conclusion

Dewatering and drying processes have large impact on the activity of enzymes in the product. Kinetic modelling of enzyme inactivation can be of great help in evaluating and optimising the impact of thermal processing or more specific drying on enzyme activity. Although it is generally known that temperature and moisture content have both impact on the inactivation kinetics, the coupled effect of both variables on enzyme inactivation within a broad temperature-moisture content range are still not well understood. This applies especially to the evaluation of processes which involve many different temperatures and moisture levels, for example cooking (baking, boiling), drying, spray drying, and evaporation.

The effect of temperature and moisture content on the β-galactosidase inactivation kinetic constant was described by a new kinetic model (Model 2), assuming a two-step inactivation mechanism. This model used the theory on conformational stability to describe enzyme unfolding kinetics and Eyring's transitional-state theory to describe the dependency of enzyme inactivation on temperature. It was found that Model 2 could accurately describe the inactivation kinetics of β-galactosidase, including the transition from reversible unfolding limited to irreversible inactivation limited inactivation. From statistical analysis it was further concluded that the proposed model performs better than Luyben's model (114), despite the fact that the model has three more parameters.

Finally, a contour plot was constructed to sketch the temperature and moisture content history of a combined evaporation and drying process. Such a plot provides immediate understanding of the effect of processing history on enzyme inactivation and indicates the critical points in the process with respect to enzyme inactivation.

Nomenclature

A	Enzyme activity	–
E_a	Activation energy	$J \cdot mol^{-1}$
$\Delta\Delta G$	Gibbs' free energy difference for protein unfolding in a solution with infinite dilution ($x_w = 1$) and in pure solid form ($x_w = 0$)	$J \cdot mol^{-1}$

h	Planck's constant ($6.626 \cdot 10^{-34}$)	J.s
$\Delta H^{\ddagger}$	Activation enthalpy	$J \cdot mol^{-1}$
$\Delta\Delta H^{\ddagger}$	Activation enthalpy difference between unfolding and refolding reaction	$J \cdot mol^{-1}$
I	Inactivated enzyme	–
k	inactivation kinetic constant	s^{-1}
k_B	Boltzmann's constant ($1.381 \cdot 10^{-23}$)	$J.K^{-1}$
K_1	Reversible unfolding equilibrium constant	$mol \cdot mol^{-1}$ or $s \cdot s^{-1}$
m	Parameter to describe the effect of moisture content on the conformational stability of protein	–
N	Native enzyme	–
p	Parameter in the Model 1 to describe the effect of moisture content on inactivation kinetic constant	–
P	The uncertainty of the parameters	–
r	Inactivation rate	$mol \cdot s^{-1}$
R	Ideal gas constant (8.314)	$J \cdot mol^{-1}K^{-1}$
S	Concentration of solids	mol
$\Delta S^{\ddagger}$	Activation entropy	$J \cdot mol^{-1}K^{-1}$
$\Delta\Delta S^{\ddagger}$	Activation entropy difference between unfolding and refolding reaction	$J \cdot mol^{-1}K^{-1}$
t	Time	s
T	Temperature	K
U	Unfolded enzyme	–
x	Mass fraction	$(kg \cdot kgtotal^{-1})$

Subscript:

0	Initial condition
1	First step inactivation: unfolding reaction
-1	First step inactivation: refolding reaction

2	Second step inactivation, i.e. irreversible inactivation
crit	Critical
I	Inactivated enzyme
int	Intercept
obs	Observed
ref	Reference
s	In pure solid form ($x_w = 0$)
w	In a solution with infinite dilution ($x_w = 1$)

Appendix

Derivation of Eq. 4-5

The effect of temperature and moisture content on the inactivation kinetics constant is described by

$$k = k_{ref}\ exp\left[-\frac{E_a}{\mathrm{R}}\left(\frac{1}{T}-\frac{1}{T_{ref}}\right)\right] \tag{4-A1}$$

The effect of moisture content on k_{ref} and E_a are described by parameter p is as follows:

$$ln\left(k_{ref}\right) = ln\left(k_{ref,w}\right) + \left[ln\left(k_{ref,s}\right) - ln\left(k_{ref,w}\right)\right]exp\left(-p\cdot\frac{x_w}{1-x_w}\right) \tag{4-A2}$$

$$E_a = E_{a,w} + \left(E_{a,s} - E_{a,w}\right)exp\left(-p\cdot\frac{x_w}{1-x_w}\right) \tag{4-A3}$$

Substitution of Eq. 4-A2 and 4-A3 to Eq. 4-A1 gives

$$k = k_{ref,w}\,exp\left[\left[ln\left(k_{ref,s}\right) - ln\left(k_{ref,w}\right)\right]exp\left(-p\cdot\frac{x_w}{1-x_w}\right)\right]$$
$$exp\left[-\frac{E_{a,w} + \left(E_{a,s} - E_{a,w}\right)exp\left(-p\cdot\frac{x_w}{1-x_w}\right)}{\mathrm{R}}\left(\frac{1}{T}-\frac{1}{T_{ref}}\right)\right]$$

The equation above can be rewritten into

$$k = k_{ref,w}\, exp\left[-\frac{E_{a,w}}{\mathrm{R}}\left(\frac{1}{T}-\frac{1}{T_{ref}}\right)\right]$$
$$exp\left[\left(\left[ln\left(k_{ref,s}\right)-ln\left(k_{ref,w}\right)\right]-\frac{\left(E_{a,s}-E_{a,w}\right)\left(\frac{1}{T}-\frac{1}{T_{ref}}\right)}{\mathrm{R}}\right)exp\left(-p\cdot\frac{x_w}{1-x_w}\right)\right]$$

Rearrangement of the equation above returns

$$k = k_{ref,w}\exp\left[-\frac{E_{a,w}}{\mathrm{R}}\left(\frac{1}{T}-\frac{1}{T_{ref}}\right)\right]\exp\left[\left(\begin{array}{l}\ln\left(k_{ref,s}\right)-\frac{E_{a,s}}{\mathrm{R}}\left(\frac{1}{T}-\frac{1}{T_{ref}}\right)-\ln\left(k_{ref,w}\right)+\\ \frac{E_{a,w}}{\mathrm{R}}\left(\frac{1}{T}-\frac{1}{T_{ref}}\right)\end{array}\right)\exp\left(-p\cdot\frac{x_w}{1-x_w}\right)\right]$$

Equation above can be simplified into

$$k = k_w\, exp\left[ln\left(\frac{k_s}{k_w}\right)exp\left(-p\cdot\frac{x_w}{1-x_w}\right)\right] \qquad (4\text{-A4})$$

Chapter 5

Mimicking spray drying by drying of single droplets deposited on a flat surface

Published as:
J. Perdana, M.B. Fox, M.A.I. Schutyser, and R.M. Boom. 2013. Mimicking Spray Drying by Drying of Single Droplets Deposited on a Flat Surface. Food Bioprocess Tech. 6:964-977.

Abstract

The inactivation of bioactive ingredients during spray drying is often matrix specific. Therefore, the design of new processes or the optimisation of existing spray drying processes is usually highly product specific and requires numerous experiments. Rapid experimentation methods that facilitate fast data generation are therefore desired.

A novel method for drying single droplets to mimic spray drying is proposed. The approach involves droplet deposition on a hydrophobic flat surface followed by controlled drying. A heat and mass transfer model is applied to predict the drying history of the single droplets. The approach is successfully evaluated through studying the inactivation of β-galactosidase during drying. The heat and mass transfer model supplemented with inactivation kinetics provided reasonable prediction of the residual enzyme activity after drying. In addition, the inactivation kinetics could be directly extracted from single droplet experiments rather than using the kinetics from separate heating experiments. Finally, it was demonstrated that the inactivation kinetics found with the single drop experiments could satisfactorily predict the residual activity of β-galactosidase dried with a laboratory scale spray dryer.

Keywords: enzyme, temperature, moisture content, inactivation kinetics, spray drying, single droplet

Introduction

Spray drying belongs to the most common drying techniques for liquid food products. The fine atomisation of the product and the subsequent fast evaporation of water makes it especially suitable to formulate heat-sensitive products (11, 131). Despite the relative mild conditions during drying, (partial) inactivation of bioactive compounds such as enzymes, antioxidants, and vitamins cannot be avoided. Optimisation of the spray drying conditions and addition of stabilizers is often required to retain maximum activity (2, 8, 132). In practice, numerous expensive pilot-scale trials are executed to explore different product formulations and to find optimum drying conditions.

Modelling tools are frequently used to accelerate process development and optimisation in spray drying. The availability of reliable inactivation kinetics – usually highly product-specific – is a prerequisite for this. Kinetic models require experimental data from drying experiments for parameter calibration. Pilot scale experiments are not ideal for this as they are expensive, time consuming, and involve the evaluation of complex process conditions. A more efficient alternative is the application of small-scale representative drying experiments.

Once reliable inactivation kinetics are obtained, a process model of the dryer can be used to predict the impact of the drying on the remaining ingredient activity. Subsequently, the model can be used to approximate optimal drying conditions and product formulations in a more systematic way (9, 10, 114, 133, 134).

Small-scale spray drying has been carried out in laboratory scale spray dryers (102, 135, 136). However, major differences between laboratory and industrial spray dryers are the smaller droplet size, caused by the different method of atomisation, and the shorter residence time in the laboratory spray dryer (11, 137). Since the laboratory spray dryer can (due to its design and dimensions) only cover a limited range of droplet sizes and drying times and it produces droplets with a size distribution (not monodisperse), it is virtually impossible to extract sufficient representative experimental data to calibrate a kinetic model.

Another approach is the drying of single droplets under well-controlled conditions. In this approach a small droplet is generated, immobilized, and subsequently dried by contacting it with well-defined drying air. Examples are drying of a droplet that is non-intrusively

levitated using for example acoustic, aerodynamic, or electromagnetic levitation (49, 59, 138), intrusively levitated that is in pendant or filament (139, 140), or that is deposited on a flat surface (67).

In this study, the latter method is followed (67). The major advantages of this method are the possibility to vary droplet size and residence time, and to dry multiple droplets at once to obtain higher volume of sample. The minimum droplet diameter can be adjusted to 150 μm which is only slightly bigger than the typical droplet size in industrial spray dryers; a comparable droplet size is critical to accurately mimic the kinetics in spray drying (138, 141). The challenge in using this approach is the presence of the flat surface. This surface for example affects the spherical shape of the droplet. Therefore, a hydrophobic surface is used to minimize the contact between the droplet and the surface and to retain the spherical shape. Other differences introduced by the presence of the surface are the air flow velocity and the air temperature near the droplet, which deviate from the bulk conditions (142). By monitoring the air temperature near the droplet and by modelling the air flow and heat transfer across the drying surface, the influence of the surface on the drying conditions can be quantified.

This study focuses on the drying of the enzyme β-galactosidase suspended in a maltodextrin matrix. The enzyme β-galactosidase is selected as the model enzyme in this study, because it is an industrial relevant enzyme applied for production of lactose-hydrolysed milk and whey. Additionally, its activity can be easily determined and its inactivation kinetics has been studied before, though under steady-state conditions, providing strong basis for this study (6, 68, 143). The inactivation kinetics of β-galactosidase from the previous studies were combined with the heat and mass transfer model to predict the residual activity of β-galactosidase during the single droplet drying experiments. Finally, the predictive value of the model was also checked by drying of β-galactosidase in a laboratory spray dryer system.

Modelling and statistical evaluation

This section consists of four parts: 1) model description for a single droplet drying, 2) modelling temperature and air flow distribution across the flat plate, 3) inactivation kinetics of β-galactosidase, and 4) parameter optimisation and statistical evaluation.

Model description for single droplet drying

In analogy to several previous studies a heat and mass transfer model is used to describe the drying of a sessile single droplet (50, 59, 144). The sessile droplet is approximated as a spherical droplet and it is thus assumed that the diffusion occurs only in the radial direction. For the small droplet sizes considered the temperature gradient inside the droplet could be neglected. This assumption is valid if Bi <0.1. The Biot number (Bi) is defined as the ratio of external heat transfer (between air and droplet) and the internal heat transfer (in the droplet) (145).

$$Bi = \frac{hd_d}{\lambda_d} \tag{5-1}$$

In this study, Bi is around 0.02.

The following differential equation is used to describe the droplet mass change in time

$$-\frac{dm_d}{dt} = k_c 4\pi R_d^2 \frac{M_w}{R}\left(\frac{a_w P_w^{sat}}{T_d} - \frac{P_\infty}{T_\infty}\right) \tag{5-2}$$

where m_d is the mass of the droplet, t is the time, k_c is the mass transfer coefficient, R_d is the droplet radius, M_w is the molecular weight of water, R is the ideal gas constant, a_w is the water activity, P_w^{sat} is the saturated vapour of water at T_d, T_d is the temperature of the droplet, P_∞ is the vapour partial pressure in the bulk air, and T_∞ is the bulk air temperature.

The developing moisture gradient inside the droplet is described by Fickian diffusion

$$\frac{\partial C_w}{\partial t} = D_{w,d}\frac{\partial}{\partial r}\left(\frac{\partial C_w}{\partial r}\right) \tag{5-3}$$

With C_w is the water concentration, $D_{w,d}$ is the effective diffusion coefficient of water in the droplet, and r is the radial coordinate. The boundary conditions applied here are

$$t = 0, 0 \le r \le R_d; \quad \frac{dC_w}{dr} = 0$$

$$t = t, r = 0; \quad \frac{dC_w}{dr} = 0$$

$$t = t, r = R_d; \quad -D_{w,d}\frac{dC_w}{dr} = k_c 4\pi {R_d}^2 \frac{M_w}{\mathrm{R}}\left(\frac{a_w P_w^{sat}}{T_d} - \frac{P_\infty}{T_\infty}\right)$$

The temperature change of the droplet is described by the following enthalpy balance:

$$\left(m_w c_{p,w} + m_s c_{p,s}\right)\frac{dT_d}{dt} = h_d 4\pi {R_d}^2 (T_\infty - T_d) - \frac{dm_d}{dt} H_{lv} \tag{5-4}$$

with m_s is the mass of the solute, $c_{p,w}$ and $c_{p,s}$ the heat capacity of the water and the solute respectively, h_d the heat transfer coefficient to the droplet through convection, and H_{lv} is the evaporation enthalpy of water.

The coupled heat and mass transfer models were solved numerically using 100 radial layers in the droplet. In each layer the same solute mass (m_s) was calculated according to

$$m_s = C_{s,0}\frac{V_{d,0}}{n} \tag{5-5}$$

with $C_{s,0}$ is the initial solute concentration and $V_{d,0}$ is the initial volume of the droplet.

Since the initial solute concentration is assumed homogenous, the initial solute mass distribution is approximated with the initial volume distribution. The radial position of the i^{th} layer from the centre of the droplet can be calculated as follows

$$r_i = \left(i \cdot \frac{{R_d}^3}{n}\right)^{1/3} \tag{5-6}$$

with n is the total number of layers for numerical integration. The layer thickness Δr is

$$\Delta r_i = \begin{cases} r_i, & i = 1 \\ r_i - r_{i-1}, & i \geq 2 \end{cases} \tag{5-7}$$

The volume of each layer V is then

$$V = \frac{m_w}{\rho_w} + \frac{m_s}{\rho_s} \tag{5-8}$$

with ρ_w and ρ_s are the densities of water and solute, respectively. The average water concentration is then defined as

$$C_w = \frac{m_w}{V} = \frac{m_w}{\frac{m_w}{\rho_w} + \frac{m_s}{\rho_s}} \tag{5-9}$$

Reorganizing Eq. 5-9 results in

$$m_w = \frac{m_s}{\rho_s}\frac{C_w}{\left(1 - \frac{C_w}{\rho_w}\right)} \tag{5-10}$$

The droplet shrinks upon drying due to the evaporation of water. This shrinkage influences the heat and mass transfer within the droplet. The model was therefore corrected to describe the decrease of layer thickness due to shrinkage (146). This correction was based on the water concentration in every layer at t > 0 that is calculated from Eq. 5-3 (147). From the water concentration, the new volume of the layer was recalculated as

$$V = \frac{m_s}{\rho_s}\left(1 + \frac{1}{(\rho_w - C_w)}\right) \tag{5-11}$$

The radial coordinate of every partition was corrected using this new volume. The radius of the i^{th} partition is

$$r_i = \left(\frac{3\left(\sum_0^i V_i\right)}{4\pi}\right)^{1/3} \tag{5-12}$$

The thickness of every partition could be recalculated using Eq. 5-7. To solve the model, several closure equations like heat and mass transfer coefficient, water activity, moisture diffusion coefficient, and vapour pressure are required, which are tabulated in Appendix (Table 5-A1).

Modelling temperature and air flow distribution across the flat plate

In this study, the droplet was deposited on a flat plate. The drawback of this configuration is that in addition to heat transfer from the air to the droplet, also heat is transferred from the air to the flat plate through convection. This heat is further transferred from the plate to the droplet through conduction. It is of major importance to quantify the heat transfer between the flat plate and the droplet and compare this to the convective heat transfer via the drying air. The conductive heat transfer between the flat plate and the droplet is preferably as low as possible, when one wants to mimic the drying of a droplet suspended in air. By using a hydrophobic surface, the contact area for conductive heat transfer has already been reduced. Furthermore, the temperature in the air near the flat plate deviates from the bulk air temperature affecting the drying process. Therefore a model description of the temperature gradients within the plate and in the air near the plate was developed.

To minimize turbulence (eddy formation) near the edge of the depositing plate, a thin flat plate is used rather than a blunt-edged plate. However, the presence of the flat plate still influences the flow pattern of the drying air above the plate, i.e. near the droplet (Figure

5-1). A boundary layer model according to Mosaad (148) is used to describe the air flow and temperature distribution across the flat plate: a hydrodynamic boundary layer is defined for the air flow distribution and a thermal boundary layer for the temperature distribution

$$\frac{u}{u_\infty} = \frac{3}{2}\left(\frac{z}{\delta}\right) - \frac{1}{2}\left(\frac{z}{\delta}\right)^3; \quad 0 \le z \le \delta \tag{5-13}$$

$$\frac{T-T_\infty}{T_{p,x}-T_\infty} = 1 - \frac{3}{2}\left(\frac{z}{\delta_t}\right) + \frac{1}{2}\left(\frac{z}{\delta_t}\right)^3; \quad 0 \le z \le \delta_t \tag{5-14}$$

with z is the height coordinate from the surface of the flat plate, u is the air velocity at z, u_∞ is the bulk velocity of air, υ is the kinematics viscosity of air, $T_{p,x}$ is the temperature of the surface of the flat plate at distance x (at the front edge of the flat plate, $x = 0$), T_∞ is the bulk air temperature, δ is the hydrodynamic boundary layer at distance x, and δ_t is the thermal boundary layer. The hydrodynamic boundary layer for $u = 0.99u_\infty$ is (142)

$$\delta = 5\sqrt{\frac{\upsilon x}{u_\infty}} \qquad \textit{5-15} \tag{5-16}$$

and δ_t is thermal boundary layer at distance x

$$\delta_t = \begin{cases} Pr^{-1/3}, & Pr \le 1 \\ Pr, & Pr > 1 \end{cases} \tag{5-17}$$

The heat transfer coefficient between the air and the flat plate h_p is approximated by (149)

$$h_p = 0.332\frac{\lambda_a}{x^{1/2}}\left(\frac{u_\infty}{v}\right)Pr^{1/3}; \qquad Pr = \frac{c_{p,a}\mu_a}{\lambda_a} \tag{5-18}$$

with λ_a is the thermal conductivity of air, Pr is the Prandtl number of air, $c_{p,a}$ is the heat capacity of air, and μ_a is the dynamic viscosity of air. The value of λ_a, $c_{p,a}$, and μ_a are temperature dependent; in Eq. 5-18, the value are evaluated at $T = (T_p+T_\infty)/2$.

The heat transfer coefficient decreases as a function of the x-coordinate (Eq. 5-18) and is calculated locally. It was estimated numerically; i.e. assuming a Δx at distance L from the front side of the plate, the average heat transfer coefficient is obtained by integrating h_p along Δx

$$h_{p,avg} = 0.664\frac{\lambda_a}{v^{1/2}}Pr^{1/3}\left(\left(\frac{u_\infty}{L}\right)^{1/2} - \left(\frac{u_\infty}{L+\Delta x}\right)^{1/2}\right) \tag{5-19}$$

where $h_{p,avg}$ is the average local heat transfer coefficient.

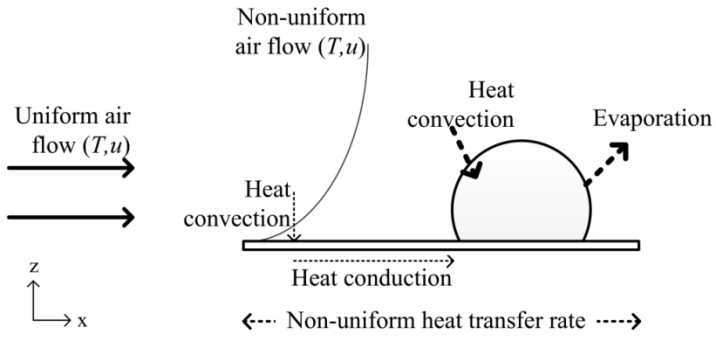

Figure 5-1. Sketch of a single droplet drying on a flat plate with the air flow pattern and governing heat transfer processes indicated. The sessile droplet is dried on a thin plate consisting of a hydrophobic membrane (0.15 mm) on top of a stainless steel platform (1.00 mm).

The non-uniform heat transfer rate across the plate contributes to the development of a temperature gradient within the plate. The temperature distribution within the plate is described with a one-dimensional partial differential equation (150). It is assumed that no temperature gradient in the y-direction (perpendicular to the air flow direction) and in the z-direction (within the plate; because of the small thickness, i.e. 150 μm)

$$\frac{\partial T_p}{\partial t} = \frac{\lambda_p}{\rho_p c_{p,p}} \left(\frac{\partial^2 T_p}{\partial x^2} + \frac{h_{p,avg}(T_\infty - T_p)}{Z \lambda_p} \right) \qquad (5\text{-}20)$$

with ρ_p is the density of the plate, Z is the thickness of the flat plate, and λ_p is the thermal conductivity of the flat plate. The boundary layer applied here are that near the droplet the flat plate temperature is equal to the droplet temperature and at the edge of the flat plate (far from the droplet) the temperature gradient of the flat plate is 0.

Equations 5-14 and 5-20 were solved numerically to estimate the temperature distribution history within and above the flat plate. The predictions were validated by simple temperature measurements at different heights above the plate.

To estimate the conductive heat transfer between the surface and the droplet and compare it to the convective heat transfer between the air and the droplet, the conductive heat flux Q through the contact surface of the droplet was estimated according to

$$Q = \lambda_p 2\pi R_d z \frac{\Delta T_{cond}}{\Delta x_{cond}} \tag{5-21}$$

with $\Delta T_{cond}/\Delta x_{cond}$ is the temperature gradient in the partition layer of the flat plate that is closest the droplet. It was found that the conductive heat flux was smaller than 5 % of the total heat transferred to the droplet regardless of its position. Therefore, it can be safely assumed that most heat is transferred via convective heat transfer.

Inactivation kinetics of β-galactosidase

The inactivation rate of the β-galactosidase is affected by the temperature and moisture content of the droplet, which both change with time. A kinetic inactivation model for β-galactosidase is developed in earlier work and calibrated using constant heating experiments (68). In the latter experiments, the suspended enzyme is exposed to various temperature-moisture value combinations for a specific time and the remaining enzyme activity is measured. The inactivation kinetics are described by a two-step inactivation process and the observed inactivation coefficient (k_{obs}) is described as

$$k_{obs} = \left(\frac{K_1}{1+K_1}\right) k_2 \tag{5-22}$$

with

$$K_1 = exp\left(\frac{\Delta\Delta S^{\ddagger}_{1,w}}{R} - \frac{\Delta\Delta H^{\ddagger}_{1,w}}{RT_{ref}}\right) exp\left(-\frac{\Delta\Delta H^{\ddagger}_{1,w}}{R}\left(\frac{1}{T} - \frac{1}{T_{ref}}\right)\right) exp\left(-\frac{f(1-x_w)}{RT}\right) \tag{5-23}$$

$$k_2 = \frac{k_B T}{h} exp\left(\frac{\Delta S^{\ddagger}_{2,w}}{R} - \frac{\Delta H^{\ddagger}_{2,w}}{RT_{ref}}\right) exp\left(\frac{\Delta H^{\ddagger}_{2,w}}{RT}\left(\frac{1}{T} - \frac{1}{T_{ref}}\right)\right) exp\left(-\frac{\Delta H^{\ddagger}_{2,m} - \Delta H^{\ddagger}_{2,w}}{R}\left(\frac{1}{T} - \frac{1}{T_{int}}\right) exp\left(-g\frac{x_w}{1-x_w}\right)\right) \tag{5-24}$$

where K_1 is the reversible unfolding equilibrium constant, k_2 is the complete denaturation rate constant, $\Delta\Delta S^{\ddagger}_{1,w}$ is the activation entropy difference between the unfolding and refolding reactions in pure water, $\Delta\Delta H^{\ddagger}_{1,w}$ is the activation enthalpy difference between the

unfolding and refolding reactions in pure water, k_B is Boltzmann's constant, h is Planck's constant, the $\Delta S^{\ddagger}_{2,w}$ is the activation entropy of complete denaturation in pure water, $\Delta H^{\ddagger}_{2,w}$ is the activation enthalpy in pure water, $\Delta H^{\ddagger}_{2,m}$ is the activation enthalpy in pure solid form (i.e. no moisture), f describes the effect of moisture content on conformational stability of the enzyme, g describes the effect of moisture content on the irreversible inactivation (second step) kinetic constant of the enzyme, and T_{in} is the intercept temperature at which $k_{2,w}/k_{2,s}= 1$.

Alternatively, the enzyme inactivation can also be regarded as a one-step inactivation process in which the native enzyme is irreversibly inactivated. Then

$$k_{obs} = k_2 \qquad (5\text{-}25)$$

An advantage is that this approach involves only 5 parameters to fit instead of 8 in the two-step model. The effect of the temperature is then still described using the transitional state theory as shown in Eq. 5-24.

Parameter optimization and statistical evaluation

To directly extract the kinetics from single droplet drying experiments the following approach was taken:

1. The temperature and moisture content histories of several droplets were predicted using the drying model (Eq. 5-3 and 5-4).
2. The inactivation kinetic constants were optimised to fit the measured residual enzyme activities after the drying for all droplets simultaneously.

The parameter optimisation was carried out using a non-linear least square method solved using the Levenberg-Marquardt algorithm (128). The confidence interval of the parameters (p = 0.95) were estimated using the Hessian matrix, which was again derived from the Jacobian matrix of the solution (129). All calculations were performed with MATLAB version 7.10.

Materials and methods

Sample preparation

The enzyme, β-galactosidase from *Aspergillus oryzae* (Sigma-Aldrich, Germany) was dissolved in a buffer solution. The solution was then filtered with a 0.2 μm Minisart sterile sieve (Sartorius Stedim Biotech SA, Germany) and stored overnight in a refrigerator. The maltodextrin, with DE 4-7 (Sigma-Aldrich, Germany) was dissolved in a buffer. The buffer was prepared from 0.2 M Na_2HPO_4 (Sigma-Aldrich, Germany) and 0.1 M Citric Acid ($C_6H_8O_7$) solutions (Sigma-Aldrich, Germany). The pH of the buffer was adjusted to 6.00±0.01.

The feed for single droplet drying experiments was prepared by mixing 600 μl 2.5 % $^{w}/_{w}$ enzyme solution and 2400 μl 25 % maltodextrin solution. The feed for the laboratory scale spray dryer was prepared by mixing 4 ml 2 % $^{w}/_{w}$ enzyme solution and 96 ml 20.8 % $^{w}/_{w}$ maltodextrin solution. A lower enzyme concentration is used during the laboratory scale spray dryer experiments. The major reason was that a larger sample volume could be easily obtained for performing the enzyme activity test. This is allowed, since at low enzyme concentration, the inactivation kinetics of β-galactosidase is not affected by its concentration (6).

Deposited droplet drying experiments

The single droplet drying experiments involved the subsequent steps: droplet generation, droplet drying, rehydration, and enzyme activity measurement. A micro-dispenser was used to generate the droplet as described by Perdana *et al*. (67). The droplet was deposited on a polypropylene membrane (Akzo Nobel Faser Ag., The Netherlands) positioned on a platform from stainless steel slab; the thickness of the membrane was 0.15 mm and the stainless steel slab was 1 mm. The droplet was then positioned in a drying tunnel (Figure 5-2). By guiding the drying air through a porous medium, a uniform flow distribution could be achieved within the tunnel. The tunnel was insulated and heated with heating oil to ensure that the air temperature was constant. The temperature and relative humidity of the air bulk air was monitored using SHT75 temperature and humidity sensor (Sensiron AG, Switzerland). The temperature near the droplet was monitored using a thermocouple Type K (NiCr-NiAl) (RS Component, United Kingdom) with probe diameter 250 μm. Furthermore, the setup was equipped with a μEye 1480ME CCD camera with a lens with

9x magnification ratio (Imaging Development Systems GMBH, Germany) to monitor the droplet geometry evolution during drying.

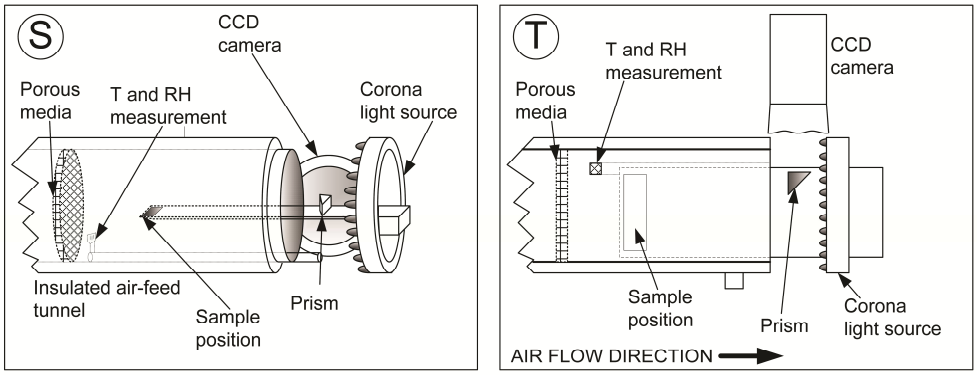

Figure 5-2. Schematic drawing of the drying tunnel, side view (S) and top view (T).

The single droplet drying experiments were performed using dry air (RH = 0.0 %), preheated to a temperature between 80 and 110 °C and a bulk air velocity of 0.20 m/s. After drying, the resulting powder particle was dissolved in 50 µl buffer solution, stored overnight in the refrigerator, and then the enzyme activity was measured.

Laboratory scale spray drying experiments

The enzyme solution was dried with a Buchi B-190 spray dryer (Buchi Labortechnik AG, Switzerland). The residence time of the particle inside this small spray dryer can be as short as 1 s. Based on the equipment specification, the particle diameter after drying was between 2 and 25 µm. The inlet air temperature was 180 °C and the outlet air temperature varied between 80 and 130 °C. Subsequently, around 1 g of powder was taken and dried further in a heating chamber at 105 °C for 72 h to determine the moisture content of the powder after spray drying. Additionally, a 0.200 g powder sample was reconstituted to 3.80 ml buffer solution and analysed for its residual enzyme activity.

Measurement of the residual activity of β-galactosidase

The residual activity of β-galactosidase was measured using an o-nitrophenyl-β-D-galactopyranoside (ONPG) assay (Sigma-Aldrich, Germany) according to Perdana *et al.* (68). The absorbance of the samples incubated in ONPG solution was immediately

measured after incubation at a wavelength 420 nm using a spectrophotometer (Beckman Coulter, Inc., USA).

Particle size measurement

Approximately 1 gram of the spray dried sample was dried further in a heating chamber at 105 °C for 72 h to reduce the moisture content and to avoid particle agglomeration. Afterwards, the particle size distribution of the sample was measured using Mastersizer Scirocco 2000 (Malvern Instrument LTD, England).

Results and discussion

Droplet geometry evolution

Snapshots of a deposited droplet during the drying process are shown in Figure 5-3. The droplet shrinks uniformly before 30 s, and then starts to develop wrinkles. The uneven shrinkage after 60 s suggests that a thin non-flowing layer is developed, which cannot accommodate a homogenous shrinkage (151). Instead, it collapses which leads to an irregular shape of the particle.

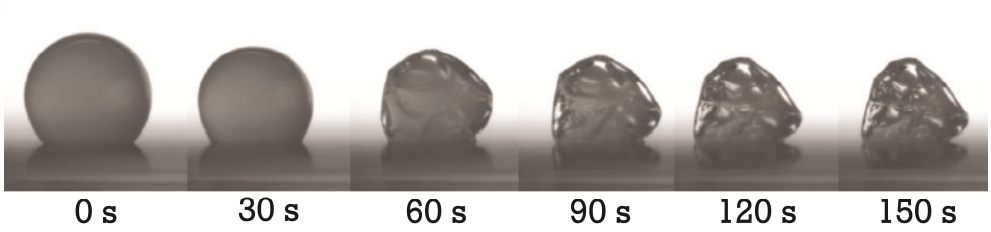

Figure 5-3. Droplet geometry change during a single droplet drying experiment at an air temperature of 80 °C, an absolute air humidity of 0 g/kg dry air, a bulk air velocity of 0.20 m/s, an initial droplet height of 800 μm, and an initial droplet moisture content of 80 % $^{w}/_{w}$.

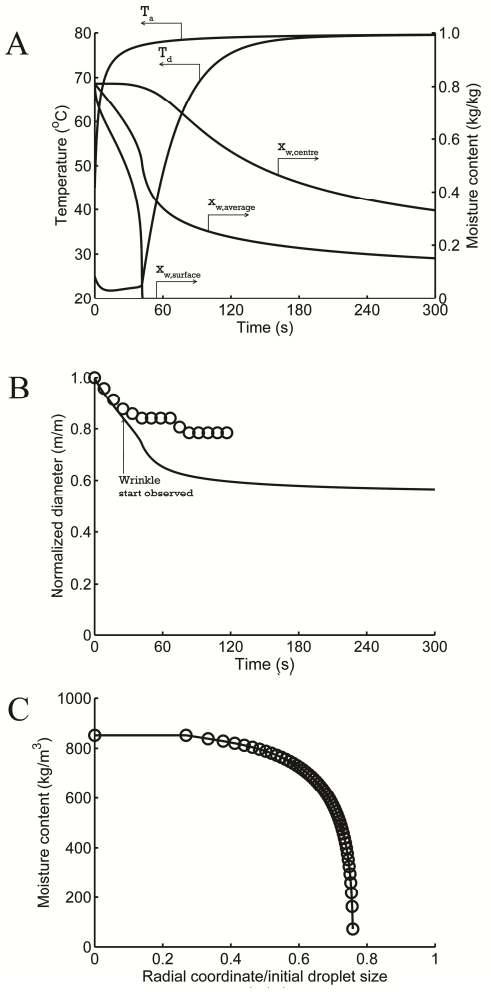

Figure 5-4. A: Temperature and moisture content history of a droplet dried during a single droplet drying experiment; T_a is the air temperature contacting the droplet; averaged as the air temperature at half droplet height, T_d is the droplet temperature, and xw is the moisture content. B: Droplet radius change during drying from the visual monitoring (symbol) and the model (line). C: Moisture content distribution inside the droplet at t = 32 s, the symbols show the border of the partition for each layer. The drying is carried out at an air temperature of 80 °C, a bulk air velocity of 0.20 m/s, and an absolute air humidity of 0 kg/kg dry air. The initial moisture content is 80 % $^{w}/_{w}$ and the initial droplet height is 800 μm.

Drying model

In the heat and mass transfer model the sessile droplet is assumed to be a perfect sphere. This assumption reduces the complexity of the model and is acceptable since the initial sessile droplet has a very high contact angle (>130 °C) and also the final powder particle remains approximately spherical, as shown in Figure 5-3. The predicted temperature and moisture profiles are shown in Figure 5-4.

The model predicts that the moisture content at the surface decreases faster than in the centre of the droplet and reaches a moisture content close to 0 % at around 35 s. This is in line with the visual observations, i.e. the occurrence of wrinkles indicating the presence of a thin dry layer. As shown in Figure 5-4B, at t = 31 s, the moisture content gradient near the surface of the droplet is very steep, indicating that a very thin layer near the droplet surface is very dry. The model also predicts that the droplet radius does not change any more after approximately 60 s of drying. This is also in line with the visual observations.

The droplet temperature at the beginning (t < 40 s) of the drying process is equal to the corresponding wet bulb temperature of the heating air (Figure 5-4A). When the moisture content near the surface of the droplet decreases to less than 100 kg/m^3, the droplet temperature starts to increase. At this point the water evaporation rate decreases together with the lower vapour pressure at the droplet surface (a_w < 1). While the evaporation rate decreases, the heat transfer into the droplet continues and causes an accumulation of heat; observed as an increase in droplet temperature.

Predicting the residual enzyme activity after drying

The single droplet drying method is applied to dry β-galactosidase suspended in a maltodextrin matrix. The inactivation kinetics of β-galactosidase determined with independent experimental data was combined with the heat and mass transfer model to predict the residual enzyme activity after drying (68). Subsequently, the predicted enzyme activity is compared to the drying results. In modelling the inactivation of β-galactosidase, the pH change due to decreasing moisture content was neglected. This is allowed since most of the enzyme activity loss takes place at high moisture content where the presence of the added buffer stabilizes the pH. Furthermore, at lower moisture content, the enzyme activity loss is negligible at the time scale of drying applied. The model predictions and the experimental data are shown in Figure 5-5.

As shown in Figure 5-5, the heat and mass transfer model using the independent kinetic inactivation model for β-galactosidase is in reasonable agreement with the experimental data. Both the predictions and the experimental data show that the enzyme activity does not decrease during the initial drying period (< 40 s) because the temperature of the droplet, which is near the (low) wet bulb temperature. Then, a rapid inactivation rate is observed, which slowly declines to result in a final enzyme activity. The subsequent rapid inactivation can be explained by an increase in particle temperature. At this point the heat transfer is not compensated by sufficient water evaporation. The increase in temperature has especially impact on the enzyme present in the centre of the droplet as the moisture content in the centre is still high as also reported for drying of other heat sensitive products (44, 152).

After a while the enzyme inactivation rate decreases and the residual enzyme activity in the particle is obtained. The enzyme inactivation rate decreases because of the decreasing moisture content, especially near the surface of the droplet and finally also in the centre of the droplet. Most of the residual active enzyme is located near the surface of the particle as shown in Figure 5-5C. It can be concluded that the different moisture content history at different locations in the droplet determines the large differences in residual enzyme activity across the droplet radius.

A strategy that might be followed to retain maximum enzyme activity is to minimize the presence of enzyme in the centre of the droplet. This can for example be achieved by drying the enzyme in a droplet that forms a hollow sphere upon drying (113) or by applying a coating of a concentrated enzyme solution on pre-dried particles.

The results also show that the initial droplet diameter determines the residual enzyme activity to a large extent. Figure 5-5 indicates that the residual activity is higher for smaller droplets. Although inactivation starts earlier in a smaller droplet, the critical region is shorter (i.e. the combination of high temperature and high moisture content in the centre of the droplet) compared to that in the larger droplet. This implies that with respect to enzyme inactivation a smaller droplet size is preferred for spray drying.

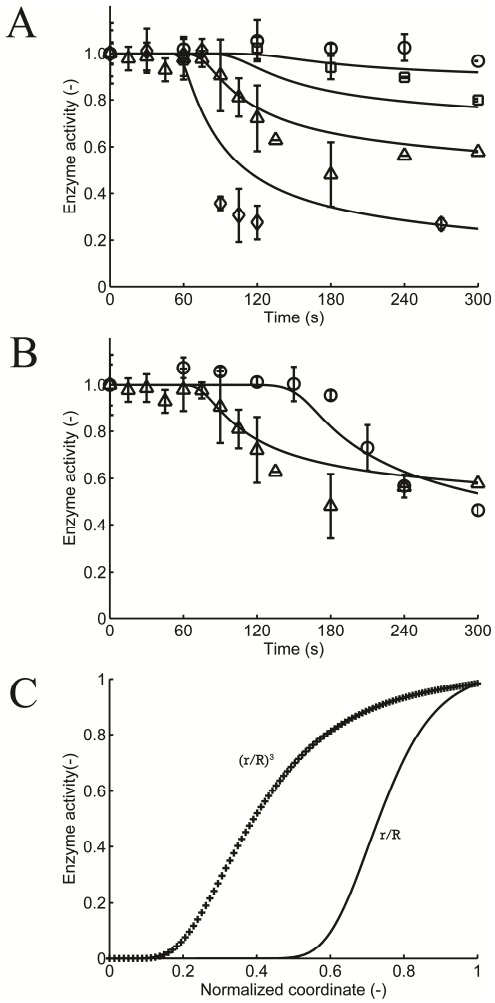

Figure 5-5. A: Residual enzyme activity after drying of a single sessile droplet at air temperatures of 80 (○), 87 (□), 95 (Δ), and 110 °C (◊) for an initial droplet diameter of 800 μm. B: The effect of initial droplet size on residual enzyme activity for an initial droplet diameter of 800 μm (Δ), and 1400 μm (○). The error bar shows the standard deviation of the data. The predictions (solid line) are based on the inactivation kinetics of β-galactosidase from the constant heating experiments. C: Residual activity of β-galactosidase as a function of the radial coordinate (solid line) and of the volumetric coordinate (symbols) after drying of a droplet with an initial diameter of 800 μm at an air temperature of 95 °C for 300 s.

Direct extraction of inactivation kinetic parameters from drying experiments

The parameters describing the specific inactivation kinetics of β-galactosidase in maltodextrin may be extracted directly from the single droplet drying results. This is preferred as these experiments are much less labour intensive and can be scaled out to facilitate a high throughput approach. If the method is reliable, the parameters for β-galactosidase inactivation directly obtained from single droplet drying experiments should be similar to the ones obtained from the separate heating experiments (68).

Both the one-step and the two-step inactivation models were evaluated to describe the experimental drying data. The results of the parameter optimisation are compared to the parameters from the earlier study (Table 5-1). It can be observed that the parameters obtained from the drying experiments differ from the parameter values from the heating experiments (Table 5-1). This can be explained by the fact that the inactivation during single droplet drying experiments occurs primarily during a very short critical period. This critical period is dictated by the drying history and involves temperatures and moisture content values that lead to rapid inactivation. Therefore, the parameter values are optimised such that they specifically describe the inactivation during this critical period. This explanation is further confirmed by implementing the one-step inactivation model, which is also able to describe the inactivation during drying experiments well. The data from the heating experiments were obtained at many different temperature and moisture content combinations and could be varied independently. Therefore, the values are based on a much wider data set, but having less data in the specific range that is relevant for spray drying.

Another reason for the difference between the kinetic parameters is that the parameter optimisation procedure forces the model to describe the residual enzyme activity after the drying. By doing so, any uncertainties in the heat and mass transfer model are neglected. However, from earlier observations it was concluded that the heat and mass transfer model could predict the droplet shrinkage and the residual enzyme activity using the kinetic parameters from the heating experiments reasonably accurate. Therefore, it is believed that the uncertainties involved are not very large and that the kinetic parameters of the single droplet experiments remain valid. This conclusion is supported by laboratory spray drying experiments.

Table 5-1. The parameter values for the inactivation kinetic constant of β-galactosidase estimated from heating experiments and from single droplet drying experiments

Estimated parameter[a]	Heating experiments[b]	Drying experiments	
		Two-step inactivation model (Eq. 5-22)	One-step inactivation model (Eq. 5-24)
$\Delta\Delta S^{\ddagger}_1$ (J·mol^{-1}K^{-1})	$1.08\cdot10^{3}$ ($0.25\cdot10^{3}$)	$1.31\cdot10^{3}$ ($0.0063\cdot10^{3}$)	NA
$\Delta\Delta H^{\ddagger}_1$ (J·mol^{-1})	$3.57\cdot10^{5}$ ($0.81\cdot10^{5}$)	$4.86\cdot10^{5}$ ($0.023\cdot10^{5}$)	NA
$\Delta S^{\ddagger}_{2,w}$ (J·mol^{-1}K^{-1})	$6.75\cdot10^{2}$ ($1.17\cdot10^{2}$)	$5.49\cdot10^{2}$ ($0.097\cdot10^{2}$)	$1.88\cdot10^{3}$ ($0.00010\cdot10^{3}$)
$\Delta H^{\ddagger}_{2,w}$ (J·mol^{-1})	$3.28\cdot10^{5}$ ($0.40\cdot10^{5}$)	$2.76\cdot10^{5}$ ($0.063\cdot10^{5}$)	$7.74\cdot10^{5}$ ($0.00023\cdot10^{5}$)
$\Delta H^{\ddagger}_{2,s}$ (J·mol^{-1})	$1.28\cdot10^{5}$ ($0.20\cdot10^{5}$)	$1.57\cdot10^{5}$ ($0.027\cdot10^{5}$)	$4.77\cdot10^{5}$ ($0.0010\cdot10^{5}$)
m	$2.60\cdot10^{4}$ ($0.00094\cdot10^{4}$)	$8.92\cdot10^{3}$ ($0.0010\cdot10^{3}$)	NA
p	1.16 (0.0056	5.37 (0.011)	5.67 (0.00038)
T_{int} (°C)	33.85 (0.065)	-49.65 (8.80)	8.25 (0.026)
T_{ref} (°C)[c]	68.50	68.50	68.50

[a] The uncertainty of the parameters at 95 % confidence interval

b The values of the parameters are according to Perdana et *al*. (68)

[c] Not optimized

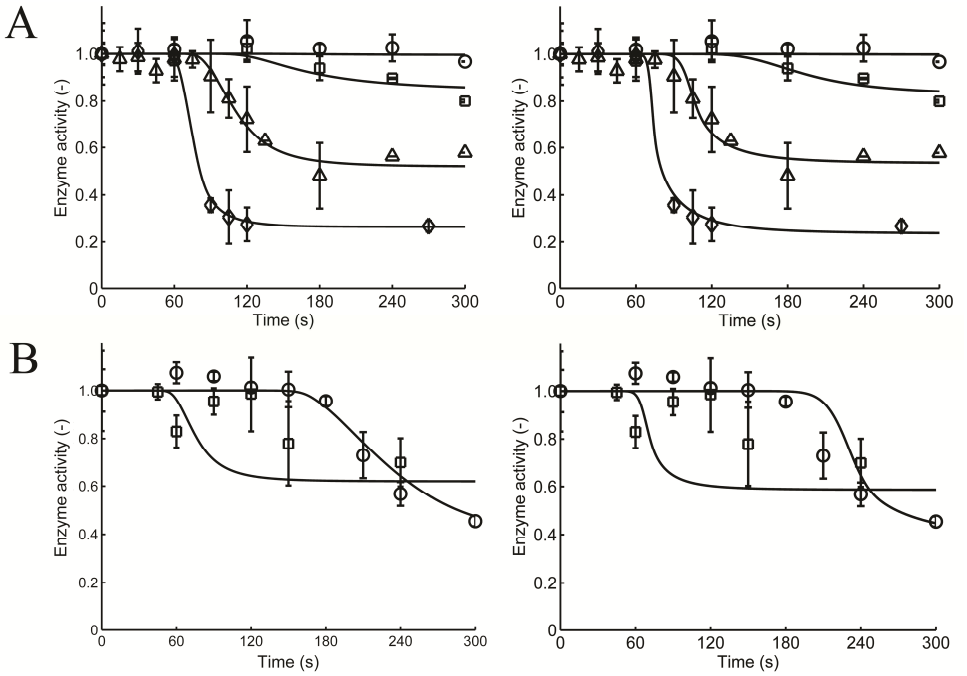

Figure 5-6. A: Fitted residual enzyme activity obtained from single droplet drying experiments at varying air temperatures of 80 (○), 87 (□), 95 (Δ), and 110 °C (◊) for an initial droplet diameter of 800 μm. B: Residual enzyme activity predicted using the inactivation kinetics extracted from drying data at various heating air temperatures compared to the drying results from different initial droplet diameter: 500 μm (□) and 1400 μm (○). The β-galactosidase inactivation is described by the two-step inactivation model (left) and the one-step inactivation model (right).

In Figure 5-6B, the effect of the initial droplet diameter on the residual β-galactosidase activity after drying is shown. The figure shows that the model accurately predicts the experimental data. Therefore, it can be concluded that although the values for the parameters in the model for inactivation kinetics obtained from the drying experiments may be less precise, the inactivation kinetics are accurate enough to predict the effect of drying on the inactivation of the enzyme. This is because the critical drying period dictates the end-product properties.

Table 5-1 shows that the values of the confidence intervals of the parameters are smaller for the one-step inactivation compared to the two-step inactivation model. Therefore, it may be concluded that the one step inactivation model is more favourable than the two-step inactivation model to describe the effect of drying on enzyme activity loss. From practical point of view the one-step inactivation model may be sufficient to translate the measured inactivation from single droplet experiments into useful inactivation kinetics.

Laboratory-scale spray drying

The models were also applied to predict the residual enzyme activity after drying on a laboratory scale spray dryer. The results indicate that at an outlet air temperature below 100 °C, the enzyme is hardly inactivated upon drying, while with an outlet air temperature higher than 100 °C, the enzyme is increasingly inactivated with higher temperature as also observed by Yamamoto and Sano (6) (Figure 5-7).

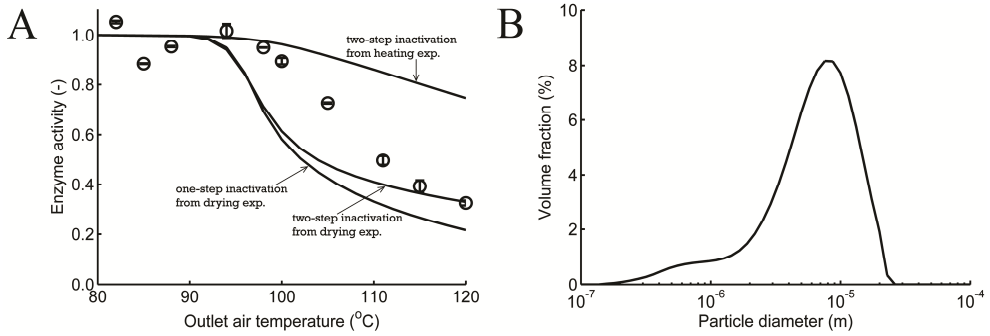

Figure 5-7. A: the residual activity of β-galactosidase after spray drying in a laboratory scale spray dryer. The symbols represent the experimental results at an inlet air temperature of 180 °C and varied outlet air temperature. The lines represent the predicted enzyme activity using the inactivation kinetics obtained from the single droplet drying experiments and from the constant heating experiments. B: the particle size distribution of the powder obtained from the laboratory scale spray dryer.

The volume weighted mean diameter ($d_{4,3}$) of the spray dried particle is 6.94 µm; fed into the drying model to predict the residual enzyme activity. By assuming that the volumetric

droplet shrinkage is equal to the amount of water removed, the initial droplet diameter was estimated at 11.8 µm (initial moisture content 80 % $^{w}/_{w}$) (152).

The model can predict the drying results reasonably accurate, but at temperatures between 100 and 120^{o}C, the predicted value of the residual activity of β-galactosidase is slightly lower than the experimental results. This may be due to the lower initial droplet size in reality due to non-ideal shrinkage leading to more rapid drying and thus lower inactivation (see also Figure 5-3).

Furthermore, Figure 5-7 shows that there is only a small difference between the two inactivation models at temperatures larger than 100 °C. This is probably because the inactivation kinetic constant of the one-step inactivation model increases more quickly with temperature. This may lead to an overestimation of the inactivation kinetic constant at high temperatures.

Conclusion

A newly developed, small scale experimental setup to mimic spray drying was presented which involves the drying of single droplets deposited on a hydrophobic flat plate. This approach ensures rapid and inexpensive trials while maintaining key parameters similar to the process condition on spray drying. In this study, the setup is used to evaluate the inactivation of β-galactosidase during drying.

To describe the physical and chemical changes during drying, a model based on heat and mass transfer is presented. The model, combined with the inactivation kinetics of β-galactosidase from separate heating experiments was used to predict the loss in enzyme activity after drying. It is found that the model can provide a reasonably accurate prediction on the residual enzyme activity.

It was also shown that the inactivation kinetics of β-galactosidase can be directly extracted from the single droplets drying experiments rather than using the kinetics from separate heating experiments. The parameters that were obtained in this way were used to predict other experimental results both from other single droplet drying experiments and from a laboratory scale spray dryer. The new inactivation kinetics provides reasonably accurate prediction on the residual enzyme activity for both procedures.

Nomenclature

A	Area	m^2
a_w	Water activity	–
c_p	Heat capacity	$J \cdot kg^{-1}K^{-1}$
C	Concentration	$kg \cdot m^{-3}$
C_g	Constant in GAB sorption model	–
d	Diameter ($2R_d$)	m
D	Diffusion coefficient	m^2s^{-1}
E_a	Arrhenius-type diffusion activation energy	$J.mol^{-1}$
f	Parameter to describe the effect of moisture content on conformational stability of the enzyme	–
g	Parameter to describe the effect of moisture content on the irreversible inactivation (second step) kinetic constant of the enzyme	–
h	Planck's constant (6.626×10^{-34})	$J.s^{-1}$
h	Convective heat transfer coefficient	$J \cdot s^{-1}m^{-2}K^{-1}$
ΔH_{lv}	Enthalpy of evaporation	$J \cdot kg^{-1}$
$\Delta H^{\ddagger}$	Activation enthalpy	$J \cdot mol^{-1}$
$\Delta\Delta H^{\ddagger}$	Activation enthalpy difference between unfolding and refolding reaction	$J \cdot mol^{-1}$
J	Evaporation rate	$kg \cdot s^{-1}$
k_B	Boltzmann's constant (1.380×10^{-23})	$J.K^{-1}$
k_{obs}	Observed inactivation kinetic constant of β-galactosidase	s^{-1}
k_2	Irreversible complete denaturation rate constant of β-galactosidase	s^{-1}
k_c	Mass transfer coefficient	$m \cdot s^{-1}$
K_g	Constant in GAB sorption model	–
K_1	Unfolding equilibrium constant of β-galactosidase	$s.s^{-1}$
L	Length	m
m	Mass	kg

m_u	Parameter to describe the effect of moisture content on unfolding equilibrium of β-galactosidase	–
M_w	Molecular weight of water ($18 \cdot 10^{-3}$)	$kg \cdot mol^{-1}$
n	Number of partition	–
p	The uncertainty of the parameters	–
p_i	Parameter to describe the effect of moisture content on irreversible complete denaturation rate constant of β-galactosidase	–
P	Pressure	Pa
Pr	Prandtl number	–
Q	Heat	$J.s^{-1}$
r	Distance in radial coordinate	M
R	Ideal gas constant (8.314)	$J \cdot mol^{-1} \cdot K^{-1}$
Re	Reynolds number	–
R_d	Droplet radius	m
$\Delta S^{\ddagger}$	Activation entropy	$J \cdot mol^{-1} K^{-1}$
$\Delta\Delta S^{\ddagger}$	Activation entropy difference between unfolding and refolding reaction	$J \cdot mol^{-1} K^{-1}$
Sc	Schmidt number	–
t	Time	S
T	Temperature	°C
u	Velocity	$m \cdot s^{-1}$
V	Volume	m^3
x	Distance in Cartesian coordinate	m
x_w	Mass fraction of water	$kg \cdot kg^{-1}$
X_w	$\frac{x_w}{1-x_w}$, moisture content	$kg \cdot kg^{-1}$ DM
X_{wm}	Monolayer moisture content in GAB sorption model	$kg \cdot kg^{-1}$ DM
y	Distance in Cartesian coordinate	m
z	Distance in Cartesian coordinate	m
Z	Thickness	m

Greek symbols

δ	Hydrodynamic boundary layer thickness	m
δ_t	Thermal boundary layer thickness	m
λ	Thermal conductivity	$J{\cdot}s^{-1}m^{-1}K^{-1}$
μ	Dynamic viscosity	Pa·s
ρ	Density	$kg{\cdot}m^{-3}$
υ	Kinematic viscosity	m^2s^{-1}

Subscript

a	Air
avg	Average
cond	Conduction
d	Droplet
int	Intercept
m	Very dry matrix
obs	Observed
p	Flat plate for droplet deposition
ref	Reference
s	Solute
sat	Saturated
w	Water
0	Initial
∞	Bulk air

Appendix

Table 5-A1. The closure equations used in drying model

Equation name	Equation	Reference
Saturated vapour pressure	$\log\left(\frac{P_W^{sat}}{100}\right) = -7.90298\left(\frac{T_{st}}{T}-1\right)+$	(153)

	$5.02808 \log\left(\frac{T_{st}}{T}\right) - 1.3816 \cdot 10^{-7}\left(10^{11.344\left(1-\frac{T_{st}}{T}\right)} - 1\right) + 8.1328 \cdot 10^{-3}\left(10^{-3.49149\left(\frac{T_{st}}{T}-1\right)} - 1\right) + \log(e_{st})$ For vapour at total pressure 1 atm, T_{st} is 373.15 K and e_{st} is 1013.25 (in hPa).	
Water activity (Guggenheim-Anderson-de Boer model)	$\frac{X_w}{X_{wm}} = \frac{C_g \cdot K_g \cdot a_w}{(1-K \cdot a_w)(1-K_g \cdot a_w + C_g \cdot K_g \cdot a_w)}$	(154)
Heat and mass transfer coefficients	For a droplet suspended in air, used in the drying model for laboratory scale spray dryer $\frac{hd_d}{\lambda_a} = 2 + 0.6Re^{0.51}Pr^{0.33}$ $\frac{k_c d_d}{D_{w,a}} = 2 + 0.6Re^{0.51}Sc^{0.33}$ For a sessile droplet, used in the drying model for single droplet drying $\frac{hd_d}{\lambda_a} = 0.24 + 0.63Re^{0.51}Pr^{0.33}$ $\frac{k_c d_d}{D_{w,a}} = 0.24 + 0.63Re^{0.51}Sc^{0.33}$ with $Re = \frac{\rho_a d_d u_\infty}{\mu_a}$; $Pr = \frac{c_{p,a}\mu_a}{\lambda_a}$; $Sc = \frac{\mu_a \rho_a}{D_{w,a}}$	(62, 67)
Diffusion coefficient of water in maltodextrin solution	$D_{w,d,T=30°C} = exp\left(-\frac{35.8+215X_w}{1+10.2X_w}\right)$ $D_{w,d} = D_{w,d,T=30°C} exp\left(-\frac{E_a}{R}\left(\frac{1}{T} - \frac{1}{303.15}\right)\right)$ with $E_a = \frac{d+190X_w}{1+10X_w}$	(155)
Diffusion coefficient of water in air	$D_{w,a} = -2.775 \cdot 10^{-6} + 4.479 \cdot 10^{-8}T + 1.656 \cdot 10^{-10}T^2$	(156)

Chapter 6

Novel method for viability enumeration for single-droplet drying of *Lactobacillus plantarum* WCFS1

Published as:

Perdana, J., L. Bereschenko, M. Roghair, M. B. Fox, R.M. Boom, M. Kleerebezem, and M.A.I. Schutyser. 2012. Novel Method for Enumeration of Viable *Lactobacillus plantarum* WCFS1 Cells after Single-Droplet Drying. Appl. Environ. Microbiol. 78:8082-8088.

Abstract

Survival of probiotic bacteria during drying is not trivial. Survival percentages are very specific for each probiotic strain and can be improved by careful selection of drying conditions and proper drying carrier formulation. An experimental approach is presented, comprising a single droplet drying method and a subsequent novel screening methodology to assess the microbial viability within single particles. The drying method involves the drying of a single droplet deposited on a flat, hydrophobic surface under well-defined drying conditions and carrier formulations. (Semi-) dried particles were subjected to rehydration, fluorescence staining, and live/dead enumeration using fluorescence microscopy. The novel screening methodology provided accurate survival percentages in line with conventional plating enumeration and was evaluated in single droplet drying experiments with *Lactobacillus plantarum* WCFS1 as a model probiotic strain. Parameters such as bulk air temperatures and the carrier matrices (glucose, trehalose, and maltodextrin DE 6) were varied. Following the experimental approach, the influence on the viability as a function of the drying history could be monitored. Finally, the applicability of the novel viability assessment was demonstrated for samples obtained from drying experiments at a larger scale.

Keywords: viability, enumeration, probiotics, Anopore, single droplet drying

Introduction

Probiotics are defined as “live microorganisms, which when administered in adequate amounts, confer a health benefit on the host” (157). Health benefits are usually related to the influence of probiotic bacteria on the microbial balance in the hosts’ intestine or via modulation of the gut-associated immune system (158-162). Probiotics are delivered to the gastrointestinal tract as food products or dietary supplements; supplied on the market either as fermented food commodities, freeze-dried or frozen cultures, which enhances their stability and facilitates their implementation in appropriate product formulations (76, 163, 164). When compared to freeze drying and freezing, spray drying could be an interesting alternative for providing shelf-life to probiotic ingredients. Spray drying is more energy and cost efficient and can be operated continuously at higher production capacities (2, 5, 165). The major drawback of spray drying is the limited survival of probiotics (3, 24). Several studies have successfully explored approaches to increase the survival percentages after spray drying (18, 166-168). However, most of the results so far are very specific and difficult to translate between different species. It was for example found that a high variability exists between different strains of the same species (169, 170). In addition, the process conditions applied during spray drying (75, 165) and the protective carrier-materials added (3, 166) have strong influence on the final viability. Since these parameters need to be optimized for each specific case (different process parameters, different strains or species, and different carrier formulations used during drying), many cost-, time- and labour-intensive experiments are required.

This paper presents an experimental approach to assess probiotic survival during drying, starting with the drying of small single droplets deposited on a flat hydrophobic surface (67) followed by cell rehydration on Anopore chips (171), and subsequent evaluation of the microbial viability by fluorescence microscopy.

A recently developed single droplet drying method is used to produce powder particles dried under well-defined conditions to investigate the influence of drying process conditions and carrier formulations (64, 67). Specifically, drying parameters, such as droplet size, and temperature, relative humidity and flow rates of the air, can be varied effectively and systematically over wide ranges.

Critical to the assessment of the viability after drying is the availability of a rapid and reliable live/dead assay. The assay developed here employs a micro-porous aluminium oxide chip (Anopore) (171, 172). Following rehydration of the droplets, fluorescence probes are used for live/death enumeration using fluorescence-microscopy. This assay is compatible with medium- to high-throughput techniques, especially when compared to more conventional enumeration by plating. Moreover, the proposed method allows direct visualization of live and dead populations after drying without the requirement for growth. It has the potential to measure the viability in small sample volumes, i.e. the viability of bacteria present in a single powder particle. Subsequently, the method is applied to just as well assess the microbial viability in the particles obtained from single droplet drying experiments and from stabilization experiments at a larger scale. In our experiments, *Lactobacillus plantarum* WCFS1 was selected as the model bacterium. This selection is based on the fact that this *Lactobacillus* strain has been topic of extensive studies before (173) without per se *L. plantarum* being a probiotic bacterium.

Materials and methods

The entire experimental procedure can be divided into: 1) microbial culture preparation, 2) drying of single droplets, 3) particle rehydration and fluorescence-probe staining, and 4) fluorescence microscopy analysis automated relative viable cell enumeration (Figure 6-1).

Microbial culture preparation

A culture with high viability (> 99 %) was acquired by growing *L. plantarum* WCFS1 in 10 ml sterilized lactobacilli culture medium, MRS (BD Difco, USA) at 30 °C for 16 h. The final cell density approximated 10^9 colony forming unit (cfu) per ml.

The overnight culture was centrifuged using Eppendorf Centrifuge 5804R with F-34-6-38 rotor at 13.5 × g at 4 °C for 10 minutes. The resulting pellet was washed twice with phosphate buffered saline (PBS) solution (BD Difco, USA). To minimize washing stress, the pH of the PBS solution was adjusted to pH of 4, which is similar to the pH of the culture at the end of growth.

Single droplet drying experiments

Directly before the drying experiment was initiated, the washed bacterial cells were suspended in a carrier matrix, consisting of 20 % $^{w}/_{w}$ maltodextrin DE 6 (Glucidex 6,

Roquette, France), trehalose (Sigma-Aldrich, Germany) or glucose (Sigma-Aldrich, Germany). These carbohydrates are known to provide protection to bacterial cells (174, 175).

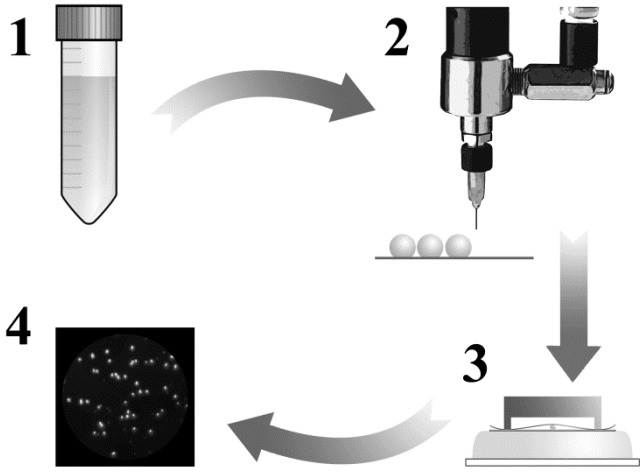

Figure 6-1. Schematic overview of the experimental procedure including 1) microbial culture preparation, 2) single droplet drying, 3) particle rehydration and fluorescence-probe staining, and 4) fluorescence microscopy analysis automated relative viable cell enumeration

The drying experiments were performed using the same equipment as described by Perdana et al. (64). The droplets were generated using a pneumatic dispenser of the Microdot 741 MD-SS series (Engineered Fluid Dispensing-Nordson, USA). The droplet deposition on the flat surface (5 x 20 x 0.2 mm) was automated using a XYZ positioning platform Ultra 525 TT Automation series (Engineered Fluid Dispensing-Nordson, USA). The dispensing needle AKA740TK precision tips (Engineered Fluid Dispensing-Nordson, USA) were coated with DOW Corning 340 heat sink compound (Dow Chemical, USA) to avoid droplets from creeping up along the outside of the needle.

Prior to the deposition of the droplets, the micro-dispensing system was flushed with sterilized Milli-Q water (Millipore, USA) followed by 70 % $^{v}/_{v}$ ethanol solution (VWR

International, France) and then rinsed again with Milli-Q water. The droplets were deposited on a flat hydrophobic membrane Accurel® type PP 2E HF (Akzo Nobel Faser AG, The Netherlands). To prevent microbial contamination, the membrane was sterilized with 70 % $^{v}/_{v}$ ethanol solution and dried under aseptic conditions at room temperature.

The droplets were dried using preconditioned, filtered (dust/microbes and oil free) drying air, heated to the desired temperature by leading it through a coil that was submerged in an oil bath (Julabo EH-5, Germany). The heated air was then fed to an insulated tunnel which acted as the drying chamber. The air temperature in the tunnel was monitored using a thermocouple Type K (NiCr-NiAl) (RS Component, United Kingdom) with a probe diameter of 500 µm. The air flow velocity was monitored (Type 1355, Brooks Instruments, The Netherlands). The tunnel was filled with a highly porous medium to develop an air flow with a uniform velocity. Meanwhile, the temperature was maintained by insulating the tunnel with heating oil. After the deposition of the droplets, the samples were placed in the drying chamber and dried using various drying times and regimes. The setup was equipped with a µEye 1480ME CCD camera with a lens with x9 magnification ratio (Imaging Development Systems GMBH, Germany) to monitor the droplet geometry evolution during drying.

The single droplet drying experiments were performed using dry air (RH = 0.0 %), preheated to a temperature between 25–70 °C and a bulk air velocity of 0.12–0.52 m/s. For each experiment, three identical droplets were dispensed and dried simultaneously. Biological duplicates were performed by repeating the experiments twice.

Rehydration and staining chip

The substrate for cell rehydration and staining was prepared by applying an Anopore chip (171) on a low-melting point (LMP) agarose gel (Sigma, The Netherlands). The gel was prepared by dissolving 1 g of agarose in 100 ml of Milli-Q water (Millipore, USA) and autoclaved (121 °C) for 20 min. The agarose solution was allowed to cool; after the temperature reached approx. 40 °C, 2 µL of a fluorescence staining probe Live/Dead BacLight Bacterial Viability Kit (Invitrogen, USA) was added to 10 ml of the agarose solution. The agarose solution was then spread on microscope slides (76 x 26 mm) and allowed to solidify for 30 minutes in a dark environment. Afterwards, a sterilized Anopore chip (8 x 35.6 mm; 60 µm thick; 0.2 µm pore size; 3×10^9 pores per cm^2; Microdish BV,

The Netherlands) was carefully placed on the agarose gel. The Anopore chips were sterilized by submerging it into 70 % $^{v}/_{v}$ ethanol solution for 2 h in falcon tubes. Subsequently, ethanol was decanted and the chips were dried in a sterile flow chamber for 12 h and then the tubes were tightly closed for storage. The Anopore chips were positioned on the agarose gel for at least 30 min prior to the rehydration of the dried particles. All preparations were carried out under aseptic conditions.

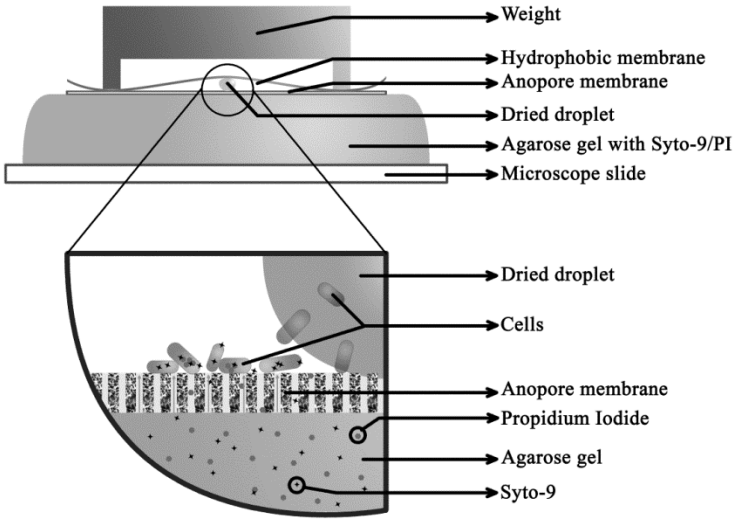

Figure 6-2. Schematic drawing of the rehydration and staining chip

Cell rehydration and enumeration

After drying, the powder particles were directly transferred to the rehydration and fluorescence staining substrate. The powder particles were transferred to the Anopore chip by turning the hydrophobic membrane upside down on the Anopore chip (Figure 6-2). A small weight providing 1.25 g/cm^2 pressure was put on top of the membrane to ensure contact between the membrane and the Anopore surface for the entire membrane surface. Therefore, rehydration could be considered as being universal and complete. After rehydration, the weight and hydrophobic membrane were removed carefully from the Anopore chip.

The rehydrated samples on the Anopore chip were analysed using a fluorescent microscope Axioskop 40FL (Carl Zeiss, Germany). Fluorescence images were captured with a magnification of x630 using an Olympus XC30 camera (Olympus, Japan) and Cell^{B} imaging software (Olympus, Japan). Due to decrease of fluorescence signal of the sample in time due to bleaching, the sample was not exposed to the light source for more than 5 min.

The BacLight Bacterial Viability Kit (Invitrogen) is composed of two nucleic acid-binding stains: Syto 9 and propidium iodide. Syto 9 can be internalized in cells depending on their membrane integrity and membrane potential, resulting in green fluorescent staining of cells that are alive. In contrast, propidium iodide can passively penetrate cells that have damaged membranes and therefore can be considered to be dead. The presence of propidium iodide within the cell can override the green signal of Syto 9, results in red fluorescent cells (176). The total viability is therefore calculated by differential enumeration of green and red cells. This method can be automated using an image processing routine as shown in Figure 6-3.

An in-house coded routine in Matlab 7.10.0 was developed to perform automated image processing and extract live/dead enumerations. First, the red and green channels of the resulting image from microscopy analysis were selectively split. Subsequently, the routine counted the number of cells for red and green channels separately (Figure 6-3). The package was able to evaluate multiple images at once; the resulting live and dead enumerations were automatically summarized.

Cell enumeration through plating

The results of the rehydration and enumeration method developed here were compared to the conventional enumeration of viable cells using plating on MRS agar. For this method, powder particles were suspended and dissolved in a 1 ml PBS solution for 30 min and subsequently diluted further to an appropriate dilution (10^{-1} and 10^{-2}). Subsequently, cfu enumeration was performed in duplicate by plating 50 µl of the suspension on MRS agar plates using an Eddy Jet 2 spiral plater (IUL Instrument, Spain). The plates were incubated at 30 °C for 48 h, following colony counting of the dilutions having between 30 and 300 colonies. The viability fraction was determined by dividing the number of colony for each treatment to the colony of the untreated sample, assuming 100 % viability in the untreated sample.

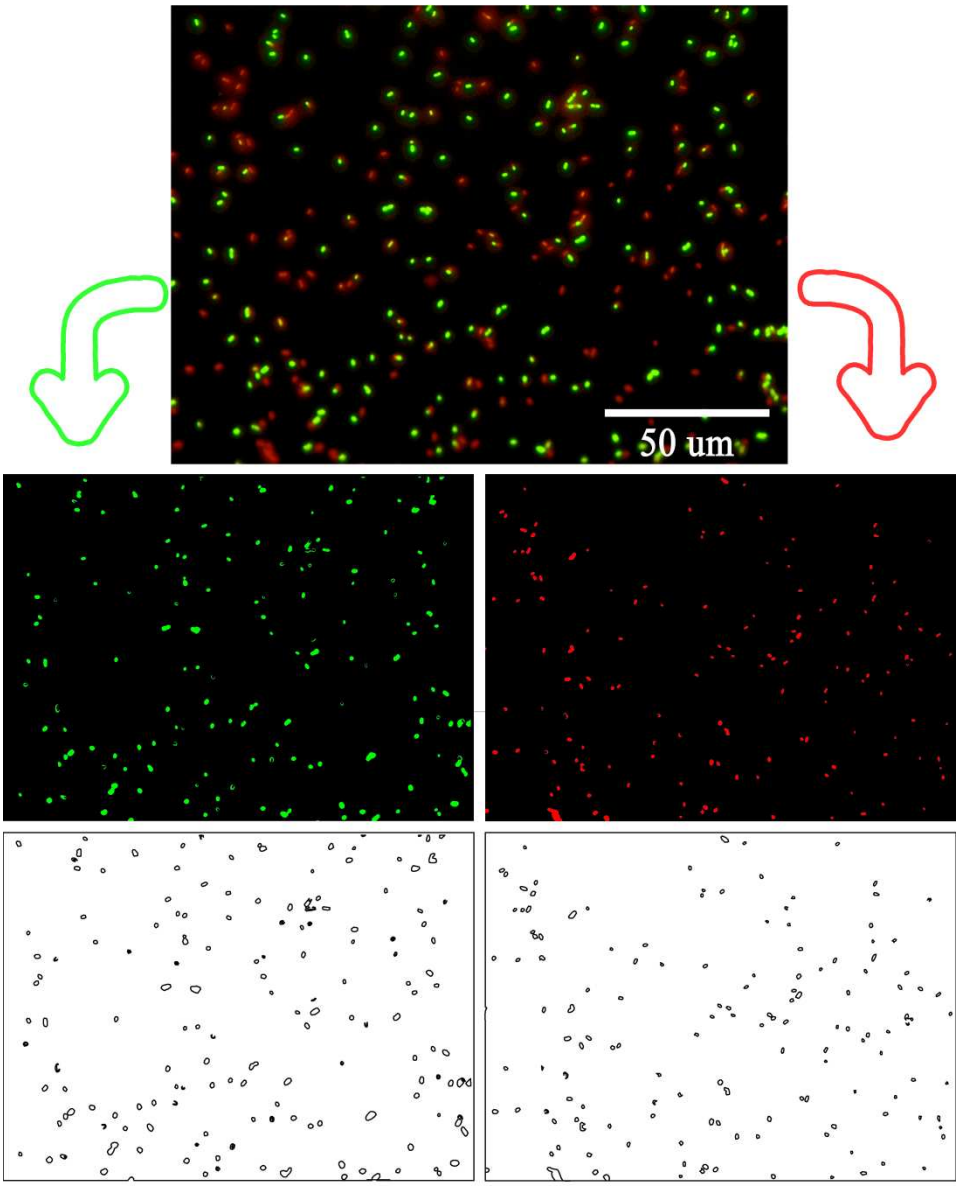

Figure 6-3. Live/dead counting. Top: Original fluorescence microscopy image of *L. plantarum* WCFS1 cells rehydrated on an Anopore chip observed with ×630 magnification. Middle: Red and green channels are separated. Bottom: Cell counting to determine the number of live (left) and dead (right) cells.

Spray drying experiments

Spray drying experiments were carried out in a Buchi B-190 spray dryer (Buchi Labortechnik AG, Switzerland). The outlet temperatures of the spray dryer were set between 50 and 90 °C and the inlet temperatures were set 30 °C higher than the applied outlet temperature. The resulting powder was further dried using contact air drying (ambient temperature, RH = 0 %) for 24 h, and was analysed for viability before and after drying. The viability analyses were done by spreading a small amount of the powder (approx.: 1 mg) to the rehydration and fluorescence staining substrate. Subsequently, a similar treatment was applied as to the droplets dried using single droplet drying method.

Moisture content analysis

The moisture content of the samples was analysed using the Sartorius MA 30 (Sartorius Mechatronic, Germany) gravimetric analyser. Approximately 1 g of sample was spread on an aluminium pan and put in the moisture content analyser, which heated the sample up to 130 °C for approximately 5 min.

Results and discussion

Method development

Optimum cell density for microscopic evaluation

The microbial enumeration is affected by too high or too low cell densities. High cell densities may induce flocking or lead to visual overlap of cells. Conversely, low cell densities may not provide sufficient numbers of cells for statistically significant enumeration. Therefore, an optimum cell density for the enumeration needs to be established. The current method allowed to determine viability percentages for maximally ~500 cells per image (2080x1544 pixels). For higher cell densities the enumeration routine may not provide accurate results due to the frequent overlapping fluorescence signals from different individual cells. Additionally, the viability fraction was evaluated as a function of the number of counted cells within an image, showing stable viability fraction between 200 and 500 cell density per image.

Rehydration time

The rehydration time is defined as the time between the transfer of the dried powder particle from the hydrophobic membrane to the Anopore chip and the subsequent removal of the hydrophobic membrane. The rehydration time is critical, since too short rehydration times may lead to transfer of only a small percentage of the cells to the Anopore surface.

We found that more than 90 % of the cells were transferred to the Anopore chip using rehydration times between 15 and 90 minutes. Additionally, the fluorescent dyes could be detected immediately following the transfer. During further experiments 15 minutes of rehydration time were used for transfer of the cells.

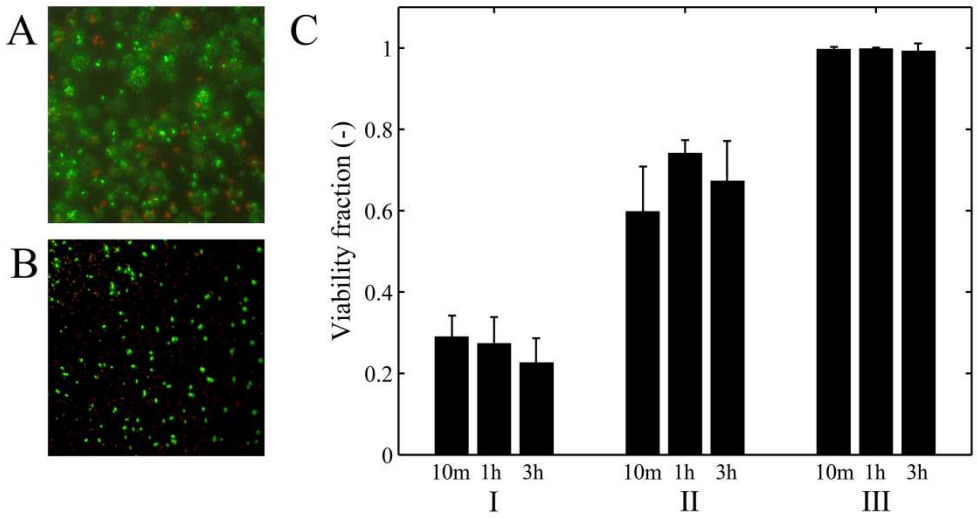

Figure 6-4. A: Image of a rehydrated particle observed under the microscope after 0 minutes of delay time. B: Image of a rehydrated particle observed under the microscope after 10 minutes of delay time. C: Residual microbial viability of particles dried under three different circumstances; droplet size of 600 μm dried with air temperature of 60 °C for 1 minute (I), air temperature of 25 °C for 5 minute (II), and air temperature of 25 °C for 1 minute (III), with varied delay times during particle rehydration for 10 minutes, 1 hour, and 3 hour. The error bars represent the standard deviation.

Time period between rehydration and microscopic analysis

For practical purposes it was evaluated whether a delay time between rehydration and fluorescence microscopy would be of influence to the final viability assessment. The major advantage of this delay time is that it facilitates the combination of the results from multiple drying experiments with a single subsequent viability assessment run. The delay time was evaluated for a time period between 0 and 3 hours. The delay time did not have significant impact on the viability assessment outcome (Figure 6-4C).

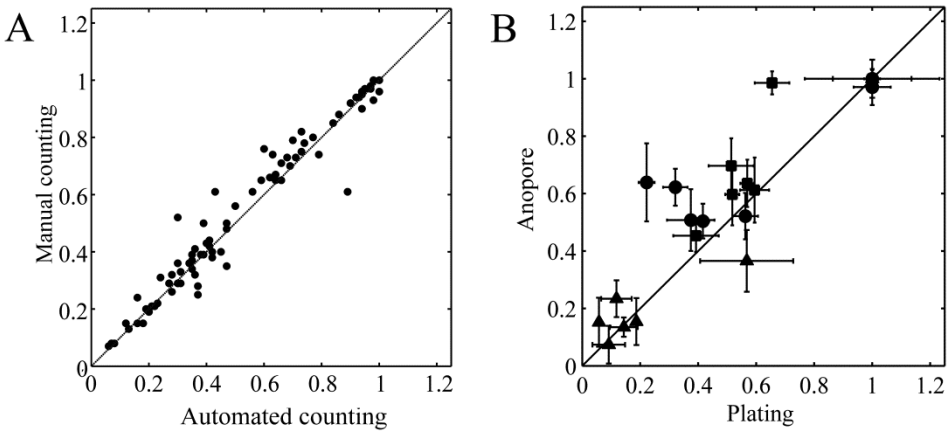

Figure 6-5. A: parity plot of the viability fractions obtained via the Matlab enumeration routine (x-axis) and the manual enumeration method (y-axis). B: parity plot of the viability fraction of *L. plantarum* WCFS1 assessed by conventional plating (x-axis) and the new enumeration method (y-axis). The samples were obtained by drying the *L. plantarum* WCFS1 in a 20 % maltodextrin for 10 min with hot dry air of 25 (●), 50 (■) and 70 °C (▲), a droplet size of 600 μm and an air velocity of 0.52 m/s.

However, the microscopic images obtained directly after removal of the hydrophobic membrane were substantially less sharp than the images obtained 10 min after membrane removal (Figure 6-4A and B). This might be explained by the presence of a thin water layer on the surface of the Anopore chip after the removal of the hydrophobic membrane, which

disappears upon exposure to air, either by evaporation or reabsorption into the agarose gel. The presence of a water layer may negatively affect the sharpness of the image due to the focus depth of the microscope. Therefore, a minimum delay time of 10 minutes was used between membrane removal and microscopy analysis, while the maximum delay time was fixed at 3 hours.

Final evaluation of the viability assessment method

The enumeration of live and dead cells was carried out with a Matlab routine. These results were compared to manual enumeration. Eighty images were selected randomly; the viability fraction for every image was determined manually and compared to the result from the Matlab enumeration routine. Both methods generated similar counts (Figure 6-5A), which validates the automated enumeration routine. The total number of counted cells should be such that an accurate value of the viability fraction is obtained. A total number of 200 cells was found sufficient to obtain an accurate value. From this and previous results it can be concluded that the ideal cell density lies between 200 and 500 per image. Finally, the fluorescence microscopy based viability enumeration was compared to results obtained via conventional plating. Both enumeration methods generate similar viability counts (Figure 6-5B), which validates the fluorescence microscopy method.

Application of the viability assessment method

Inactivation during single droplet drying

The novel and validated assessment method was subsequently applied to evaluate the effect of the drying history on the viability loss of *L. plantarum* WCFS1. A single drying droplet method was used to generate droplets with the bacteria suspended in different carbohydrates (20 % $^{w}/_{w}$).

The residual viability decreased with drying time at different bulk air temperatures (Figure 6-6). A higher bulk air temperature led to a significantly increased loss in viability. Almost all loss in viability occurs in the first minutes of the process ($t < 5$ minutes), after which the residual viability remained more or less constant. This loss in viability corresponds to a period of rapid drying, while the subsequent period with constant viability shows little or no further decrease in moisture content. The small decrease in residual viability during the

latter period can be explained by the immobilization of the bacteria in a rigid matrix, which slows down the inactivation process (174).

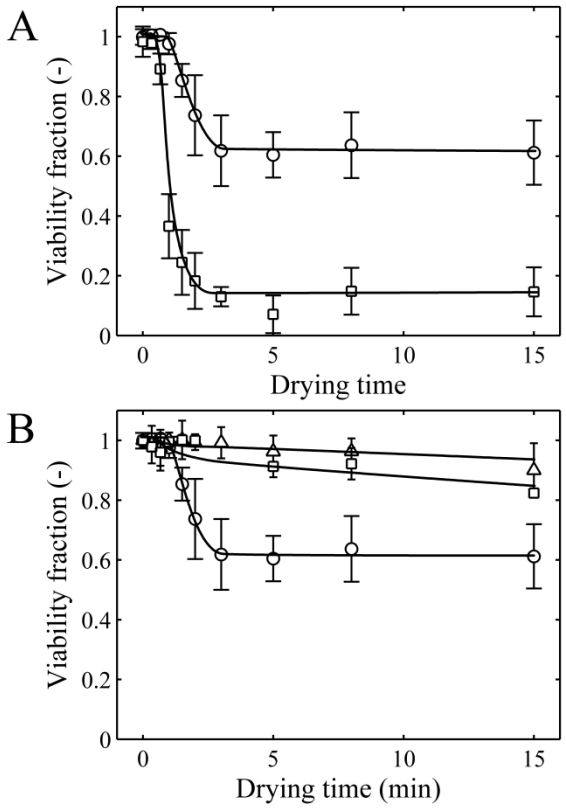

Figure 6-6. A: Viability fractions after drying with air temperatures of 25 (○) and 70 °C (□), and an air velocity of 0.52 m/s. B: Viability fractions after drying with different carrier formulations of glucose (Δ), trehalose (□), and maltodextrin DE6 (○) dried with air temperature of 25 °C and an velocity of 0.52 m/s. Initial concentrations of the formulations were 20 % $^{w}/_{w}$. The average droplet size was 600 μm. The error bars represent the standard deviation and the solid lines are guidelines.

Subsequently, the influence of the carrier-matrix on survival was examined. Low molecular weight carbohydrates (glucose and trehalose) provided better protection to the cells during drying than maltodextrin DE 6 (Figure 6-6).

Two hypothetical mechanisms exist on how sugar molecules protect the cell membrane from leakage by minimizing the chance of membrane phase transition (177). The first mechanism is proposed to act via water replacement. In fully hydrated conditions, the cell membrane lipids are in undisturbed liquid-crystalline form. According to this hypothesis, sugar molecules replace water in the hydration shell of the cell membrane; thereby maintaining the spacing between the phospholipid molecules (178). In this case, lower molecular weight sugars, e.g. glucose and trehalose, can provide better protection because of their better ability to enter the spacing between phospholipid molecules compared to higher molecular weight molecules or polymers, in this case maltodextrin (179). The second mechanism is proposed to act via the hydration force (vitrification hypothesis) (24). During drying the presence of sugar molecules hinders water removal from the surface of the cell membrane due to the high osmotic pressure. At the same mass concentration, lower molecular weight molecules are able to provide a higher osmotic pressure and thus provide more protection than larger molecules or polymers. In the glassy state, the rigidity and the mechanical properties of the sugar matrix limits the possibility for the cell membrane to collapse. Therefore, the protective ability of different sugars can be related to their glassy forming ability; where higher glass transition temperature of the sugar is found to contribute to increased protection. Based on this, trehalose could be expected to provide more protection than glucose due to its higher glass transition temperature. However, the viability results do not confirm this effect (Figure 6-6); although the differences in (high) viability were not significant.

Inactivation in a laboratory-scale spray dryer

Since the viability assessment method allows more rapid detection compared to conventional plating, it was applied to check the viability loss of *L. plantarum* WCFS1 during spray drying at a larger scale than single droplets. The method selected was spray drying with a laboratory scale spray dryer at various inlet-outlet temperature combinations, followed by (ambient temperature) air drying.

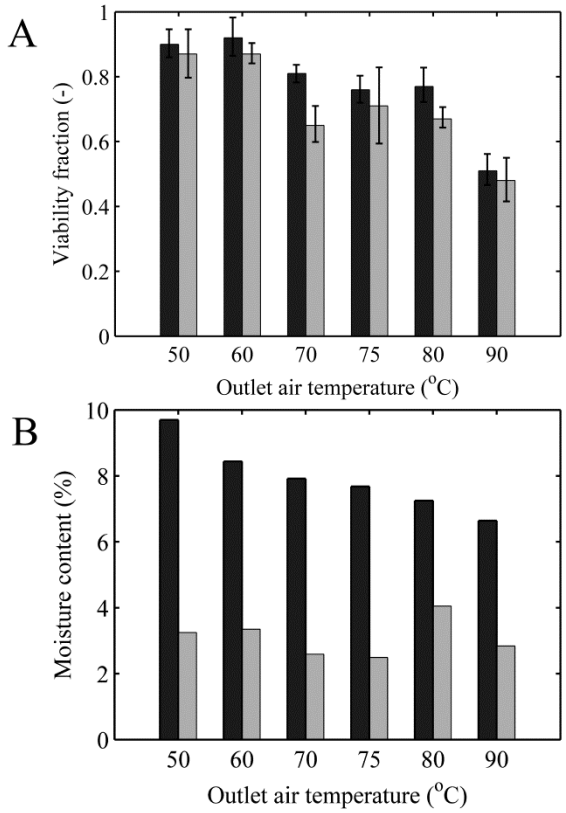

Figure 6-7. A: The viability fraction of *L. plantarum* WCFS1 after spray drying in 20 % $^{w}/_{w}$ maltodextrin DE 6 at various outlet air temperatures (black bars). Subsequently, samples were dried for 24 h in a desiccator at ambient temperature and viability was assessed again (grey bars). The inlet temperatures of the spray drying air were fixed 30 °C above the outlet temperatures. B: The corresponding moisture contents of the powder after spray drying (black bars) and after the subsequent drying for 24 h (grey bars).

Lactobacillus plantarum WCFS1 was found to be susceptible to inactivation even with a mild spray drying process. Although drying in a laboratory-scale spray dryer was very fast (less than 1 s residence time) more than 10 % reduction in viability was observed, which

increased considerably with applied air temperatures (Figure 6-7). Subsequent additional drying for 24 h at ambient temperature reduced the residual viability only slightly, which again can be related to vitrification due to glassification (15, 24).

Outlook on the application of the new viability enumeration method

The enumeration method developed here is generic as the stains applied in the method are widely applied to detect viability of micro-organisms. Furthermore, powder particles formulated with different drying or stabilization methods at different scales or the impact of storage conditions on microbial viability can be assessed using this new method.

The proposed enumeration method is complementary to the traditional plating method. Traditional plating provides information on cell numbers of living bacteria on a log10 scale, whereas the new method provides a live-dead ratio, i.e. 1 to 100 % viability. The new method can distinguish for example between 20 % and 60 % viability, while traditional plating is able to distinguish between living cell concentrations, e.g. 10^7 and 10^5 cfu/ml. For optimisation of microbial viability during drying processes, the live-dead ratio may be preferred as it is most sensitive and accurate near the maximum percentage living cells. A possible drawback of the new method is that it is less sensitive at small living cell numbers.

Conclusion

A novel method was developed to determine the microbial viability of probiotics in small samples, such as single powder particles. The method employs Anopore carrier chips for rehydration of (semi-) dried particles followed by live/dead staining using fluorescence probe methodology. The enumeration was carried out by microscopy and automated image analysis using a Matlab routine. The robustness of the method was evaluated and validated with conventional plating. In combination with a single droplet drying approach the influence of the drying air temperature and carrier formulation on viability loss of *L. plantarum* WCFS1 was mapped as a function of drying time. The latter approach can be also of major support in determining optimal drying conditions and formulations for spray drying of probiotics.

Chapter 7

Dehydration and thermal inactivation of *Lactobacillus plantarum* WCFS1: comparing single droplet drying to spray and freeze drying

Submitted for publication as:

J. Perdana, L. Bereschenko, M.B. Fox, J.H. Kuperus, M. Kleerebezem, R.M. Boom, and M.A.I. Schutyser. Dehydration and thermal inactivation of *Lactobacillus plantarum* WCFS1 by comparing single droplet drying to spray and freeze drying.

Abstract

We demonstrated that viability loss during single droplet drying can be explained by the sum of dehydration and thermal inactivation. For *Lactobacillus plantarum* WCFS1, dehydration inactivation predominantly occurred at drying temperatures below 45 °C and only depended on the moisture content. Above 45 °C the inactivation was due to a combination of dehydration and thermal inactivation, which depended on the moisture content, temperature, and drying time. A Weibull model was successfully applied to describe the thermal and dehydration inactivation and enabled the prediction of residual viability of *L. plantarum* WCFS1 after single droplet drying. Subsequently, the model was evaluated to predict the viability loss during laboratory scale spray drying, showing a remarkable agreement if assumed that only thermal inactivation occurred. This indicated that very high drying rates in laboratory scale spray drying could induce instant fixation of the cell suspensions in a vitrified matrix and thereby preventing dehydration inactivation. Finally, the influence of drying rate on remaining viability was evaluated by comparing single droplet drying, freeze drying and laboratory scale spray drying of the same bacterial suspension. It was shown that slow drying leads to large dehydration inactivation, which diminished in fast drying processes such as laboratory scale spray drying where thermal inactivation appears to be the predominant mechanism of inactivation.

Keywords: probiotics, inactivation mechanism, spray drying, freeze drying, single droplet, predictive modelling

Introduction

Drying is a common method to stabilize ingredient formulations or foods containing micro-organisms such as bacteria and yeast for a prolonged period of time (1, 43, 76, 180). In dehydrated form, stored under appropriate constant conditions, micro-organisms can remain viable in a unique vitrified state for very long times, even years. Upon rehydration, cells rapidly swell and resume their active living state. This phenomenon is known as anhydrobiosis (43), which is literally translated as "survival without water". For example, spray drying is a frequently applied industrial technique to dehydrate yeast cells and other micro-organisms (181). Unfortunately, drying of heat-vulnerable micro-organisms such as probiotics is problematic because of relatively poor survival rates (1, 5). Therefore, for the latter micro-organisms, lyophilisation (freeze drying) is applied, a more energy-consuming operation, which is commonly operated in a batch-wise manner (12).

Inactivation of micro-organisms during drying is elicited by dehydration and/or thermal shocks (5, 24, 44, 182). The inactivation by dehydration is hypothesized to be related to a loss of lipid bilayer integrity and impairment of cell membrane functions. Removal of the hydration layers around the lipid bilayer may cause loss of the plasticity of the membrane (gelling), which is held responsible for the collapse of the bilayer, finally resulting in loss of viability (43, 177-179). Thermal inactivation is related to structural damage and/or denaturation of key cell components such as ribosomes, nucleic acids, enzymes, and the cell membranes (183).

In previous studies we developed an experimental set-up that allows the drying of diminutive single droplets deposited on a surface under well controlled conditions (67). The drying of these droplets mimics the drying of a droplet in a spray dryer. Subsequently, this approach was used to determine the inactivation kinetics of the enzyme β-galactosidase as a function of the moisture content and the temperature during drying (64).

In this study the single droplet drying method was combined with a recently developed rapid cell enumeration method based on rehydration of dried particles on a micro-porous aluminium oxide (Anopore) chip and live-dead enumeration using fluorescence microscopy (5) to test the microbial inactivation during drying. Using this approach, we investigated the dehydration and thermal inactivation mechanisms for *Lactobacillus plantarum* WCFS1 and translated this insight to predict the residual viability during laboratory spray drying under

various conditions. *Lactobacillus plantarum* WCFS1 was also used as an exemplary lactic acid bacterium in our previous study (5, 173) and has been extensively studied in relation to its host microbe interactions in the gastrointestinal tract (for reviews see: (161, 162)).

The two inactivation mechanisms were modelled to describe the effect of the drying history on residual viability of *L. plantarum* WCFS1. The model considers the combined effects of the history in temperature and moisture content. The predictions from single droplet drying experiments were further validated and explored using laboratory scale spray drying trials. Finally, three drying methods (single droplet drying, freeze drying and spray drying) were compared to specifically evaluate the effect of the drying rate on inactivation by dehydration.

Materials and methods

Preparation of the samples for drying experiments

The strain of *Lactobacillus plantarum* WCFS1 was obtained from NIZO Food Research (The Netherlands). The frozen strain (-26 °C) was grown in 10 ml sterilized *Lactobacilli* MRS broth (BD Difco, USA) at 30 °C for 16 h. An aliquot of 1 % of the culture was transferred and re-grown in the same conditions to obtain the second generation culture. An aliquot of 1 % of the culture was again transferred and re-grown in the same conditions. This overnight culture contained approximately 10^9 cfu/ml. Bacteria were harvested by centrifugation (10 minutes at 13,500 g at 4 °C). The pH of the culture supernatant was determined. The bacterial pellet was washed twice with 10 ml phosphate buffered saline (PBS) solution (BD Difco, USA) adjusted to pH 4.0.

The samples for drying experiments were prepared by 10-fold diluting the cell suspension in PBS solution. The diluted cell suspension was again 2-fold diluted with sterilized maltodextrin (DE 4-8, Glucidex 6; Roquette, France), fructose, galactose, sucrose, lactose, sorbitol, mannitol, or trehalose (Sigma-Aldrich, Germany) solutions with solid content of 40 % $^{w}/_{w}$. By this, a working solution with approximately $5 \cdot 10^7$ cfu/ml cell concentration and 20 % $^{w}/_{w}$ maltodextrin was obtained and used for single droplet drying, spray drying, and freeze drying experiments.

Single droplet drying experiments

The drying experiments were done in the single droplet drying equipment developed in our previous research (67, 75). A micro-dispenser was used to deposit three identical droplets on a flat hydrophobic membrane. Subsequently, the deposited droplet was dried in a well-defined air flow with specific temperature and relative humidity as specified in the results and discussion section. The experiments were carried out in duplicate. Subsequent viability analyses were done by blotting the (semi-) dried droplets on an Anopore chip.

Spray drying experiments

Spray drying experiments were carried out in a Buchi B-190 spray dryer equipped with a two-fluid nozzle (Buchi Labortechnik AG, Switzerland). The process parameters for spray drying experiments are specified in the results and discussion section. Batches of 20 ml feed solution were spray dried, which requires approximately 5 minutes. The experiments were carried out in duplicate. The viability analysis involved spreading and rehydration of a small amount of powder (approx. 1 mg) on an Anopore chip.

Freeze drying experiments

Five ml aliquots of working solution were frozen to -26 °C for 24 h. After freezing, the residual viability of *L. plantarum* WCFS1 was always higher than 95 %. The frozen samples were directly transferred to a Christ Epsilon 2-6d freeze dryer (Martin Christ, Germany) for the lyophilization. The samples were frozen at -20 °C for 2 h prior to the main drying step at -20 °C for 0.2 h at a pressure of 1.03 mbar. Subsequently, the temperature was raised to -10 °C in 4 h. The subsequent drying was done at -10 °C for 4h, while maintaining the pressure at 1.03 mbar. Afterwards, the shelf temperature was raised to -5 °C at 1.03 bar for 12 h. Finally, the pressure was decreased to 0.001 mbar for 6.5 h for final drying. The typical water content of the freeze-dried sample was between 5 and 8 %.

Moisture content measurement

The moisture content on wet basis was determined using a Sartorius MA 30 (Sartorius Mechatronic, Germany) gravimetric analyser. Approximately 2 g of powder was spread on an aluminium pan and put in the moisture content analyser, which heated the powder up to 130 °C until the mass equilibrated to a final value; approximately 5 min heating time was needed.

Cell rehydration and viability enumeration

For viability enumeration, approximately 10 mg of powder was transferred and rehydrated on a sterilized Anopore (aluminium oxide nanoporous) chip (Microdish BV, The Netherlands) that was on top of a 1 % low melting point (LMP) agarose (Invitrogen, USA) gel containing 0.02 % fluorescent stains of Live/Dead BacLight bacterial viability kit (Invitrogen, USA). This viability kit is composed of the reagents Propidium Iodide (1.67 mM) and Syto 9 (1.67 mM) dissolved in dimethyl sulfoxide (DMSO). The rehydrated powder were incubated for 30 minutes and subsequently excited by 470 nm light to induce a fluorescent spectral shift to green (life) or red (dead), which could be observed with the microscope. The viability values were obtained from the number ratio of green cells and total cells in the image. Approximately 20 images with 200 to500 cells per images were taken for each viability assessment. A more detailed description of the method is provided in Perdana et al. [28].

Description of temperature and moisture content for single droplets

It is virtually impossible to measure the temperature and moisture content history of a single dried particle. Therefore, temperature and moisture content (including the moisture developing gradient) were predicted using an effective diffusion model. This model is extensively described by Perdana et al. (64, 67). To describe the temperature and moisture content history of spray dried particles, the model was modified by taking into account the heat and mass balance within the spray drying tower. To reduce the modelling complexity, the sizes and drying times of all particles were assumed identical. The average particle diameter of spray dried particles ($d_{4,3}$) was determined by a Mastersizer Scirocco 2000 (Malvern Instrument LTD, England) and the drying times were assumed to be 1.5 s according to the technical specifications of the spray dryer (184, 185).

Model implementation and statistical evaluation

The parameter optimisation was carried out using a non-linear least square method solved using the Levenberg-Marquardt algorithm (128). The confidence intervals of the parameters ($p = 0.95$) were estimated using the Hessian matrix, which was again derived from the Jacobian matrix of the solution (129). All calculations were performed with MATLAB version 7.10.0.

Results and discussion

Single droplet experiments were carried out to assess the inactivation kinetics at different drying temperatures for *L. plantarum* WCFS1. In the next two sections, we separately discuss the experiments carried out at low temperatures (< 45 °C) and at high temperatures (>45 °C), because different inactivation behaviour was observed.

Viability loss during single droplet drying at low temperature

The residual viability of *L. plantarum* WCFS1 is shown in Figure 7-1B for single droplet drying experiments at air temperatures between 25 °C and 45 °C. It was observed that viability remained constant during the initial phase of the drying (1 to 2 minutes), followed by a sharp decrease and subsequent levelling off (Figure 7-1A and 1B). The decrease in viability occurred faster with smaller droplets because these droplets dry faster. Despite different time periods of the initial drying until viability decrease was observed, the final residual viability was similar for all droplet sizes and drying air temperatures evaluated (Figure 7-1B).

By plotting the residual viability as a function of the average moisture content of the particle, one can see that viability loss strongly correlates with the moisture content (Figure 7-1C), in a manner that is independent of the drying time and drying rate applied (e.g. by varying the drop size). The highest inactivation rates were found to occur within a narrow range of moisture contents between approx. 0.1 and 0.35 kg/kg (Figure 7-1C). When considering the state diagram of maltodextrin (30), this critical region corresponds to the rubbery state, whereas the region below 0.1 kg/kg corresponds to the glassy state. In the latter region the dehydration inactivation rate observed was considerably lower.

The sharp viability loss in the critical region may be explained by two potentially co-occurring phenomena, or a combination of these: (i) during drying, water is removed from the hydration layer of the lipid bilayer of the cells causing destabilization, especially when the availability of free water is minimal. At this critical level, the bound water starts being removed from the solid matrix outside the cells or even the intracellular water (177, 178) and (ii) removal of water leads to an increase of the difference in osmotic pressure across the cell membrane due to the accumulation of solute outside the cell, which becomes a driving force for water migration across the cell membrane. This process can lead to an irreversible collapse of the cell membrane (14, 24, 186).

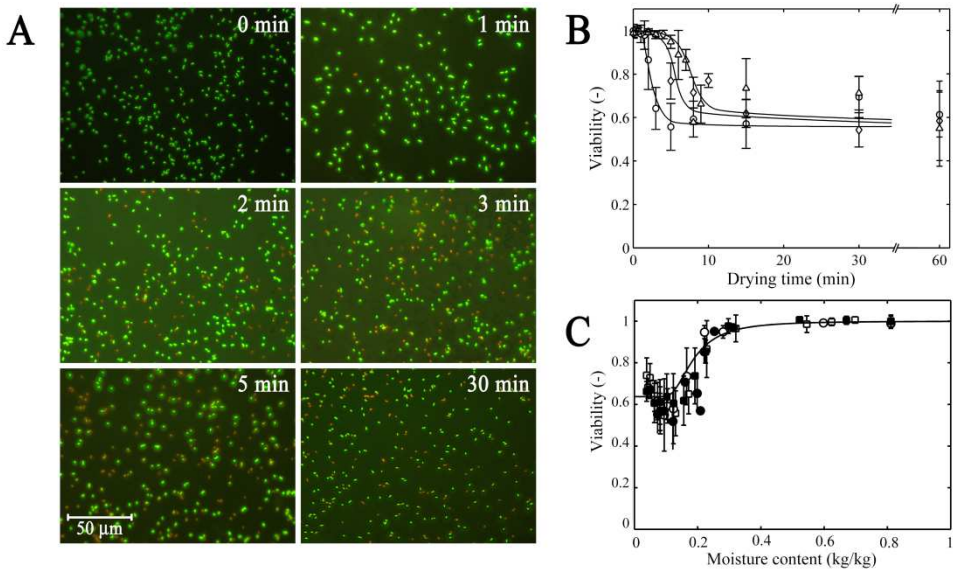

Figure 7-1. A: Microscopy images of *L. plantarum* WCFS1 dried by single drop drying using air at 25 °C for 0, 1, 2, 3, 5, and 30 min with a drop size of 600 µm following subsequent rehydration on Anopore chips and staining with live/dead probes. B: Residual viability of *L. plantarum* WCFS1 as a function of the drying time, dried using air at 25 °C with a droplet size of 600 (○), 900 (◊), and 1500 µm (Δ) µm. C: Residual viability of *L. plantarum* WCFS1 as a function of the average, time dependent moisture content of the droplet, dried using air at 25 (open symbols) and 40 °C (closed symbols) with droplet sizes of 600 (○), and 1500 µm (Δ), air of 40 °C at droplet size of 600 µm (▲), and air temperature at 45 °C with a droplet size of 600 (■), and 1500 µm (♦). For representation, not all data for optimization were presented here. The initial formulation is 20 % $^{w}/_{w}$ maltodextrin DE 6 and a cell concentration of approximately 5.0×10^{7} cfu/ml. The relative humidity of the drying air was set to 0 %.

One can conclude from Figure 7-1C that at the respected drying rate (with approximately 1 to 10 minutes of drying time) primarily the moisture content as such is determining dehydration inactivation and not the rate at which water is removed. The limited

availability of water in the matrix is the key factor for destabilisation of the cell membrane at mild temperatures. It can also be concluded that at drying temperatures below 45 °C, the effect of temperature on inactivation is not critical as the residual viability does not decrease below a certain minimum level.

A modified Weibull model was used to describe the relation between moisture content and viability loss during drying. This was based on the assumption that only moisture content determines viability loss at the lower drying temperatures (< 45 °C). Furthermore, biological variation was taken into account as the Weibull model is basically a statistical model of distribution of inactivation (35)

$$A_D - A_\infty = (A_0 - A_\infty) exp\left(-\left(\frac{x_w}{x_{crit}}\right)^{\beta_w}\right) \quad (7\text{-}1)$$

in which A_D is the cumulative amount of residual viable cells after dehydration inactivation, A_0 and A_∞ the fraction of residual viable cells in the initial ($x_w >> 0$) and in the final drying state ($x_w = 0$) respectively, x_w the moisture content, and x_{crit} and β_w the Weibull distribution parameters. The parameter x_{crit} can be related to the critical moisture content at which the inactivation rate is highest, while the parameter β_w to the sensitivity of the viable cells to the moisture content. The model accurately described the viability loss of *L. plantarum* WCFS1 during mild temperature drying. The model optimization result showed these critical conditions during drying on the viability loss (Table 7-1).

Table 7-1. Optimized parameter values for dehydration inactivation model

Parameter	Value	Confidence interval[a]	
x_{crit}	0.17	(0.0069)	4.1 %
β	-3.14	(0.48)	15.4 %
A_∞	0.64	(0.0098)	1.5 %

[a] The uncertainty of the parameters at 95 % confidence interval

Viability loss during single droplet drying at high temperature

With air drying temperatures above 45 °C, the residual viability decreased with increasing air temperature and droplet diameter. Thus, besides dehydration inactivation also thermal inactivation should play a role in loss of viability under these conditions. It was assumed that both inactivation mechanisms were co-occurring but uncoupled; a cell might lose its viability due either to dehydration, to thermal, or to both shocks.

The total viability loss was calculated by accumulating the effects of dehydration and thermal inactivation. Based on the previous observation, the dehydration inactivation in single droplet drying is only dependent on the moisture content. Meanwhile, the thermal inactivation is a function of temperature, moisture content, and time as well. To combine both mechanisms, the average moisture content of the droplet has to be described as a function of drying time. The latter can be approximated with an effective diffusion model for drying of single droplets (64). Residual viability is calculated by first accounting for inactivation for dehydration inactivation (Eq. 7-1). Subsequently additional thermal inactivation is accounted for.

$$A = A_D \cdot A_T \tag{7-2}$$

where A is the residual viability at drying time t, and A_D and A_T are the residual viability after dehydration inactivation (as a function of x_w, calculated using Eq. 7-1) and after thermal inactivation respectively. The thermal inactivation can be described using a Weibull model. Finally, the residual viability taking into account both dehydration and thermal inactivation could be estimated as

$$A = A_D \exp\left(-\left(\frac{t}{\alpha}\right)^{\beta_T}\right) \tag{7-3}$$

where α and β_T are the Weibull parameters for thermal inactivation. It was found appropriate for our viability range of interest to assume that $\beta_T = 1$ (see Appendix and its Figure 7-A1).

Similar to our previous research on enzyme inactivation, we assumed that both temperature and moisture content influence the thermal inactivation (68), which could be described with the Weibull parameter α:

$$\alpha = \alpha_{w,T} exp\left[\ln\left(\frac{\alpha_{s,T}}{\alpha_{w,T}}\right) exp\left(-p\frac{x_w}{1-x_w}\right)\right] \quad (7\text{-}4)$$

with

$$\log(\alpha_{w,T}) = \log(a_{w,Tref}) - b_w(T - T_{ref})$$

and

$$\log(\alpha_{s,T}) = \log(a_{s,Tref}) - b_s(T - T_{ref}) \quad (7\text{-}5)$$

in which α_w and α_s are the Weibull inactivation parameters at x_w = 1 and x_w = 0, respectively, at temperature T, and p is a parameter that describes the dependency of parameter α on the moisture content. The temperature dependencies of parameter α_w and α_s are described with the empirical model (Eq. 7-5) with optimized parameters of α_{Tref} and b (36).

Table 7-2. Optimized parameter values for the thermal inactivation model

Parameter	Value	Confidence interval[a]	
$\alpha_{w,Tref}$[b]	3.48	0.64	18.3 %
b_w[b]	0.18	0.013	7.6 %
$\alpha_{s,Tref}$	$108.49 \cdot 10^3$	$32.14 \cdot 10^3$	29.6 %
b_s[b]	0.11	0.0046	4.2 %
p	0.98	0.11	11.5 %
β_T[c]	1		
T_{ref}[c]	50 °C		

[a] The uncertainty of the parameters at 95 % confidence interval

[b] Parameter values from separate isothermal heating experiments

[c] Not optimized

The parameters ($\alpha_{w,Tref}$ and b_w) that determine the parameter α_w were obtained from separate isothermal heating experiments. These experiments were carried out at a moisture content of 80 % $^{w}/_{w}$ to obtain the microbial inactivation kinetics under dilute conditions, where α is not sensitive to the moisture content (Figure 7-2C, see also Appendix).

The values of parameters $\alpha_{s,Tref}$ and b_s were obtained from isothermal heating experiments at a moisture content of 8 %. At this low moisture content, the parameter $\alpha_{s,Tref}$ is sensitive to the moisture content, but parameter b_s is less sensitive, which resembles the observations made while studying enzyme inactivation kinetics during drying (68). Based on this, $\alpha_{w,Tref}$, b_w, and b_s could be fixed, which improves the accuracy of the fitting because only two parameters now had to be found through fitting, i.e. parameters $a_{s,Tref}$ and p (Table 7-2). The data were collected at drying temperatures of 50, 60, and 70 °C and varying droplet sizes of 600, 900, and 1500 µm.

The residual viability as a function of drying time for *L. plantarum* WCFS1 shows a similar trend as that observed for drying at temperatures below 45 °C; i.e. at first the viability remains more or less constant for a very short period of time, then decreases rapidly, and finally remains at a relatively stable value. The final residual viabilities were lower at a higher drying temperature (Figure 7-2A), which is different from the observation with drying below 45 °C. Nevertheless, the final residual viability remained unaffected by extended periods of exposure to high temperatures provided that the cells were appropriately dehydrated. This was confirmed by the optimization results provided in the contour plot showing that at a moisture content lower than e.g. 0.2 the thermal inactivation kinetic parameter (α) was already irrelevant: it could not change the residual viability in the course of the drying time; e.g. at 80 °C, the value of α for x_w = 0.05 is approx. 40 min, which requires 5 min for 10 % viability loss at this low moisture content (Figure 7-2C).

Thus, we observe good agreement between the model and the residual viability data from single droplet drying experiments. This provides a basis to predict the viability loss in larger scale spray drying.

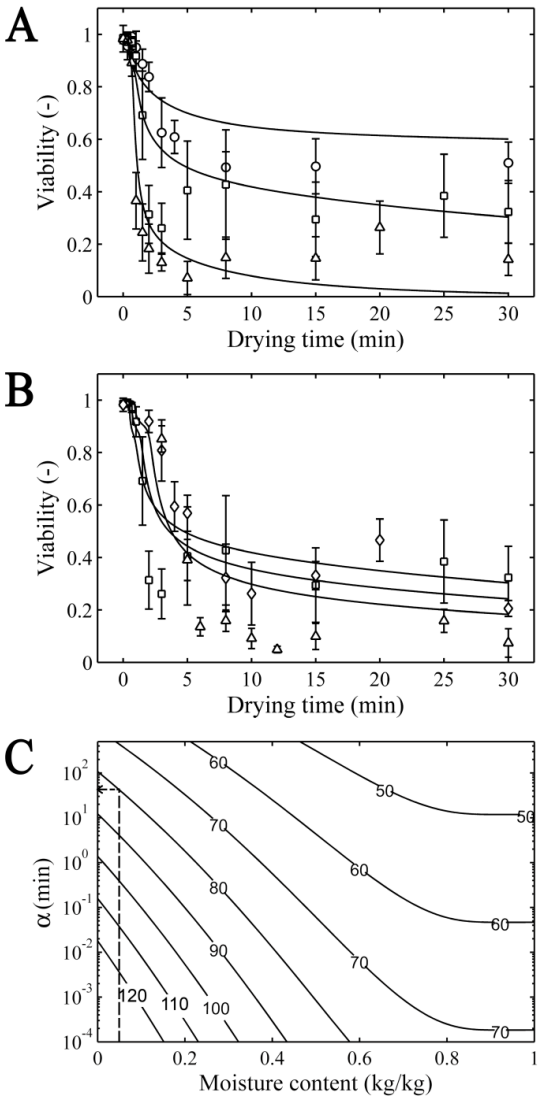

Figure 7-2. A: Residual viability of *L. plantarum* WCFS1 dried with air at 50 (○), 60 (□), and 70 °C (Δ), relative humidity of 0 %, and droplets of 600 µm. B: Residual viability of *L. plantarum* WCFS1 dried with air at 60 °C, relative humidity of 0 %, and droplets of 600 (□), 900 (◊), and 1500 µm (Δ). Solid lines represent the fitted model and error bars represent the standard deviation. C: Contour plot of T as a function of x_w and α.

Translating the results from single droplet drying approach to spray drying

The predictive model developed to describe the viability loss of *L. plantarum* WCFS1 was evaluated for spray drying on laboratory scale. The effective diffusion model was used to estimate the temperature and moisture content history of a single droplet during spray drying (64, 75). The temperature and moisture content history of powder particles was approximated with the assumption that particle size and particle residence time during spray drying are identical for all powders. The microbial inactivation model was incorporated into the diffusion model. Subsequently, the residual viability of *L. plantarum* WCFS1 was predicted for varying spray drying conditions and compared to experimental drying results.

Spray drying experiments were carried out at varying inlet and outlet temperatures. The residual viability and the final moisture content of the powders were monitored (Figure 7-3). In contrast to the results from single droplet drying experiments, a very high fraction of cells remained viable (more than 95 % compared to the cell viability in the original suspension) at outlet air temperatures below 70 °C. This high survival is in agreement with previous studies (15, 45, 175). It may be explained by the absence of dehydration inactivation during laboratory-scale spray drying, in which the drying rate is very high (typical drying time of a droplet is between 1 and 1.5 s according to the technical specification of the dryer (184, 185)) compared to that in the single droplet drying experiments (typical drying time of a droplet is about 300 s). During spray drying, fast removal of water leads to instantaneous vitrification of the solid matrix surrounding the cells, which fixates the cell membranes and thereby minimizes the damage to the cell integrity (187, 188). At outlet air temperatures above 70 °C, the residual viability decreases with increasing outlet air temperatures. When comparing the experimental results to the model prediction based on thermal inactivation, it can be concluded that this viability loss can be explained entirely by thermal inactivation. This finding was further confirmed by comparing model predictions and spray drying experiments at different inlet air temperatures, while maintaining the outlet air temperature at 75 °C. At inlet air temperatures above 190 °C all cells were inactivated very rapidly because the droplets reached a critical combination of high temperature and moisture content at the beginning of the drying.

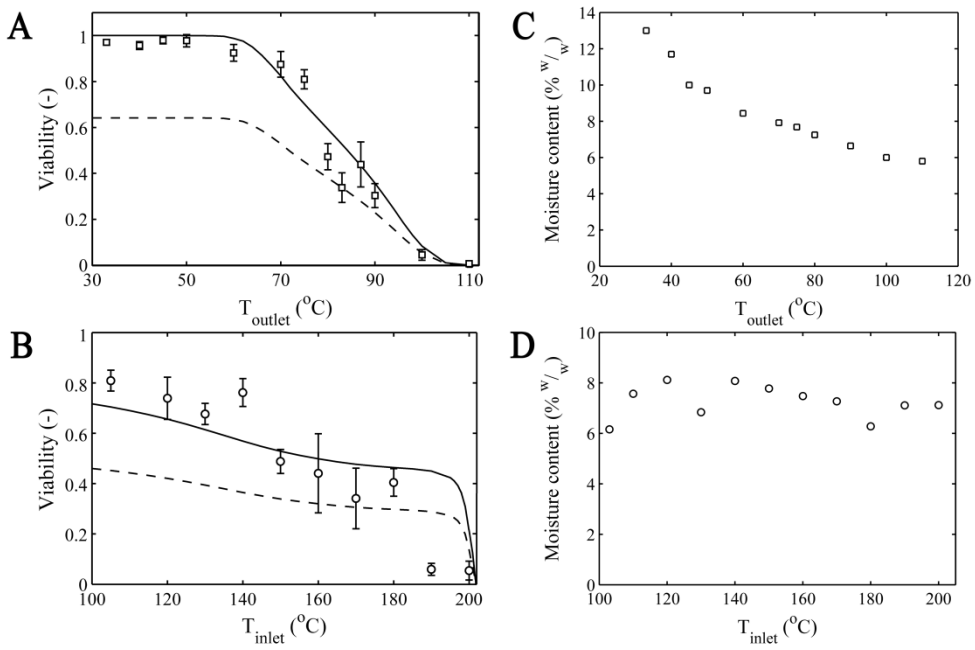

Figure 7-3. Residual viability of *L. plantarum* WCFS1 dried in a laboratory scale spray dryer at different outlet air temperatures (between 33 and 110 °C) where the inlet air temperatures were set 30 °C higher than the respective outlet temperature (A), at different inlet air temperatures (between 105 and 200 °C) where the outlet air temperature was set to 75 °C (B), and their respective moisture contents after drying (C and D). The symbols represent the experimental data, the solid lines represent the residual viability prediction taking into account thermal inactivation, the dashed lines represent the residual viability prediction taking into account both thermal and dehydration inactivation, and the error bars represent standard deviation.

At high inlet air temperatures (i.e. higher than 180 °C), the droplet experiences temperatures higher than 70 °C, even from the beginning of the drying. The prediction of inactivation under such conditions in the spray dryer could only be obtained through extrapolation, which can explain the difference between experimental and predicted

viability values (Figure 7-3A and 3B). It is noted however that these high inlet air temperatures are less relevant, since lower levels of residual viability were obtained.

The effect of the drying rate on viability loss

Because dehydration inactivation was found to be negligible when drying quickly, the influence of the drying rate on dehydration inactivation was studied by comparing three different methods of drying: freeze drying, single droplet drying to mimic slow drying at low temperature, and very fast spray drying using a laboratory spray dryer. The drying time for these processes are in the order of 24 h for freeze drying, 30 min for single droplet drying, and about 1.5 s for laboratory spray drying. Spray drying provides the highest residual viability (Figure 7-4A). This was reported previously for the dehydration of TBC vaccine (70). As discussed before, the high residual viability during spray drying can be explained by the high drying rate providing immediate vitrification of the solid matrix without negatively affecting the stability of the cell membrane. For slow convective drying a residual viability of 65 % was measured, due to dehydration inactivation. After freezing (the first step in freeze drying) a residual viability of 90 % was found. After subsequent freeze-drying, the residual viability of *L. plantarum* WCFS1 decreased to 50 %. Thus, approximately 45 % of the cell population lost its viability during the freeze drying step, which is in line with results from another study (189). Another study by van Baarlen *et al.* (105) shows that more than 85 % viability could be retained by freeze drying of *L. plantarum* in a mixture of 20 % $^{w}/_{w}$ maltodextrin + 2 % $^{w}/_{w}$ glucose solution. However, the dextrose equivalent (DE) of the maltodextrin was not reported. It may well possible that a higher DE, which means shorter chain, of maltodextrin was used as the shorter chain of carbohydrates could give better stabilization to the cell membrane during dehydration (24).

The viability loss during freezing can be attributed to either (i) the formation of intracellular ice crystals (190) or (ii) a phase transition in the lipid bilayer, which damages the cell membrane (189, 191). During freeze drying, a first step of drying occurs when freezing down to e.g. -20 °C, during which about 65-90 % of the water is sublimated. The remaining water, so called “bound water”, (0.10-0.35 g/g (14), 0.2-0.25 g/g solid (186)) cannot be frozen at this temperature but has to be removed through evaporation in the second step of drying to achieve approx. 5-8 % final moisture content (14). If this drying procedure is compared to single droplet drying, in which most viability loss took place between moisture

contents of 0.1 and 0.35 kg/kg (Figure 7-1C), it is hypothesized that the viability loss during freeze drying will primarily occur during the second step as a consequence of dehydration inactivation. The observation that the residual viability after freeze-drying for different solid matrices was never higher than the residual viability after single droplet drying supports this hypothesis (Figure 7-4B). At the same time, the fact that using different matrices influences the viability is an indication that indeed the phase behaviour of the lipid bilayer is important. This is in agreement with the fact that below 45 °C, thermal inactivation did not take place. Inactivation by dehydration may still occur, as the removal of water will cause differences in osmotic pressure, and may cause deformation and rupture due to local crystallisation or other effects (24, 192, 193). The same may happen during freeze drying with even some additional inactivation due to cold stress or crystallization (194).

In contrary to “slow drying”, the absence of dehydration inactivation during laboratory scale spray dryer indicated that at this nearly instantaneous drying rate dehydration inactivation can be avoided. However, in slow drying, the drying rate does not influence the viability loss due to dehydration. Therefore, it is hypothesized that, within the moisture content range between 0.35 and 0.1 where dehydration inactivation takes place, the drying rate influences the dehydration inactivation in a step function; the time during which the drying crosses this so-called critical moisture content is hypothesized to determine whether dehydration inactivation will occur or not. Thus, to eliminate the dehydration inactivation, the drying rate should be faster than a certain “critical drying rate” to eliminate dehydration inactivation. This “critical drying rate” should be obtained from relating the drying time (to dehydrate the particles from moisture content above 0.35 to 0.1) to retention of cell viability.

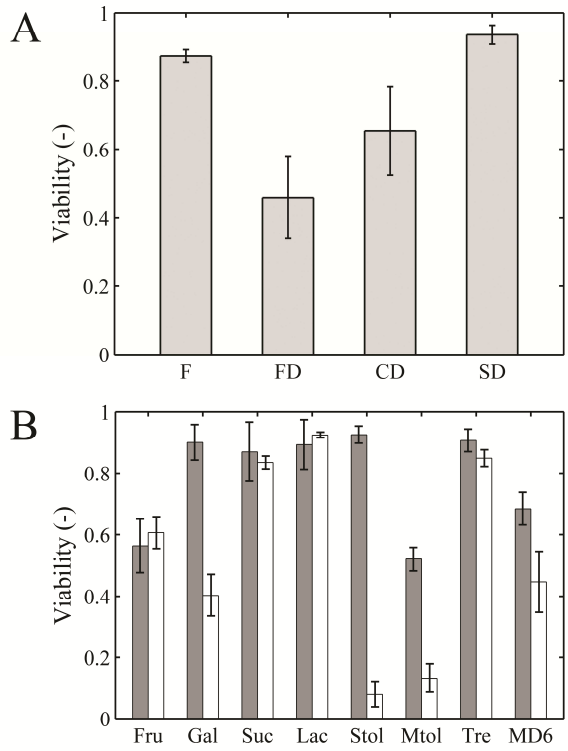

Figure 7-4. A: Residual viability of *L. plantarum* WCFS1 subjected to freezing at -26 °C for 24 h (F) and subsequent freeze drying (FD), convective drying at 25 °C on single droplet drying equipment (CD), and laboratory scale spray drying at 50 °C (SD). B: Residual viability of *L. plantarum* WCFS1 after convective drying at 25 °C on single droplet drying equipment (grey bars) and freeze drying (white bars) in solid matrices of fructose (Fru), galactose (Gal), sucrose (Suc), lactose (Lac), sorbitol (Stol), mannitol (Mtol), trehalose (Tre), and maltodextrin DE 6 (MD6). The error bars represent the standard deviation.

Outlook for the industrial application of spray drying to dehydrate probiotics

The positive results from lab scale spray drying experiments provide an indication that spray drying may be a superior technique to dehydrate probiotics. However, to confidently and accurately translate the insight gained from single droplet drying and lab scale spray

drying to industrial-scale spray drying of probiotics, the droplet size and the related drying rate and drying time should be controlled.

Industrial spray drying requires much longer drying times (~30 s) compared to lab scale spray drying (between 1 and 1.5 s (184)), which is mainly due to the difference in particle size. The longer drying time in industrial spray drying leads to higher viability losses. To minimize loss of viability, lower drying temperatures should be applied. This negatively affects energy efficiency or leads to high residual moisture content and operational difficulties due to sticky powders. The drying rate relates to the droplet size and determines whether dehydration inactivation occurs. The drying rate is preferably higher than a "critical drying rate" for instantaneous vitrification. It is questionable whether this can be achieved in industrial spray drying systems. Another route that can be taken is to reduce the droplet size by e.g. implementation of a different atomization method. Rapid drying of small droplets is favourable for retention of viability and avoiding dehydration inactivation. Atomization is not expected to have negative impact on residual viability, because a residual viability above 95 % was found for spray dried *L. plantarum* WCFS1 ($d_{4,3}$ = 8.1 μm with $d_{0.1}$ = 1.4 μm). This has also been observed in previous studies (189, 195). However, the use of very small droplets in conventional spray dryers involves redesign of drying chambers, but could contribute to process intensification of spray dryers used for drying of probiotics or other food or pharmaceutical applications.

This study shows that spray drying is capable in retaining more than 95 % of viability of probiotic cells (in this research represented by *L. plantarum* WCFS1) after drying. However, it should be realised that loss of viability during storage can have large influence on shelf-life of the probiotic formulation. However, this was beyond the scope of this study.

Conclusion

The inactivation of micro-organisms during drying can be ascribed to the effects of the dehydration and the effects of the thermal shock. Using the single droplet drying platform (drying time between 2 to 5 min), the dehydration inactivation of *Lactobacillus plantarum* WCFS1 predominantly occurred at drying temperatures below 45 °C and only depended on the moisture content. Above 45 °C the inactivation was however due to a combination of dehydration and thermal inactivation, which depended simultaneously on the moisture content, temperature, and drying time.

A model was developed to describe the thermal and dehydration inactivation of the cells during single droplet drying, based on the Weibull probability distribution, which could describe the inactivation and enabled the prediction of residual viability of *L. plantarum* WCFS1 after single droplet drying.

Subsequently, the model was implemented to predict the viability loss of *L. plantarum* WCFS1 dried in a laboratory scale spray dryer (drying time between 1 and 1.5 s). A good agreement between the model prediction and the experimental data was observed if assumed that only thermal inactivation occurred. This implies that fast drying in laboratory scale spray drying could induce instant fixation of the cells in a vitrifying matrix and thereby prevent dehydration inactivation. Finally, the influence of the drying rate on the residual viability was evaluated by comparing single droplet drying, freeze drying and laboratory scale spray drying of the same bacterial suspension. The results indicated that slow drying leads to significant dehydration inactivation, which is strongly reduced in fast drying processes such as laboratory scale spray drying where thermal inactivation is the predominant mechanism of inactivation.

Nomenclature

A	Residual viability	–
A_D	Residual viability due to dehydration inactivation	–
A_∞	Fraction of viable cells at $x_w = 0$ (after drying)	–
b	Temperature dependency parameter of parameter α for thermal inactivation	–
p	Moisture content dependency of parameter α for thermal inactivation	–
T	Temperature	°C
t	Time	s or minute
x	Mass fraction	$kg \cdot kg^{-1}$
x_{crit}	Weibull distribution parameter for dehydration inactivation to describe the critical moisture content where the inactivation rate is highest	$kg \cdot kg^{-1}$

Greek symbols:

α	Weibull distribution parameter for thermal inactivation	minute
β_T	Weibull distribution parameter for thermal inactivation	–
β_w	Weibull distribution parameter for dehydration inactivation	–

Subscripts:

ref	Reference
D	Dehydration
s	Solid
T	temperature, thermal
w	Water
0	Initial

Appendix

The thermal inactivation kinetics of *L. plantarum* WCFS1 is dependent on the temperature, moisture content, and drying time. Here, we provide the steps to determine the thermal inactivation kinetics of *L. plantarum* WCFS1 described using a Weibull model.

$$A = A_0 exp\left(-\left(\frac{t}{\alpha}\right)^{\beta_T}\right) \quad \text{(7-A1)}$$

The temperature dependency of parameter α was described by the semi-empirical Bigelow model:

$$\log(\alpha_T) = \log\left(a_{Tref}\right) - b\left(T - T_{ref}\right) \quad \text{(7-A2)}$$

The temperature dependency of parameter α was extracted from isothermal heating experiments for both wet (x_w = 0.80) and dry condition (x_w = 0.08) by nonlinear fitting of parameter *A* against *t* and *T*

$$A = A_0 exp\left(-\left(\frac{t}{a_{Tref} \cdot 10^{\left(-b\left(T-T_{ref}\right)\right)}}\right)^{\beta_T}\right) \quad \text{(7-A3)}$$

Table 7-A1. The optimized parameter values for temperature-moisture content dependency of thermal inactivation parameters

Parameter	Value	Confidence interval[a]	
$\alpha_{w,Tref}$	3.48	0.64	18.3 %
b_w	0.18	0.013	7.6 %
$\alpha_{s,Tref}$	$24.36 \cdot 10^3$	$4.98 \cdot 10^3$	20.4 %
b_s	0.11	0.0046	4.2 %
β_T[b]	1		
T_{ref}[b]	50 °C		

[a] The uncertainty of the parameters at 95 % confidence interval

[b] Not optimized

Analogous to the combined effect of temperature and moisture content on enzyme inactivation kinetics (68), the sensitivity of parameter α on moisture content increases at lower moisture contents. According to the model (Eqs. 7-A4 and 7-A7-5), parameter a is more sensitive to the change of moisture content than parameter b. Therefore, although the model was fitted to x_w = 0.8 and x_w = 0.08 instead of x_w = 1.0 and x_w = 0.00, the approximation of a_w, b_w, and b_s from these experimental data will be accurate. Parameter value a_s is obtained from fitting the model to the single droplet drying data.

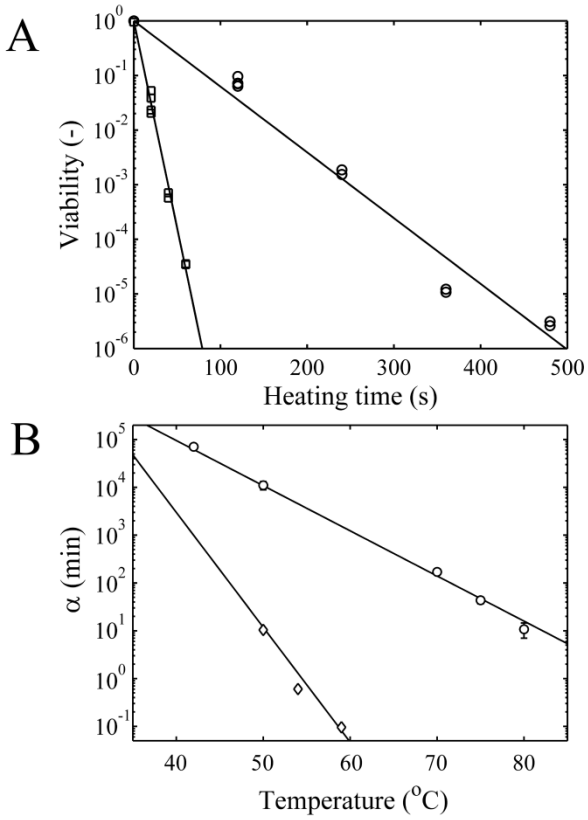

Figure 7-A1. A: Residual viability of *L. plantarum* WCFS1 after isothermal heating at 55 °C (○) and 60 °C (□). Solid lines represent the fitted model based on Weibull model (Eq. 7-3) with $\beta_T = 1$. B: The temperature dependence of parameter α for water content of 0.8 (◊) and 0.08 (○). Solid lines represent the fitted model based on Eq. 7-5.

Chapter 8

Interactions between formulation and spray drying conditions related to survival of *Lactobacillus plantarum* WCFS1

Submitted for publication as:

J. Perdana, M.B. Fox, S. Chen, R.M. Boom, and M.A.I. Schutyser. Interactions between formulation and spray drying conditions related to survival of *Lactobacillus plantarum* WCFS1.

Abstract

Protective solid carriers are commonly added to probiotic cultures prior to drying. The selection of suitable carriers is not trivial and related to the applied drying conditions. We present a systematic study into the influence of formulation parameters on the survival of *L. plantarum* WCFS1 during single droplet and spray drying at various operational conditions. The combination of low molecular weight carbohydrates (less than 2 kDa) and high molecular weight is concluded most appropriate to provide protection at both low (25 °C) and high (50 °C or higher) temperature drying. Low molecular weight compounds provide stabilization by closely interacting with the lipid bilayer of the cell membranes, whereas high molecular weight carriers provide stabilisation by their high glass transition temperature yielding a glassy powder. We showed that depending on the crystal geometry, crystallization during drying can be either beneficial (e.g. with mannitol or sorbitol) or detrimental (e.g. with lactose) to the survival of *L. plantarum* WCFS1. The minimum amount of solid carrier required to provide sufficient protection to the cells during drying was determined at 2 % $^{w}/_{w}$ for trehalose. An acceptable decimal reduction time of approximately 300 days was found when spray dried *L. plantarum* WCFS1 powders were stored at temperatures below 40 °C. Finally, a generalised diagram was constructed to indicate combinations of outlet air temperature and residual moisture content to maximally retain viability and operate at highest dryer efficiency. In this diagram it is assumed that a formulation with a specific glass transition temperature is applied.

Keywords: Feed formulation, spray drying, viability, probiotics, vitrification

Introduction

Spray drying is an attractive route to enhance and prolong the stability of probiotic cell cultures (1-4, 75). When stored under appropriate conditions, cells enclosed in a glassy powder remain viable and resume their active living state after reconstitution (33, 43). Dedicated formulations are used to enhance survival of cells during spray drying and subsequent storage (75, 76, 196). They consist usually of protective agents such as carbohydrates and, to a lesser extent, proteins, which are approved as food additives (3, 15, 175). The protective effect is often related to the high glass transition temperatures of the selected components providing stability to bacteria when enclosed in a glassy matrix (33, 197).

Generally, the presence of protective agents may depress the phase transition temperature of the phospholipid in the cell membrane (T_m) between liquid crystalline phase and gel phase (45, 188, 198). In the absence of protective agents, this T_m increases with decreasing moisture content (199). For example, the T_m of *E. coli* and *B. thuringiensis* increases from 30 (hydrated) to 40 °C (dried). In the presence of trehalose or sucrose, the T_m of dried cells is maintained around 30 °C (45). Due to the variability of the chain length of the phospholipid molecules in the cell membrane, the T_m may also vary, resulting in uneven transformation of the phospholipids from liquid crystalline phase to gel phase. This uneven transformation might cause a leakage of the cell membrane, which could lead to viability loss (199, 200). Thus, it is desirable to keep the cell membrane in the liquid crystalline phase (as when it is hydrated) upon drying, for example with the addition of protective agents.

Several mechanisms were proposed to explain the depression of T_m in the presence of protective agents, of which the most important are the water replacement theory (45, 201) and the hydration force theory (187, 202, 203) indicating whether there is specific interaction between the protective molecules and the phospholipid head-group or not. The ability of protective agents to influence the T_m of cell membrane depends on the type of the protective agents and also on the cell. Therefore, in practice the selection of suitable protective agents is often bacterial strain-specific (204-206).

In our previous study we showed that the inactivation behaviour of *Lactobacillus plantarum* WCFS1 during spray drying was different at low and high drying temperatures

(207). At a low drying temperature, only dehydration inactivation occurred, while at high temperatures inactivation occurred due to both dehydration and thermal inactivation (182, 207). It was also demonstrated that fast drying at low temperatures leads to a minimal viability loss, which is explained by the absence of dehydration inactivation during the fast drying process. This is probably due to the instant vitrification of the solid matrix surrounding the bacterial cells (207). Fast drying at higher temperatures only invokes thermal inactivation. Obviously, the addition of protective agents influences the degree of survival during the drying at the above mentioned drying conditions. It is hypothesized that protective agents may have different effects in combination with the two different inactivation mechanisms.

Therefore, this study explores the protective effect of different solid carriers on the survival of *Lactobacillus plantarum* WCFS1 at different drying and subsequent storage conditions. The latter is of importance because significant viability losses may occur during storage that could compensate for good retention of the viability during drying (15, 208). The final aim is to provide guidelines for optimal spray drying and storage that provide maximum retention of viability of *L. plantarum* WCFS1.

Firstly, the influence of protective formulations on survival of *Lactobacillus plantarum* WCFS1 was investigated for the two specific drying conditions:

1. Single droplet drying at low temperature inducing only dehydration inactivation
2. Fast drying in a laboratory-scale dryer inducing only thermal inactivation

The survival of *L. plantarum* WCFS1 was monitored for various protective agents including low and high molecular weight carbohydrates and proteins. The survival was determined by a cell-integrity based enumeration method that is also suitable for single powder particles (75). Subsequently, the correlation was investigated between the survival and the physical properties of the protective formulation such as glass transition temperature, molecular weight and presence of crystals. Also the amount of added solid carrier was examined as a formulation parameter. Next, the inactivation during storage was taken into account, for which the survival was monitored as a function of the storage conditions (at different times and temperatures). Finally, guidelines were derived aiming at optimal retention of viability of spray dried *L. plantarum* WCFS1.

Materials and Methods

Materials

Maltodextrin DE = 6 and DE = 16 (Roquette, France) was used as received. Sorbitol, mannitol, xylose, glucose, sucrose, maltose, trehalose, lactose, l-glutamine, glycine, glutamic acid, lysine, and lactalbumin hydrolisate were analytical grade, purchased from Sigma-Aldrich (USA) and used as received. Inulin (Orafti HP) and fructo-oligosaccharides (Orafti L85) were purchased from Beneo-Orafti (Belgium), galacto-oligosaccharide (Vivinal GOS) from FrieslandCampina (The Netherlands), and potato starch from Sigma-Aldrich (USA) were used as received.

Preparation of bacterial culture

The strain *Lactobacillus plantarum* WCFS1 was obtained from NIZO Food Research (The Netherlands). The deep frozen culture (-26 °C) was grown in 10 ml sterilized *Lactobacilli* MRS broth (BD Difco, USA) at 30 °C for 16 h. An aliquot of 1 % of the grown culture was transferred and re-grown at the same conditions. Approximately 10^9 cfu/ml cell density was obtained after incubation. The culture was then centrifuged for 10 minutes at 4000 rpm (13500 g) at 4 °C. The supernatant was collected for pH measurement, while the pellet was twice washed with 10 ml of sterilized phosphate buffer saline (PBS; BD Difco, USA) solution (pH = 4.0).

Preparation of the samples for the drying experiments

The samples for the drying experiments were prepared by diluting the cell culture 10 times in PBS (pH = 4.0) solution. The diluted cell culture was again diluted 2 times with the sterilized carrier solutions containing 40 % $^{w}/_{w}$ of solid content. By this, a suspension with approximately $5{\cdot}10^7$ cfu/ml cells in a 20 % $^{w}/_{w}$ solid carrier was obtained. Subsequently, this suspension was directly used for single droplet or spray drying experiments.

Single droplet drying experiments

These were carried out with the single droplet drying platform consisting of a pneumatic micro-dispenser to deposit droplets on a flat hydrophobic membrane (Accurel PP 2E-HF, Akzo Nobel, The Netherlands) and a channel with well-defined drying air flow at specific temperature and relative humidity (RH) (67, 75). The RH of air was 0.0 %. Three identical

droplets (d = 600 μm) were dried simultaneously for 30 min in each experiment. The experiments were carried out in duplicate.

Spray drying experiments

A Buchi B-290 spray dryer (Buchi Labortechnik AG, Switzerland) was used for spray drying experiments. The experiments were carried out in duplicate. The relative humidity of the inlet air was 0.0 %. Small amounts of powder (approx.: 10 mg) were subjected to rehydration and viability enumeration.

Moisture content measurement

The moisture content of spray dried powder was analysed using the Sartorius MA 35 (Sartorius Mechatronic, Germany) gravimetric analyser. Approximately 2 g of powder was spread on an aluminium pan and put in the moisture content analyser, which heated the powder up to 130 °C until the mass equilibrated to a final value; approximately 5 min heating time was needed. The moisture content of the powders after single droplet drying was not measured. It was assumed that the moisture content is lower than 5 % $^{w}/_{w}$.

Cell rehydration and viability enumeration

Powder particles were transferred and rehydrated on a sterilized Anopore (aluminium oxide nanoporous) chip (Microdish BV, The Netherlands) positioned on top of a 1 % low melting point agarose (Invitrogen, USA) gel containing 0.02 % fluorescent stains (Live/Dead BacLight bacterial viability kits, Invitrogen, USA). The viability kit contained Propidium Iodide (1.67 mM) and Syto 9 (1.67 mM) reagent in dimethyl sulfoxide (DMSO). The rehydrated powder particles were incubated for 30 minutes; then excited by 470 nm light to induce a fluorescent spectral shift to green (life) or red (dead), which could be observed with the microscope. Approximately 20 images were taken for each viability measurement. A more detailed description of the method is provided by Perdana *et al*. (75).

Scanning electron microscopy (SEM) measurement

Samples were fixed on sample holders by carbon adhesive tabs (EMS, Washington, USA) and subsequently sputter coated with 5 nm Tungsten (MED 020, Leica, Vienna, Austria). Samples were analysed at 2 kV at room temperature in a field emission scanning electron

microscope (Magellan 400, FEI, Eindhoven, The Netherlands). Images were digitally recorded.

X-ray diffraction for measurement of the degree of crystallinity in powder samples

Approximately 0.5 gram sample powder was placed in the sample holder for X-ray diffraction spectroscopy (XRD) experiments. XRD was conducted with a PANalytical Expert Pro System (The Netherlands) by using nickel-filtered CuKα radiation (tube operating at 40 kV and 40 mA). The data were collected using an automated divergence slit (5mm irradiated length) and a 0.5 mm receiving slit. Data were obtained by step counting at 0.02° intervals for 2 seconds per data point.

Amorphous powder samples were used as a reference and obtained by spray drying 20 % $^{w}/_{w}$ samples diluted in Milli-Q water (Millipore, USA) in the Buchi 190 mini spray dryer at an inlet air temperature of 120 °C (RH_{in} = 0.0 %) and an outlet air temperature of 85 °C.

The degree of crystallinity was determined using an external standard method (87). The volume fraction of the crystalline phase in the mixture was calculated from the measured integrated intensities of diffraction peaks produced by the samples compared to the amorphous samples

$$W_i = 1 - \frac{I_i}{I_a} \tag{8-1}$$

where W_i is the weight fraction of the crystalline phase, I_i is the integrated intensity of the samples and I_a is the integrated intensity of the reference phase (amorphous sample).

Glass transition temperature of powder formulations

Glass transition temperature (T_g) of a powder is dependent on the material composition and the water content. When a mixture of components is used (e.g. solid and water or two solids and water), glass transition temperature is a function of the glass transition temperature of the components and their mass fractions, which could be estimated using the Couchman-Karasz relation (30, 209, 210):

$$T_g = \frac{\sum y_i \Delta c_{p,i} T_{g,i}}{\sum y_i \Delta c_{p,i}} \tag{8-2}$$

with y the mass fraction, Δc_p the transition of isobaric heat capacity increment, and T_g the glass transition of the pure components. The data for Δc_p and T_g of the components are listed in the Appendix. It is important to realize that presence of residual moisture has significant impact on the T_g of a formulation, since the T_g of pure water is very low (-138 °C).

Results and discussion

We showed earlier that *L. plantarum* WCFS1 loses viability during drying due to dehydration, thermal inactivation or both types of inactivation simultaneously (182, 207). To study the cell survival during drying with both types of inactivation behaviours, two different drying methods were used:

1. Single droplet drying (droplet diameter of 600 μm) at drying air temperatures of 25 °C
2. Laboratory scale spray drying to achieve fast, nearly instantaneous, drying at drying temperatures 50 °C or higher.

Another reason for using both methods is that drying at low temperature is impossible in the laboratory-scale drying equipment because of the short residence time in the dryer, while fast drying at high temperature cannot be carried out with the single droplet drying equipment.

Single droplet drying at an air temperature of 25 °C

For drying at an air temperature of 25 °C it can be safely assumed that inactivation is dehydration driven. Drying under these conditions leads to relatively extended drying times (approximately 2-5 min). Different formulations were prepared and dried with *L. plantarum* WCFS1. The survival was experimentally measured and related to the glass transition temperatures and molecular weights of the added components (Figure 8-1). To facilitate the interpretation of the data, the components were grouped into ‘carbohydrates’ and ‘proteins’.

The residual viability of *L. plantarum* WCFS1 dried with carbohydrates decreased with increasing molecular weight of the carbohydrates, while the glass transition temperature had a smaller influence (Figure 8-1 A & B). The effect of the molecular weight may be explained by interactions between small carbohydrates and the phospholipids stabilizing the bilayer in the liquid crystalline phase (45, 46). Only low molecular weight solutes are able

to closely interact with the lipid bilayer of the cell membranes, which seems possible still for maltodextrins DE16 with a molecular weight equal or less than 2 kDa (Figure 8-1B) (187, 188). With increasing molecular weight the interactions weaken and therefore the residual viability decreases, e.g. for maltodextrins DE6 or starch (Figure 8-1B). The reason that also larger carbohydrates still provide some protection is probably due to the fixation of cells in a glassy matrix, which hinders mobility of the lipid bilayer (179, 203). With fructose or xylose, cells were not enclosed in a glassy matrix because the glass transition temperatures were below the drying temperature. The same is true for sorbitol and mannitol but here crystallization was observed during single droplet drying at 25 ^{o}C, which could provide protection to cells by enclosing them in a crystalline matrix (211, 212).

When proteins or amino acids were used as solid carrier, the residual viability after drying was not clearly related to the molecular weight or the glass transition temperature (Figure 8-1C). The residual viabilities with glycine and lactalbumin hydrolysate were relatively low. The low residual viability with glycine is surprising as it has a high T_g and is considered to prevent cell lysis (213). Probably, the large concentration of glycine during drying increases the intra- and extracellular osmotic pressure difference that cannot be tolerated by *L. plantarum* WCFS1, leading to cell death.

Laboratory-scale spray drying at air temperatures of 50 °C or higher

Thermal inactivation occurs in addition to dehydration inactivation when drying at air temperatures of 50 °C or higher. However, when fast drying is applied (using laboratory scale spray drying, with a drying time of approximately 1.3 s) the effect of dehydration on the viability loss was small for *L. plantarum* WCFS1 spray dried in maltodextrin DE6 (207). For other tested solid carriers the viability losses were small when spray drying at outlet air temperature below 70 °C (Figure 8-2). At these drying temperatures, thermal inactivation is minimal because the cells are rapidly entrapped in a solid glassy matrix (38, 214).

At outlet air temperatures above 70 °C, the residual viability decreases significantly with increasing drying air temperature (Figure 8-2). This decrease was more pronounced when the cells were suspended in high molecular weight carriers. Apparently, low molecular weight components provide more stability with respect to thermal inactivation. This

stabilization is likely to occur via a similar mechanism as was described for protection against dehydration inactivation (70, 215, 216).

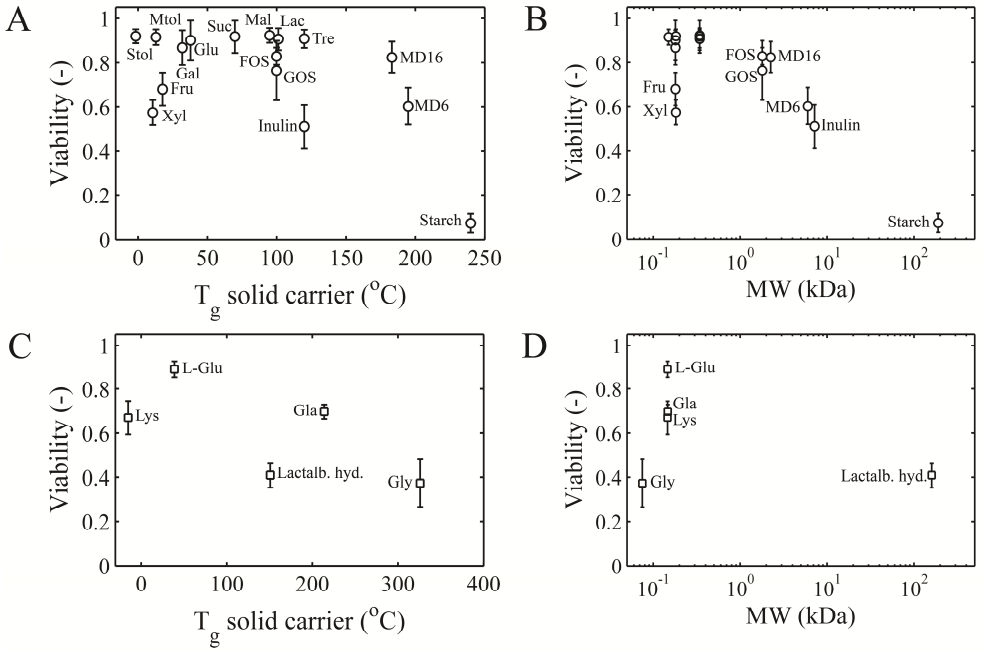

Figure 8-1. Residual viability of *L. plantarum* WCFS1 after drying for 30 min in single droplet drying apparatus in various solid carriers at 25 °C as a function of the glass transition temperature, carbohydrates (A) and proteins (C) and as a function of molecular weight, carbohydrates (B) and proteins (D). The error bars represent the standard deviation of the viability measurements. The final moisture content of the powder is approximately 2 %. The complete description of the abbreviated solid carriers is listed in Appendix (Table 8A-1).

The effect of the glass transition temperature on thermal inactivation of *L. plantarum* WCFS1 was investigated by preparation of different mixtures of solid carriers with different T_g. By doing so, mixtures could be prepared, that cover a range of glass transition temperatures. Subsequently, *L. plantarum* WCFS1 was suspended in these mixtures and spray dried at inlet and outlet air temperatures of 120 and 85 °C, respectively.

The residual viability decreased when the T_g of the spray dried powders was below 40 °C, which is much lower than T_a (85 °C) (Figure 8-3A and B). This may be explained by the rapid cooling in the collected powder in the glass container of the laboratory-scale dryer, leading to the formation of a glassy powder (30). The temperature in the small glass container tank was determined at about 40 °C. It was also observed that when drying powder mixtures with a lower T_g (< 40 °C), only a small amount of powder could be collected, due to fouling of the walls. The residual viability decreased further with decreasing T_g, indicating that the powder mixtures obtained with T_g below 40 °C were not glassy (Figure 8-3A and B). This is in agreement with a previous study that showed that thermal inactivation becomes more pronounced in matrices being in a more 'liquid-like' state (212). The mechanism may be analogous to the influence of increasing moisture content on thermal inactivation (207).

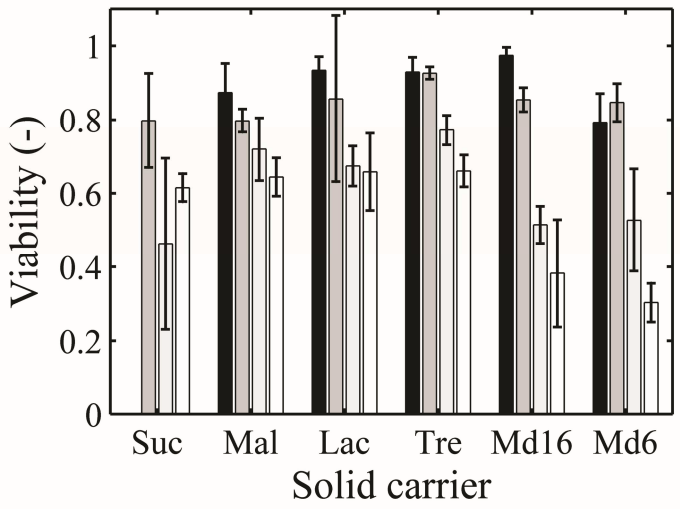

Figure 8-2. Residual viability of *L. plantarum* WCFS1 spray dried in various matrices at spray drying outlet air temperature of 50 (black), 70 (dark grey), 85 (light grey), and 90 °C (white) with $T_{in} = T_{out} + 50$ °C. The error bars represent the standard deviation of viability measurements. Sucrose could not be spray dried at T_{out} 50 °C.

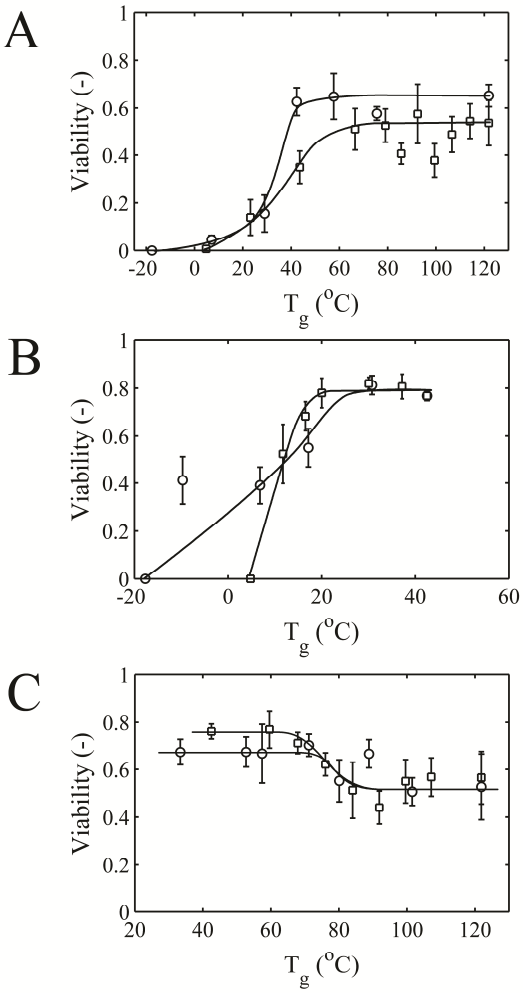

Figure 8-3. Residual viability of *L. plantarum* WCFS1 spray dried at inlet and outlet air temperature of 120 and 85 °C, respectively as a function of the glass transition temperature of the solid matrices. The cells were spray dried in mixtures of: A) trehalose and glucose (□) and trehalose and sorbitol (○), B) maltodextrin DE 6 and glucose (□) and maltodextrin DE6 and sorbitol (○), C) maltodextrin DE 6 and trehalose (□) and maltodextrin DE6 and lactose (○). The glass transition temperatures of the powders were adjusted to a moisture content of 5 %, relevant to the measurement data. Solid lines are drawn to guide the eye and the error bars represent the standard deviation of viability measurements.

The powders with maltodextrin DE6 and lactose or trehalose have a minimum T_g around 40 °C. Therefore, all powder mixtures of these components obtained are glassy. The residual viability is found to change at approximately equivalent amounts of both components with a higher residual viability for disaccharide-rich mixtures and a lower viability for the maltodextrin-rich mixtures (Figure 8-3C). Apparently, the residual viability depends on the component with larger fraction in the mixture.

In conclusion, a higher glass transition temperature of the solid carriers is not necessarily related to higher retention of viability. It is more important to ensure that the cells are rapidly fixated into a glassy matrix after drying to achieve maximum retention of viability. A high glass transition temperature of the formulation is desired only because it could easily reach a glassy state than the formulation with lower T_g.

Presence of crystals affects survival

Depending on the rate of drying and the components present, crystallization may occur. In the case of sorbitol and mannitol, crystal structure appears enclose the bacteria and may thereby provide protection to the cells. However, depending on the crystal architecture, crystals may also detrimental to the bacteria. For example, lactose is a disaccharide that can form needle-like crystals (217), which may puncture cells. This effect was investigated by drying *L. plantarum* WCFS1 with various concentrations of lactose crystals in the feed solution. Two different drying experiments were carried out in which a fraction of lactose in the feed was replaced by lactose crystals: i) single droplet drying at an air temperature of 25 °C and a droplet size of ~600 μm (drying time approx. 5 min) and ii) laboratory-scale spray drying at an air temperature of 50 °C (drying time approx. 1.5 s). It was assumed that thermal inactivation during these experiments was negligible.

When no lactose crystals were present in the feed solution, the residual viability was equal to 95 % for both experiments (Figure 8-4). When a fraction of the lactose was present as a crystal, the residual viability for the single droplet drying decreased rapidly to approximately 60 %. This is independent of the initial fraction of lactose in the crystalline state. The initial lactose acts as a seed for crystal growth during drying (218). In the absence crystalline lactose in the feed, the crystallization was hindered by the absence of crystal seeds.

When the feed solution is rapidly dried in the spray drier, the residual viability was very high (> 90 %) despite the presence of lactose crystals. The rapid drying and solidification of the matrix hinders the growth of the crystal, and thus hinders the detrimental effect of lactose crystals penetrating bacterial cells.

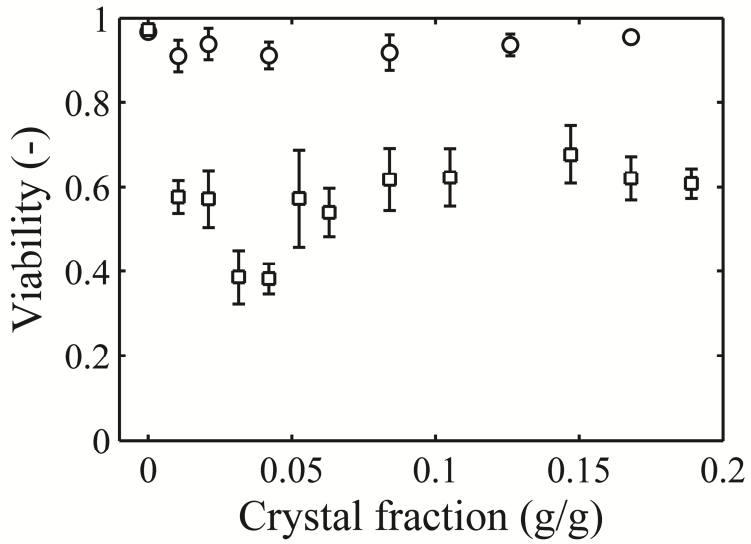

Figure 8-4. Residual viability of *L. plantarum* WCFS1 dried in the presence of different amounts of lactose crystals in the feed. The crystal concentration was presented as the fraction to the total lactose concentration. The lactose concentration in the feed was 20 % $^{w}/_{w}$. The drying was performed by single droplet drying (slow drying) at 25 °C air temperature and a droplet size of 600 µm (□) and by laboratory-scale spray drying at an air temperature of 50 °C (○). The error bars represent the standard deviation for the viability measurements.

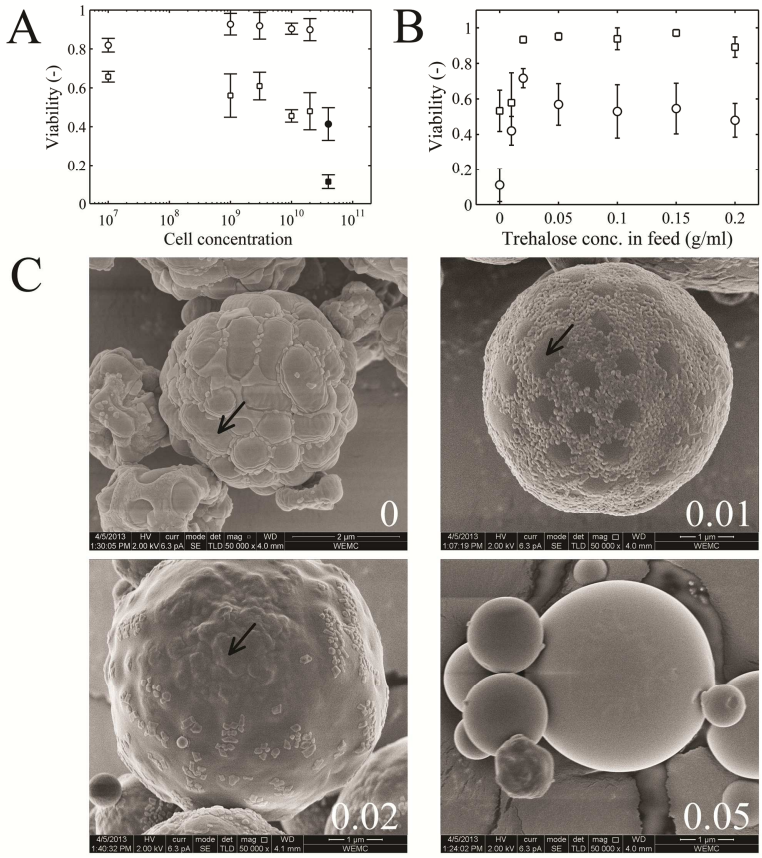

Figure 8-5. A: Residual viability of *L. plantarum* WCFS1 spray dried in feed solution containing 20 % $^{w}/_{w}$ trehalose at various cell concentrations under outlet spray drying temperatures of 50 (○) and 85 °C (□). The closed symbols represent the residual viability of cells spray dried without addition of any protective agent. B: Residual viability of *L. plantarum* WCFS1 spray dried in feed solution containing 10^{10} cfu/ml cell concentration and various trehalose concentrations under outlet spray drying temperatures of 50 (○) and 85 °C (□). The inlet air temperature was fixed 50 °C above the outlet air temperature during spray drying. The error bars represent the standard deviation. C: SEM pictogram of collected powder spray dried at outlet air temperatures of 50 °C with *L. plantarum* WCFS1 (10^{10} cfu/ml cells) and 0, 0.01, 0.02, and 0.05 g/ml trehalose concentration. The black arrows indicated the exposed cells.

Effect of the solids concentration on survival

The absence of a solid carrier is detrimental to the survival of *L. plantarum* WCFS1 (Figure 8-5A). A minimum amount of solid carrier is required to protect *L. plantarum* WCFS1 during drying. A small amount of trehalose (2 % $^{w}/_{w}$ trehalose in feed solution containing 10^{10} cfu/ml cell concentration) was sufficient to retain the viability during spray drying (Figure 8-5B). Scanning electron microscope (SEM) observation shows that the addition of 2 % $^{w}/_{w}$ trehalose was sufficient to obtain powder particles with a surface that is perfectly covered by trehalose, which apparently provided adequate protection to the cells (Figure 8-5C).

At lower concentrations, the individual cells could be observed at the surface of the powder particles (Figure 8-5B). These cells were exposed to the hot drying air, which explains the large decrease in their viability. The residual viability did not further increase with increasing trehalose concentration in the feed solution (Figure 8-5B), probably related to the minimal coverage of cells required to provide full protection. The cell concentration in the feed solution also did not influence the retention of viability after spray drying as long as a sufficiently high concentration of trehalose was added to the feed (Figure 8-5A).

Survival during storage

In the previous section we showed that viability of *L. plantarum* WCFS1 is affected by the drying process itself and can be influenced by formulation. However, as already mentioned in the introduction, loss of viability may occur also during subsequent storage. This effect varies with the selected formulation. Therefore, spray dried powders were stored at different conditions and subsequently analysed for residual viability of *L. plantarum* WCFS1.

The residual viability was similar for spray dried *L. plantarum* WCFS1 with maltodextrin DE=6 (x_w ~ 7 %) stored at temperatures below 40 °C, but decreased slowly in time as described by a decimal viability loss time (*D value* (34), see Appendix). The viability decreased more severely when stored at temperatures above 40 °C (Figure 8-6A). The decimal viability loss time (D value) exponentially decreases with increasing temperature, which is in alignment with the temperature dependency of reactions as described by the Bigelow model. After 300 days of storage at temperatures below 40 °C, 10 % of the initial

viability was reached. This period might be extended to 600 days for powders with a moisture content of 4 % $^{w}/_{w}$.

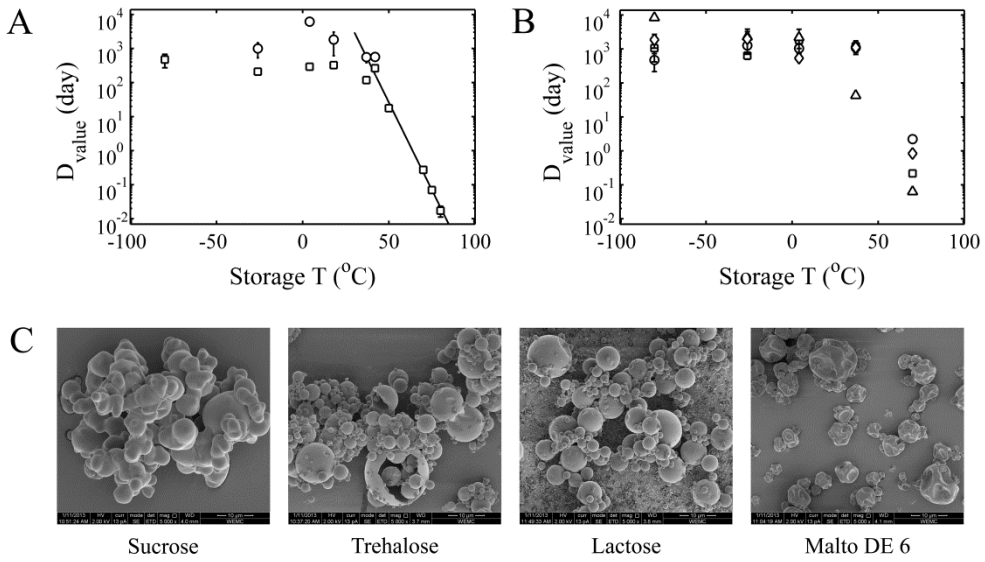

Figure 8-6. Decimal reduction value of residual viability of *L. plantarum* WCFS1 during storage at various temperatures. A. The cultures were spray dried in maltodextrin DE=6 at inlet and outlet air temperature of 110 and 70 °C (x_w ~ 7 %, □) followed by after drying at 25 °C for 24 h (x_w ~ 4 %, ○). B. The cultures were spray dried at inlet and outlet air temperature of 110 and 70 °C (x_w ~ 7 %) in lactose (○), maltodextrin DE = 6 (□), sucrose (Δ), and trehalose (◊). The error bars represent the confidence interval of the optimized parameter (p = 0.95). C: Scanning electron microscope (SEM) images of spray dried *L. plantarum* WCFS1 with solid formulation of 20 % lactose (A), sucrose (B), trehalose (C), and maltodextrin DE 6 (D).

No significant differences in viability loss were found with different solid carriers when samples were stored at temperatures below 0 °C. At a temperature of 40 °C, sucrose was less effective in protecting *L. plantarum* WCFS1. At a temperature of 50 °C, lactose and trehalose provided better retention of viability than sucrose and maltodextrin DE 6 (Figure

8-6B). Microscopic analysis revealed that the spray dried lactose and trehalose powders consisted of perfect spherical particles, showing rigid glassy powders. The particles with sucrose powder were partially merged together due to rubbery behaviour during or after drying. The maltodextrin powder contained particles with wrinkled surface despite its high T_g, possibly vitrified maltodextrin is more elastic while vitrified trehalose or lactose is rigid (Figure 8-6 C). The latter observations indicate that trehalose and lactose are preferred for protecting bacterial cells during storage at elevated temperatures (219).

Optimal spray drying and storage of *L. plantarum* WCFS1

Spray drying and storage conditions should be optimized towards overall survival. Depending on the selected formulation, different conditions are required. For example, the storage temperature should be below the glass transition temperature of the powder. For spray drying, generally low outlet air temperatures are advisable (also related to the T_g of the formulation) to have minimal thermal inactivation. However, at these low temperatures the spray dryer capacity is low, and thus the efficiency of the process is low. Higher energy efficiency can be achieved by increasing the inlet air temperatures; however, this increase is also restricted by risk of viability loss. Thus, maximum drying temperatures should be identified to avoid excessive loss of viability due to thermal inactivation. In spray drying, the thermal inactivation is generally dependent on the combined effect of i) the outlet air temperature (T_{out}) and ii) the spray dried particle size, which determines the drying time.

Two different approaches may be used for spray drying depending on the glass transition temperature of the formulation (Figure 8-7). The optimum conditions depend strongly on the residual moisture content of the powder and the outlet air temperature. The residual moisture content has large influence on thermal inactivation, while both parameters influence the glass transition temperature of the formulation at the end of the process, and thus also strongly affect the residual viability.

Region A in Figure 8-7 represents combinations of the residual moisture content and the outlet air temperature for a formulation with a glass transition temperature ($T_{g,2}$) that is optimal for maximum retention of viability in combination with the largest drying efficiency possible.

Region B represents combinations of residual moisture content and outlet air temperature with a formulation with a lower glass transition temperature ($T_{g,1}$). For this formulation

more intensive drying is required to reach a lower residual powder moisture content in the glassy region, with the constraint that the outlet air temperature should be kept low. This can be achieved by drying at low spray dryer capacity (to ensure the low final moisture content of the powder). Alternatively, spray drying at higher capacity may be followed by rapid cooling or a combination of drying and rapid cooling (e.g. in a fluidized bed dryer) to reach region C.

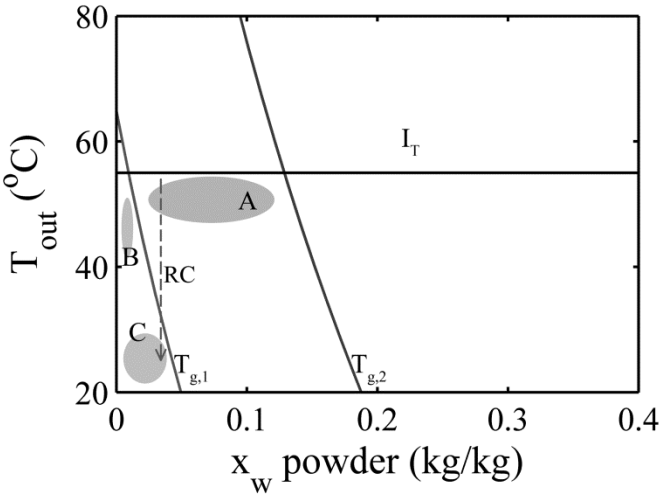

Figure 8-7. Combinations of residual powder moisture content and outlet air temperature. Line (I_T) represents acceptable viability loss due to thermal inactivation (depending on the spray dried particle size and the decision of optimization). Glass transition temperatures of two different formulations are drawn, i.e. $T_{g,1}$ (red) and $T_{g,2}$ (blue). The regions represent the drying combinations that lead to maximum viability retention for formulation 1 (A), for formulation 2 (B), and for formulation 2 but then spray drying is followed by rapid cooling or a combination of drying and rapid cooling (e.g. in a fluidised bed dryer) to obtain a glassy powder (C).

For industrial purposes, spray drying of *L. plantarum* WCFS1 can be carried out at cell concentration as high as 10^{10} cfu/ml with additions of protective materials as small as 2 % $^{w}/_{w}$. The advisable protective material for this strain is either trehalose or lactose. For

economic reasons, lactose might be more attractive than trehalose. However, trehalose is a better choice than lactose if retention of viability is the priority. This is relevant especially because only a small concentration (2 % $^{w}/_{w}$) of protective agent is needed. Sometimes, lactose cannot be added to food products, for example for the products aimed for lactose intolerant people.

Conclusions

The influence of solid carriers was evaluated in combination with low temperature (25 °C, single droplet drying) and high temperature drying (≥ 50 ^{o}C, laboratory-scale spray drying) for survival of *L. plantarum* WCFS1. At a low temperature and slow drying only dehydration inactivation was expected. This dehydration inactivation was minimal in combination with the addition of low molecular weight carbohydrates (mono- and disaccharides), which increased with molecular weight for molecules larger than 2 kDa. Similar results were obtained during lab-scale drying experiments in which only thermal inactivation of *L. plantarum* WCFS1 was expected. Besides the effect of molecular weight, carriers are preferred having a higher glass transition temperature, since this allows drying at higher outlet air temperatures while still providing a glassy powder at higher residual moisture content.

A high residual viability of *L. plantarum* WCFS1 was observed when dried in sorbitol or mannitol. Meanwhile, a low residual viability of *L. plantarum* WCFS1 was observed when dried with the presence of needle-like lactose crystals. For slow drying a small fraction of crystals was already detrimental to cells. This was not observed when drying was fairly rapid, e.g. in a laboratory scale spray dryer. Finally, different ratios of bacteria and solid materials were evaluated on retention of viability. The maximum viability was achieved with addition of at least 2 % $^{w}/_{w}$ trehalose. Microscopic observations indicated that these powder particles were smooth, i.e. the trehalose provides sufficient coverage for protection.

The residual viability of spray dried *L. plantarum* WCFS1 decreased with storage time. A decimal viability loss time (D-value) of approximately 600 days was determined when stored at temperatures below 40 °C for different carriers. At higher temperatures, the D-value decreased with an exponential dependency on the temperature for maltodextrin DE = 6. Furthermore, the storage at temperatures higher than the T_g of the formulation lead to significant residual viability reduction (e.g. for sucrose).

The spray drying of *L. plantarum* WCFS1 is restricted by dehydration and thermal inactivation. A diagram was constructed that indicates combinations of outlet air temperature and residual moisture content that are optimal with respect to retention of viability and dryer efficiency. The latter combinations are specifically influenced by a minimal thermal inactivation line and the glass transition temperature of the formulation. This diagram can be applied to explore preferred combinations of solid carriers and spray drying conditions.

Nomenclature

A	Viability fraction	–
c_p	Heat capacity	$J \cdot kg^{-1}K^{-1}$
D	Decimal reduction time	day
I	Integrated intensity (area under the curve)	–
t	Time	day
T_g	Glass transition temperature	K
W	Weight fraction of crystalline phase	–
y	Mass fraction	–

Subscripts:

a	Reference crystal phase
i	Sample
0	Initial

Appendices

Prediction of glass transition temperature of powder mixtures

The glass transition temperature of powders mixtures was calculated using the Couchman-Karasz relation (30, 209, 210):

$$\boldsymbol{T_g} = \frac{\sum \boldsymbol{y_i \Delta c_{p,i} T_{g,i}}}{\sum \boldsymbol{y_i \Delta c_{p,i}}} \qquad \text{(8-A1)}$$

with y the mass fraction, Δc_p the transition of isobaric heat capacity increment, and T_g the glass transition of the pure component i. The data for Δc_p and T_g of the components are listed in Table 8-A1. Examples of glass transition temperatures of mixtures of solid components as a function of moisture content are shown in Figure 8-A1.

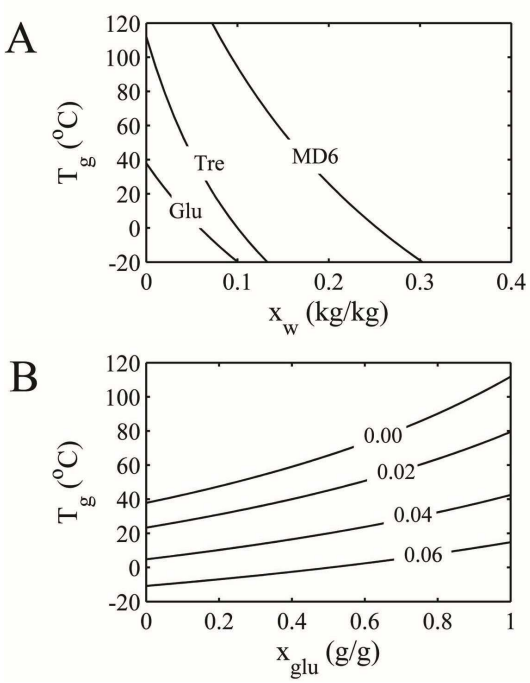

Figure 8-A1 A: Glass transition temperatures of maltodextrin DE 6 (MD6), trehalose (Tre), and glucose (Glu) as a function of moisture content. B: Glass transition temperatures of trehalose-glucose mixtures as a function of the glucose mass fraction (x_{glu}) at 0, 0.02, 0.04, and 0.06 moisture contents.

Table 8-A1. An overview of carrier materials and their anhydrous glass transition temperature

Pure components	Abbreviated	T_g (°C)	Δc_p ($J \cdot g^{-1}K^{-1}$)	Reference
Water	Water	-138	1.93	(220)
Sorbitol	Stol	-3	1.17	(221)
Mannitol	Mtol	10	1.27	(221)
Xylose	Xyl	13	0.95	(210)
Galactose	Gal	32	0.86	(210)
Glucose	Glu	38	0.88	(210)
Sucrose	Suc	70	0.77	(210)
Maltose	Mal	95	0.79	(210)
Lactose	Lac	101	0.26[a]	(222)
Trehalose	Tre	112	0.37 [a]	(84, 223)
Fructo-oligosaccharides	FOS	100	0.43	(30)
Galacto-oligosaccharides	GOS	100	0.43	(30)
Inulin	Inulin	119	0.43	(30)
Maltodextrin DE 16	MD16	183	0.43	(30)
Maltodextrin DE 6	MD6	195	0.43	(30)
Potato starch	Starch	243	0.43	(30, 224)
Lysine	Lys	-15	NA	(225)
L-glutamine	L-Glu	39	NA	(225)
Lactalbumin hydrolisate	Lactal hyd.	151	NA	(225)
Glutamic acid	Gla	214	NA	(225)
Glycine	Gly	326	NA	(225)

[a] Estimated from Gordon-Taylor constant (222)

[b] Estimated based on the molecular weight using Fox-Flory relation (30)

Analysis of the inactivation kinetics during storage

The inactivation kinetics of *L. plantarum* WCFS1 during storage was represented with a decimal reduction time *D* (Figure 8-6). The decimal reduction time is calculated as (34)

$$\log(A/A_0) = -t/D \qquad \text{(8-A2)}$$

Equation 8-A2 was fitted to experimental results to determine the *D* value of *L. plantarum* WCFS1 spray dried with different carriers and stored at specific temperatures (Figure 8-A2).

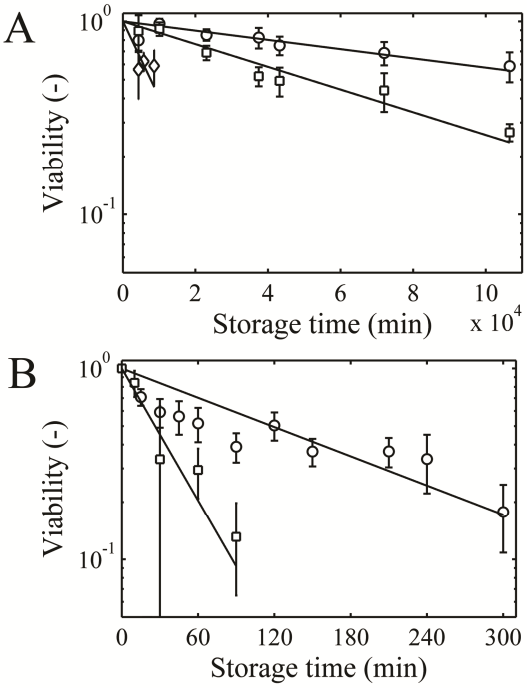

Figure 8-A2. A: Residual viability of *L. plantarum* WCFS1 spray dried with maltodextrin DE 6 during storage at 4 (○), 37 (□), and 50 °C (◊). B: Residual viability of *L. plantarum* WCFS1 spray dried with maltodextrin DE 6 during storage at 70 (○) and 75 °C (□). The error bars represent the standard deviation of the viability measurement results. The spray drying was carried out in a laboratory scale spray dryer at inlet and outlet air temperatures of 100 and 50 °C, respectively.

Chapter 9

Inactivation of *L. plantarum* WCFS1 during spray drying and storage assessed with three complementary enumeration methods

Submitted for publication as:

J. Perdana, H.M.W. den Besten, O. Kutahya, D.C. Aryani, M.B. Fox, M. Kleerebezem, R.M. Boom, and M.A.I. Schutyser. Inactivation of *L. plantarum* WCFS1 during spray drying and storage assessed with three complementary enumeration methods.

Abstract

In this study residual viability of *L. plantarum* WCFS1 spray-dried under different conditions was investigated. Three different enumeration methods were evaluated to assess whether inactivation is due to cell membrane damage and/or due to damage to intracellular components. The first method involved characterisation of the cell growth in a liquid medium by means of detection time, the second a membrane integrity viability-based method, and the third is carried out by conventional plating. At mild spray drying conditions with an outlet air temperature of 50 °C, all enumeration methods indicated very high residual viability values (> 95 %), which decreased when higher outlet spray drying temperatures were applied. At outlet temperatures of 80 °C or higher, residual viabilities determined using a detection time method and by conventional plating were lower compared to those determined using the membrane integrity method. This suggests that under the latter conditions cell membrane damage is probably not determining loss of viability but damage to intracellular components. Residual viability of the spray-dried cells was also evaluated as function of storage time and temperature. The cell membrane integrity method showed a slower viability loss rate as function of storage time compared to when determined with the other methods. Therefore, it is hypothesized that during storage, cell inactivation and/or prolonged repair time occurs primarily due to damage to intracellular components.

Keywords: viability enumeration, growth parameters, detection time, membrane integrity, probiotics drying

Introduction

In our previous study we investigated spray drying as an alternative for freeze drying to dehydrate probiotic bacteria (207). During spray drying at low outlet temperatures (up to 50 °C), membrane damage was discussed to be the main reason for viability loss (182, 226-229). However, at elevated outlet air temperatures (i.e. when cells are exposed to temperatures >65 °C) it was hypothesized that intracellular components such as ribosomes and nucleic acids are primarily affected (183, 226, 230). This will hamper cells to resume growth or at least the repair time before growth starts will be increased (231). In this case, the cell membrane-integrity method will not be able to detect all the lethally injured cells resulting in overestimation of viability (75, 176, 232-235). Therefore, this study adds two enumeration methods to assess viability loss based on growth behaviour. Plate counting is the standard enumeration method involving the cultivation of cells on a nutrient agar surface and subsequent colony counting. However, it requires elaborate preparations and takes approximately 2 days for cells to be incubated and counted (236, 237). Another method is the detection time method which is based on cell growth capacity in a liquid medium (238, 239).

This study aims at obtaining more insight in the effect of spray drying of probiotics and its subsequent storage on the loss of viability. Moreover, it relates decreased viability to loss of integrity of the cell membrane and/or to damage to internal cell components. The three complementary methods are used to assess the residual viability of *Lactobacillus plantarum* WCFS1, which is selected as a model micro-organism for probiotic lactobacilli (161, 162). The comparative analysis of these techniques is applied to obtain better understanding of the subcellular lethal damage (e.g. membrane damage and/or intracellular component damage) that may occur during spray drying and storage (38, 182, 226, 229).

Materials and methods

Culture preparation

Lactobacillus plantarum WCFS1 was grown in de Man, Rogosa and Sharpes (MRS) broth (BD Difco, USA) at 30 °C for 24 h. An aliquot of 1 % of the culture was transferred and re-cultured in the same conditions for 16 h. This overnight culture contained approximately 10^9 cfu/ml. The bacteria were harvested by centrifugation for 10 minutes at 13,500 × *g* at 4 °C using Eppendorf Centrifuge 5804R with F-34-6-38 rotor (Eppendorf, Germany). The pH

of the spent culture medium was usually between 3.9 and 4.1. The bacterial pellet was washed twice with 10 ml phosphate buffered saline (PBS) solution (Sigma-Aldrich, Germany) adjusted to pH 4.0.

The samples for the drying experiments were prepared by diluting the cell suspension to approximately 10^8 cells per ml in PBS (pH 4.0). The diluted cell suspension was mixed with an equal volume of 40 % ($^w/_w$) solutions of maltodextrin (DE 4-8, Glucidex 6; Roquette, France), fructose, galactose, sucrose, lactose, sorbitol, mannitol, or trehalose (Sigma-Aldrich, Germany) in PBS (pH 4.0) and used for spray drying experiments.

Spray drying

Spray drying experiments were carried out in a Buchi B-190 spray dryer (Buchi Labortechnik AG, Switzerland). The implemented drying regimes included outlet air temperatures of 50 and 90 °C with inlet air temperatures that were set 45 °C higher than the outlet air temperatures. The moisture content of the resulting powders, determined using Sartorius MA 35 (Sartorius Mechatronic, Germany) gravimetric analyser, was between 4 and 8 %. Spray drying experiments were performed in duplicate for independently prepared cell suspensions.

Viability assessment on the basis of cell membrane integrity

One drop of the of the 200-folds diluted washed cell culture (in PBS pH = 7.4) prior to spray drying experiments (reference sample) or approximately 1 mg of spray-dried particles (treated sample) containing *L. plantarum* WCFS1 were transferred and rehydrated on a sterilized Anopore (aluminium oxide nanoporous) chip (Microdish BV, The Netherlands) positioned on top of a 1 % low melting point agarose gel (Invitrogen, USA) containing 0.34 μM Propidium Iodide and 0.34 μM Syto 9 as the membrane integrity probes (Live/Dead BacLight bacterial viability kit, Invitrogen, USA). The samples were incubated for 30 minutes on Anopore, then excited by 470 nm light to induce a fluorescent spectral shift to green (intact cell membrane) or red (damaged cell membrane) and imaged using a Zeiss Axioplan 2 Imaging microscope equipped with a Zeiss LD Plan-Neofluar 63_/0.75 Corr Ph2 objective lens and a single-band fluorescein isothiocyanate (FITC) filter. Twenty images containing approximately 4000 individual cells were captured using charge-coupled device (CCD) camera controlled by Cell^B imaging acquisition software (Olympus, Japan). Automated viability determination was performed via an image analysis routine written in

Matlab (MathWorks, USA). More detailed description of the method has previously been reported (75, 234, 235).

Viability assessment using plate counting

A reference sample was prepared by taking an aliquot of washed cell culture prior to spray drying experiments and diluting it 200-fold in PBS (pH = 7.4). The treated (spray-dried) samples were prepared by re-suspending a 100 mg of the spray-dried particles containing *L. plantarum* WCFS1 to a 5 ml sterilized PBS solution (pH = 7.4), which also generates a 200-fold dilution from the original cell suspension, thereby having a comparable absolute cell density (live and dead cells together) as the reference sample. The resulting suspensions were decimally diluted in PBS (up to 8 dilutions), and 50 µl of these dilutions was plated on MRS agar (BD Difco, USA) plates using an Eddy Jet 2 spiral plater (IUL Instrument, Spain). Plating was done in duplicate for each dilution. The plates were incubated at 30 °C for 48 h, followed by colony counting of the dilutions that generated between 30 and 300 colonies per plate. The fractional viability was determined by the ratio of the recovered colonies after each treatment and the colony count of the reference sample.

Growth experiments and optical density measurements

The growth experiments in liquid medium were performed in a Bioscreen C MBR (Bioscreen, Finland). For that, the reference sample was prepared by taking an aliquot of washed cell culture prior to spray drying experiments and diluting it 200-folds in PBS (pH = 7.4). The treated (spray-dried) samples were prepared by re-suspending a 100 mg of the spray-dried particles containing *L. plantarum* WCFS1 to a 5 ml sterilized PBS solution (pH = 7.4). Serial two-fold dilutions of the initial cell suspensions in MRS were prepared by subsequent dilution in a honeycomb format 10×10 micro-plate (Bioscreen, Finland) with 15 wells per dilution series. Growth was measured in terms of optical density (OD) at 600 nm every 5 minutes during incubation for 48 h at 30 °C with intermittent 30 s shaking at medium intensity. These growth experiments were performed in triplicate for each spray drying batch.

Estimating residual viability using detection time method

The ability of *L. plantarum* WCFS1 to resume growth was measured for fresh and spray-dried cultures. A method was followed that evaluates the bacterial growth in terms of the

detection time (239), which is here defined as the time required for a culture starting with an initial cell number of x_0 to reach a cell number of x_{det} while still being in the exponential growth phase. This detection time (denoted as t_{det}) may be determined with

$$\boldsymbol{t_{det}(x_0) = \lambda(x_0) + \frac{\ln(x_{det}/x_0)}{\mu}} \quad (9\text{-}1)$$

with $\lambda(x_0)$ the population lag time for x_0 number of initial cell concentration, and μ the specific growth rate of cell.

Cell growth was monitored indirectly as a function of the optical density (240), which allowed an inline measurement at short time intervals (order of magnitude: minutes). The prerequisite for this is that a correlation between the cell concentration and the optical density reading is available. When the detection time t_{det} is assessed in term of the optical density *OD*, OD_{det} needs to be set instead of x_{det}. For our system, an arbitrary optical density value of 0.5 was selected. Then, a relation between t_{det} and $\ln(x_0)$ for all dilution ratio was constructed; the specific growth rate was estimated from the slope between t_{det} and $\ln(x_0)$ when the culture is still in the exponential growth phase.

The initial viable cell concentration ($x_{0,s}$) in the processed (spray-dried and subsequently stored) samples was determined relative to a reference sample ($x_{0,ref}$).

$$\ln(x_{0,ref}/x_{0,s}) = \mu[t_{det}(x_{0,s}) - t_{det}(x_{0,ref})] \quad (9\text{-}2)$$

with $t_{det}(x_{0,s})$ and $t_{det}(x_{0,ref})$ the time required to reach an OD value of 0.5 for the sample (treated) and the reference sample respectively. Fresh cultures from the working solution prior to spray drying were used as reference samples.

The viability value determined using this approach should be interpreted with care because it is composed of at least two contributing factors, (1) the increase of lethally injured cells during spray drying, and (2) the delayed regrowth of sub-lethally injured cells as a consequence of the required time for resuscitation (231, 241).

Calculations and statistical analyses

The specific growth rate and the viability values were estimated using a non-linear least square method solved using the Levenberg-Marquardt algorithm (128). The confidence interval of the parameters (p = 0.95) were estimated using the Hessian matrix, which was

derived from the Jacobian matrix of the solution (129). All calculations were performed with MATLAB version 7.10.

Analysis of trehalose concentration within the cells

To assess whether the drying process not only removed intracellular water, but also led to transfer of solid carrier material into bacterial cells, the concentration of solid carrier within the spray-dried cell cultures was measured. A *Lactobacillus plantarum* WCFS1 (approximately 10^9 cfu/ml) suspension in a 20 % ($^{w}/_{w}$) trehalose solution was spray-dried at 95 (inlet air temperature) and 50 °C (outlet air temperature) using a Buchi B-190 Mini Spray Dryer (Buchi Labortechnik, Switzerland). The resulting powder (approximately 10^9 cfu per 0.2 g) was washed twice in 40 ml PBS (pH = 7.4). Washed cells were re-suspended in 100 µl lysis buffer (Lysis buffer: 0.4 g sodium dodecyl sulphate (SDS), 0.15 g dithiotreitol (DTT), and 10 ml of 100 mM Tris/HCl pH 7.6) in a 1.5 ml sterile micro Mini-BeadBeater vial with 0.1 mm glass bead (Biospeck, USA). The sample was vortexed with FastPrep (FP120, BIO101/Savent) at 6000 mm/s speed 4 times 45 s. Between runs, the sample was cooled on ice for 1 minute. Subsequently, cell debris was removed by centrifugation at 21,000 × *g* for 10 minutes at 4 °C and supernatant was collected. The supernatant was 10-fold diluted in Milli-Q water (Millipore, USA) and aliquots of 0.1 ml sample were analysed by high performance liquid chromatography (HPLC) with Rezex RSO oligosaccharide column (Phenomenex, The Netherlands) at 80 °C. The column was eluted with Milli-Q water at a flow rate of 0.3 ml/minute. A refractive index detector was used to quantify the amount of trehalose.

Results and discussion

Validation of the detection time method

In Figure 9-1A, the growth curves of *L. plantarum* WCFS1 with series of two-fold dilutions are shown. The time axes of the individual curves were shifted such that all curves reached an OD = 0.5 at the same time. It was found that all curves overlapped. This suggests that the growth behaviour of the cultures is identical and independent of initial cell concentration. It also means that dilutions only affect the time to reach the detection point.

Exponential growth of *L. plantarum* WCFS1 was observed between OD 0.3 and 1.0 (Figure 9-1A). The OD in this range is proportional to the cell concentration (Figure 9-1B). At an OD value of 0.5 (used to determine the detection time) we may therefore safely assume that *L. plantarum* WCFS1 is in the exponential growth phase.

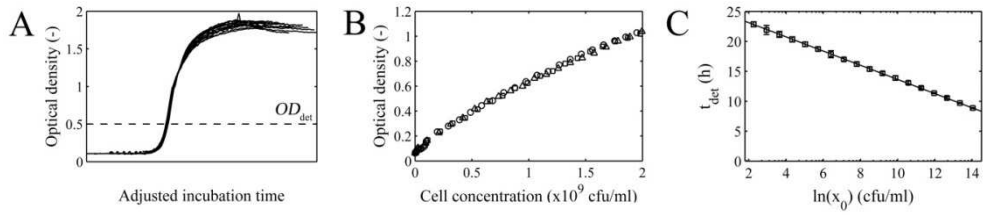

Figure 9-1. A: The growth curves of *L. plantarum* WCFS1 from series of two-fold dilution after shifting of the incubation time. B: Optical density at wavelength of 600 nm as a function of cell concentration of *L. plantarum* WCFS1. C: Time required to reach optical density value of 0.5 as a function of initial viable cell concentration. The symbols represent the experimental data, the error bars represent the 95 % confidence interval of data, and the solid line represents the data fitting with Eq. 9-2. The *L. plantarum* WCFS1 culture was obtained after incubation at 30 °C for 16 h.

A logarithmic relationship between detection time (t_{det}) and initial cell concentration (x_0) is found (Figure 9-1C), which is in line with Eq. 9-2. Thus, the specific growth rate can be determined from the slope of the line between t_{det} and ln(x_0) (Eq. 9-2), yielding μ = 0.84 ± 0.0070 h^{-1} for 95 % confidence interval of the parameter.

A cell culture may lose (part of) its viability upon spray drying and subsequent storage. Increasing growth detection time while using the same initial cell concentration in the feed can be considered indicative of a decrease in viability ($\boldsymbol{x_{0,s}}$) induced by drying, which includes 1) lethally damaged cells and 2) sub-lethally damaged cells requiring longer resuscitation time. The viability fraction that remains after spray drying ($\boldsymbol{x_{0,s}/x_{0,ref}}$) is estimated using Eq. 9-2, which is graphically represented in Figure 9-2. The prerequisite for this method is that the specific growth rate (μ) remains unaffected by the spray drying treatment. This assumption is valid because similar slope values for *L. plantarum* WCFS1

spray-dried at various conditions are obtained, indicating the same specific growth rate (Figure 9-2).

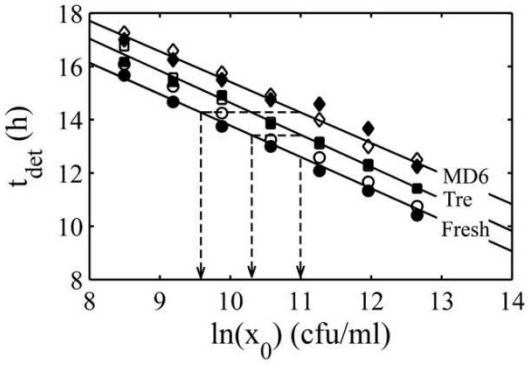

Figure 9-2. The times required to reach an OD of 0.5 in a two-fold dilution series of *L. plantarum* WCFS1 from fresh cultures (○, Fresh), spray-dried cultures in trehalose at air temperature of 90 °C (□, Tre), and spray-dried cultures in maltodextrin DE 6 at an air temperature of 80 °C (◊, MD6). The symbols represent the measurement data from two independent experiments and the lines represent the fitting results. The dashed lines represent the residual viability compared to that in fresh cultures.

Comparison of the three methods to determine residual viability of spray-dried cells

The residual viability of *L. plantarum* WCFS1 spray-dried in various matrices was assessed using the membrane integrity determination and the detection time method directly after spray drying (with inlet and outlet air temperatures of 95 and 50 °C, respectively). Viability values close to 100 % were measured (Figure 9-3A). It can be concluded that under these conditions the cell membrane and intracellular components remained mostly intact and thus growth is not hampered (183, 226). This can be explained by the relatively low temperature and short drying time (between 1 and 1.5 s according to the dryer specification (184)) in the laboratory scale spray dryer.

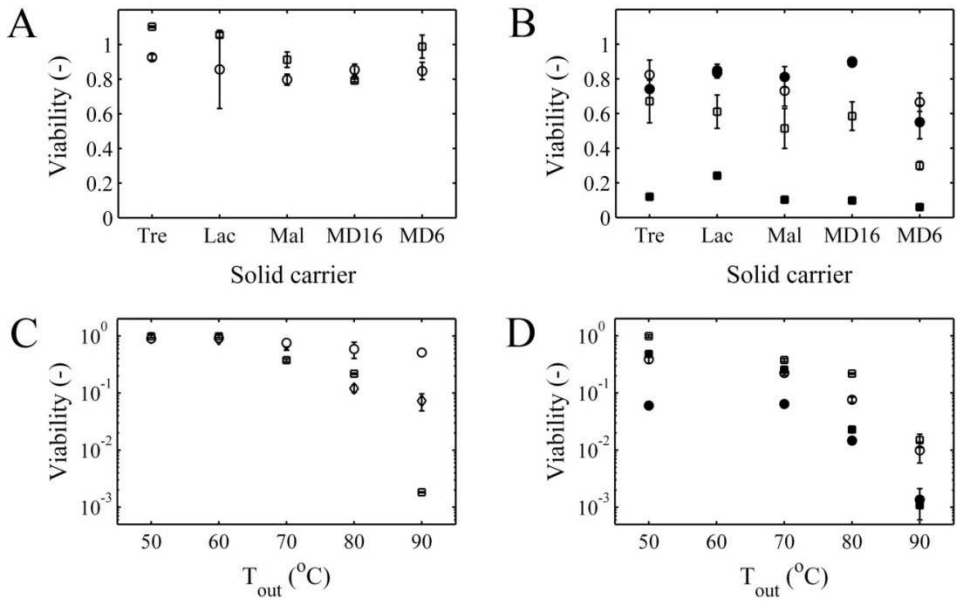

Figure 9-3. A: Residual viability of *L. plantarum* WCFS1 spray-dried in trehalose (Tre), lactose (Lac), maltose (Mal), maltodextrin DE 16 (MD16), and maltodextrin DE 6 (MD6) directly assessed after spray drying using the detection time method (□) and using the membrane integrity method (○). The spray drying was carried out at inlet and outlet air temperatures of 95 and 50 °C, respectively.

B: Residual viability of *L. plantarum* WCFS1 spray-dried in trehalose (Tre), lactose (Lac), maltose (Mal), maltodextrin DE 16 (MD16), and maltodextrin DE 6 (MD6) assessed using membrane integrity method after storage for 60 days at -26 °C (○) and at 4 °C (●) and using the detection time method after storage for 60 days at -26 °C (□) and at 4 °C (■).

C: Residual viability of *L. plantarum* WCFS1 spray-dried in a 20 % ($^{w}/_{w}$) maltodextrin DE 6 solution at outlet air temperatures between 50 and 90 °C (the inlet air temperatures was set 45 °C higher than the outlet air temperatures) assessed using the membrane integrity method (○), detection time method (□), and plating (◊). Error bars represent the standard deviation of the viability measurements.

D: Residual viability of *L. plantarum* WCFS1 spray-dried in maltodextrin DE 6 at outlet air temperatures between 50 and 90 °C (inlet air temperature was set 45 °C higher than the outlet air temperature) after storage for 1 day (□) and for 60 days (○) at -26 °C and after storage for 1 day (■) and for 60 days (●) at 4 °C assessed using the detection time method. Error bars represent the standard deviation of the viability measurements.

The residual viability of spray-dried *L. plantarum* WCFS1 in a 20 % $^{w}/_{w}$ maltodextrin DE 6 solution was more than 95 % for outlet air temperatures 60 °C or lower (Figure 9-3C). At outlet temperatures of 70 °C or higher, the residual viability decreased. At higher spray drying temperatures, the conventional plating and detection time methods indicated a stronger reduction of viability compared to the results from the membrane integrity method, in particular when outlet temperature was 80 °C or higher (Figure 9-3C). It may be that at these high outlet temperatures, significant part of the viability loss is due to intracellular damage (226, 230). The limited damage to the cell membrane could be explained by rapid fixation of the cells in a vitrifying matrix during spray drying (33, 45, 183). The lower detection time viability values compared to those from plating for spray dried *L. plantarum* WCFS1 at an outlet temperature of 90 °C could indicate an increased degree of sub-lethal damage that requires longer resuscitation time before growth can be resumed. Plate count enumeration allows individual sub-lethally damaged cells to repair successfully and thus these cells will be counted as viable.

Residual viability of spray-dried *L. plantarum* WCFS1 during storage

A higher retention of the cell-membrane integrity based viability after storage for 1 and 60 days is observed for *L. plantarum* WCFS1 spray-dried in low molecular weight solid carriers compared to those dried in maltodextrin DE 6 (molecular weight > 3 kDa) carrier (Figure 9-3B). This suggests that low molecular weight solid carriers are more suited for stabilization of the cell membrane, which is in agreement with previous studies (188, 197). However, the detection time method indicated no large differences in viability after storage for 60 days when *L. plantarum* WCFS1 is spray dried in the presence of different solid carriers (Figure 9-3B). Thus, during storage the addition of solid carriers can only enhance the stability of the cell membrane but not that of the intracellular components. This is in

agreement with our separate observation that solid carriers do not penetrate or accumulate in the cells, which can be explained by the barrier imposed by the intact cell membrane (242, 243). As shown in Figure 9-4, only a very small amount of trehalose (3.33 mg/ml) is present inside the *L. plantarum* WCFS1 cells. These value were obtained for cells spray-dried in 20 % ($^{w}/_{w}$) trehalose solution at a low outlet temperature (T_{out} = 50 °C) to retain a high viability. In other studies, it has been explored that at least 20 % internal trehalose per wet cell weight is required, to enhance stability of intracellular components against desiccation and subsequent storage (244, 245). It is hypothesized that trehalose acts as an osmolyte to stabilize intracellular macromolecules and thereby extend shelf life (25, 244-249). Values of 20 % of intracellular trehalose were not obtained with spray drying (Figure 9-4).

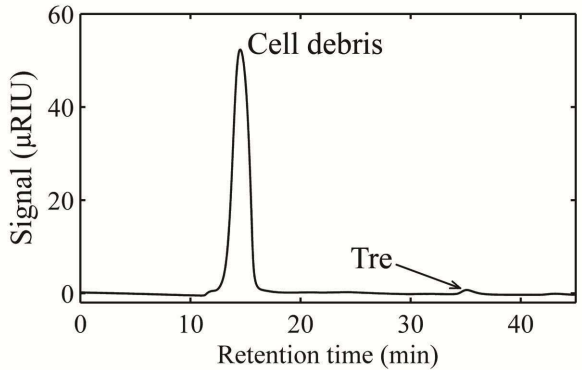

Figure 9-4. HPLC analysis is applied to measure intracellular trehalose concentration after spray drying. The feed contained 10^9 cfu/ml *L. plantarum* WCFS1 in a 20 % ($^{w}/_{w}$) trehalose solution. The dashed line represents an approximation of the expected peak height when the intracellular trehalose concentration would be 2 % of trehalose weight per wet cell weight.

The residual viability of spray-dried *L. plantarum* WCFS1 in a 20 % $^{w}/_{w}$ maltodextrin DE 6 solution at outlet temperatures between 50 and 90 °C also decreased with storage time. The detection time method yielded a higher residual viability when spray-dried *L. plantarum* WCFS1was stored at -26 °C compared to when it was stored at 4 °C (Figure 9-3D). At -26 °C, the degradation of constituents (by enzymatic or non-enzymatic

reactions) is expected to be slower due to smaller reaction rates and limited molecular mobility (68, 80, 250-253). After storage for 60 days, the membrane integrity method resulted in a higher degree of residual viability as compared to the viability measured by the detection time method (Figure 9-3D). This suggests that the damage to the cell membrane is less critical than the damage to the other cellular components (i.e. intracellular constituents). It is because the cell membrane is fixated in the vitrified matrix, whereas the intracellular constituents are detrimentally affected due to for example Maillard reactions, lipid oxidation, the decreased activity of enzymes, or other reactions (226, 246, 254).

Conclusion

We presented a detection time method to assess and analyse the residual viability of spray dried *L. plantarum* WCFS1. This method is based on the time needed to reach a specific concentration of cells by growth in a liquid medium. The residual viability based on growth behaviour was compared to the residual viability determined by the cell membrane integrity method. At mild drying conditions (outlet drying air temperature 50 °C), both methods indicated similar viability values higher than 95 %, which indicates limited influence of spray drying on cell viability. At higher spray drying temperatures (80 °C or higher), a significant difference was found between the methods, which suggests that the inactivation at these temperatures has to be related to degradation of the intracellular components and not to cell membrane damage.

The residual viability of the cells decreases during storage. Both the membrane integrity and the detection time methods gave the same, small decrease in viability at -26 °C. By contrast, at 4 °C, the membrane integrity remained high during storage, whereas the detection period indicated a strong decrease in viability, indicating that again intracellular damage is likely responsible for the reduction in viability.

Nomenclature

A_{det}	Optical density to determine the detection time	–
t_{det}	Detection time	h
x	Number of cell concentration	cfu

Greek symbols

λ	Population lag time	h
μ	Specific growth rate	h^{-1}

Subscripts:

0	Initial
det	Detection
ref	Reference

Chapter 10

General discussion

Introduction

In the research reported in this thesis, an experimental platform was developed to explore the conditions for optimal spray drying of heat sensitive products. The platform is based on controlled drying of single sessile droplets deposited on a flat hydrophobic surface followed by analysis of the resulting dried particles. It was successfully applied to establish the inactivation kinetics of the enzyme β-galactosidase and the probiotic bacterium *Lactobacillus plantarum* WCFS1 during drying. The experimental work was combined with modelling of 1) the drying kinetics of sessile droplets (including temperature and moisture content histories and their distribution across the droplet) and 2) the inactivation kinetics of the enzyme or the bacterium. The predicted residual activity of the enzyme and residual viability of the bacterium were in agreement with the data obtained from single droplet drying experiments. The validity of the models was further confirmed when predicting and analysing inactivation during laboratory spray drying experiments. Finally, insight was gained into the optimum spray drying conditions relevant for industrial production scale.

In this chapter we will discuss the following topics:

- Section I: The combination of a single droplet platform and modelling approaches as a tool to identify optimum spray drying conditions
- Section II: General recommendations for optimum spray drying conditions of probiotics at the industrial scale
- Section III: Conceptual design of an optimal drying process for probiotics
- Section IV: Economic and efficiency analysis including a comparison between spray and freeze drying
- Section V: Future outlook for research on drying of probiotics

The combination of a single droplet platform and modelling approaches for identifying optimum spray drying conditions

The need for screening methodologies is clear when considering the costs of pilot scale experimentation and the number of parameters involved in the optimisation of spray drying, e.g. processing conditions, formulation, and component-specific sensitivity. Use of

laboratory-scale spray dryers for the optimisation is often problematic, since especially drying time and particle size distribution cannot be easily translated to spray drying at the industrial scale (11, 137, 255). Moreover, the drying behaviour at the laboratory-scale induces specific physical and chemical changes which might not be comparable to the industrial scale (256-258).

An attractive alternative approach for screening of optimal spray drying conditions is via a single droplet drying approach combined with predictive modelling (64). During single droplet drying, the conditions such as drying air temperature, drying time, air flow rate (and slip velocity between the air and the dried particles), and particle size) are well defined. Therefore, this approach is well suited for the generation of data required for model development and can be applied to systematically investigate the drying kinetics. Different single droplet approaches have been described to study the influence of drying on inactivation, such as acoustic levitation and droplets drying at the outlet of a capillary. The latter methods have been applied to study the influence of drying on the residual activity of enzymes, on the residual count of viable cells, on the quality of milk and of flavours (6, 133, 197, 259-261). The single droplet drying approach in this thesis is based on drying of sessile droplets on a hydrophobic surface, which has the major advantage that it allows the development of a high throughput approach.

The retention of the functionality of the activity of the product is usually dependent on the drying trajectory of an individual droplet, including the specific histories of the moisture content and temperature (6, 64, 75, 207). Directly monitoring the temperature and moisture gradients within very small drying droplets is virtually impossible (< 200 μm). Therefore many studies choose to work with larger droplets and measure the internal temperature with a thermocouple and the mass change due to dehydration with an analytical balance. In our studies we decided to rely on the commonly applied effective diffusion model to describe the evolving temperature and moisture content histories during single droplet drying (49, 59, 64, 167).

A schematic overview of the combined use of an experimental single droplet drying platform and modelling to arrive at improved drying procedures is shown in Figure 10-1. The experimental single droplet data can be used to establish the inactivation kinetics or change in functionality. Modelling can be used to quantify the changes in moisture and

temperature in location and time. These can then be combined with the (descriptive) functionality model from the experiments. A final step is then to confirm (validate) the predictive models with experimental data from e.g. pilot-scale spray drying experiments, which was demonstrated for drying of β-galactosidase and *Lactobacillus plantarum* WCFS1 (64, 207). After this validation the predictive model may be used to optimise spray drying at the industrial scale. The kinetic models also may be applied in more advanced simulations at the industrial scale, e.g. using computational fluid dynamics (CFD).

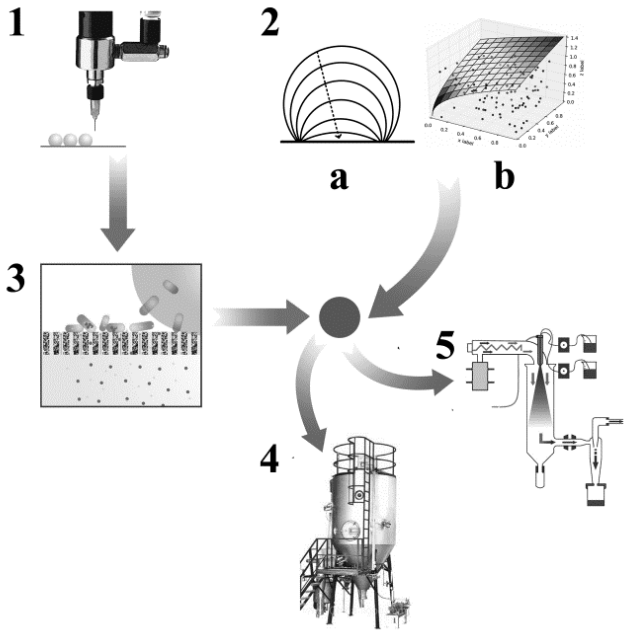

Figure 10-1. Flow diagram of the spray drying experimentation approach involving single droplet drying (1), predictive modelling (2) of drying kinetics (a) and inactivation kinetics (b), residual activity or survival measurement (3), optimization of the existing spray drying procedures (4), and new design for drying system (5).

In addition, the single droplet drying approach can provide insight on different types of spray drying applications, for example, encapsulation of volatile components or healthy

oils. Within many applications, the morphology of the particle changes during the drying process (e.g. formation of vacuoles, crystals, pores). These changes can be monitored visually and studied as a function of drying conditions and selected matrices. Finally, it is well known that drying can affect the spatial distribution of components within a particle, for example by segregation of components (e.g.: fat and lactose) during drying (258, 262, 263). The single droplet approach may well be used to explore such behaviour.

General recommendations for optimum spray drying conditions of probiotics at the industrial scale

Optimisation of (spray) drying of probiotics involves 1) proper culture preparation, 2) adequate carrier formulation, and 3) application of optimum drying conditions. This thesis focused primarily on the influence of carrier formulation and drying parameters on inactivation of *L. plantarum WCFS 1*.

Carrier formulation

This research indicated that solid carriers should be selected that have a high glass transition temperature and exert minimum dehydration inactivation to bacteria (197). Dehydration inactivation can be avoided by fast vitrification, e.g. when very small droplets are generated leading to a fast drying process (e.g. in a laboratory scale spray dryer). If slower drying cannot be avoided, the selection of the solid carriers is crucial to the residual viability of bacteria after drying.

In Figure 10-2, two different carriers are shown (maltodextrin and sucrose) which have different glass transitions. Maltodextrin with a higher T_g is preferred as a carrier because of its higher glass transition temperature providing more rapid vitrification. With respect to drying conditions, a low drying temperature is not preferred, since it results in a lower drying capacity or a higher water content in the final product. Most optimum drying conditions are indicated with the grey filled circles in Figure 10-2 (region A for maltodextrin and region B for sucrose) in which vitrification can still be realized and the drying rate is reasonable, while the thermal inactivation is minimal. However, from shelf life point of view, lower final moisture content is preferred because of the slower viability loss during storage (Chapter 8). Therefore, for cells dried in maltodextrin, it is advisable to further dry the powder to region A' to obtain a longer retention of viability. In practice,

further drying to region A' can be realized via e.g. fluidized bed drying. A slightly elevated temperature in the first part of fluidized bed drying is usually needed to enable the drying. It is important to assure that viability does not drop during fluidized bed drying.

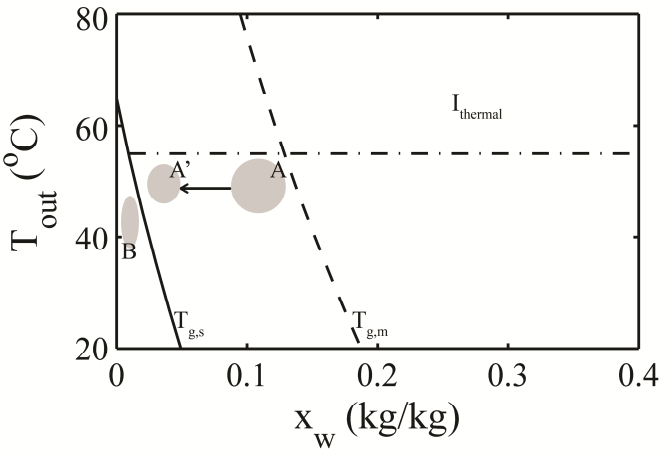

Figure 10-2. Optimum drying conditions for maximum viability considering the thermal inactivation (I), and different glass transition temperatures of maltodextrin ($T_{g,m}$) and sucrose ($T_{g,s}$). The grey regions represent the optimum conditions for drying or storage.

Drying conditions

Loss of viability of *L. plantarum* WCFS1 during drying occurs due to dehydration and/or thermal inactivation (Chapter 7). Inactivation due to dehydration can be minimized by (nearly) instant vitrification of the matrix: this does not allow micro-organisms to respond metabolically to the changing conditions; in addition some physical responses (e.g., phase changes in the phospholipid bilayer) may also be prevented. This assumption has been validated for very short drying times (1.3 s) in a laboratory scale spray dryer. One may assume that also for larger spray dryers (e.g. in a spray dryer with a typical drying time shorter than 30 s) the loss of viability is mostly determined by thermal inactivation.

The rate of viability loss due to thermal inactivation decreases considerably with the moisture content. Therefore, fast drying is preferred to minimize the thermal inactivation.

This can be achieved by reducing the droplet size (207). In Figure 10-3A, a contour plot is provided to show the combined effect of droplet size and outlet air temperature on estimated residual activity. Almost 90 % viability can be achieved for a droplet with an initial diameter of 100 μm when spray dried at an outlet air temperature of 50 °C.

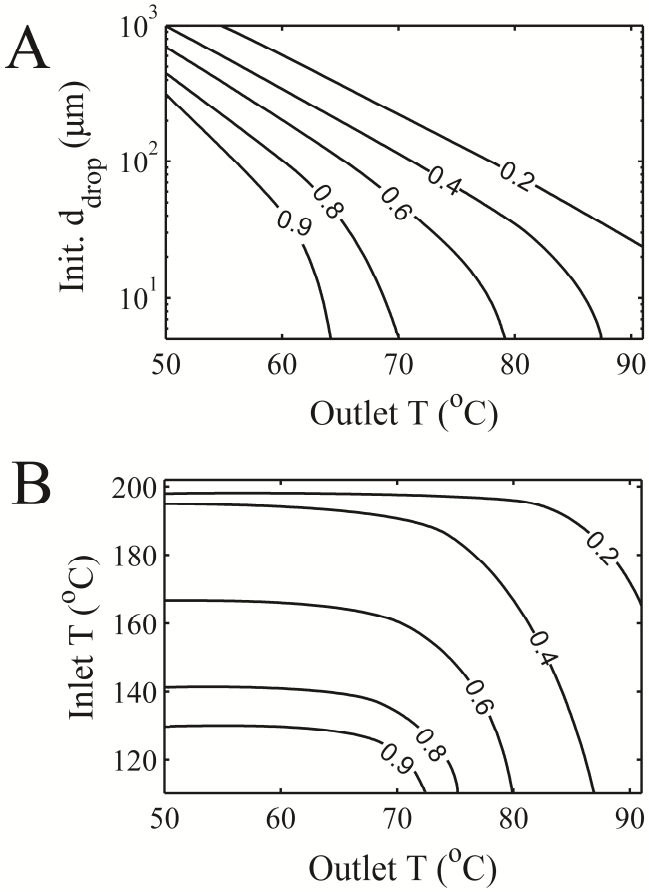

Figure 10-3. Contour plots of residual viability of *L. plantarum* WCFS1 as a function of initial droplet diameter and the spray drying outlet air temperature, while the inlet air temperature was set 30 °C higher than the outlet air temperature (A) and as a function of inlet and outlet air temperature, while the initial droplet diameter was set to 10 μm. The feed formulation contains 20 % $^{w}/_{w}$ maltodextrin and approx. 10^{8} cfu/ml cell cultures. The plots were smoothen for representation.

The inlet and outlet air temperatures of the spray dryer are essential to the retention of the viability (Figure 10-3B), but it is much more sensitive to the outlet air temperature. This is logical: while the droplet does not assume the inlet temperature due to evaporative cooling, it does assume the outlet temperatures in the later stages of the spray drying process. As shown in the contour plot (Figure 10-3B), the residual viability decreases rapidly when the outlet air temperature increases from 70 to 90 °C. The inlet air temperature has large influence between 190 and 200 °C: under these conditions the droplet which is not fully dried yet will still rapidly heat up towards a temperature that induces thermal inactivation.

Conceptual design of an optimal drying process for probiotics

A conceptual design is proposed for spray drying at a high drying rate and outlet air temperatures between 20 and 60 °C, thus avoiding both dehydration and thermal inactivation. Another advantage of using low temperature drying is that solid carriers with high glass transition temperatures can provide glassy powders; however, the use of low molecular weight carbohydrates (MW < 2 kDa) in the formulation is generally recommended for their stabilising effect on the cell membrane despite their glass transition temperature being lower (Chapter 8).

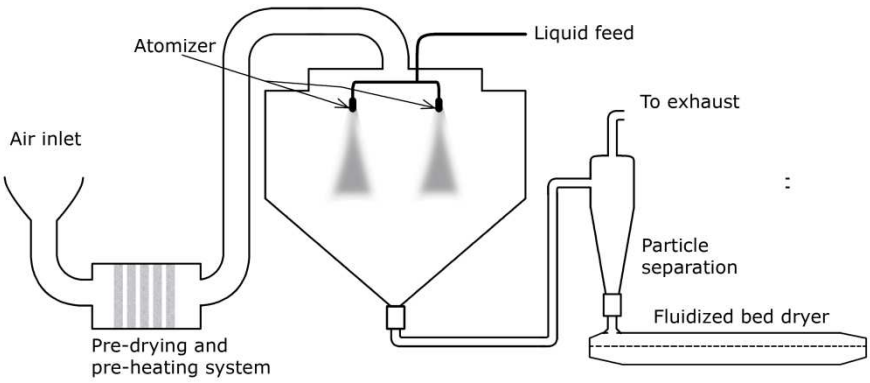

Figure 10-4. Schematic design of the low temperature spray drying system

Several challenges remain for low temperature drying, because of the slow drying and the large volumes of drying air required. Therefore, the following aspects should be considered in the conceptual design of the spray dryer:

1. It is recommended to reduce the particle size compared to conventional spray driers to decrease the drying time. At the same time the (initial) drying temperature should be as high as possible, such that viability is retained with highest drying efficiency possible (Figure 10-3A and Figure 10-5A). The recommended droplet diameter is between 5 and 50 μm. A narrow distribution of droplet diameters is desired to ensure uniform drying conditions. To generate the recommended droplet diameters, one could explore novel atomization techniques, e.g. piezo-driven atomization or microfluidic nozzles (264). To operate at acceptable capacity, large volumes of drying air are required (Figure 10-5B). This may be achieved by design of a drying chamber with a large diameter in combination with many low capacity nozzles in parallel or several narrow drying chambers in parallel. The height of the drying chamber can be small because of the shorter drying times Figure 10-5A.
2. It is advisable to pre-dry the drying air to maximise the uptake of water per kg supplied drying air. This is important because often the maximum allowable temperature is still relatively low (i.e. between 40 and 70 °C) depending on the bacterial strain and the carrier formulation used. For example, adsorptive drying (e.g. using zeolites) can be used to pre- or re-dry the drying air ((265, 266)
3. Agglomeration is usually applied to increase particle size for easier and safer handling of the powder; particles smaller than 10 μm can be dangerous if inhaled, while agglomerated particles are easier to dissolve. However, it should be noted that the process of agglomeration involving powder rewetting (267, 268) may involve the risk of reduced survival. Therefore, it is recommended to carry out the agglomeration using a binding agent.
4. A high performance cyclone or a bag-house filter or fibrous filter is required to collect small particles from the air.
5. A second dryer (fluidized bed) may be required to achieve sufficiently low powder moisture content. To maximise survival, it is preferred that the powder directly after spray drying is already in the glassy state. This second drying will be beneficial to maintain viability during storage (Chapter 8).

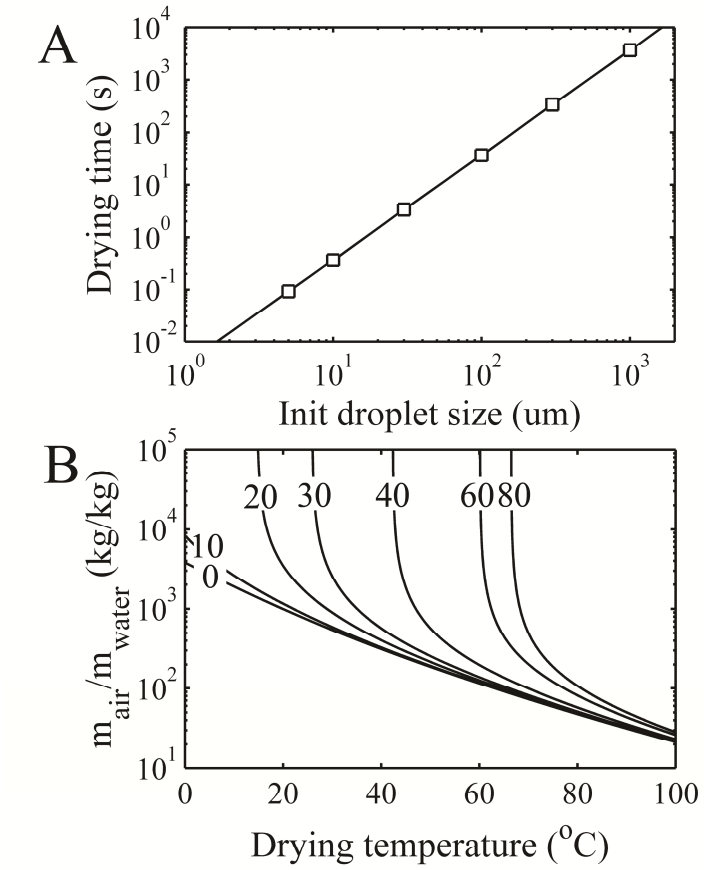

Figure 10-5. A: Drying time as a function of initial droplet size to achieve 7 % water content. We assumed that the droplets were dried at high air flow rate at temperature of 40 °C. Initial moisture was assumed 80 % $^{w}/_{w}$. B: The mass ratio of drying air required and the water removed during drying as a function of temperature to achieve a residual water content of 7 % $^{w}/_{w}$. The solid lines represent this ratio for different initial relative humidity of the drying air at 25 °C ranging between 0 and 80 %.

Comparison between spray and freeze drying on the basis of economics and energy

Spray drying could be an attractive alternative to freeze drying to preserve probiotics. To support the latter statement analyses were made of costs and energy consumption of spray and freeze drying of probiotics at an industrial scale.

Energy analyses were made on the basis of the energy required to remove 1 kg of water. For spray drying, the energy required for removal of 1 kg of water is can be interpolated from available data (269) as:

$$H_{lv} = 2499.90 - 2.11T - 3.09 \cdot 10^{-3}T^2 \quad (10\text{-}1)$$

with H_{lv} is the enthalpy of evaporation and T is the temperature. If the final moisture content of the dried powder is fixed to 5 % (a_w ~ 0.2) (270, 271), the drying air required to evaporate 1 kg of water is

$$m_a = Mw_a \frac{Mw_w}{0.2 \cdot P_{sat}^w} \quad (10\text{-}2)$$

with Mw_a and Mw_w are the molecular weight of air and water, respectively, and P_{sat}^w the saturated pressure of water in air, which is estimated following the Antoine equation (272)

$$P_{sat}^w = \frac{101325}{760} \cdot 10^{\left(8.071 - \frac{1730.63}{233.43+T}\right)} \quad (10\text{-}3)$$

with P_{sat}^win bar and T in °C. The spray drying outlet air temperatures were set between 40 and 80 °C, while the inlet air temperatures were calculated from the enthalpy balance:

$$m_a c_{p,a}\left(T_{a,in} - T_{a,out}\right) = m_w\left[c_{p,w}\left(T_{w,in} - T_{w,out}\right) + H_{lv}\right] \quad (10\text{-}4)$$

Finally, the total energy required for spray drying (Q_{SD}) per kg of water evaporated is calculated as

$$Q_{SD} = m_a c_{p,a}\left(T_{a,in} - T_{a,amb}\right) \quad (10\text{-}5)$$

with $T_{a,amb}$ the ambient temperature of feed air (set to 20 °C).

In freeze drying, sublimation requires most (45 %) of the total energy (273) and requires for 1 kg of water:

$$H_{sv} = 2834.1 - 0.290T - 0.004T^2 \quad (10\text{-}6)$$

with H_{sv} is the enthalpy of sublimation. Thus, the total energy required per kg evaporated water in freeze drying can be roughly estimated as

$$Q_{FD} = H_{sv}/0.45 \quad (10\text{-}7)$$

which is comparable (Figure 10-6) to other studies indicating total energy requirements of 7330 kJ (274) or 6467 kJ (275).

It can be concluded from Figure 10-6 that spray drying requires approximately 40 % less energy than freeze drying to remove 1 kg of water. For freeze drying, the energy required is not a function of the drying temperature, while in a spray drying, it decreases with the increase of outlet air temperature.

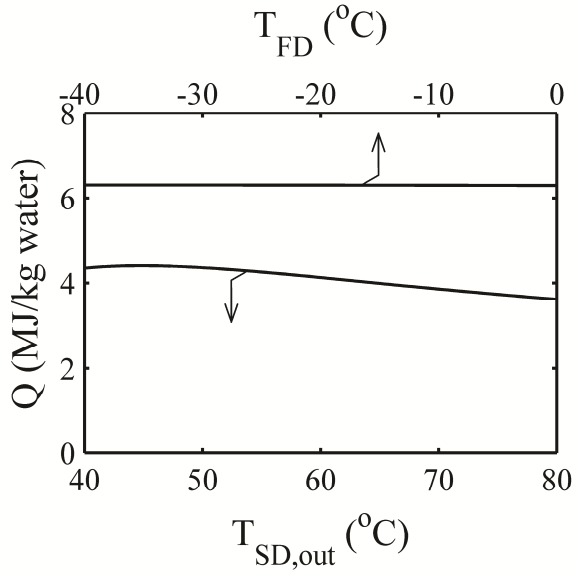

Figure 10-6. Comparison of energy required to evaporate 1 kg of water using freeze drying (FD) and spray drying (SD) as a function of operating temperatures.

For the economic analysis, the moisture content in the feed and the product were fixed to 80 % and 6 %, respectively. It was assumed that 240 batch productions could be carried out per year.

The capital investments for a spray dryer (C_{SD}) may be estimated with (276):

$$C_{SD} = 323 + 1.74 \times S^{0.7} \quad (10\text{-}8)$$

for purchasing in January 2013 in k€ and with *S* being the evaporation capacity in kg water per hour for a capacity range between 400 and 4000. To retain the maximum viability of probiotics after spray drying, a low spray drying outlet temperature (T_{out} = 50–60 °C) and small particle size ($d_{atomizer}$ ~ 10 µm) are assumed. The result of the latter assumptions is that the spray dryer capacity decreases to about 28 % or 46 % for outlet air temperatures of 50 and 60 °C, respectively, when compared to spray drying at 80 °C.

The capital investments for a freeze dryer in k€ are estimated as (277):

$$C_{FD} = 12.2 \times S^{0.564} \quad (10\text{-}9)$$

recalculated from purchasing costs in 2004 to purchasing costs in January 2013 with C_{FD} are the costs of the freeze dryer with condenser capacity *S*.

The overall production facility capital costs were roughly estimated using the Lang Factor (276) to provide a more accurate cost calculation per kg product

$$C = F \times \sum C_e \quad (10\text{-}10)$$

in which *C* are the production facility capital costs, *F* is the installation factor (3.63 for mixed solid-fluid products), and C_e are the capital costs for the major unit operations in the facility, in this case either a spray or a freeze dryer. The capital investments corrected with the installation factor (Eq. 10-10) for every kg product (assuming 10 year depreciation with 240 production days per year) are in shown Figure 10-7A.

The variable costs for freeze drying depend mostly on the volume of the chamber and the operational parameters applied. Adjusted to 2013, the variable costs to evaporate 1 kg of ice varies between €1.20 (16) and €1.90 per kg of water evaporated (13, 278).

For spray drying, adjusted to 2013 the variable costs vary between € 0.055 (capacity 250 kg/h) and € 0.013 (capacity 6000 kg/h) per kg of water evaporated with only half of the cost

is required for the utility expenses (21, 103). The work of Holsinger and co-worker (103) indicated costs of € 0.03 for a spray drying capacity of 2400 kg/h water evaporated at outlet air temperature of 40-50°C, which is comparable to our calculation. To dehydrate probiotics, low drying temperatures (Tout = 50–60°C) and small droplet sizes (e.g. 10 µm) are assumed, increasing the variable costs (Figure 10-7B).

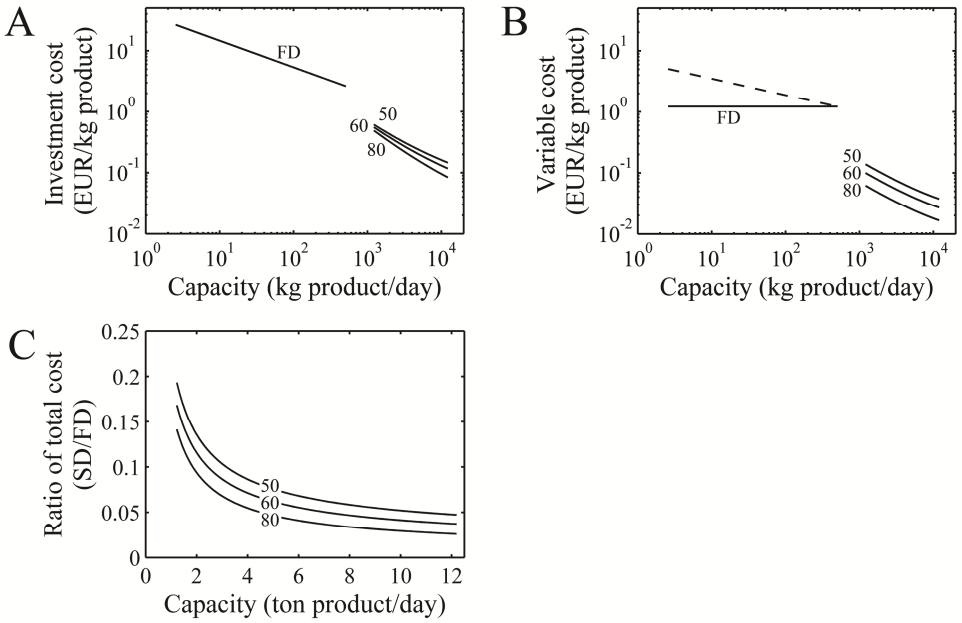

Figure 10-7. Comparison of investment cost (A), variable cost (B), and total cost (C) per kg of dried probiotic cultures for freeze drying (FD), spray drying with outlet air temperature of 50 (50), 60 (60), and 80 °C (80). The drying parameters were more elaborately described in the text.

The variable costs for spray drying are thus 8 to 50 times lower than freeze drying, which is in the same order of magnitude reported in literature (279). Compared to the lowest freeze drying costs (for a freeze dryer with 2000 kg ice condenser capacity, square symbol in Figure 10-7), spray drying with capacity higher than 1000 kg product per day still is at least 5 times less costly than freeze drying in term of total cost per kg dried product, which is the sum of investment and operational costs. The costs of spray drying compared to freeze

drying decrease further with increasing outlet air temperature and spray drying capacity. On the basis of this economic evaluation, spray drying is an attractive alternative to freeze drying to dehydrate probiotics, especially for a large production volume (e.g. above 2 ton product per day), despite the use of low temperatures and small particle size limiting the capacity of the equipment. Spray drying becomes more cost attractive than freeze drying with the increase of production capacity (Figure 10-7C); above a production volume of 100 kg/day, spray drying is more cost effective. Vice versa, spray drying becomes less attractive when the production capacity approximately 100 kg product per day (~4 product kg/h, based on extrapolation from Figure 10-7A and B). Thus, whether freeze drying or spray drying is the best route to dehydrate probiotics probably depends on the production capacity.

Future outlook for research on drying of probiotics

In this section we sketch a perspective on the scientific state of affairs, and provide an outlook on the research that should be explored in the future, in line with the results reported in this thesis. The following directions were identified:

Pilot spray drying tests

A first series of pilot scale spray drying experiments with *L. plantarum* WCFS1 suspended in a maltodextrin DE 6 formulation has been carried out. The residual viability decreased with spray drying outlet air temperatures and particle size (Figure 10-8). This is in agreement with our previous prediction (Chapter 7). A residual viability close to 100 % was only obtained for outlet air temperatures below 60 °C and a particle diameter below 20 μm (when assuming ideal shrinkage during drying this size can be translated to an initial droplet diameter of less than 35 μm). These results suggest that dehydration and thermal inactivation are absent for small particles that were quickly dried in the pilot-scale dryer as well. However, thermal inactivation is still very relevant for large particles.

The predicted viability values, which is based on the kinetics from single droplet drying experiments (**Chapter 7**) and the drying kinetics of the single droplets relevant to the pilot scale spray drying (NIRO 25) estimated using NIZO Premia software (280, 281), are in a good agreement with the viability data from the experiments. This suggests that the modelling approach is translate-able to a larger scale.

Further optimization of pilot scale spray drying can be done by improving the formulation (e.g. using trehalose or lactose as the solid carrier) as suggested in this thesis. Additionally, it should be tested whether the cell concentrations could be increased (e.g. 10^{10} cfu/ml compared to the current formulation with approximately $5 \cdot 10^{8}$ cfu/ml) or the amount of solid carrier could be reduced.

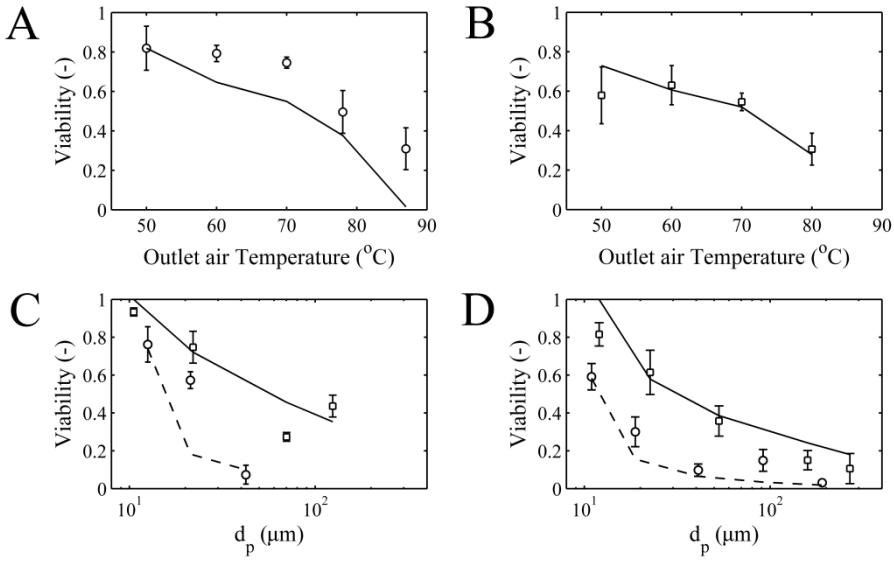

Figure 10-8. Residual viability of *L. plantarum* WCS1 spray dried in pilot scale experiments. Outlet air temperatures were varied between 50 and 90 °C and inlet air temperature of 140 °C and atomization with a high pressure (figure A) or a two-fluid nozzle (figure B). Symbols represent the experimental data and lines represent the predicted viability values.

Residual viability of *L. plantarum* WCS1 spray dried in pilot scale experiments as a function of dried particle size. Outlet air temperatures of 50 (□) and 80 °C (○) and atomization with a high pressure (figure C) or a two-fluid nozzle (figure D). Lines represent the predicted viability values for 50 (solid lines) and 80 °C (dashed lines).

The feed formulation consisted of approximately $5 \cdot 10^{7}$ cfu/ml cells suspended in 20 % w/w maltodextrin DE 6 in PBS pH = 4.0.

In depth study of viability loss during storage

Spray drying can, at specific conditions, provide at least the same degree of viability of *L. plantarum* WCFS1 compared to freeze drying. However, during storage time the residual viability declines; the reason for this is not yet fully understood. Comparative studies on storage of spray- and freeze dried probiotic formulations should be carried out to explore spray drying as an alternative to freeze drying. The loss of viability during storage depends on the formulation, storage temperature, moisture content, and possibly also the cell strains and their cultivation method (173, 214). It should be investigated whether the type of drying process itself is a factor of importance as well.

Elucidation of dehydration and thermal inactivation mechanisms at the cellular level

It is hypothesized that the inactivation of microbial cells during drying is very much related to the state of the cell membrane. Abrupt transition from liquid crystalline to gel phase may induce membrane leakage leading to viability loss (22). Specific solid carrier can protect the cell membrane from damage (leakage) upon drying. This for example is explained using water replacement and vitrification hypothesis (33, 45) or hydration force theory (282). More in depth studies should be carried out to find more details the mechanism leading to cell membrane leakage. Critical is the monitoring of membrane stability during dehydration. Several techniques that might be of interest to study the integrity of cell membranes during storage or (de- or re-) hydration are tabulated in Table 10-1.

Cell membrane leakage can be detected for example by monitoring the presence of metabolites in the incubation medium (20, 227) or by using fluorescence staining (75, 176). Since an intact cell will not leak metabolites, the amount of metabolites that can be detected outside the cells can be used as a direct measure for the degree of degradation of the cell membrane. Using fluorescence staining, specific stains can be used that only internalize when cell membranes are damaged via passive transport (diffusion). Subsequently, stains can have specific interaction with internal cell components, e.g. nucleic acids. Differential scanning calorimetry (DSC) is used to monitor the denaturation behaviour of proteins. It can be used to identify protein denaturation during drying or heating inside cells (226, 249). Recently, also atomic force and super resolution microscopy have been applied to detect development of leakage in cell membranes. For the latter technique, chemicals or

fluorescence protein tags are required to stain the cell membrane, which enables the discrimination between the cell membrane and other cell components.

Table 10-1. Techniques to study the integrity of cell membrane during storage or de- or rehydration

Technique	Reference
Monitoring the leakage of potassium or hydrolysed DNA products into the incubation medium	(20, 227)
Fluorescence staining	(75, 176)
Differential scanning calorimetry (DSC)	(226, 249)
Atomic force microscopy (AFM)	(135, 283)
Super-resolution microscopes combined with chemical tag or green fluorescence proteins (GFP)	(284-288)

Conclusion

The single droplet drying platform in combination with predictive modelling tools provides a promising approach for establishing optimum spray drying conditions for heat sensitive products. Optimal spray drying conditions for probiotics are proposed and translated into a conceptual design of a spray dryer operating at low temperature and with small primary droplet diameter (< 50 µm). An energy evaluation showed that spray drying at low temperature is 40 % more energy efficient than freeze drying. An economic evaluation showed that spray drying of probiotics at low temperature is more cost effective (up to a factor 5) than freeze drying for production volumes larger than approximately 2000 kg per day. First series of pilot-scale experiments indicated that spray drying of probiotic formulations is indeed promising at a larger-scale given that low temperatures are applied and small droplets are dried. Finally, future research challenges were identified as a follow-up of this study. These involve amongst others the need for further understanding of the viability loss during storage and elucidation of dehydration and thermal inactivation mechanisms at the cellular level.

Nomenclature

c_p	Heat capacity	$kJ \cdot kg^{-1}K^{-1}$
C	Capital investment	k€
C_e	Capital costs for the major unit operation facility	k€
d	Diameter	m
F	Installation factor	–
H_{lv}	Enthalpy of evaporation	$kJ \cdot kg^{-1}$
H_{sv}	Enthalpy of sublimation	$kJ \cdot kg^{-1}$
m	Mass	kg
Mw	Molecular mass	$kg \cdot mol^{-1}$
P_{sat}^{w}	Saturated pressure of water	bar
Q	Energy/heat	kJ
S	Evaporation capacity	kg/h
T	Temperature	°C

Greek symbols

λ	Population lag time	h
μ	Specific growth rate	h^{-1}

Subscripts:

a	Air
amb	Ambient
atomizer	Atomizer
FD	Freeze drying
in	Inlet
out	Outlet
SD	Spray drying
w	Water/feed samples

Summary

Spray drying is a widely used drying method to preserve foods and food ingredients. Because of the very short drying time and the relative low temperatures to which the products are exposed, spray drying is considered a mild drying method. Still, in practice freeze drying (or lyophilisation) of heat vulnerable products such as enzymes or probiotic bacteria is often preferred. The main reason is that already moderately elevated temperatures can lead to unacceptable loss of activity or lower survival. However, spray drying is also more energy and cost effective as it can process larger volumes and operate at higher energy efficiencies. Therefore, studies have been carried out to optimise spray drying, including development of tailored formulations, to obtain minimal loss of activity or viability. Most (optimisation) studies have been carried out through pilot-scale experimentation. Drawbacks of such experimental investigations are that they are costly, time consuming, and difficult to translate to other products or dryer configurations. The latter is especially difficult because the drying conditions in dryers depend on numerous parameters (e.g. atomisation, chamber design) resulting in a unique residence time distribution and particle size distribution.

This thesis describes the development of an alternative approach to study drying behaviour, involving single droplet experimentation in combination with predictive modelling. During single droplet drying, conditions such as drying air temperature, drying time, air flow rate, and particle size can be well controlled. Therefore, it has been applied to systematically investigate inactivation kinetics of heat vulnerable components. This provides a sound basis for model development, and can be used as a tool for screening of optimal spray drying conditions.

A single droplet drying platform has been developed allowing the controlled drying of droplets, mimicking the drying of droplets during spray drying. Small droplets (150 μm or larger) are dispensed pneumatically on a hydrophobic membrane and are subsequently dried of the droplets under well-defined drying air conditions for a defined time. In principle, the system allows high throughput experimentation for screening purposes, in contrast to other methods such as single droplets that are dried at the tip of a capillary or that are acoustically levitated. The pneumatic dispensing process was characterised by

dispensing various liquids and modelling the dispensing behaviour with Bernoulli's law. Next, single droplet drying of water droplets was investigated at different temperatures and air flow rates. A Sherwood correlation was derived to describe the mass transfer between the sessile water droplets and the drying air.

Subsequently, the single droplet drying platform was used to investigate the drying behaviour of maltodextrin suspensions. An effective diffusion model was developed to describe the drying history of the droplets. The model could predict the developing temperature and moisture gradients inside the drying droplets. It was verified that the heat transfer via the contacting surface was minimal compared to the heat transfer via the air.

As an input for the effective diffusion model, a method was developed to quantitatively determine the moisture diffusivities in solid matrices as a function of the temperature and the moisture content. This method was based on gravimetric analysis of thin film drying in a dynamic vapour sorption (DVS) analyser. The results indicated that the moisture diffusivity decreases with decreasing moisture content and temperature. The latter could also be modelled on the basis of first principles. The moisture diffusivities are similar for various carbohydrate matrices, but are different for different types of systems (e.g. skimmed milk, glycerol).

An enzyme (β-galactosidase) was selected as a model to verify our approach in assessing the influence of drying on the degradation (inactivation) of a heat sensitive ingredient during (spray) drying. For this enzyme we characterised first the effect of the temperature and the moisture content on the loss of activity. A mathematical model was developed to describe the inactivation kinetics of this enzyme as a function of these two parameters. The model for the inactivation kinetics was then combined with the effective diffusion model to form a predictive tool for the influence of drying on the residual activity. This model was then used to reversely estimate the parameters of the inactivation kinetics from the single droplet drying experiments. Finally, the full inactivation kinetics was verified by comparing the model predictions to the experimental data obtained from laboratory-scale spray drying experiments.

Single droplet drying was subsequently used to investigate the influence of drying on the survival of *Lactobacillus plantarum* WCFS1, which was selected as a model probiotic bacterium. As interface with the single droplet drying platform, a novel viability

enumeration method was developed. A requirement for this method was that it should be suitable for high throughput experimentation. The method employs a micro-porous aluminium oxide (Anopore) chip. (Semi-) dried particles were rehydrated on this micro-porous chip in a medium containing fluorescence probes for live/death enumeration. Subsequently, fluorescence-microscopy and image analysis are used to determine the live/dead ratio of bacteria. The method provided survival percentages in agreement with those found with conventional plating. The novel viability enumeration method was also successfully applied in combination with laboratory-scale spray drying experiments.

The viability enumeration method was used to study the inactivation of *L. plantarum WCFS1* during drying. Two inactivation mechanisms during drying can be distinguished. The first is inactivation by dehydration, which occurs at varying temperatures, due to the destabilisation of the cell membrane during removal of water. The second is inactivation by heat (for *L. plantarum* WCFS1 at temperatures above 45 ^{o}C) and is most probably related to loss of functionality of critical components, such as cell membrane, ribosomes, or intracellular proteins. Inactivation by dehydration can be minimised by drying very rapidly. Fast drying leads to instant vitrification of the solid matrix preventing destabilisation of the cell membrane, which needs time. For slow drying processes (e.g. during hot air or freeze drying) lower survival rates were observed.

The retention of viability of spray dried *L. plantarum* WCFS1 is influenced by the formulation applied. Rapid fixation of the cells in a vitrifying protective matrix is desirable to retain maximum residual viability. Thus, in practice, maximum viability can achieved via the addition of an adequate concentration of protective agents (preferably with high T_g, which can be vitrified at high drying temperatures) combined with an instant drying process (e.g. in spray dryer). During drying, crystallization can be either beneficial (e.g. with mannitol and sorbitol) or detrimental (e.g. with lactose). In general, the effect of crystallization is smaller with rapid drying. Finally, the viability loss in terms of membrane integrity of *L. plantarum* WCFS1 stored in various conditions was monitored. The viability loss is not temperature dependent when stored at temperatures between -80 and 18 °C but a lower moisture content is desirable to enhance the retention of viability.

Another viability enumeration technique based on cell growth behaviour in liquid media was explored and compared to the enumeration based on the fluorescent staining. This new

technique is based on the detection time method to determine the residual viability of *L. plantarum* WCFS1 after spray drying. At spray drying (outlet) air temperatures higher than 70 °C, the residual viability of *L. plantarum* WCFS1 determined using a fluorescence probe is generally higher than that determined using traditional plating or the growth behaviour. This indicates that at such high spray drying temperatures damage to the intracellular components is most critical to the loss of viability.

In the general discussion, the combined use of single droplet drying experimentation and predictive modelling was presented to establish optimum conditions for heat sensitive products. General guidelines were provided for optimal spray drying of probiotics and translated into a conceptual design of a spray dryer operating at low temperature and drying small droplets. An economic analysis was made to compare spray drying at these conditions to conventional freeze drying. The overall costs for spray drying were lower by more than a factor 5 compared to those for freeze drying. Finally, a first series of pilot-scale experiments showed that spray drying of probiotic formulations is indeed promising at a larger-scale provided that low drying temperatures are applied and the products is atomized into very small droplets.

References

1. **Meng, X. C., C. Stanton, G. F. Fitzgerald, C. Daly, and R. P. Ross.** 2008. Anhydrobiotics: The challenges of drying probiotic cultures. Food Chem **106:**1406-1416.
2. **Peighambardoust, S. H., A. G. Tafti, M. A. Hejazi, and J. Hesari.** 2011. Application of spray drying for preservation of lactic acid starter cultures: a review. Trends Food Sci Tech.
3. **Rokka, S., and P. Rantamäki.** 2010. Protecting probiotic bacteria by microencapsulation: challenges for industrial applications. Eur Food Res Technol **231:**1-12.
4. **Mattila-Sandholm, T., P. Myllärinen, R. Crittenden, G. Mogensen, R. Fondén, and M. Saarela.** 2002. Technological challenges for future probiotic foods. Int Dairy J **12:**173-182.
5. **Schutyser, M. A. I., J. Perdana, and R. M. Boom.** 2012. Single droplet drying for optimal spray drying of enzymes and probiotics. Trends Food Sci Tech **27:**73-82.
6. **Yamamoto, S., and Y. Sano.** 1992. Drying of enzymes: enzyme retention during drying of a single droplet. Chem Eng Sci **47:**177-183.
7. **Sanchez, V., and A. Pilosof.** 2006. Drying of enzymes, Handbook of Industrial Drying, Third Edition. CRC Press.
8. **Ré, M. I.** 1998. Microencapsulation by spray drying. Dry Technol **16:**1195 - 1236.
9. **Millqvist-Fureby, A., M. Malmsten, and B. Bergenståhl.** 1999. Spray-drying of trypsin - surface characterisation and activity preservation. Int J Pharm **188:**243-253.
10. **Meerdink, G., and K. van't Riet.** 1991. Inactivation of thermostable α-amylase during drying. J Food Eng **14:**83-102.

11. **Filková, I., L. X. Huang, and A. Mujumdar.** 2006. Industrial spray drying systems. *In* A. Mujumdar (ed.), Handbook of Industrial Drying, Third Edition. CRC Press.

12. **Saxelin, M., B. Grenov, U. Svensson, R. Fondén, R. Reniero, and T. Mattila-Sandholm.** 1999. The technology of probiotics. Trends Food Sci Tech **10:**387-392.

13. **Franks, F.** 2008. Freeze-drying of pharmaceuticals and biopharmaceuticals. Royal Society of Chemistry.

14. **Roberto, B., and L. Athanasios.** 2006. Freeze drying. *In* A. S. Mujumdar (ed.), Handbook of Industrial Drying, 3 ed. CRC Press.

15. **Ananta, E., M. Volkert, and D. Knorr.** 2005. Cellular injuries and storage stability of spray-dried *Lactobacillus rhamnosus* GG. Int Dairy J **15:**399-409.

16. **Roser, B.** 1991. Trehalose, a new approach to premium dried foods. Trends Food Sci Tech **2:**166-169.

17. **Silva, J., R. Freixo, P. Gibbs, and P. Teixeira.** 2011. Spray-drying for the production of dried cultures. Int J Dairy Technol **64:**321-335.

18. **Mauriello, G., M. Aponte, R. Andolfi, G. Moschetti, and F. Villani.** 1999. Spray-drying of bacteriocin-producing lactic acid bacteria. J Food Prot **62:**773-777.

19. **Thybo, P., L. Hovgaard, J. Lindeløv, A. Brask, and S. Andersen.** 2008. Scaling up the spray drying process from pilot to production scale using an atomized droplet size criterion. Pharmaceut Res **25:**1610-1620.

20. **Lievense, L., M. M. Verbreek, A. Noomen, and K. van't Riet.** 1994. Mechanism of dehydration inactivation of *Lactobacillus plantarum*. Appl Microbiol Biotechnol **41:**90-94.

21. **Quinn, J. J.** 1965. The economics of spray drying. Ind Eng Chem **57:**35-37.

22. **Santivarangkna, C., U. Kulozik, and P. Foerst.** 2008. Inactivation mechanisms of lactic acid starter cultures preserved by drying processes. J Appl Microbiol **105:**1-13.

23. **Zhou, X., J. Dong, J. Gao, and Z. Yu.** 2008. Activity-loss characteristics of spores of *Bacillus thuringiensis* during spray drying. Food Bioprod Process **86:**37-42.

24. **Santivarangkna, C., B. Higl, and P. Foerst.** 2008. Protection mechanisms of sugars during different stages of preparation process of dried lactic acid starter cultures. Food Microbiol **25:**429-441.

25. **Guo, N., I. Puhlev, D. R. Brown, J. Mansbridge, and F. Levine.** 2000. Trehalose expression confers desiccation tolerance on human cells. Nat Biotechnol **18:**168-171.

26. **Soesanto, T., and M. C. Williams.** 1981. Volumetric interpretation of viscosity for concentrated and dilute sugar solutions. J Phys Chem **85:**3338-3341.

27. **Johari, G. P., and M. Goldstein.** 1970. Viscous liquids and the glass transition. II. Secondary relaxations in glasses of rigid molecules. J Chem Phys **53:**2372-2388.

28. **Cavaille, J. Y., J. Perez, and G. P. Johari.** 1989. Molecular theory for the rheology of glasses and polymers. Phys Rev B **39:**2411-2422.

29. **Cuq, B., J. Abecassis, and S. Guilbert.** 2003. State diagrams to help describe wheat bread processing. Int J Food Sci Tech **38:**759-766.

30. **van der Sman, R. G. M., and M. B. J. Meinders.** 2011. Prediction of the state diagram of starch water mixtures using the Flory-Huggins free volume theory. Soft Matter **7:**429-442.

31. **Rahman, M. S.** 2006. State diagram of foods: Its potential use in food processing and product stability. Trends Food Sci Tech **17:**129-141.

32. **Chang, L. Q., and M. J. Pikal.** 2009. Mechanisms of protein stabilization in the solid state. J Pharm Sci **98:**2886-2908.

33. **Crowe, J. H., J. F. Carpenter, and L. M. Crowe.** 1998. The role of vitrification in anhydrobiosis. Annu Rev Physiol **60:**73-103.

34. **Bigelow, W. D.** 1921. The logarithmic nature of thermal death time curves. J Infect Dis **29:**528-536.

35. **van Boekel, M. A. J. S.** 2002. On the use of the Weibull model to describe thermal inactivation of microbial vegetative cells. Int J Food Microbiol **74:**139-159.

36. **van Boekel, M. A. J. S.** 2009. Kinetics of protein and enzyme denaturation, Kinetic Modeling of Reactions in Foods. CRC Press, Boca Raton.

37. **Van Boekel, M. A. J. S.** 1996. Statistical aspects of kinetic modeling for food science problems. J Food Sci **61:**477-486.

38. **den Besten, H. M. W., and M. H. Zwietering.** 2012. Meta-analysis for quantitative microbiological risk assessments and benchmarking data. Trends Food Sci Technol **25:**34-39.

39. **Stanton, C., G. Gardiner, H. Meehan, K. Collins, G. Fitzgerald, P. B. Lynch, and R. P. Ross.** 2001. Market potential for probiotics. Am J Clin Nutr **73:**476s-483s.

40. **Stanton, C., R. P. Ross, G. F. Fitzgerald, and D. V. Sinderen.** 2005. Fermented functional foods based on probiotics and their biogenic metabolites. Curr Opin Biotechnol **16:**198-203.

41. **Saxelin, M.** 2008. Probiotic formulations and applications, the current probiotics market, and changes in the marketplace: A European perspective. Clin Infect Dis **46:**S76-S79.

42. **Yakult.** 2013. Yakult nutritional information.

43. **Crowe, J. H., F. A. Hoekstra, and L. M. Crowe.** 1992. Anhydrobiosis. Annu Rev Physiol **54:**579-599.

44. **Chen, X. D., and K. C. Patel.** 2007. Micro-organism inactivation during drying of small droplets or thin-layer slabs – A critical review of existing kinetics models and an appraisal of the drying rate dependent model. J Food Eng **82:**1-10.

45. **Leslie, S. B., E. Israeli, B. Lighthart, J. H. Crowe, and L. M. Crowe.** 1995. Trehalose and sucrose protect both membranes and proteins in intact bacteria during drying. Appl Environ Microbiol **61:**3592-3597.

46. **Crowe, J. H., L. M. Crowe, J. F. Carpenter, A. S. Rudolph, C. A. Wistrom, B. J. Spargo, and T. J. Anchordoguy.** 1988. Interactions of sugars with membranes. BBA-Rev Biomembranes **947:**367-384.

47. **Pierre, S.** 2002. Spray drying of dairy products: State of the art. Le Lait **82:**375-382.

48. **Brask, A., T. Ullum, P. Thybo, and M. Wahlberg.** 2007. High-temperature ultrasonic levitator for investigating drying kinetics of single droplets. Niro A/S.

49. **Schiffter, H., and G. Lee.** 2007. Single-droplet evaporation kinetics and particle formation in an acoustic levitator. Part 1: Evaporation of water microdroplets assessed using boundary-layer and acoustic levitation theories. J Pharm Sci **96:**2274-2283.

50. **Mezhericher, M., A. Levy, and I. Borde.** 2008. Heat and mass transfer of single droplet/wet particle drying. Chem Eng Sci **63:**12-23.

51. **Darby, R.** 2001. Chemical engineering fluid mechanics. Marcel Dekker, Inc, New York.

52. **Steffe, J. F., and R. P. Singh.** 1997. Pipeline design calculations for Newtonian and non-Newtonian fluids, Handbook of Food Engineering Practice. CRC Press.

53. **Deplanque, J. P., and R. H. Rangel.** 1998. A comparison of models, numerical simulation, and experimental results in droplet deposition processes. Acta Mater **46(14):**4925-4933.

54. **Sylvester, N. D., and S. L. Rosen.** 1970. Laminar flow in the entrance region of a cylindrical tube: Part I. Newtonian fluids. AIChE J **16:**964-966.

55. **Picknett, R. G., and R. Bexon.** 1976. The evaporation of sessile or pendant drops in still air. J Colloid Interf Sci **61:**336-350.

56. **Ranz, W. E., and W. R. Marshall.** 1952. Evaporation from drops. Chem Eng Prog **48:**141-146; 173-180.

57. **Oliveira, F. A. R., and J. C. Oliveira.** 2003. Sherwood Number, p. 895-901. Taylor & Francis.

58. **Baines, W. D., and D. F. James.** 1994. Evaporation of a droplet on a surface. Ind Eng Chem Res **33:**411-416.

59. **Sloth, J., S. Kiil, A. D. Jensen, S. K. Andersen, K. Jørgensen, H. Schiffter, and G. Lee.** 2006. Model based analysis of the drying of a single solution droplet in an ultrasonic levitator. Chem Eng Sci **61:**2701-2709.

60. **Písecký, J.** 1995. Evaporation and spray drying in the dairy industry. *In* A. S. Mujumdar (ed.), Handbook of Industrial Drying, 2 ed, vol. 1. CRC Press, Boca Raton.

61. **Hu, H., and R. G. Larson.** 2002. Evaporation of a sessile droplet on a substrate. J Phys Chem B **106:**1334-1344.

62. **Ranz, W. E., and J. M. Marshall.** 1952. Evaporation from drops, Part 1. Chem Eng Prog **48:**173.

63. **Desai, S. J., A. P. Simonelli, and W. I. Higuchi.** 1965. Investigation of factors influencing release of solid drug dispersed in inert matrices. J Pharm Sci **54:**1459-1464.

64. **Perdana, J., M. Fox, M. A. I. Schutyser, and R. Boom.** 2013. Mimicking spray drying by drying of single droplets deposited on a flat surface. Food Bioprocess Technol **6:**964-977.

65. **Berendsen, W. R., A. Lapin, and M. Reuss.** 2006. Investigations of reaction kinetics for immobilized enzymes – Identification of parameters in the presence of diffusion limitation. Biotechnol Prog **22:**1305-1312.

66. **Ubbink, J., and J. Krüger.** 2006. Physical approaches for the delivery of active ingredients in foods. Trends Food Sci Tech **17:**244-254.

67. **Perdana, J., M. B. Fox, M. A. I. Schutyser, and R. M. Boom.** 2011. Single-droplet experimentation on spray drying: evaporation of a sessile droplet. Chem Eng Technol **34:**1151-1158.

68. **Perdana, J., M. B. Fox, M. A. I. Schutyser, and R. M. Boom.** 2012. Enzyme inactivation kinetics: coupled effects of temperature and moisture content. Food Chem **133:**116-123.

69. **Sonner, C., Y.-F. Maa, and G. Lee.** 2002. Spray-freeze-drying for protein powder preparation: Particle characterization and a case study with trypsinogen stability. J Pharm Sci **91:**2122-2139.

70. **Wong, Y.-L., S. Sampson, W. A. Germishuizen, S. Goonesekera, G. Caponetti, J. Sadoff, B. R. Bloom, and D. Edwards.** 2007. Drying a tuberculosis vaccine without freezing. Proc Nat Acad Sci USA **104:**2591-2595.

71. **Ruan, R., S. J. Schmidt, A. R. Schmidt, and J. B. Litchfield.** 1991. Nondestructive measurement of transient moisture profiles and the moisture diffusion coefficient in a potato during drying and absorption by NMR imaging. J Food Process Eng **14:**297-313.

72. **McCarthy, M. J., D. Lasseux, and J. E. Maneval.** 1994. NMR imaging in the study of diffusion of water in foods. J Food Eng **22:**211-224.

73. **Chary, S. R., and R. K. Jain.** 1989. Direct measurement of interstitial convection and diffusion of albumin in normal and neoplastic tissues by fluorescence photobleaching. Proc Nat Acad Sci USA **86:**5385-5389.

74. **Reits, E. A. J., and J. J. Neefjes.** 2001. From fixed to FRAP: measuring protein mobility and activity in living cells. Nat Cell Biol **3:**E145-E147.

75. **Perdana, J., L. Bereschenko, M. Roghair, M. B. Fox, R. M. Boom, M. Kleerebezem, and M. A. Schutyser.** 2012. Novel method for enumeration of viable *Lactobacillus plantarum* WCFS1 cells after single-droplet drying. Appl Environ Microbiol **78:**8082-8088.

76. **Anal, A. K., and H. Singh.** 2007. Recent advances in microencapsulation of probiotics for industrial applications and targeted delivery. Trends Food Sci Technol **18:**240-251.

77. **Schoeber.** 1976. Regular regimes in sorption processes: Calculation of drying rates and determination of concentration dependent diffusion coefficients. Technische Hogeschool Eindhoven, Eindhoven.

78. **Coumans, W. J.** 1987. Power law diffusion in drying processes. Technical University of Eindhoven, Eindhoven.

79. **Yamamoto, S.** 2001. A short-cut method for determining concentration dependent diffusivity in liquid foods and polymer solutions from regular regime drying curves. Dry Technol **19:**1479 - 1490.

80. **van der Sman, R. G. M., and M. B. J. Meinders.** 2012. Moisture diffusivity in food materials. Food Chem.

81. **Yamamoto, S.** 1999. Effects of glycerol on the drying of gelatin and sugar solutions. Dry Technol **17:**1681-1695.

82. **Bengoechea, C., A. Arrachid, A. Guerrero, S. E. Hill, and J. R. Mitchell.** 2007. Relationship between the glass transition temperature and the melt flow behavior for gluten, casein and soya. J Cereal Sci **45:**275-284.

83. **Hancock, B. C., and G. Zografi.** 1994. The relationship between the glass transition temperature and the water content of amorphous pharmaceutical solids. Pharmaceut Res **11:**471-477.

84. **Simperler, A., A. Kornherr, R. Chopra, P. A. Bonnet, W. Jones, W. D. S. Motherwell, and G. Zifferer.** 2006. Glass transition temperature of glucose, sucrose, and trehalose: An experimental and *in silico* study. J Phys Chem B **110:**19678-19684.

85. **Nakamura, K., Y. Nishimura, T. Hatakeyama, and H. Hatakeyama.** 1995. Thermal properties of water insoluble alginate films containing di- and trivalent cations. Thermochim Acta **267:**343-353.

86. **Donth, E.** 2001. The glass transition: relaxation dynamics in liquids and disordered materials. Springer.

87. **Prevéy, P. S.** 2000. X-ray diffraction characterization of crystallinity and phase composition in plasma-sprayed hydroxyapatite coatings. J Therm Spray Technol **9:**369-376.

88. **Liou, J. K., and S. Bruin.** 1982. An approximate method for the nonlinear diffusion problem with a power relation between diffusion coefficient and concentration - I. Computation of desorption times. Int J Heat Mass Transfer **25:**1209-1220.

89. **Crank, J.** 1956. The mathematics of diffusion. Clarendon Press, Oxford.

90. **Coumans, W. J.** 2000. Models for drying kinetics based on drying curves of slabs. Chem Eng Process: Process Intensification **39:**53-68.

91. **Yamamoto, S., W. Coumans, and T. Vlugt.** 1997. Determining concentration-dependent diffusivity in food materials. Eng Food **1:**A164-A167.

92. **Darken, L. S.** 1948. Diffusion, mobility and their interrelation through free energy in binary metallic systems. Trans. AIME **175:**184–201.

93. **Krishna, R., and J. M. van Baten.** 2005. The Darken relation for multicomponent diffusion in liquid mixtures of linear alkanes: An investigation using molecular dynamics (MD) simulations. Ind Eng Chem Res **44:**6939-6947.

94. **Vrentas, J. S., and J. L. Duda.** 1977. Diffusion in polymer—solvent systems. I. Reexamination of the free-volume theory. J. Polym. Sci. Polym. Phys. Ed. **15:**403-416.

95. **Wang, J. H.** 1951. Self-diffusion and structure of liquid water. I. Measurement of self-diffusion of liquid water with deuterium as tracer. J Am Chem Soc **73:**510-513.

96. **He, X., A. Fowler, and M. Toner.** 2006. Water activity and mobility in solutions of glycerol and small molecular weight sugars: Implication for cryo- and lyopreservation. J Appl Phys **100:**074702-074711.

97. **Limbach, H. J., and J. Ubbink.** 2008. Structure and dynamics of maltooligomer-water solutions and glasses. Soft Matter **4:**1887-1898.

98. **Edward, J. T.** 1970. Molecular volumes and the Stokes-Einstein equation. J Chem Educ **47:**261.

99. **Scholte, T. G., N. L. J. Meijerink, H. M. Schoffeleers, and A. M. G. Brands.** 1984. Mark–Houwink equation and GPC calibration for linear short-chain branched polyolefines, including polypropylene and ethylene–propylene copolymers. J Appl Polym Sci **29:**3763-3782.

100. **Champion, D., H. Hervet, G. Blond, M. Le Meste, and D. Simatos.** 1997. Translational diffusion in sucrose solutions in the vicinity of their glass transition temperature. J Phys Chem B **101:**10674-10679.

101. **Russo, M. A. L., E. Strounina, M. Waret, T. Nicholson, R. Truss, and P. J. Halley.** 2006. A study of water diffusion into a high-amylose starch blend: the effect of moisture content and temperature. Biomacromolecules **8:**296-301.

102. **Alfrey, T., E. F. Gurnee, and W. G. Lloyd.** 1966. Diffusion in glassy polymers. J Polym Sci Part C: Polym Symp **12:**249-261.

103. **Holsinger, V. H., A. J. McAloon, C. I. Onwulata, and P. W. Smith.** 2000. A cost analysis of encapsulated spray-dried milk fat. J Dairy Sci **83:**2361-2365.

104. **Paluch, M., C. M. Roland, S. Pawlus, J. Zioło, and K. L. Ngai.** 2003. Does the Arrhenius temperature dependence of the Johari-Goldstein relaxation persist above Tg? Phys Rev Lett **91:**115701.

105. **van Baarlen, P., F. J. Troost, S. van Hemert, C. van der Meer, W. M. de Vos, P. J. de Groot, G. J. E. J. Hooiveld, R.-J. M. Brummer, and M. Kleerebezem.** 2009. Differential NF-κB pathways induction by *Lactobacillus plantarum* in the duodenum of healthy humans correlating with immune tolerance. Proc Nat Acad Sci USA **106:**2371-2376.

106. **Duda, J. L., Y. C. Ni, and J. S. Vrentas.** 1979. An equation relating self-diffusion and mutual diffusion coefficients in polymer-solvent systems. Macromolecules **12:**459-462.

107. **Masaro, L., and X. X. Zhu.** 1999. Physical models of diffusion for polymer solutions, gels and solids. Prog Polym Sci **24:**731-775.

108. **Molinero, V., T. Çağın, and W. A. Goddard Iii.** 2003. Sugar, water and free volume networks in concentrated sucrose solutions. Chem Phys Lett **377:**469-474.

109. **D'Errico, G., O. Ortona, F. Capuano, and V. Vitagliano.** 2004. Diffusion coefficients for the binary system glycerol + water at 25 °C. A velocity correlation study. J Chem Eng Data **49:**1665-1670.

110. **Yoshii, H., T. L. Neoh, T. Furuta, and M. Ohkawara.** 2008. Encapsulation of proteins by spray drying and crystal transformation method. Dry Technol **26:**1308-1312.

111. **Chen, X. D., and K. C. Patel.** 2008. Biological change during food drying processes, p. 90-112. *In* X. D. Chen and A. S. Mujumdar (ed.), Drying Technology in Food Processing. Blackwell Publishing LTD, Oxford.

112. **Sutter, M., S. Oliveira, N. N. Sanders, B. Lucas, A. v. Hoek, M. A. Hink, A. J. W. G. Visser, S. C. d. Smedt, W. E. Hennink, and W. Jiskoot.** 2007. Sensitive

spectroscopic detection of large and denatured protein aggregates in solution by use of the fluorescent dye Nile red. J Fluoresc **17:**181-192.

113. **Etzel, M. R., S. Y. Suen, S. L. Halverson, and S. Budijono.** 1996. Enzyme inactivation in a droplet forming a bubble during drying. J Food Eng **27:**17-34.
114. **Luyben, K. C. A. M., J. K. Liou, and S. Bruin.** 1982. Enzyme degradation during drying. Biotechnol Bioeng **24:**533-552.
115. **Liou, J. K.** 1982. An approximate method for nonlinear diffusion applied to enzyme inactivation during drying. Proefschrift Wageningen. Wageningen University, Wageningen, The Netherlands.
116. **Tanford, C., J. J. T. E. C.B. Anfinsen, and M. R. Frederic.** 1970. Protein denaturation: Part C. Theoretical models for the mechanism of denaturation, p. 1-95, Advances in Protein Chemistry, vol. 24. Academic Press.
117. **Eyring, H.** 1935. The activated complex in chemical reactions. J Chem Phys **3:**107-115.
118. **Cornish-Bowden, A.** 2004. Fundamentals of enzyme kinetics. Portland Press, London, UK.
119. **Schokker, E. P., and A. J. S. van Boekel.** 1997. Kinetic modeling of enzyme inactivation: kinetics of heat inactivation at 90−110 ^{o}C of extracellular proteinase from *Pseudomonas fluorescens* 22F. J Agri Food Chem **45:**4740-4747.
120. **Malcolm, A. D. B., and G. K. Radda.** 1970. The reaction of glutamate dehydrogenase with 4-Iodoacetamido salicylic acid. Eur J Biochem **15:**555-561.
121. **Lumry, R., and H. Eyring.** 1954. Conformation changes of proteins. J Phys Chem **58:**110-120.
122. **Jakób, A., J. Bryjak, H. Wójtowicz, V. Illeová, J. Annus, and M. Polakovic.** 2010. Inactivation kinetics of food enzymes during ohmic heating. Food Chem **123:**369-376.
123. **Apenten, R. K. O., and N. Berthalon.** 1994. Determination of enzyme global thermostability from equilibrium and kinetic analysis of heat inactivation. Food Chem **51:**15-20.

124. **Miyawaki, O.** 2009. Thermodynamic analysis of protein unfolding in aqueous solutions as a multisite reaction of protein with water and solute molecules. Biophys Chem **144:**46-52.

125. **Murphy, K. P.** 1995. Noncovalent forces important to the conformational stability of protein structures, p. 1-34, vol. 40.

126. **Greene, R. F., and C. N. Pace.** 1974. Urea and guanidine hydrochloride denaturation of ribonuclease, lysozyme, α-chymotrypsin, and β-lactoglobulin. J Biol Chem **249:**5388-5393.

127. **Pace, C. N., C. H. W. Hirs, and S. N. Timasheff.** 1986. Determination and analysis of urea and guanidine hydrochloride denaturation curves, p. 266-280, Meth Enzymol, vol. 131. Academic Press.

128. **Seber, G. A. F., and C. J. Wild.** 2005. Computational methods for nonlinear least squares, p. 619-660, Nonlinear Regression. John Wiley & Sons, Inc.

129. **Aster, R. C., B. B. Clifford, and H. Thurber.** 2005. Appendix C Review of vector calculus, p. 273-280, International Geophysics, vol. 90. Academic Press.

130. **Hurvich, C. M., and C.-l. Tsai.** 1989. Regression and time series model selection in small samples. Biometrika **76:**297-307.

131. **Fang, Z., and B. Bhandari.** 2010. Encapsulation of polyphenols - a review. Trends Food Sci Technol **21:**510-523.

132. **Sansone, F., T. Mencherini, P. Picerno, M. d'Amore, R. P. Aquino, and M. R. Lauro.** 2011. Maltodextrin/pectin microparticles by spray drying as carrier for nutraceutical extracts. J Food Eng **105:**468-476.

133. **Wijlhuizen, A. E., P. J. A. M. Kerkhof, and S. Bruin.** 1979. Theoretical study of the inactivation of phosphatase during spray drying of skim-milk. Chem Eng Sci **34:**651-660.

134. **Coumans, W. J.** 2000. Models for drying kinetics based on drying curves of slabs. Chem Eng Process **39:**53-68.

135. **Fantner, G. E., R. J. Barbero, D. S. Gray, and A. M. Belcher.** 2010. Kinetics of antimicrobial peptide activity measured on individual bacterial cells using high-speed atomic force microscopy. Nat Nano **5:**280-285.

136. **Gianfrancesco, A., C. Turchiuli, D. Flick, and E. Dumoulin.** 2010. CFD modeling and simulation of maltodextrin solutions spray drying to control stickiness. Food Bioprocess Technol **3:**946-955.

137. **Goula, A. M., and K. G. Adamopoulos.** 2004. Influence of spray drying conditions on residue accumulation-simulation using CFD. Dry Technol **22:**1107-1128.

138. **Adhikari, B., T. Howes, B. R. Bhandari, and V. Truong.** 2000. Experimental studies and kinetics of single drop drying and their relevance in drying of sugar-rich foods: A review. Int Journal Food Prop **3:**323-351.

139. **Chuchottaworn, P., A. Fujinami, and K. Asano.** 1984. Experimental study of evaporation of a volatile pendant drop under high mass flux conditions. J Chem Eng Jap **17:**7-13.

140. **Ali Al Zaitone, B., and C. Tropea.** 2011. Evaporation of pure liquid droplets: Comparison of droplet evaporation in an acoustic field versus glass-filament. Chem Eng Sci **66:**3914-3921.

141. **Vehring, R., W. R. Foss, and D. Lechuga-Ballesteros.** 2007. Particle formation in spray drying. J Aerosol Sci **38:**728-746.

142. **Schlichting, H., and K. Gersten.** 2000. Boundary-layer theory 8th ed. Spinger, Berlin, Germany.

143. **Yoshioka, S., Y. Aso, K.-i. Izutsu, and S. Kojima.** 1994. Is stability prediction possible for protein drugs? Denaturation kinetics of β-galactosidase in solution. Pharmaceut Res **11:**1721-1725.

144. **Straatsma, H., M. Verschueren, M. Gunsing, R. Verdurmen, and P. d. Jong.** 2007. CFD simulation of spray drying of food products, p. 249-286, Computational Fluid Dynamics in Food Processing. CRC Press.

145. **Incropera, F. P., and D. P. De Witt.** 1985. Fundamentals of heat and mass transfer, 2nd edition. John Wiley and Sons, Inc., New York, USA.

146. **Farid, M.** 2003. A new approach to modelling of single droplet drying. Chem Eng Sci **58:**2985-2993.

147. **Crank, J.** 1990. The mathematics of diffusion. Oxford University Press, London, UK.

148. **Mosaad, M.** 1999. Laminar forced convection conjugate heat transfer over a flat plate. Heat Mass Transfer **35:**371-375.

149. **Thirumaleshwar, M.** 2009. Fundamentals of heat and mass transfer. Dorling Kindersley, New Delhi, India.

150. **Kakac, S., and Y. Yener.** 1993. Heat conduction. Taylor & Francis, Washington DC, USA.

151. **Walton, D. E., and C. J. Mumford.** 1999. The morphology of spray-dried particles: the effect of process variables upon the morphology of spray-dried particles. Chem Eng Res Des **77:**442-460.

152. **Langrish, T.** 2009. Degradation of vitamin C in spray dryers and temperature and moisture content profiles in these dryers. Food Bioprocess Technol **2:**400-408.

153. **Goff, J. A., and S. Gratch.** 1946. Low-pressure properties of water from -160 to 212 F, p. 95-122, The 52nd Annual Meeting of the American Society of Heating and Ventilating Engineers, New York.

154. **Quirijns, E. J., A. J. B. v. Boxtel, W. K. P. v. Loon, and G. v. Straten.** 2005. Sorption isotherms, GAB parameters and isosteric heat of sorption. J Sci Food Agric **85:**1805-1814.

155. **Räderer, M., A. Besson, and K. Sommer.** 2002. A thin film dryer approach for the determination of water diffusion coefficients in viscous products. Chem Eng J **86:**185-191.

156. **Bolz, R. E., and G. L. Tuve.** 1973. CRC handbook of tables for applied engineering science. CRC Press, Cleveland, Ohio.

157. **FAO/WHO.** 2002. Report of a joint FAO/WHO expert consultation on guidelines for the evaluation of probiotics in food. World Health Organization and Food and Agriculture Organization of the United Nations, London Ontario, Canada.

158. **Parvez, S., K. A. Malik, S. Ah Kang, and H. Y. Kim.** 2006. Probiotics and their fermented food products are beneficial for health. J Appl Microbiol **100:**1171-1185.

159. **Fuller, R.** 1991. Probiotics in human medicine. Gut **32:**439-442.

160. **Jankovic, I., W. Sybesma, P. Phothirath, E. Ananta, and A. Mercenier.** 2010. Application of probiotics in food products—challenges and new approaches. Curr Opin Biotechnol **21:**175-181.

161. **Bron, P. A., P. van Baarlen, and M. Kleerebezem.** 2012. Emerging molecular insights into the interaction between probiotics and the host intestinal mucosa. Nat Rev Micro **10:**66-78.

162. **Kleerebezem, M., P. Hols, E. Bernard, T. Rolain, M. Zhou, R. J. Siezen, and P. A. Bron.** 2010. The extracellular biology of the lactobacilli. FEMS Microbiol Rev **34:**199-230.

163. **Ranadheera, R. D. C. S., S. K. Baines, and M. C. Adams.** 2010. Importance of food in probiotic efficacy. Food Res Int **43:**1-7.

164. **Holzapfel, W. H., P. Haberer, R. Geisen, J. Björkroth, and U. Schillinger.** 2001. Taxonomy and important features of probiotic microorganisms in food and nutrition. Am J Clin Nutr **73:**365s-373s.

165. **Ananta, E.** 2005. Impact of environmental factors on viability and stability and high pressure pretreatment on stress tolerance of *Lactobacillus rhamnosus* GG (ATCC 53103) during spray drying. Technischen Universität Berlin, Berlin.

166. **Desmond, C., R. P. Ross, E. O'Callaghan, G. Fitzgerald, and C. Stanton.** 2002. Improved survival of *Lactobacillus paracasei* NFBC 338 in spray-dried powders containing gum acacia. J Appl Microbiol **93:**1003-1011.

167. **Corcoran, B. M., R. P. Ross, G. F. Fitzgerald, and C. Stanton.** 2004. Comparative survival of probiotic lactobacilli spray-dried in the presence of prebiotic substances. J Appl Microbiol **96:**1024-1039.

168. **Gardiner, G. E., E. O'Sullivan, J. Kelly, M. A. E. Auty, G. F. Fitzgerald, J. K. Collins, R. P. Ross, and C. Stanton.** 2000. Comparative survival rates of human-derived probiotic *Lactobacillus paracasei* and *L. salivarius* strains during heat treatment and spray drying. Appl Environ Microbiol **66:**2605-2612.

169. **Guilbaud, M., M. Zagorec, S. Chaillou, and M.-C. Champomier-Vergès.** 2012. Intraspecies diversity of *Lactobacillus sakei* response to oxidative stress and

variability of strain performance in mixed strains challenges. Food Microbiol **29:**197-204.

170. **Molenaar, D., F. Bringel, F. H. Schuren, W. M. de Vos, R. J. Siezen, and M. Kleerebezem.** 2005. Exploring *Lactobacillus plantarum* genome diversity by using microarrays. J Bacteriol **187:**6119-6127.

171. **Ingham, C. J., A. Sprenkels, J. Bomer, D. Molenaar, A. van den Berg, J. E. T. van Hylckama Vlieg, and W. M. de Vos.** 2007. The micro-petri dish, a million-well growth chip for the culture and high-throughput screening of microorganisms. Proc Nat Acad Sci USA **104:**18217-18222.

172. **Ingham, C. J., M. van den Ende, D. Pijnenburg, P. C. Wever, and P. M. Schneeberger.** 2005. Growth and multiplexed analysis of microorganisms on a subdivided, highly porous, inorganic chip manufactured from anopore. Appl Environ Microbiol **71:**8978-8981.

173. **Kleerebezem, M., J. Boekhorst, R. van Kranenburg, D. Molenaar, O. P. Kuipers, R. Leer, R. Tarchini, S. A. Peters, H. M. Sandbrink, M. W. E. J. Fiers, W. Stiekema, R. M. K. Lankhorst, P. A. Bron, S. M. Hoffer, M. N. N. Groot, R. Kerkhoven, M. de Vries, B. Ursing, W. M. de Vos, and R. J. Siezen.** 2003. Complete genome sequence of *Lactobacillus plantarum* WCFS1. Proc Natl Acad Sci USA **100:**1990-1995.

174. **Augustin, M. A., and Y. Hemar.** 2009. Nano- and micro-structured assemblies for encapsulation of food ingredients. Chem Soc Rev **38**.

175. **Chávez, B. E., and A. M. Ledeboer.** 2007. Drying of probiotics: Optimization of formulation and process to enhance storage survival. Dry Technol **25:**1193-1201.

176. **Boulos, L., M. Prévost, B. Barbeau, J. Coallier, and R. Desjardins.** 1999. Live/Dead® BacLight™: application of a new rapid staining method for direct enumeration of viable and total bacteria in drinking water. J Microbiol Methods **37:**77-86.

177. **Crowe, J. H., L. M. Crowe, and F. A. Hoekstra.** 1989. Phase transitions and permeability changes in dry membranes during rehydration. J Bioenerg Biomembr **21:**77-91.

178. **Hoekstra, F. A., E. A. Golovina, and J. Buitink.** 2001. Mechanisms of plant desiccation tolerance. Trends Plant Sci. **6:**431-438.

179. **Koster, K. L., Y. P. Lei, M. Anderson, S. Martin, and G. Bryant.** 2000. Effects of vitrified and nonvitrified sugars on phosphatidylcholine fluid-to-gel phase transitions. Biophys J **78:**1932-1946.

180. **Womersley, C. Z.** 1990. Dehydration survival and anhydrobiotic potential, p. 117-137. CRC Press Inc., Boca Raton, Florida.

181. **Pereira, E. d. J., A. D. Panek, and E. C. A. Eleutherio.** 2003. Protection against oxidation during dehydration of yeast. Cell Stress Chaperon **8:**120-124.

182. **Lievense, L. C., M. A. M. Verbeek, T. Taekema, G. Meerdink, and K. V. t. Riet.** 1992. Modelling the inactivation of *Lactobacillus plantarum* during a drying process. Chem Eng Sci **47:**87-97.

183. **Abee, T., and J. A. Wouters.** 1999. Microbial stress response in minimal processing. Int J Food Microbiol **50:**65-91.

184. **Buchi.** 2012. Mini Spray Dryer B-290.

185. **Arpagaus, C., and H. Schwartzbach.** 2012. Scale-up from the Büchi Mini Spray Dryer B-290 to the Niro Mobile Minor.

186. **Crowe, J. H., J. F. Carpenter, L. M. Crowe, and T. J. Anchordoguy.** 1990. Are freezing and dehydration similar stress vectors? A comparison of modes of interaction of stabilizing solutes with biomolecules. Cryobiology **27:**219-231.

187. **Koster, K., K. Maddocks, and G. Bryant.** 2003. Exclusion of maltodextrins from phosphatidylcholine multilayers during dehydration: Effects on membrane phase behaviour. Eur Biophys J **32:**96-105.

188. **Tetsuya, S., and K. Hiroaki.** 1996. Effects of glucose and its oligomers on the stability of freeze-dried liposomes. BBA - Biomembranes **1278:**176-182.

189. **Castro, H. P., P. M. Teixeira, and R. Kirby.** 1997. Evidence of membrane damage in *Lactobacillus bulgaricus* following freeze drying. J Appl Microbiol **82:**87-94.

190. **Mazur, P., and J. J. Schmidt.** 1968. Interactions of cooling velocity, temperature, and warming velocity on the survival of frozen and thawed yeast. Cryobiology **5:**1-17.

191. **Sinskey, T. J., and G. J. Silverman.** 1970. Characterization of injury incurred by *Escherichia coli* upon freeze-drying. J Bacteriol **101:**429-437.

192. **Oliver, A. E., L. M. Crowe, and J. H. Crowe.** 1998. Methods for dehydration-tolerance: Depression of the phase transition temperature in dry membranes and carbohydrate vitrification. Seed Sci Res **8:**211-221.

193. **Sun, W. Q., T. C. Irving, and A. C. Leopold.** 1994. The role of sugar, vitrification and membrane phase transition in seed desiccation tolerance. Physiol Plantarum **90:**621-628.

194. **van de Guchte, M., P. Serror, C. Chervaux, T. Smokvina, S. Ehrlich, and E. Maguin.** 2002. Stress responses in lactic acid bacteria. Antonie Leeuwenhoek **82:**187-216.

195. **Fu, W.-Y., and M. R. Etzel.** 1995. Spray drying of *Lactococcus lactis* ssp. l*actis* C2 and cellular injury. J Food Sci **60:**195-200.

196. **Knorr, D.** 1998. Technology aspects related to microorganisms in functional foods. Trends Food Sci Tech **9:**295-306.

197. **Perdana, J., M. B. Fox, R. M. Boom, M. Kleerebezem, and M. A. I. Schutyser.** 2013. Low molecular weight sugars enhance the cell membrane stability during dehydration - submitted for publication.

198. **Leslie, S. B., S. A. Teter, L. M. Crowe, and J. H. Crowe.** 1994. Trehalose lowers membrane phase transitions in dry yeast cells. BBA - Biomembranes **1192:**7-13.

199. **Linders, L. J., W. F. Wolkers, F. A. Hoekstra, and K. van't Riet.** 1997. Effect of added carbohydrates on membrane phase behavior and survival of dried *Lactobacillus plantarum*. Cryobiology **35:**31-40.

200. **Oldenhof, H., W. F. Wolkers, F. Fonseca, S. Passot, and M. Marin.** 2005. Effect of sucrose and maltodextrin on the physical properties and survival of air-

dried *Lactobacillus bulgaricus*: an in situ Fourier transform infrared spectroscopy study. Biotechnol Prog **21:**885-892.

201. **Wiener, M., R. Suter, and J. Nagle.** 1989. Structure of the fully hydrated gel phase of dipalmitoylphosphatidylcholine. Biophys J **55:**315-325.
202. **Bryant, G., K. L. Koster, and J. Wolfe.** 2001. Membrane behaviour in seeds and other systems at low water content: the various effects of solutes. Seed Sci Res **11:**17-25.
203. **Wolfe, J., and G. Bryant.** 1999. Freezing, drying, and/or vitrification of membrane-solute-water systems. Cryobiology **39:**103-129.
204. **Zhao, G., and G. Zhang.** 2005. Effect of protective agents, freezing temperature, rehydration media on viability of malolactic bacteria subjected to freeze-drying. J Appl Microbiol **99:**333-338.
205. **de Valdez, G. F., G. S. de Giori, A. P. de Ruiz Holgado, and G. Oliver.** 1983. Comparative study of the efficiency of some additives in protecting lactic acid bacteria against freeze-drying. Cryobiology **20:**560-566.
206. **Champagne, C. P., F. Mondou, Y. Raymond, and D. Roy.** 1996. Effect of polymers and storage temperature on the stability of freeze-dried lactic acid bacteria. Food Res Int **29:**555-562.
207. **Perdana, J., M. B. Fox, R. M. Boom, M. Kleerebezem, and M. A. I. Schutyser.** 2013. Unravelling dehydration and thermal inactivation mechanisms using a single droplet approach for increased viability of *Lactobacillus plantarum* WCFS1 after spray drying - submitted for publication.
208. **O'Riordan, K., D. Andrews, K. Buckle, and P. Conway.** 2001. Evaluation of microencapsulation of a Bifidobacterium strain with starch as an approach to prolonging viability during storage. J Appl Microbiol **91:**1059-1066.
209. **Couchman, P. R., and F. E. Karasz.** 1978. A classical thermodynamic discussion of the effect of composition on glass-transition temperatures. Macromolecules **11:**117-119.

210. **Orford, P. D., R. Parker, and S. G. Ring.** 1990. Aspects of the glass transition behaviour of mixtures of carbohydrates of low molecular weight. Carbohydr Res **196:**11-18.

211. **Talja, R. A., and Y. H. Roos.** 2001. Phase and state transition effects on dielectric, mechanical, and thermal properties of polyols. Thermochim Acta **380:**109-121.

212. **Först, P., and U. Kulozik.** 2009. A low resolution 1H NMR study to investigate the protective mechanism of sorbitol during vacuum drying of a probiotic micro-organism, p. 73-80, Magnetic Resonance in Food Science: Challenges in a Changing World. Royal Society of Chemistry.

213. **Moran, J. H., and R. G. Schnellmann.** 1997. Diverse cytoprotectants prevent cell lysis and promote recovery of respiration and ion transport. Biochem Biophys Res Commun **234:**275-277.

214. **De Angelis, M., R. Di Cagno, C. Huet, C. Crecchio, P. F. Fox, and M. Gobbetti.** 2004. Heat shock response in *Lactobacillus plantarum*. Appl Environ Microbiol **70:**1336-1346.

215. **Bischof, J. C., and X. He.** 2006. Thermal stability of proteins. Ann N Y Acad Sci **1066:**12-33.

216. **Csermely, P., L. Vígh, and J. Crowe.** 2007. Trehalose as a "chemical chaperone", p. 143-158, Molecular Aspects of the Stress Response: Chaperones, Membranes and Networks, vol. 594. Springer New York.

217. **Roetman, K.** 1979. Crystalline lactose and the structure of spray-dried milk-products as observed by scanning electron-microscopy. Neth Milk Dairy J **33:**1-11.

218. **Vuataz, G.** 2002. The phase diagram of milk: A new tool for optimising the drying process. Lait **82:**485-500.

219. **Palzer, S., C. Dubois, and A. Gianfrancesco.** 2011. Generation of product structures during drying of food products. Dry Technol **30:**97-105.

220. **MacFarlane, D. R., and C. A. Angell.** 1984. Glass transition for amorphous solid water. J Phys Chem **88:**759-762.

221. **Yu, L., D. S. Mishra, and D. R. Rigsbee.** 1998. Determination of the glass properties of D-mannitol using sorbitol as an impurity. J Pharm Sci **87:**774-777.

222. **Roos, Y.** 1993. Melting and glass transitions of low molecular weight carbohydrates. Carbohydr Res **238:**39-48.

223. **Chen, T., A. Fowler, and M. Toner.** 2000. Literature review: Supplemented phase diagram of the trehalose–water binary mixture. Cryobiology **40:**277-282.

224. **Roos, Y., and M. Karel.** 1991. Water and molecular weight effects on glass transitions in amorphous carbohydrates and carbohydrate solutions. J Food Sci **56:**1676-1681.

225. **Matveev, Y. I., V. Y. Grinberg, I. V. Sochava, and V. B. Tolstoguzov.** 1997. Glass transition temperature of proteins. Calculation based on the additive contribution method and experimental data. Food Hydrocolloid **11:**125-133.

226. **Anderson, W. A., N. D. Hedges, M. V. Jones, and M. B. Cole.** 1991. Thermal inactivation of *Listeria monocytogenes* studied by differential scanning calorimetry. J Gen Microbiol **137:**1419-1424.

227. **Lambert, P. A., and S. M. Hammond.** 1973. Potassium fluxes, first indications of membrane damage in micro-organisms. Biochem Biophys Res Commun **54:**796-799.

228. **Pagán, R., and B. Mackey.** 2000. Relationship between membrane damage and cell death in pressure-treated Escherichia coli cells: differences between exponential- and stationary-phase cells and variation among strains. Appl Environ Microbiol **66:**2829-2834.

229. **Ananta, E., and D. Knorr.** 2009. Comparison of inactivation pathways of thermal or high pressure inactivated *Lactobacillus rhamnosus* ATCC 53103 by flow cytometry analysis. Food Microbiol **26:**542-546.

230. **Lee, J., and G. Kaletunç.** 2002. Evaluation of the heat inactivation of *Escherichia coli* and *Lactobacillus plantarum* by differential scanning calorimetry. Appl Environ Microbiol **68:**5379-5386.

231. **Métris, A., S. M. George, B. M. Mackey, and J. Baranyi.** 2008. Modeling the variability of single-cell lag times for *Listeria innocua* populations after sublethal and lethal heat treatments. Appl Environ Microbiol **74:**6949-6955.

232. **Breeuwer, P., and T. Abee.** 2000. Assessment of viability of microorganisms employing fluorescence techniques. Int J Food Microbiol **55:**193-200.

233. **Darzynkiewicz, Z., X. Li, and J. Gong.** 2009. Assays of cell viability: discrimination of cells dying by apoptosis, p. 437, Essential Cytometry Methods.

234. **den Besten, H. M. W., D. Garcia, R. Moezelaar, M. H. Zwietering, and T. Abee.** 2010. Direct-imaging-based quantification of *Bacillus cereus* ATCC 14579 population heterogeneity at a low incubation temperature. Appl Environ Microbiol **76:**927-930.

235. **den Besten, H. M. W., C. J. Ingham, J. E. T. van Hylckama Vlieg, M. M. Beerthuyzen, M. H. Zwietering, and T. Abee.** 2007. Quantitative analysis of population heterogeneity of the adaptive salt stress response and growth capacity of *Bacillus cereus* ATCC 14579. Appl Environ Microbiol **73:**4797-4804.

236. **Snyder, T. L.** 1947. The relative errors of bacteriological plate counting methods. J Bacteriol **54:**641.

237. **Fisher, R. A., H. Thornton, and W. Mackenzie.** 1922. The accuracy of the plating method of estimating the density of bacterial populations. Ann Appl Biol **9:**325-359.

238. **Baranyi, J., and C. Pin.** 1999. Estimating bacterial growth parameters by means of detection times. Appl Environ Microbiol **65:**732-736.

239. **Cuppers, H. G. A. M., and J. P. P. M. Smelt.** 1993. Time to turbidity measurement as a tool for modeling spoilage by *Lactobacillus*. J Ind Microbiol **12:**168-171.

240. **Mosmann, T.** 1983. Rapid colorimetric assay for cellular growth and survival: Application to proliferation and cytotoxicity assays. J Immunol Methods **65:**55-63.

241. **Guillier, L., P. Pardon, and J.-C. Augustin.** 2005. Influence of stress on individual lag time distributions of *Listeria monocytogenes*. Appl Environ Microbiol **71:**2940-2948.

242. **Carruthers, A.** 1990. Facilitated diffusion of glucose. Physiol Rev **70:**1135-1176.

243. **Briczinski, E. P., A. T. Phillips, and R. F. Roberts.** 2008. Transport of glucose by *Bifidobacterium animalis* subsp. *lactis* occurs via facilitated diffusion. Appl Environ Microbiol **74:**6941-6948.

244. **Termont, S., K. Vandenbroucke, D. Iserentant, S. Neirynck, L. Steidler, E. Remaut, and P. Rottiers.** 2006. Intracellular accumulation of trehalose protects *Lactococcus lactis* from freeze-drying damage and bile toxicity and increases gastric acid resistance. Appl Environ Microbiol **72:**7694-7700.

245. **Wiemken, A.** 1990. Trehalose in yeast, stress protectant rather than reserve carbohydrate. Antonie Leeuwenhoek **58:**209-217.

246. **Yancey, P. H.** 2001. Water stress, osmolytes and proteins. Amer Zool **41:**699-709.

247. **Arakawa, T., and S. Timasheff.** 1985. The stabilization of proteins by osmolytes. Biophys J **47:**411.

248. **Kumar, R.** 2009. Role of naturally occurring osmolytes in protein folding and stability. Arch Biochem Biophys **491:**1-6.

249. **Santoro, M. M., Y. Liu, S. M. A. Khan, L. X. Hou, and D. W. Bolen.** 1992. Increased thermal stability of proteins in the presence of naturally occurring osmolytes. Biochem **31:**5278-5283.

250. **Karmas, R., M. Pilar Buera, and M. Karel.** 1992. Effect of glass transition on rates of nonenzymic browning in food systems. J Agri Food Chem **40:**873-879.

251. **Buitink, J., M. M. Claessens, M. A. Hemminga, and F. A. Hoekstra.** 1998. Influence of water content and temperature on molecular mobility and intracellular glasses in seeds and pollen. Plant Physiol **118:**531-541.

252. **Linders, L. J. M., G. I. W. de Jong, G. Meerdink, and K. van't Riet.** 1997. Carbohydrates and the dehydration inactivation of *Lactobacillus plantarum*: The role of moisture distribution and water activity. J Food Eng **31:**237-250.

253. **Foerst, P., and U. Kulozik.** 2012. Modelling the dynamic inactivation of the probiotic bacterium *L. paracasei* subsp. *paracasei* during a low-temperature

drying process based on stationary data in concentrated systems. Food Bioprocess Tech **5:**2419-2427.

254. **Murthy, U. N., P. P. Kumar, and W. Q. Sun.** 2003. Mechanisms of seed ageing under different storage conditions for *Vigna radiata* (L.) *wilczek*: lipid peroxidation, sugar hydrolysis, Maillard reactions and their relationship to glass state transition. J Exp Bot **54:**1057-1067.

255. **Fyfe, K., O. Kravchuk, A. V. Nguyen, H. Deeth, and B. Bhandari.** 2011. Influence of dryer type on surface characteristics of milk powders. Dry Technol **29:**758-769.

256. **Walton, D. E.** 2000. The morphology of spray-dried particles a qualitative view. Dry Technol **18:**1943-1986.

257. **Nijdam, J. J., and T. A. G. Langrish.** 2005. An investigation of milk powders produced by a laboratory-scale spray dryer. Dry Technol **23:**1043-1056.

258. **Kim, E. H. J., X. D. Chen, and D. Pearce.** 2009. Surface composition of industrial spray-dried milk powders. 2. Effects of spray drying conditions on the surface composition. J Food Eng **94:**169-181.

259. **Ferrari, G., G. Meerdink, and P. Walstra.** 1989. Drying kinetics for a single droplet of skim-milk. J Food Eng **10:**215-230.

260. **Liu, X. D., T. Furuta, H. Yoshii, and P. Linko.** 2000. Retention of emulsified flavor in a single droplet during drying. Food Sci Technol Res **6:**335-339.

261. **Menting, L. C., and B. Hoogstad.** 1967. Volatiles retention during the drying of aqueous carbohydrate solutions. J Food Sci **32:**87-90.

262. **Nijdam, J. J., and T. A. G. Langrish.** 2006. The effect of surface composition on the functional properties of milk powders. J Food Eng **77:**919-925.

263. **Shrestha, A. K., T. Howes, B. P. Adhikari, B. J. Wood, and B. R. Bhandari.** 2007. Effect of protein concentration on the surface composition, water sorption and glass transition temperature of spray-dried skim milk powders. Food Chem **104:**1436-1444.

264. **Amelia, R., W. D. Wu, J. Cashion, P. Bao, R. Zheng, X. D. Chen, and C. Selomulya.** 2011. Microfluidic spray drying as a versatile assembly route of functional particles. Chem Eng Sci **66:**5531-5540.

265. **Djaeni, M., P. Bartels, J. Sanders, G. v. Straten, and A. v. Boxtel.** 2007. Process integration for food drying with air dehumidified by zeolites. Dry Technol **25:**225-239.

266. **Atuonwu, J., G. van Straten, H. van Deventer, and A. van Boxtel.** 2011. Improving adsorption dryer energy efficiency by simultaneous optimization and heat integration. Dry Technol **29:**1459-1471.

267. **Scoti, E. C.** 1959. Method and apparatus for producing granulated food products. USA.

268. **Chen, Y.-M.** 1987. Fundamentals of a centrifugal fluidized bed. AIChE J **33:**722-728.

269. **Perry, R. H., and D. W. Green.** 2007. Perry's chemical engineers' handbook. McGraw-Hill Professional Publishing.

270. **Wang, N., and J. G. Brennan.** 1991. Moisture sorption isotherm characteristics of potatoes at four temperatures. J Food Eng **14:**269-287.

271. **Al-Muhtaseb, A. H., W. A. M. McMinn, and T. R. A. Magee.** 2002. Moisture sorption isotherm characteristics of food products: a review. Food Bioprod Process **80:**118-128.

272. **Lange, N. A., and J. A. Dean.** 1979. Lange's handbook of chemistry. McGraw-Hill.

273. **Rogers, R. R.** 1979. A short course in cloud physics. Pergamon Press.

274. **Wolff, E., and H. Gibert.** 1990. Atmospheric freeze-drying part 1: Design, experimental investigation and energy-saving advantages. Dry Technol **8:**385-404.

275. **Pardo, J. M., and D. A. Letva.** 2010. Effects of different pre-treatments on energy consumption during freeze drying of pineapple pieces. Interciencia **35:**934-938.

276. **Towler, G., and R. K. Sinnott.** 2007. Chemical engineering design: Principles, practice and economics of plant and process design. Elsevier Science.

277. **Bouman, R. W., S. B. Jesen, L. Wake, and W. B. Earl.** 2005. Process capital cost estimation for New Zealand 2004. Society of Chemical Engineers New Zealand.

278. **Millman, M. J., A. I. Liapis, and J. M. Marchello.** 1985. Note on the economics of batch freeze dryers. Int J Food Sci Technol **20:**541-551.

279. **Desobry, S. A., F. M. Netto, and T. P. Labuza.** 1997. Comparison of spray-drying, drum-drying and freeze-drying for β-carotene encapsulation and preservation. J Food Sci **62:**1158-1162.

280. **Smit, F., P. D. Jong, J. Straatsma, and M. Verschueren.** 2011. NIZO-Premia enables knowledgement in the food industry. Part 1: background and application of the system. Voedingsmiddelentechnologie **34:**23-26.

281. **Jong, P. D., J. Straatsma, Z. E. H. Otten, R. J. Siezen, and H. C. v. d. Horst.** 1999. Presented at the The 25th International Dairy Federation Congress.

282. **Bryant, G., and J. Wolfe.** 1992. Interfacial forces in cryobiology and anhydrobiology. Cryo-Lett **13:**23-36.

283. **Dufrene, Y. F.** 2004. Using nanotechniques to explore microbial surfaces. Nat Rev Micro **2:**451-460.

284. **Huang, B., H. Babcock, and X. Zhuang.** 2010. Breaking the diffraction barrier: Super-resolution imaging of cells. Cell **143:**1047-1058.

285. **Fernandez-Suarez, M., and A. Y. Ting.** 2008. Fluorescent probes for super-resolution imaging in living cells. Nat Rev Mol Cell Biol **9:**929-943.

286. **Shimomura, O.** 2005. The discovery of aequorin and green fluorescent protein. J Microsc **217:**3-15.

287. **Shimomura, O., F. H. Johnson, and Y. Saiga.** 1962. Extraction, purification and properties of aequorin, a bioluminescent protein from the luminous Hydromedusan, *Aequorea*. J Cell Comp Physiol **59:**223-239.

288. **Liu, D. S., W. S. Phipps, K. H. Loh, M. Howarth, and A. Y. Ting.** 2012. Quantum dot targeting with lipoic acid ligase and Halotag for single-molecule imaging on living cells. ACS Nano **6:**11080-11087.

Acknowledgments

If you close this booklet now, you will find only one name written on the cover. I should confess that I don't deserve this much credit; too many hands have helped me to finalize this thesis booklet. Without them, I am afraid that you will not see even a single dot in this thesis. So, let me express my gratitude to those who have contributed to the completion of this thesis, either directly or indirectly.

First of all, I would like to thank Maarten, Remko, and Martijn for your support and guidance, not only within the project, but also for my personal development. Maarten, I owed you and learned from you a lot. Greetings to Susan and thanks for her encouragements. Remko, your out-of-the-box advices often could solve my cul-de-sac research problems. Martijn, before you even realize, many times you already stood in the right time in the right place to pull me out of the mud. I am proud to have three of you as supervisors and promotor. I enjoyed working with you and I hope to keep the collaboration.

I would also thank Ludmila and Oylum. Ludmila, we had a bit of hard time in the start of the project. It's sad that you left when I started enjoying our collaboration. Oylum, thanks for the good work and the fruitful discussions. Good luck with the last stretch of your Ph.D.

I am glad to meet my Pandawa; Jacob, Pengfei, Mark, Jan, and Siwei. I thank you for the good results and the large contributions in the completion of my thesis. I enjoyed the time with you and learned a lot from you. Keep in touch. You don't need to wait for tomorrow, I am already proud of you now.

I am grateful to have Michiel, Ruud, and Heidy as my co-authors. I enjoyed our fruitful discussions and collaboration. I learned a lot from you, too. I thank Marcel Giesbers for his kind assistance to operate X-ray diffraction and later to work with SEM. I thank Tiny for her kind assistance to work with SEM. I also thank Jan Willem and Boudewijn who helped me with CLSM measurements. Collin, thanks for the timely supply of Anopore. Clint, thanks for helping and teaching Ludmila and I to operate the fluorescence microscope.

Joyce, Marjan, Roelfina and Petra, thanks for your help related to the administrative works and the application of the residence permit for me and my family. Jos and Maurice, thanks for your valuable assistance. Give my greeting to the enigmatic FPE-Order. Martin, thanks for your help managing the financial matters. I promise to buy you a milk shake, one day. Peter, thanks for your assistance and help, for example during installations of some software. I would also like to thank people in Werkplaats: Hans de Rooij, Hans Meijer, Reinoud, and André. My gratitude to PoaC, especially to Varsha and Remko. I thank Huygens Scholarship Program, which enabled me to come to The Netherlands, also all Hutac-ers for the nice experiences.

Dear fellow colleagues of Food and Bio Process Engineering, it was an unforgettable and wonderful experience to be part of a dynamic, diverse, and intellectually engaging group. I thank you for the memorable labuitjes, Ph.D trips, and any other activities. Karola, Ivon, Olesya, Kashif, Nanik, it was fun to have you as the office-mate. Thanks also for taking care of me and thanks for the chats and everything. Karola and Ivon, I feel secure to have you as my paranymphs. I wish you good luck with your Ph.D. Kashif, greeting for your family and please send us some photos or at least a postcard, Nanik, can I treat you coffee in HEMA? Hans Tramper, Atze-Jan, Arjen, Anja, Karin, Albert, thank you. Dear fellow colleagues from Food Microbiology. It feels like home in your lab, despite my status as an invisible guy. Ingrid, I will never enough thanking you who helped Mark and I during our experiments. I also enjoyed our chats. Diah, thanks for the encouragement, (sneaky) collaborations, and the secret recipe of rendang. Greetings to all members of Dapur Troelstraweg. Clint, Xiao, Alicja, and Na, thanks for being OK to be disturbed. Hein, Henk, Franz, and all Dairy Science and Technology people; thanks a lot for the fascination with dairy you have infected to me.

I would thank Peter, Hans, Patrick, and Franklin from NIZO Food Research. Edwin, Jeroen, Alessandro, Martin, and Gabrie, thanks for the discussions and inputs from industrial perspective. Dong, Xin, James, Aditya, stay in touch, fellow drying guys!

Audrie and Melli Siahainenia, thanks for taking care of Nathan, Emi, and me. Next time, please cook the curry a bit less spicy. Milkha and Jeni, trimakasih banyak sudah mengasuh anak terlantar ini, buburnya enak banget. Trees and Heine Smit, you have invaluable helps done to my family, we don't even know how to repay it. Pak Hadi, mbak Adian and Adhel,

terimakasih banyak atas bantuannya, nanti saya mampir ke Semarang boleh nginap kan? Marcel and kak Tini, trimakasih banyaaaaak, kebaikan kalian betul-betul tak ternilai bagi kami; nanti kalo Nathan sudah agak terkendali, kita ke IKEA, ya kak.

Special thanks to all loyal customers of Losmen Dua Cinta, cinta Tuhan dan sesama: bang Robert (terimakasih sekali atas nasihat-nasihatmu dan kesediaanmu menampungku), Roni, and mas Probo. Mutia, you still owe me playing Nocturnes Op. 9. Syifa, jaga kesehatan baik-baik. Bang Toni, mbak Reni, adek Grace. Trimakasih sudah menerima saya dengan sangat baik di Duesseldorf. Karl-Heinz, Regina, Matthias. Psalm 25. CJ, Ich werde promoviert; see you in paradise, or in Schafheutle. Monika, thanks for the Bigos recipe. Ferdinand, sering-sering mampir ya. Affan dan Herda, good to have you, guys, a handful old friends that still remains. All Indonesian Bennekomers, mbak Anti and mas Zakir, keep the good work dan tetap guyub. PPI Wageningen, tetap berkarya dimanapun kita berada.

I thank SCW, Josine, Ingeborg, Alfred, Kat, Oscar, Robin. Alexandre and Danielle, do not forsake wisdom, and she will protect you. I am grateful to ICF: Johan and Heleen, Delano and José, Hans and Marieke, Jaap, Peter and Yuni, Koos and Carolien, Koos v.d. Ziel, and Koenrad; WBS: Beryl, Lailanie, Connie, Pulcherie, and Oscar, PubCie ICF: Annewies, Alies, Samson. I am grateful to find home away from home and family away from family, both in SCW and ICF. Do not neglect to show hospitality to strangers, for thereby some have entertained angels unawares.

I have a wonderful and encouraging time with PD Wageningen. Terimakasih atas dukungan, doa, dan kebersamaannya. I want to thank Pak Anton and Bu Isti, jaga kesehatan dan cukup istirahat. Semoga pada akhirnya kita bisa berkata “Aku telah mengakhiri pertandingan yang baik, aku telah mencapai garis akhir dan aku telah memelihara iman.”

To my parents, papah, mami, and Omega, without your support and sacrifices, I will never be I am who I am now. Terima kasih dan salam sayang selalu. Terima kasih telah memperkenalkanku sejak dini dengan kasih Tuhan. My ten minas: Emi & Nathaniel. Emi, I walk the Milky Way route to find the answer, which is YOU, with additional bonus of . Terima kasih atas dukungan dan pengertianmu. You are worth far more than rubies. Nathan, I hope that you can be like the one whom he saw under the fig tree. I thank Yeshua to let not my heart be troubled. So teach me to number my days that I may get a heart of wisdom.

Andreas Dehne once said, “Ich hatte das Glück, Dich gekannt zu haben. Ich habe das Glück, mich noch erinnern zu können an DICH. Ich wäre glücklich, Dich noch einmal wiederzusehen.” Truly, I was lucky to have known you, I am fortunate enough to remember you, and I would be happy to see you again, once more. Keep me updated.

lg, *J*

cherfrans@yahoo.fr

List of publications

J. Perdana, M.B. Fox, M.A.I. Schutyser, and R.M. Boom. 2013. Mimicking spray drying by drying of single droplets deposited on a flat surface. Food Bioprocess Tech. 6:964-977.

J. Perdana, L. Bereschenko, M. Roghair, M. B. Fox, R. M. Boom, M. Kleerebezem, and M.A.I. Schutyser. 2012. Novel method for enumeration of viable *Lactobacillus plantarum* WCFS1 cells after single-droplet drying. Appl. Environ. Microbiol. 78:8082-8088.

M.A.I. Schutyser, **J. Perdana**, and R.M. Boom. 2012. Single droplet drying for optimal spray drying of enzymes and probiotics. Trends Food Sci. Tech. 27(2), 73-82.

J. Perdana, M. B. Fox, M. A. I. Schutyser, and R. M. Boom. 2012. Enzyme inactivation kinetics: coupled effects of temperature and moisture content. Food Chem. 133:116-123.

J. Perdana, M.B. Fox, M.A.I. Schutyser, and R.M. Boom. 2011. Single-droplet experimentation on spray drying: evaporation of a sessile droplet. Chem. Eng. Technol. 34:1151-1158.

J. Perdana, R.G.M. van der Sman, M.B. Fox, R.M. Boom, and M.A.I Schutyser. Measuring and modelling of diffusivities in carbohydrate-rich matrices during thin film drying. *Submitted for publication*.

J. Perdana, L. Bereschenko, M.B. Fox, J.H. Kuperus, M. Kleerebezem, R.M. Boom, and M.A.I. Schutyser. Dehydration and thermal inactivation of *Lactobacillus plantarum* WCFS1 by comparing single droplet drying to spray and freeze drying. *Submitted for publication*.

J. Perdana, M.B. Fox, S. Chen, R.M. Boom, and M.A.I. Schutyser. Interactions between formulation and spray drying conditions related to survival of *Lactobacillus plantarum* WCFS1. *Submitted for publication*.

J. Perdana, H.M.W. den Besten, O. Kutahya, D.C. Aryani, M.B. Fox, M. Kleerebezem, R.M. Boom, and M.A.I Schutyser. Residual viability of spray dried and stored *L. plantarum* WCFS1 measured by means of growth parameters. *Submitted for publication*.

Overview of completed training activities

Discipline specific activities

Star-CD Computational Fluid Dynamics, 2009
Computational Fluid Dynamics of Multiphase Flow, 2010
Advanced Computer Aided Modelling, 2010
An Introduction to gProms, 2010
Optimization and model validation with gProms, 2010
NIZO - How to get more out of spray drying, 2010
Reaction Kinetics in Food Science, 2013
Advanced Food Analysis, 2013

Netherlands Process Technology Symposium 9, Veldhoven, The Netherlands, 2009
Netherlands Process Technology Symposium 10, Veldhoven, The Netherlands, 2010
17th International Drying Symposium, Magdeburg, Germany, 2010
8th European Congress of Chemical Engineering, Berlin, Germany, 2011
18th International Drying Symposium, Xiamen, China, 2012

General courses

PhD Career Assessment, 2009
Project and Time Management, 2009
Effective Behaviour in Your Professional Surrounding, 2011
Techniques for Writing and Presenting a Scientific Paper, 2011
Career Perspective, 2012

Optional

PhD Project Proposal, 2009
PhD Excursion, Massachusetts–New York, USA, 2010
PhD Excursion, Finland and Baltic Countries, 2012
POAC and Trans-ACTS meetings, 2009-2013

About the author

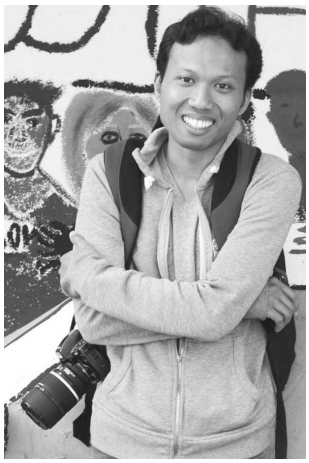

Jimmy Perdana was born in October 1983 in Klaten, Indonesia. He spent his childhood in Kebumen before moving to Bandung in 2001 to pursue a bachelor degree in Chemical Engineering in Institute Technology of Bandung. He completed the degree in March 2007. In the same year he joined Nestle Indonesia within Management Development Program framework. In July 2007, Jimmy left Nestle Indonesia to pursue a master study in Food Technology in Wageningen UR, fully funded by Huygens Scholarship Program – NUFFIC. He obtained the degree in 2009 with distinction (*cum laude*). His thesis on inline determination of model kinetics in the microheater was conducted in collaboration with NIZO Food Research. Instead of internship, Jimmy conducted a minor thesis leading to his Ph.D project within Food Process Engineering Group – Wageningen UR on the development of single droplet analysis for spray drying of foods. The results of the research are presented in this thesis.

The research described in this thesis was financially supported by Process on a Chip (PoaC) program – Advanced Chemical Technologies for Sustainability (ACTS) – Netherlands Organization for Scientific Research (NWO).